



# Mathematical modelling of coating film application onto pharmaceutical solid dosage forms

Charalampos Christodoulou

A dissertation submitted in partial  
fulfillment of the requirements for the degree of  
Doctor of Philosophy  
Department of Chemical Engineering  
University College London (UCL)

August 2019

I, Charalampos Christodoulou confirm that the work presented in this thesis is my own. Where information has been derived from other sources, I confirm that this has been indicated in the thesis.

---

Charalampos Christodoulou

*ἀρχὰς εἶναι τῶν ὅλων ἀτόμους καὶ κενόν, τὰ δ'ἄλλα πάντα νενομίσθαι*

- Democritus

# Impact statement

The application of coating films is a significant step in the manufacture of pharmaceutical tablets. In many cases, tablets are coated with an edible polymer-based film before they are administered to patients. This may be done to protect the tablet core, to separate active ingredients, to cover the unpleasant taste of some ingredients or for aesthetic reasons. Even though the tablet coating process is very popular, information related to the behavior of coating liquids on tablets under pharmaceutical coating process conditions is limited in the open literature. In this work, we therefore investigate the fundamental phenomena that are taking place at the point of contact between a tablet and a coating suspension in an effort to reduce the number of defective tablets, to maximize tablet shelf-life and to enable a more accurate selection of the optimal process conditions.

During this research project, mathematical models were developed in order to provide insight into the process of coating application on pharmaceutical tablets. This insight can be used by the pharmaceutical industry to adopt the appropriate film-coating process conditions and enhance the quality of the final product. Main outputs of the current models include predictions of the amount of coating suspension (water and polymer particles) that penetrates into the tablet and the percentage of water that evaporates from within the tablet. Knowledge of the amount of water and polymer in the tablet core can be used to optimize the shelf-life of the tablet and control the adhesion of the dry coating film.

The assumptions of the models presented in this thesis, which are solely based on physics and are specific to the tablet coating process, allow solving the coating flow problems much faster than equivalent models in commercial Computation Fluid Dynamics (CFD) software. For that reason, in this work, it was possible to perform uncertainty and variance-based sensitivity analyses to study the influence of process parameters on the coating behavior that is applied on the surface of pharmaceutical tablets. The mathematical models developed in this thesis were validated against experimental data taken from the literature and/or CFD simulations.

# Abstract

It is well understood that during the pharmaceutical aqueous film-coating process the amount of liquid water that interacts with the porous tablet core can affect the quality of the final product. Therefore, understanding and simulating the mechanisms of aqueous coating suspension spreading, drying and absorption into the tablet is crucial for controlling the process and optimizing the shelf-life of the tablets. The main aim of the work presented in this thesis is to define and describe the fundamental phenomena taking place at the point of contact between the coating suspension and the tablet during the film-coating process.

In this thesis, a mathematical model that predicts the behavior of single droplets after impact on tablets was developed and validated with experimental results from the literature (Chapter 3). The droplet behavior was divided into two phases of different dynamics and duration: the kinematic and capillary. The kinematic phase model describes the first milliseconds after impact during which inertial forces are significant and the capillary phase model concerns the droplet flow, evaporation and absorption when the capillary effects become dominant. The output of the kinematic and capillary phase models can provide useful insight into the behavior of pure liquid droplets on the surface and into the tablets.

A novel model that predicts liquid coating spreading on the surface of a tablet while it passes under a spray was developed (Chapter 4). The spray-impact model does not require prior knowledge of the process via empirical relations or experimental data. The output of the current model provides useful insight into the coating film formation, thickness and spreading rate on dry tablet cores during the film-coating process. To study the effect of coating properties and process parameters on the film spreading rate and on the final liquid film thickness a variance-based sensitivity analysis was performed. The spray-impact model predictions are in good agreement with experimental data found in the literature.

The “mixture modeling” approach and the “lubrication approximation” method were combined to simplify the equations describing the behavior of the coating liquid-particle system and to develop a model for simulating film motion and drying on tablet surfaces (Chapter 5). The influence of solvent evaporation on important physical properties of the coating suspension, such as the density and viscosity, was taken into consideration. The current model (presented in Chapter 5) also simulates the absorption of the coating suspension inside the porous tablet core, since predicting the wetting front profile inside the core provides important information about the tablet water content during the film-coating process.

Finally, a mathematical model that predicts the evaporation rate of water which has been absorbed into a pharmaceutical tablet during the film-coating process was developed (Chapter 6). The validation of the numerical results with the experimental data from the two separate papers shows that the current novel evaporation model is able to efficiently predict the water content evaporation from different materials in different conditions. The output of the evaporation model provides useful insight into the final water content of a tablet core during the film-coating process.

# Preface

This thesis is submitted in partial fulfillment of the requirements for the degree of Doctor of Philosophy of the University College London. The research has been carried out during the period of October 2015 to August 2019 at the Department of Chemical Engineering, University College London, with Dr. Luca Mazzei and Prof. Eva Sorensen as my academic supervisors and Dr. Salvador García Muñoz as my industrial supervisor.

First, I would like express my greatest thanks to my supervisors Professor Eva Sorensen and Dr. Luca Mazzei for helping me complete this project, for the many useful and critical discussions and for their commitment from the beginning until the end of this project. I would also like to thank Professor Aditya Khair for making me feel part of his group during my stay as a visiting scholar at Carnegie Mellon University. I would like to specially thank Dr. Sal García Muñoz for his support, for sharing his expertise and insight into the pharmaceutical industry processes and for his hospitality during my visit to Eli Lilly at Indianapolis.

I would like to acknowledge my sponsors. Without the financial assistance of Eli Lilly and Company and the Engineering and Physical Sciences Research Council (EPSRC) this project would not have been possible.

My thanks also go to my friends from Greece, Katerina, Adam, Aggelos, Ilias, Stavros, Kostas and Pete and to my friends from the Product and Process Systems Engineering office of the Department of Chemical Engineering at UCL. I thank Carlos, Alba, Andres, Masha, Marco, Cristian, Giannis, Laura, Adrian, Javier, Kostas, Davide, Ricardo, Panos, Katerina, Sergio, Arun and Pedro for their friendship and academic support.

I am extremely grateful to my family for always supporting me. Their encouragement and support gave me the force I needed to have a positive attitude every day. To my parents Aikaterini and Christos and my sister Penelope I dedicate this thesis.

# Contents

<b>1</b>	<b>Introduction</b>	<b>1</b>
1.1	A brief introduction to tablet film-coating . . . . .	2
1.2	Coating process parameters . . . . .	4
1.3	Phenomena during film-coating . . . . .	6
1.4	Motivation and objectives of this thesis . . . . .	7
1.4.1	Tablet defects . . . . .	7
1.4.2	Project motivation . . . . .	8
1.4.3	Summary of thesis objectives . . . . .	9
1.5	Modeling approach . . . . .	9
1.6	Outline of the thesis . . . . .	10
<b>2</b>	<b>Literature Review</b>	<b>12</b>
2.1	Review of modeling of the pharmaceutical film-coating process . . . . .	12
2.1.1	Spray atomization and droplet evaporation during flight models . . . . .	13
2.1.2	Coating drum temperature and humidity level prediction models . . . . .	15
2.1.3	Tablet motion and coating uniformity prediction models . . . . .	17
2.1.4	Single droplet behavior on solid substrates . . . . .	19
2.1.5	Spray impingement on solid substrates . . . . .	22
2.1.6	Thin film flow and absorption onto and into porous substrates . . . . .	24
2.1.7	Tablet drying and film adhesion . . . . .	25
2.2	Concluding remarks . . . . .	28
<b>3</b>	<b>Single droplet behavior on a tablet</b>	<b>29</b>
3.1	Introduction . . . . .	29
3.2	Mathematical model . . . . .	30
3.2.1	Kinematic phase . . . . .	30
3.2.2	Capillary phase . . . . .	37
3.2.3	Numerical solution . . . . .	41
3.3	Numerical results and validation . . . . .	43
3.3.1	Kinematic phase results . . . . .	44
3.3.2	Capillary phase results . . . . .	46
3.4	Concluding remarks . . . . .	50
3.5	Appendix of Chapter 3 . . . . .	51
3.5.1	Mechanical energy balance equation derivation . . . . .	51
3.5.2	Estimation of the rate of viscous dissipation in the droplet-film boundary layer . . . . .	56
<b>4</b>	<b>Spray impingement onto a tablet</b>	<b>58</b>
4.1	Introduction . . . . .	58
4.2	Mathematical model . . . . .	59
4.2.1	Initial wetting . . . . .	60
4.2.2	Droplet impingement on wetted surface - Film spreading . . . . .	62
4.2.3	Splashing of impinging droplets . . . . .	68
4.3	Numerical results and validation . . . . .	68
4.3.1	Validation of spray impingement numerical results . . . . .	69
4.3.2	Sensitivity analysis . . . . .	70
4.4	Concluding remarks . . . . .	73

<b>5</b>	<b>Suspension film behavior on a tablet</b>	<b>74</b>
5.1	Introduction . . . . .	74
5.2	Mathematical model . . . . .	75
5.2.1	Coating behavior on the tablet surface . . . . .	76
5.2.2	Coating absorption into the tablet core . . . . .	83
5.2.3	Numerical solution . . . . .	86
5.3	Numerical results and validation . . . . .	87
5.3.1	Coating film drying rate . . . . .	88
5.3.2	Pure solvent absorption rate . . . . .	89
5.3.3	Coating flow, absorption and evaporation . . . . .	91
5.4	Concluding remarks . . . . .	95
5.5	Appendix of Chapter 5 . . . . .	96
5.5.1	Simplified momentum balance equation . . . . .	96
5.5.2	Film thickness evolution equation . . . . .	98
5.5.3	Energy equation . . . . .	100
5.5.4	Heat conduction from the tablet to the film . . . . .	102
5.5.5	Particle volume fraction evolution equation . . . . .	102
5.5.6	Estimation of the Peclet and Stokes numbers . . . . .	103
5.5.7	Main equations of Section 5.2.2 expressed in cylindrical coordinates . . . . .	104
<b>6</b>	<b>Water evaporation from within a porous tablet</b>	<b>106</b>
6.1	Introduction . . . . .	106
6.2	Mathematical model . . . . .	107
6.3	Numerical solution . . . . .	111
6.4	Numerical results and validation . . . . .	113
6.4.1	Water evaporation from porous media . . . . .	113
6.4.2	Case study: Prediction of the water content of a tablet during film-coating . . . . .	115
6.5	Concluding remarks . . . . .	118
<b>7</b>	<b>Conclusions and directions for future research</b>	<b>119</b>
7.1	Single droplet behavior on a tablet . . . . .	119
7.2	Spray impingement onto a tablet . . . . .	120
7.3	Suspension film behavior on a tablet . . . . .	120
7.4	Water evaporation from within a porous tablet . . . . .	121
7.5	Summary of main contributions . . . . .	122
7.6	Directions for future research . . . . .	123
7.6.1	Extending this research . . . . .	123
7.6.2	Broader recommendations . . . . .	124

# List of Figures

1.1	Revenue of the pharmaceutical industries worldwide from 2001 to 2017 (data from Mikulic, 2017).	1
1.2	Coating equipment. a) Coating drum, b) fluidized bed.	2
1.3	Tablet defects. Pictures taken from Muliadi and Sojka (2010).	4
1.4	Coating drum with baffles.	5
1.5	Film absorption into a porous tablet core.	7
1.6	Phenomena at the point of contact between the pharmaceutical tablet and the coating formulation.	9
1.7	Overall modeling approach. The position of the tablet while going through each stage is shown in the figure on the left.	11
2.1	Pharmaceutical coating rotating drum.	17
2.2	Types of wetting on pharmaceutical tablets.	21
2.3	Spray impingement on a rigid substrate.	23
2.4	Coating film behavior on porous tablets.	25
2.5	Tablet drying during film-coating.	26
3.1	Mathematical modelling approach.	29
3.2	Spherical cap droplet on a tablet. $\vartheta$ is the dynamic contact angle and $\mathcal{S}_{rs}$ and $\gamma_{rs}$ are the interface and the interfacial tension between phases $r$ and $s$ , respectively.	31
3.3	Axisymmetric stagnation point flow. The lines denote the flow streamlines.	33
3.4	$F_d$ factor estimation. The experimental data are from Bolleddula et al. (2010).	35
3.5	VOF simulation of droplet impact ( $Re = 10$ ). a) The assumed axisymmetric stagnation point flow, b) the calculated flow streamlines from the VOF simulation.	36
3.6	$\Lambda$ factor estimation. The experimental data are from Bolleddula et al. (2010).	37
3.7	Droplet evaporation and absorption into the tablet. The model calculates the droplet height $h$ and the wetting front depth $h_p$ into the tablet.	38
3.8	Wetting front depth ( $h_p$ ) inside the tablet.	41
3.9	Kinematic phase model results. a) Normalized wetted area diameter and droplet max height (experiments by Bolleddula et al., 2010) and, b) Kinetic energy dissipation during spreading.	44
3.10	Validation of the kinematic phase model with experimental data from Bolleddula et al. (2010): a) Wetted area diameter of OpadryII 10% droplets for different impact velocities. b) Spreading factor of droplets of different viscosity after deposition.	45
3.11	Capillary phase model results. Percentage of liquid content absorbed inside porous substrate of different porosities. Experimental data from Lee et al. (2016).	47
3.12	a) Droplet height profile on the surface after 1, 5 and 10s, and b) wetting front profile in the substrate after 1, 5 and 12s. The red lines denote the propagated error of the model input parameters	48
3.13	Comparison between simulation and experimental data for a) the maximum droplet height on the substrate surface, and b) the maximum wetting depth in the substrate. Experimental data from Lee et al. (2016).	49
3.14	Effect of evaporation in liquid absorption during the capillary phase, a) Droplet height profiles after 3s. b) Final wetting front profile inside the porous matrix.	49

4.1	Outline of the coating application process during pharmaceutical coating. . .	59
4.2	a) Droplet array, and b) single droplet impact on a dry tablet. . . . .	60
4.3	Droplet-droplet interaction on a rigid surface. Volume-Of-Fluid simulation. .	61
4.4	Successive droplet impact onto the tablet. a) Side and b) top view of the tablet. . . . .	62
4.5	Shear flow velocity field. The dotted lines denote the streamlines. . . . .	64
4.6	a) Droplet impact on a film, b) Volume-Of-Fluid CFD simulation of droplet-film impingement. . . . .	65
4.7	Vertical to the solid substrate velocity component during droplet impingement on a film ( $Re = 250$ , $U_0 = 1\text{ m/s}$ , $D_0 = 2.5\text{ mm}$ , $\mu_1 = 10\text{ cP}$ , $\rho_1 = 1000\text{ kg/m}^3$ ). .	66
4.8	Droplet impingement on a film and merging. a) Volume-Of-Fluid CFD simulation, and b) current modeling approach. . . . .	67
4.9	Film height as a function of the droplet impact Reynolds number. Comparison with a) experimental data, and b) empirical equation by Kalantari and Tropea (2007). . . . .	69
4.10	Film thickness variation with changing: a) droplet velocity ( $D_0 = 150\mu\text{m}$ , $\mu_1 = 10\text{ cP}$ , $\dot{Q} = 200\text{ g/min}$ ), b) droplet diameter ( $U_0 = 5\text{ m/s}$ , $\mu_1 = 10\text{ cP}$ , $\dot{Q} = 200\text{ g/min}$ ), c) viscosity ( $D_0 = 150\mu\text{m}$ , $\dot{Q} = 200\text{ g/min}$ , $U_0 = 5\text{ m/s}$ ), d) spray rate ( $D_0 = 150\mu\text{m}$ , $\mu_1 = 15\text{ cP}$ , $U_0 = 5\text{ m/s}$ ). . . . .	72
5.1	Coating film applied on the surface of a porous tablet core. . . . .	75
5.2	a) Coating film on a tablet surface, b) Tablet top view. . . . .	79
5.3	Wetting front depth inside the tablet. . . . .	84
5.4	Particle passing through a tablet pore. The random lines denote the retained solid coating. . . . .	86
5.5	Validation of numerical results for pharmaceutical coating (Aquarius Prime) drying rate. Comparison with data by Niblett et. al. (2017). . . . .	89
5.6	Validation of numerical results for pure liquid (a. water, b. glycerol) absorption rate into porous substrates. Comparison with experimental data reported by Léang et al. (2019). . . . .	91
5.7	a) Suspension film thickness and penetration depth profiles, and b) particle volume fraction distribution, in the film after 7 s. . . . .	92
5.8	Effect of the a) evaporation velocity, b) initial solid volume fraction, c) tablet initial permeability, and d) filter coefficient on the coating suspension absorption rate. . . . .	93
5.9	Effect of the particle diameter/pore diameter ratio on the suspension wetting front depth. . . . .	94
6.1	Second stage of a spray drying process. . . . .	107
6.2	Liquid evaporation from within a porous matrix. . . . .	108
6.3	Evaporation front within a tablet. . . . .	109
6.4	Domains $z_1^*$ and $z_2^*$ . . . . .	112
6.5	Evaporation of water inside a) $\text{CaCO}_3$ tablets and b) glass beads during the evaporation phase. Experiments from a) Tag et al. (2010) and b) Reis et al. (2003). . . . .	113
6.6	Wetted region profile in glass beads during evaporation. (Substrate porosity $= 0.30$ ; initial water droplet volume $= 4.3\mu\text{L}$ ). . . . .	114
6.7	Wetting front depth profile during the evaporation phase under coating process conditions. (Substrate porosity $= 0.30$ ; initial water droplet volume $= 4.3\mu\text{L}$ ). . . . .	115

6.8	a) Water that has evaporated or is inside the film or inside porous tablet core.	
	b) Water evaporation rate from within the suspension film crust. . . . .	117
6.9	Reduction of the water content of the tablet after it leaves the spray zone. . .	118

# List of Tables

1.1	Coating process parameters (Agrawal and Pandey, 2015). . . . .	3
2.1	Atomization models available in the literature for the prediction of pharmaceutical coating spray droplet Sauter mean diameter. . . . .	13
2.2	Models available in the literature that can predict the conditions (temperature, humidity, moisture levels) inside a coating drum. . . . .	16
2.3	Models available in the literature that can simulate tablet movement. . . . .	17
2.4	Overview of models that predict droplet behavior on pharmaceutical tablets. . . . .	19
2.5	Overview of models that predict spray impact on rigid substrates. . . . .	22
2.6	Overview of models that predict film behavior on porous substrates. . . . .	23
2.7	Overview of the main studies regarding film and tablet drying and film adhesion. . . . .	26
3.1	Coating droplets rheology properties. Taken from Bolleddula et al. (2010). . . . .	45
3.2	Comparison of the current model with the model from Roisman et al. (2002) in terms of the final spreading factor. Experiments from Bolleddula et al. (2010). . . . .	46
3.3	Validation of the numerical results and experimental data for the maximum wetting front depth during the capillary phase. Experiments by Lee et al. (2016). . . . .	47
4.1	Droplet-droplet interaction effect on the wetted area diameter at $t_i = D_0/U_0$ . . . . .	61
4.2	Film thickness at the moment when the entire target surface is wetted ( $t = \tau_F$ ). Validation of the spray model against the empirical equation by Kalantari and Tropea (2007). . . . .	70
4.3	Sensitivity analysis. Variance-based method by Saltelli et al. (2010). . . . .	71
5.1	Current model predictions for coating solvent evaporation mass flux $\dot{m}_e$ . Validation with numerical results by Niblett et al. (2017). . . . .	89
6.1	Process parameters for the case studies. . . . .	116
6.2	Coating suspension properties for the case studies (from: Amidon et al., 1999). . . . .	116

# CHAPTER 1

## Introduction

---

This thesis is concerned with the mathematical modeling of pharmaceutical coating film behavior during application onto tablets. In this chapter, tablet film coating is introduced, the phenomena involved in the process are described, the main goals of this work are summarized and finally a brief outline of the thesis is presented.

---

The pharmaceutical industry discovers, develops and produces medications (pharmaceutical drugs) that are intended to cure or alleviate symptoms of patients. Therefore, its high significance as a global sector is indisputable. In less than 20 years (2001-2017), the worldwide revenue of pharmaceutical industries has increased from 390.2 to 1143 billion U.S. dollars (Mikulic, 2017). In 2014, the revenue of the global pharmaceutical market for the first time increased to over one trillion U.S. dollars (Fig. 1.1).

In 2015, two-thirds of all prescribed medications to patients were solid dosage forms, with half of them being tablets (Alam et al., 2015). Today, pharmaceutical tablets are easily administered to the patients (accurate dosing), are relatively cheap to produce and are easy to package and transport. Thus, tablets are the dosage form of choice for a large number of pharmaceutical companies (Hein, 2017).

In many cases tablets are coated with an edible polymer-based film before they are administered to patients (Cole et al., 1995). This may be done to protect the tablet core (e.g. from humidity), to cover the unpleasant taste of some ingredients or for aesthetic reasons. This thesis is concerned with the film-coating process, which is part of the overall solid tablet production process, and aims to provide insight that can enhance the quality of the final pharmaceutical product.

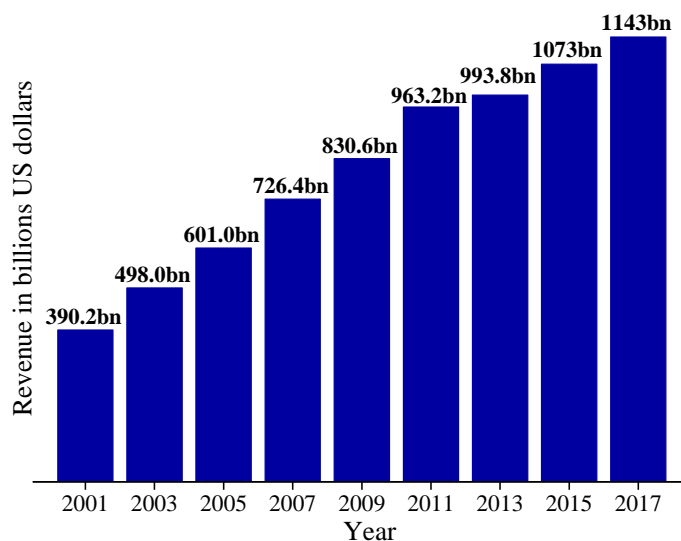


Figure 1.1: Revenue of the pharmaceutical industries worldwide from 2001 to 2017 (data from Mikulic, 2017).

## 1.1 A brief introduction to tablet film-coating

Coating of tablet cores is one of the oldest manufacturing processes used by the pharmaceutical industry dating back to the mid 19<sup>th</sup> century. At first, coating was carried out by slowly applying sugar coating at the rough surface of tablets. The confectionery industry still makes use of sugar coating regardless of its flaws (time consuming, expensive). On the other hand, the modern pharmaceutical process has evolved over the years to provide attractive appearance, protection and special properties to tablets (Chen and Porter, 2008).

Before describing the modern process, one should address the question “Why are tablets coated?”. A number of equally important reasons can be proposed (Cole et al., 1995):

- The tablet core needs to be modified for aesthetic reasons (e.g. change in color)
- The active ingredients have unpleasant taste which needs to be masked
- The drug release profile needs to be modified (by changing the coating film thickness one can control the release of the active ingredient)
- The tablet core is sensitive to light, atmospheric oxygen or humidity and needs to be protected by a polymer film
- Incompatible substances need to be kept separate inside the same tablet (one ingredient can be part of the tablet core, whereas the second can be inside the polymer film)

This list is of course not exhaustive, but it shows the importance of coating in the pharmaceutical industry.

Tablet film-coating first appeared in 1930, but it took more than two decades until the first film-coated tablets were commercially available (Cole et al., 1995). In the following years, polymer-based coating formulations - *which consist of polymer particles dispersed or dissolved in water or organic solvents* - gained popularity replacing sugar coatings, mainly because their application was not as complex and expensive (Muliadi and Sojka, 2010). During the next twenty years (1954-1975), aqueous coating suspensions (polymer particles + water) did not receive attention compared to the ones using organic solvents because it was mistakenly perceived that they would produce weaker films (Cole et al., 1995).

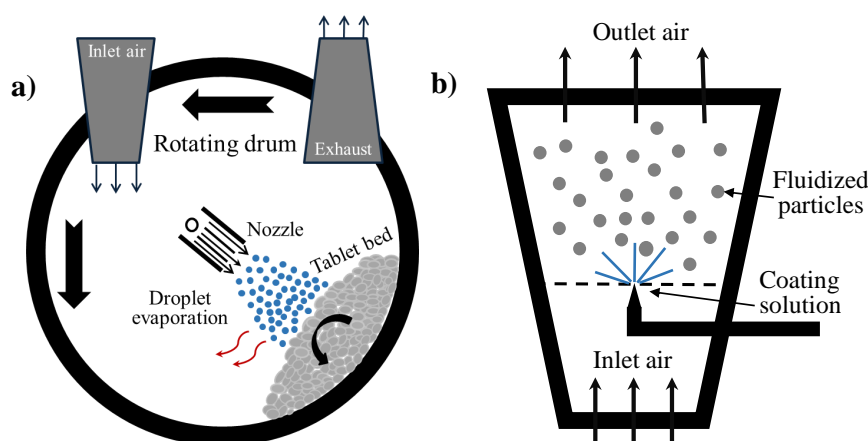


Figure 1.2: Coating equipment. a) Coating drum, b) fluidized bed.

However, in recent years, aqueous coating liquids are gaining ground for many reasons:

- The cost of aqueous coating suspensions is lower than that of the solvent-based ones
- Environmental concerns for the organic solvents were raised especially after chlorinated hydrocarbon solvents were banned by many regulatory authorities
- Modern coating equipment allowed the application of aqueous coating suspensions

The uncoated tablet cores are usually placed inside a rotating drum (Fig. 1.2.a) before being sprayed with the coating formulation. Another configuration is the fluidized bed coater where the tablets are moved around in the fluidized bed and at the same time they are sprayed with coating (Fig. 1.2.b). This thesis is mainly focused on the much more common film-coating process utilizing a rotating pan/drum. Furthermore, tablet coating can be done in either a batch or continuous process. Even though the continuous tablet-coating processes are gaining in popularity, the focus of the current thesis is on batch-coating processes as they are used far more often in commercial manufacturing (Ketterhagen et al., 2017).

The film coating process commences by preparing the coating formulation. This is usually an aqueous suspension that contains polymer particles as well as plasticizer and pigment (Colorcon, 2019). In this thesis, simple aqueous coating liquids (particles + water) are mainly considered. After preparation, the coating formulation is then atomized to produce a spray. The spray droplets are directed with a pattern air stream to the tablet bed. During the flight from the spray nozzle to the bed the droplets evaporate and decelerate. After the droplets impinge on the tablets the remaining water is depleted (evaporates) from the surface, leaving a dry film behind (Muliadi and Sojka, 2010). The application of coating spray on the tablets continues until a dry film that adheres to the substrate has formed. The duration of a coating process can range from 20 to 130 minutes based on the type of drum, coating liquid and process conditions (Colorcon, 2019).

The appropriate temperature for tablet drying is achieved by applying a hot air stream through the tablet bed (Agrawal and Pandey, 2015). The way the drying air is supplied is not always the same and depends on the type of equipment. Modern pan-coaters (e.g. Manesty, Glatt) allow controlling the temperature inside the drum but cannot solve main problems such as tablet defects and coating non-uniformity (Muliadi and Sojka, 2010). Mowery et al. (2002) reported that in a typical coating run, inter- and intra-tablet film thickness variations can be significantly high. To address these issues, one needs to investigate the phenomena taking place during tablet film-coating and provide insight regarding the important parameters of this complex process (Table 1.1).

Table 1.1: Coating process parameters (Agrawal and Pandey, 2015).

Coating equipment	Spray/Atomisation	Tablet properties
Coater dimensions	No. spray nozzles	Hardness, friability
Tablet load	Inlet/outlet air temperature	Friction coefficient
Baffle set-up	Inlet/outlet air humidity	Core shape and size
Drum perforation	Coating viscosity & density	Tablet porosity & tortuosity

## 1.2 Coating process parameters

Due to the complexity of the film-coating process, one often encounters problems with the final product (Muliadi and Sojka, 2010). Some of the most common tablet defects are coating non-uniformity, film peeling and cracking (Cole et al., 1995; Fig. 1.3). The main cause of these defects is not choosing the right values for the process parameters such as spray flow rate, air temperature and relative humidity, which leads to uneven distribution of the coating film on the tablet surface and therefore to coating imperfections. Here the most important coating process parameters which affect the quality of the tablets (Table 1.1) are discussed.

Parameters such as the dimensions of the coating drum, the baffle number and configuration (Fig. 1.4), and the tablet batch-size (tablet load), influence the coating process. The shape and dimensions of the coating equipment should enable coating drying by allowing sufficient air to reach the surface of the tablets. The drum rotation speed, shape and configuration affect the tablet mixing dynamics and thus influence the tablet coating uniformity (Agrawal and Pandey, 2015). Additionally, coating process parameters such as the pan rotation speed and the tablet load need to be taken into account during scale-up (Cole et al., 1995).

Tablet properties can significantly influence the coating process and the quality of the final product. The tablet size and shape can affect tablet movement and coating application. Differently shaped tablets require different coating levels to be adequately coated and to ensure the desired product performance (Agrawal and Pandey, 2015).

When designing a coating process one needs to take into account the tablet hardness to reduce the manifestation of defects caused by edge chipping or tablet cracking (Agrawal and Pandey, 2015). Furthermore, tablet properties, such as porosity and tortuosity, affect liquid coating absorption into the porous core, which is directly linked to coating adhesion and water content in the tablet (Aulton and Twitchell, 1995).

Spray properties such as the atomizing air pressure, the design and the configuration of the guns/nozzles and the spray mass flow rate have a significant effect on the mean droplet size and mean droplet velocity, as well as the spray density and area which play an important role in controlling the process and optimizing the quality of the tablets (Aliseda et al., 2008).

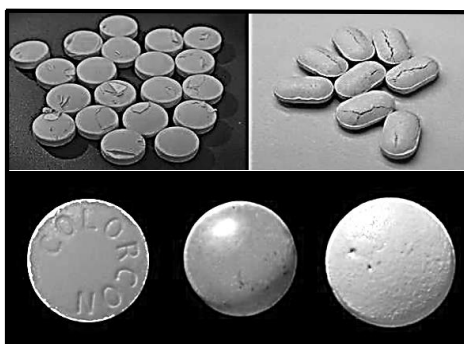


Figure 1.3: Tablet defects. Pictures taken from Muliadi and Sojka (2010).

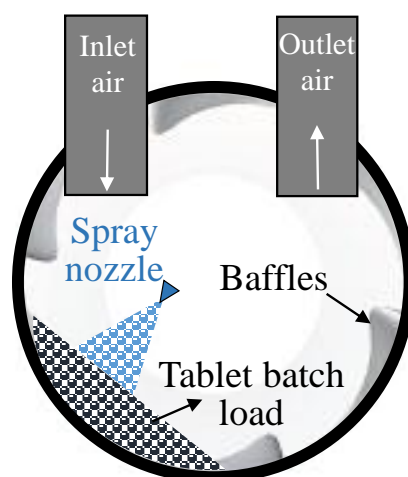


Figure 1.4: Coating drum with baffles.

It is well known in the pharmaceutical industry that high spray mass flow rates might cause tablet defects (e.g. tablet sticking and logo bridging), whereas significantly low spray mass flow rates can lead to spray drying phenomena which affect the duration and efficiency of the coating process (Agrawal and Pandey, 2015). Droplet mean size and velocity are also important spray characteristics since if the droplets are too small or too slow, then most of the water can evaporate before it impinges on the tablet bed, whereas large droplets might result in problems with the film drying and over-wetting of the cores which cause tablet defects (Niblett et al., 2017).

As mentioned earlier in this chapter, coating formulations are usually aqueous or non-aqueous polymer-based suspensions. Modern coating formulations may include active pharmaceutical ingredients or excipients which can enhance tablet properties. Important properties of the coating formulations include the viscosity, the density, the surface tension, the solids content and the evaporation rate of the carrier fluid. Higher particle concentration in the coating suspension can reduce the process run time (more polymer is applied per unit time), but at the same time may cause problems due to difficulties in handling and spraying viscous coatings (Agrawal and Pandey, 2015). Adjusting the solids content and choosing the appropriate carrier fluid in the coating formulation can increase the amount of coating applied uniformly onto the tablets per unit time (Aliseda et al., 2008).

When designing a coating process or considering scale-up, one needs to take into account the relationship between the inlet and exhaust air streams (e.g. volume flow rate, temperature, relative humidity), the coating formulation and the coating equipment (e.g. dimensions, tablet load). Controlling the coating drying rate by adjusting the temperature and flow rate of the inlet air stream accordingly is important for products which are sensitive to humidity. Failing to control the droplet drying rate, by not choosing the equipment, the coating formulation and the inlet air conditions appropriately, gives rise to the possibility of water penetrating and staying in the tablet core for a significant length of time. This can result in tablet degradation, active ingredient disintegration and reduction of tablet shelf-life and overall quality (Cole et al., 1995). To conclude, choosing the right values of the process parameters is not an easy task. It is imperative that one understands the phenomena that take place during tablet film-coating before optimizing the process.

### 1.3 Phenomena during film-coating

A thorough investigation and understanding of the fundamental phenomena taking place during the coating process provides essential information needed to reduce the number of defective tablets and to select the optimal conditions for the process. This section concerns the behavior of the coating liquid from the moment it leaves the nozzle until it coats the tablet, thus including droplet atomization and evaporation as well as film spreading, drying and absorption in the tablet core.

Spray atomization is the breakdown of coating liquid into droplets. In most pharmaceutical coating processes, atomization is achieved when a high velocity air stream impinges on a coating liquid jet. In the literature, there are various theories which address the complex multi-factor process of atomization. A proposed physical mechanism, which is in good agreement with experimental data, is the two-stage jet instability mechanism (Varga et al., 2003). Varga et al. (2003) suggested that a primary shear instability acting on the coating formulation produces liquid jets which then break down into droplets when a secondary instability develops.

The main parameters that influence atomization include the rheological properties of the coating liquid, the spray gun/nozzle type and geometry, and the spray characteristics such as the spray rate and pattern air streams (Ketterhagen et al., 2017). All of the above parameters may change significantly during scale-up or due to different coating equipment. As is discussed in the literature review (Chapter 2), several researchers have investigated spray atomization in an attempt to predict the mean droplet size exiting the nozzle.

During pharmaceutical tablet film-coating, as the droplets travel towards the tablets they experience solvent evaporation due to the differences in relative humidity, velocity and temperature among the surface of the droplets and the drying air (Niblett et al., 2017). When the droplets produced during atomization are small, the effect of droplet evaporation during flight becomes significant since spray-drying comes into play. If spray-drying occurs the efficiency of the coating process reduces. Moreover, pharmaceutical coating droplets contain solid particles which affect the rheological properties and the evaporation kinetics. As the droplet water content decreases, the mass fraction of the solid particles increases leading to the droplets becoming more viscous and also evaporate more slowly. The decrease of the evaporation rate is due to the inability of the solvent to reach the droplet surface when the solids concentration is high in the droplet (Kadja and Bergeles, 2003).

Tablet wetting takes place when spray droplets impinge on the surface of the tablet core. After impingement, the droplets spread over the surface and penetrate into the tablet core (Aulton and Twitchell, 1995). As the film dries, the viscosity of the coating liquid increases and becomes effectively infinite when the solids volume fraction approaches a critical value (Weidner et al., 1996). After this point, coating wetting and absorption are negligible and evaporation is affected by polymer concentration. When the concentration of the solids reaches a new critical value, a porous crust develops at the surface of the film (Kiil, 2006). At this stage, evaporation of the solvent from beneath the film porous crust takes place.

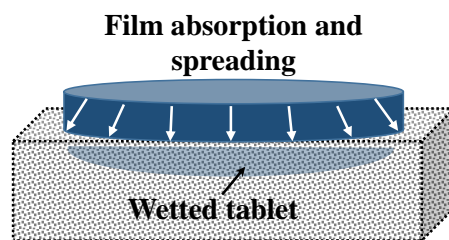


Figure 1.5: Film absorption into a porous tablet core.

Coating absorption into the tablet core (Fig. 1.5) can influence film-tablet adhesion and tablet shelf-life (high water content promotes the degradation of the excipients and the active ingredients). Wetting characteristics also affect the film surface roughness and could promote film splitting. The drying rate plays an important role in the final appearance of the tablets. Slow drying rates might result in problems with over-wetting and tablet tackiness whereas fast drying might affect the quality of the final product.

Water has been found to influence solid-state interactions in a pharmaceutical tablet due to its ability to act as a reactant in several situations (e.g. hydrolytic reactions). Water also enhances degradation mechanisms and affects drug stability (Chen and Porter, 2008). To describe solid-water interactions the concept of “bound” and “unbound” water is introduced; the “bound” water is considered to be unavailable for degradation, whereas “unbound water” is responsible for instability and degradation. Coating suspension penetration into tablets during film-coating affects the water content of the final product (Cole et al., 1995).

## 1.4 Motivation and objectives of this thesis

Information related to coating spray impingement onto tablets and coating formulation drying and absorption into porous tablets is limited in the open literature. Providing this missing insight into the film-coating process is the main goal of this thesis. In this section, the most common tablet defects are discussed and in this way the motivations for studying the behavior of a coating formulation onto and into a tablet are highlighted.

### 1.4.1 Tablet defects

#### **Excess water content in the core**

It is reported in the literature (Muliadi and Sojka, 2010; Cole et al., 1995) that the shelf-life of pharmaceutical tablets depends on the amount of humidity to which they are exposed during the coating process and water present during the handling of the coated product and the packaging. Excess water inside the tablet core can lead to the acceleration of degradation mechanisms thus affecting the tablet quality.

#### **Coating film non-uniformity**

Coating film uniformity is not only crucial for the appearance of the tablets; it can also affect the functionality of solid-dosage drugs and it is especially important for controlled release tablets. Defects such as film cracking, splitting and orange-peel roughness appear when the coating application (spreading, drying) is not optimal.

### **Film peeling/flaking**

Peeling and flaking are important tablet defects. In both cases, the unfinished tablet core surface is exposed. It is reported in the literature that film adhesion (resistance to peeling and flaking) is connected to the amount of coating that dries into the tablet (Amidon, 1999). If the tablet core is impermeable to coating liquid then the final film may not adhere properly.

#### **1.4.2 Project motivation**

Based on the issues highlighted above (Section 1.4.1), it is clear that the pharmaceutical industry needs to be able to understand and to predict the mechanisms of coating spreading and absorption onto and into tablets to avoid accelerating the degradation mechanisms caused by high water content. Moreover, by expanding the knowledge regarding the fundamentals of coating film formation (insight into droplet spreading) on the surface of a pharmaceutical tablet, product defects such as film cracking and peeling can be reduced.

Recent research studying coating behavior on tablets is limited and has been mainly focused on single droplet impact cases (Bolleddula et al., 2010; Niblett et al., 2017). Mathematical models which aim to predict the phenomena at the point of contact between the coating and the tablet are either computationally expensive (CFD simulations) or for simplicity neglect water penetration into the tablet cores or consider coating suspensions as pure liquids (Shaari, 2007; Niblett et al., 2017). The aforementioned mathematical models have shortcomings which do not allow the prediction of the water content inside the tablet core or the occurrence of defects.

The general aim of this work is to investigate the fundamental phenomena that are taking place at the point of contact between the tablet and the coating (Fig. 1.6) in an effort to reduce the number of defective tablets, to maximize tablet shelf-life and to enable a more accurate selection of the optimal process conditions. In this thesis, mathematical models are developed which are able to:

- 1) Predict film formation on tablets during spray impingement
- 2) Provide insight into coating film behavior on a tablet
- 3) Estimate the tablet water content which may affect the quality of the final product

The current models assumptions, which are solely based on physics and are specific to the tablet coating process, allow the solution of coating flow problems much faster than equivalent models developed in commercial CFD software. More importantly, the models developed in this work can be easily combined with an overall model that takes into account tablet movement, drum rotation, tablet exposure and resident time under the spray, spray atomization and evaporation (Aliseda et al., 2008; Ketterhagen, 2011; am Ende and Berchielli, 2005). The final “combined” model will be able to provide useful information regarding the entire coating process and help optimize it. To conclude, the model presented in the following chapters can assist the end user (the pharmaceutical company) in choosing the appropriate process conditions which will maximize the overall quality of the tablets.

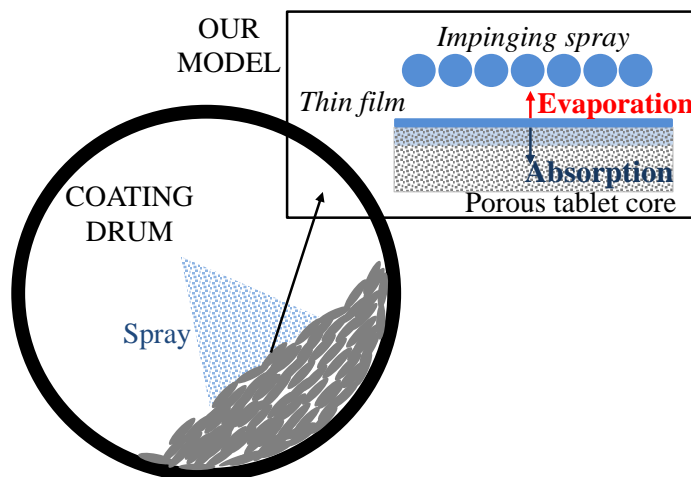


Figure 1.6: Phenomena at the point of contact between the pharmaceutical tablet and the coating formulation.

### 1.4.3 Summary of thesis objectives

Sponsored by Eli Lilly and Company and the Engineering Physical Science Research Council (EPSRC), the specific objectives of this research project are:

- To develop mathematical models that can predict coating film behavior after the film has been applied on a pharmaceutical tablet.
- To validate the mathematical models with experimental data from the literature and/or CFD simulations.
- To use the validated models to gain insight into the spreading of coating droplets which impinge onto tablet surfaces.
- To analyze the numerical results of the models to understand the interactions between pharmaceutical coatings and solid dosage forms and to investigate coating film motion and drying on tablets during the coating process.
- To assist the pharmaceutical industry in choosing the appropriate process conditions which maximize the quality of the final product.

## 1.5 Modeling approach

This section concerns the modeling approach followed in this work to simulate the phenomena at the point of contact between a porous pharmaceutical tablet and a coating formulation inside a film-coating drum (Fig. 1.6), and thus to achieve the thesis objectives listed above.

In this thesis, the process of coating-formulation application onto a tablet surface is divided into four stages (Fig. 1.7) and a model is developed for each stage. These stages are discussed below.

During the 1<sup>st</sup> stage, the tablet enters the spray zone (area under the spray) and the first droplet impinges onto the dry tablet surface. The spreading of the first single droplet is modeled in this work (Chapter 3) by adopting an approach based on the mechanical energy balance equation. The 1<sup>st</sup> stage is completed when a second droplet impinges on the surface of the first.

As the tablet moves into the spray-zone (2<sup>nd</sup> stage), more droplets impinge onto the tablet surface. The individual droplets spread (as described by the model for the 1<sup>st</sup> stage) and locally merge and form disjointed films. As the spray impingement continues, the disjointed films expand, merge and cover the entire tablet surface facing the spray. In this thesis (Chapter 4), a one-dimensional spreading model is developed in order to describe the liquid coating layer formation on the tablet surface while the tablet is under the spray. The time scale of the 2<sup>nd</sup> stage is much shorter than the time scales of absorption and evaporation (Bolledulla et al., 2010) and so these processes are neglected during this stage.

The 3<sup>rd</sup> stage commences when the tablet leaves the spray-zone and the liquid coating layer that has just formed during the 2<sup>nd</sup> stage flows on the tablet and concurrently absorbs into the tablet and evaporates. Eventually, a solid crust forms on the tablet surface. In this work (Chapter 5), the “mixture modeling” approach (Manninen et al., 1996) and the “lubrication approximation” (Szeri, 2010) method are used to simplify the equations describing the behavior of the coating layer (water-particle system) and to develop a mathematical model for simulating coating suspension flow, evaporation and absorption into the tablet.

During the 4<sup>th</sup> stage, water evaporates from within the solid crust that forms at the end of the 3<sup>rd</sup> stage and covers the tablet surface. The tablet during this stage may be located inside the tablet bed where drying air is supplied (Suzzi et al., 2012). The output of the evaporation model developed in this work (Chapter 6) provides insight into the water content of a tablet core when it re-enters the spray-zone (1<sup>st</sup> stage) as well as when the film-coating process is completed. This output is useful to the pharmaceutical industry since the presence of water inside the tablet may accelerate degradation mechanisms of the active ingredients and reduce the shelf-life of the tablet.

During the film-coating process, the tablet enters the spray-zone several times (Kumar et al., 2015) and goes through stages 1 to 4 until a dry film of the desirable thickness has formed. The models developed in the following chapters (see the outline of the thesis in the next section) can be used to describe these stages at any moment during the process.

## 1.6 Outline of the thesis

**Chapter 2** presents a critical survey of selected literature on modeling the pharmaceutical film-coating process. Additionally, numerical models that are not specific to pharmaceutical coatings are presented. These models can, however, be used to predict general film behavior on porous substrates and serve as a background for the current work.

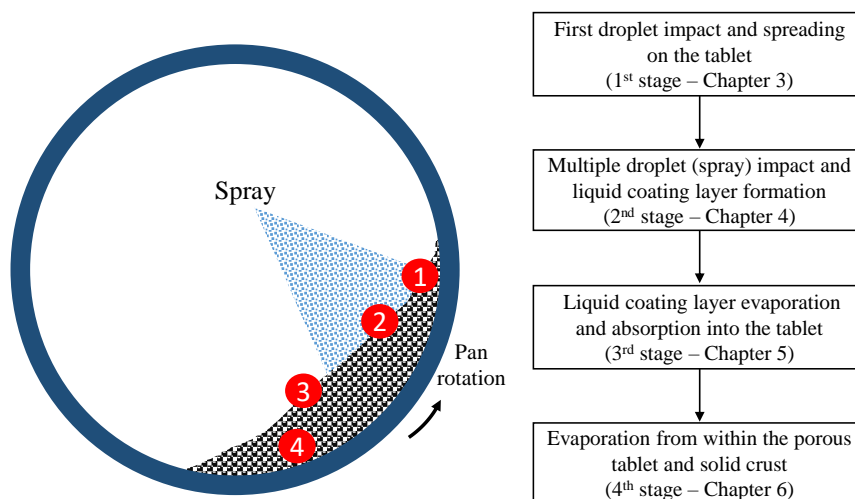


Figure 1.7: Overall modeling approach. The position of the tablet while going through each stage is shown in the figure on the left.

**Chapter 3** deals with single droplet (1<sup>st</sup> stage) impact, spreading, absorption and evaporation onto and into tablet cores. A model that predicts the behavior of single droplets after impingement on a tablet is developed and validated with experimental results from the literature.

In **Chapter 4**, a mathematical model that predicts coating spray impingement and film formation (2<sup>nd</sup> stage) on pharmaceutical tablets is presented. The numerical results are validated by experimental data from the literature.

In **Chapter 5**, a model that calculates film flow and drying on the surface of porous tablets (3<sup>rd</sup> stage) is developed. The model is able to estimate the amount of coating absorbed into the porous core. Again, the model is validated with experimental data taken from the literature.

In **Chapter 6**, a mathematical model that estimates water evaporation from porous media (4<sup>th</sup> stage) is derived. It aims to calculate the final water content in the tablet core and it is validated with experimental data from the literature. A case study that highlights the overall modeling approach, which is described in Section 1.5, is presented.

Finally, in **Chapter 7**, the overall conclusions and main contributions of this PhD project are highlighted. This thesis concludes with an outline of potential future work.

# CHAPTER 2

## Literature Review

---

In this chapter, mathematical models regarding the overall pharmaceutical film-coating process, the impingement of droplets and sprays on solid substrates and the flow, absorption, drying and adhesion of coating films are reviewed. This review aims to give an overview of the level of understanding of the film-coating process up to this day.

---

### 2.1 Review of modeling of the pharmaceutical film-coating process

The topic of tablet film-coating has been extensively studied in recent years and the industrial method is well developed in terms of production capability and economy. However, film-coating is arguably not fully optimized in terms of aesthetic elegance and quality of the final product (Muliadi and Sodjka, 2010). Few researchers have developed mathematical models that simulate the film-coated process in order to enhance the quality and/or appearance of the coated tablet. In this chapter, previous work from the open literature is presented to give an overview of the level of understanding of the process up to this day. The most important mathematical models, found in the literature, that concern the phenomena which take place during the pharmaceutical coating process are reviewed.

The main categories of mathematical models developed for the film-coating process are:

- Models which describe coating spray atomization and droplet evaporation.
- Thermodynamic models which estimate temperature and humidity in a coating drum.
- Models which simulate tablet movement/orientation inside a coating drum.
- Models which predict single coating droplet spreading on a dry tablet core.

The aforementioned models, which have been developed so far for the pharmaceutical film-coating process, cannot currently provide insight into coating film formation and absorption, nor into solvent evaporation from within the tablet core. Thus, with these models accurate prediction of the water content inside the tablets is not currently possible.

In this chapter, previous work that describes aspects or phenomena that affect the film-coating process is also discussed:

- Spray impingement on rigid substrates.
- Liquid film/droplet absorption into porous substrates.
- Polymeric film drying.
- Liquid evaporation from within a porous substrate.

The above studies are crucial in understanding the fundamental phenomena that take place at the tablet-coating point of contact and are investigated in this thesis to help develop a novel model that can predict coating film formation and tablet water content.

Table 2.1: Atomization models available in the literature for the prediction of pharmaceutical coating spray droplet Sauter mean diameter.

References	Model type	Type of atomized liquid
Lefebvre et al. (1988)	Empirical (fitting of experimental data)	Newtonian
Varga et al. (2003)	Theoretical (RT-instability model)	Newtonian
Aliseda et al. (2008)	Theoretical (RT-instability model)	non-Newtonian

### 2.1.1 Spray atomization and droplet evaporation during flight models

To create a spray that impinges onto the tablets inside the rotating drum the coating formulation is supplied through a nozzle at a low velocity; at the same time gas is introduced at much higher velocity, thereby atomizing the coating liquid into droplets. The pharmaceutical industry has employed spray atomization models (Table 2.1) to gain insight into the spray characteristics of different coating formulations.

It is apparent that spray atomization models can help to design the coating process since they reduce the need for experiments and trial runs. The currently available atomization models can estimate the mean droplet size at the exit of the spray gun nozzle (Aliseda et al., 2008), which are typically difficult - if not impossible - to measure experimentally (Ketterhagen et al., 2017). The droplet size predictions play an important role in calculating the amount of coating applied on a tablet per unit time. This section of the chapter concerns the main modeling approaches which can be employed to simulate pharmaceutical coating spray atomization.

In the simplest cases, the atomization parameters, such as the spray rate and airflows, can be selected based on experimental trial and error runs (Ketterhagen et al., 2017). However, in cases where process optimization is required, mathematical models allow for a more accurate selection of the coating formulation properties and the coating process parameters. By using models one can estimate a preferable mean droplet size and in turn an optimal amount of applied coating per tablet per unit time in order to enhance the tablet quality.

Three main factors that affect coating spray atomization (Ketterhagen et al., 2017) are:

- the spray nozzle geometry and type
- the rheological properties of the coating formulation
- the coating spray rate and airflows

An appropriate mathematical model for film-coating atomization should take all the above factors into consideration.

Several types of atomizers (nozzle types) have been proposed for film-coating, although air-assist atomizers are mainly used today (Cole et al., 1995). For the different atomizers, there are a few empirical models in the literature which can estimate the droplet Sauter mean diameter (*SMD*). According to Lefebvre et al. (1988), most of the empirical relations are in the form of  $SMD \propto U_g^{-n}$  where  $U_g$  is the atomizing gas velocity and  $0.7 \leq n \leq 0.9$ .

Based on the experimental data, Varga et al. (2003) presented a model that predicts the size of the droplets when exiting a nozzle of specific geometry. They considered a Rayleigh-Taylor (RT) instability model for the liquid atomization and they derived an expression for the estimation of *SMD*:

$$SMD = \frac{0.68 \psi^{1/2} (\rho_l \nu_g)^{1/4}}{\rho_g^{3/4} \left[ U_g \left( 1 + \sqrt{\rho_g / \rho_l} \right) - U_l \right] U_g^{1/4}} \quad (2.1)$$

where  $\psi$  is an atomizer-specific shape proportionality factor,  $\nu_g$  is the gas kinematic viscosity and  $\rho_g$ ,  $\rho_l$ ,  $U_g$ ,  $U_l$  are the densities and velocities of the gas and the coating, respectively.

More recently, Aliseda et al. (2008) also derived an expression for the droplet *SMD* of viscous and non-Newtonian coating liquids:

$$\begin{aligned} \frac{SMD}{D_l} = & \left[ C_1 (1 + m_r) \left( \frac{b_g}{D_l} \right)^2 \frac{(\rho_l / \rho_g)^{1/4}}{\text{Re}_g} \frac{1}{\sqrt{\text{We}}} \right] \\ & \times \left[ 1 + C_2 \left( \frac{D_l}{b_g} \right)^{1/6} \left( \frac{\text{Re}_g}{\rho_l / \rho_g} \right)^{1/12} \text{We}^{1/6} \text{Oh}^{2/3} \right] \end{aligned} \quad (2.2)$$

where  $C_1$  and  $C_2$  are coefficients of proportionality that depend on nozzle design,  $D_l$ ,  $b_g$  are dimensions of the nozzle (diameter of the nozzle orifice and thickness of the atomizing gas jet, respectively),  $m_r$  is the dimensionless liquid/gas mass flux ratio and  $\text{Re}_g$ ,  $\text{We}$  and  $\text{Oh}$  are the Reynolds, Weber and Ohnesorge dimensionless numbers, respectively. These dimensionless numbers are thus defined:

$$\text{Re}_g \equiv \frac{U_g b_g}{\nu_g} ; \quad \text{We} \equiv \frac{\rho_g (U_g - U_c) D_l}{\gamma_s} ; \quad \text{Oh} \equiv \frac{\eta}{\sqrt{\rho \gamma_s D_l}} \quad (2.3)$$

where  $\gamma_s$  and  $\eta$  are the coating surface tension and shear viscosity, respectively, whereas  $U_c$  denotes the velocity of the liquid tongues resulting from a Rayleigh-Taylor instability.

The numerical results of the mathematical models developed by Varga et al. (2003) and Aliseda et al. (2008) are in good agreement with experimental data found in the literature (Muller and Kleinebudde, 2006). As it is shown in Equations (2.1) and (2.2), the coating formulation rheology affects the size of the droplets at the exit of the spray nozzle. Typically, the coating density, viscosity and surface tension are dependent on the coating composition (polymer and solvent type) and are also functions of the solid content.

For most coating formulations (aqueous suspensions), their viscosity increases exponentially with increasing solid content leading to a large difference in droplet sizes. Another factor which affects the viscosity of the coating - and in turn the droplet size - is the coating temperature. High coating temperature leads to lower viscosity and thus influences atomization (Amidon, 1999; Ketterhagen et al., 2017). Under the conditions of interest for pharmaceutical film-coating, the spray/jet flow at the exit of the spray gun nozzle is laminar. The fluid jets under the nozzle might become turbulent if the liquid or gas flow rates are significantly increased. The drying air usually has no effect on droplet break-up but does affect the size of the droplets that finally impinge onto the tablets.

Evaporation while the droplet is travelling from the nozzle to the tablets has been investigated by a few researchers. Wang et al. (2012) modelled dynamically coating droplet evaporation. They calculated single droplet evaporation in a stagnant flow field by solving the heat, mass and momentum transfer equations. In his book, Sirignano (1999) described in detail the dynamics of droplet arrays (spray). He reported issues encountered when modeling the behavior of a whole evaporating spray which include computational expense and numerical stiffness.

Cole et al. (1995) derived a simple semi-empirical expression for the evaporation rate of single droplets that travel from the nozzle to the tablet bed:

$$\frac{dD}{dt} = -\frac{a}{D} \left(1 + b\sqrt{Dv}\right) \quad (2.4)$$

where  $D$  is the droplet diameter,  $v$  is the velocity of the droplet relative to the surrounding air,  $a$  and  $b$  are constant parameters depending only on ambient conditions and liquid properties. Since the model of Cole et al. (1995) is semi-empirical it requires the fitting of parameters by using experimental data.

More recently, Niblett et al. (2017) developed a theoretical mathematical model that predicts the rate of mass loss of a single spherical coating suspension droplet during flight from the spray nozzle to the tablet. They derived the following equation:

$$\frac{dm}{dt} = k_m 4\pi R_d^2 \frac{\mathcal{M}_w p}{\mathfrak{R}T} (y_v - y_\infty) \quad (2.5)$$

where  $R_d$  is the droplet radius,  $\mathfrak{R}$  is the universal gas constant,  $k_m$  is the mass transfer coefficient,  $\mathcal{M}_w$  is the water molar mass,  $p$  is the ambient pressure,  $T$  is the temperature of the drying air and  $y_v$  and  $y_\infty$  are the water mole fraction at the droplet surface and in the air bulk, respectively.

By using the theoretical model of Niblett et al. (2017), one can predict the mean size of the coating droplets before they impinge onto the tablets. The Sauter mean diameter calculated from the models of Varga et al. (for Newtonian liquids) or Aliseda et al. (for non-Newtonian liquids) can be used as an initial condition at the exit of the nozzle gun. Combining models for atomization and droplet evaporation during their flight can help to estimate the amount of coating liquid applied onto the surface of the tablets (Niblett et al., 2017).

### 2.1.2 Coating drum temperature and humidity level prediction models

The temperature and humidity levels inside the rotating drum play an important role in the film-coating process. Drum temperature and relative humidity affect water evaporation rate and thus can influence the coating efficiency (Page et al., 2006; Niblett et al., 2017). To optimize these process parameters one can consider the pharmaceutical film-coating process as an evaporative cooling process where the First Law of Thermodynamics applies (Ketterhagen et al., 2017). Thermodynamic film-coating models have been developed over the past years to enhance our understanding of the coating process (Table 2.2).

Table 2.2: Models available in the literature that can predict the conditions (temperature, humidity, moisture levels) inside a coating drum.

References	Model output	
	Exhaust air stream	Tablet bed
am Ende and Berchielli (2005)	Temperature, humidity	-
Page et al. (2006)	Temperature, humidity	Temperature, moisture
Pandey et al. (2006)	-	Moisture, coating efficiency
García Muñoz et al. (2012)	Temperature, humidity	-

The thermodynamic models use the First Law of Thermodynamics and conservation of mass principles to complete a material-energy balance of the coating unit operation for a closed, non-isolated system (Fig. 2.1). The model can successfully connect the inlet air properties to the coating solution and exhaust air properties (relative humidity, temperature, flow rate). Am Ende and Berchielli (2005) derived the following equation that predicts the exhaust air temperature ( $T_{out}$ ) which serves as an indication of the temperature inside the coating drum:

$$T_{out} = \frac{m_{ai}c_{pa}T_{ai} + x_w m_c c_{pw} T_c - x_w m_c \Delta H_e + T_b HLF}{m_{ai}c_{pa} + x_w m_c c_{pw} + HLF} \quad (2.6)$$

where  $\Delta H_e$  is the water latent heat of vaporisation,  $x_w$  is the water mass fraction in the coating,  $HLF$  is the heat transfer coefficient multiplied by the coating drum surface area and is estimated empirically,  $c_{pa}$  and  $c_{pw}$  denote the specific heat capacities of air and water, respectively,  $m_a$  and  $m_c$  are the mass flow rates of the inlet gas and coating formulation, respectively, and  $T_{ai}$  and  $T_c$  are the temperatures of the inlet air and coating liquid, respectively. Equation (2.6) is applicable for aqueous pharmaceutical coatings and was validated against experimental data by am Ende and Berchielli (2005).

The model developed by am Ende and Berchielli (2005) provides information on the temperature of the outlet stream (exhaust stream) which can be assumed to be close to the temperature of the air above the tablets. Once the  $HLF$  is determined empirically for a specific coating pan, this model can be used to predict the effect of changing spray rate or other inlet conditions on the temperature inside the coating drum.

Additionally the model by am Ende and Berchielli (2005) can also predict the percent relative humidity ( $RH$ ) of the exhaust air stream from a ratio of the partial pressure of water vapor in the outlet ( $p_{vp}$ ) to the vapor pressure of water at the outlet temperature ( $p_{vb}$ ):

$$\% RH = \frac{p_{vp}}{p_{vb}} \cdot 100\%$$

Recent advances in thermodynamic modeling of the film-coating process include predicting the moisture inside the tablet bed (Page et al., 2006) and adding parameter estimation (e.g. for  $HLF$ ) and process dynamic modeling (García-Muñoz et al., 2012). Pandey et al. (2006), who studied coating process scale-up methods, reported that changes in thermodynamic factors influence the quality of the coating film. Thus, it is important to first understand and then control the thermodynamic behavior of the coating process.

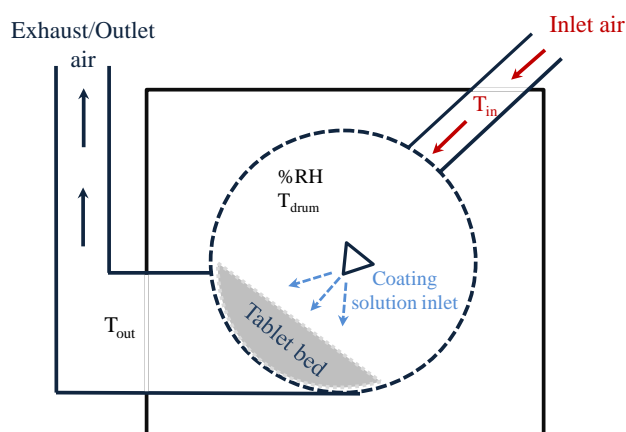


Figure 2.1: Pharmaceutical coating rotating drum.

### 2.1.3 Tablet motion and coating uniformity prediction models

During the film-coating process the coating liquid may be deposited preferentially on some tablet cores (Ketterhagen et al., 2017). This might lead to lack of sufficient coating uniformity and poor final product quality. Tablet cores that have passed under the spray more times will have thicker coatings. Additionally, tablets that have stayed under the spray for longer duration will receive more coating liquid. Thus, modeling pharmaceutical tablet motion inside the coating drum can provide insight into the final coating uniformity and in turn the overall product quality. Table 2.3 shows the most important numerical models that can be found in the literature for simulating tablet movement during the film-coating process.

Several researchers have attempted to perform Discrete Element Method (DEM) simulations to obtain tablet cycle and spray-zone residence times in a rotating drum (Table 2.3). Yamane et al. (1995) were the first who attempted to use DEM to compute the trajectories of pharmaceutical tablets in a rotating drum and to calculate if a particle is inside the spray-zone (area directly under the spray). Kalbag and Wassgren (2008) also used DEM to predict the spray-zone residence time of tablets. They were able to predict accurately the time a tablet spends under the coating spray by partitioning the drum into three-dimensional grids (voxels) and identifying the particles that pass through the voxels that form the computational spray-zone.

Table 2.3: Models available in the literature that can simulate tablet movement.

References	DEM	PBM	Coating uniformity prediction	
			Inter-tablet	Intra-tablet
Yamane et al. (1995)	✓	-	-	-
Kalbag and Wassgren (2008)	✓	-	✓	-
Freireich et al. (2011)	✓	✓	✓	-
Ketterhagen (2011)	✓	-	✓	✓
Kumar et al. (2015)	✓	✓	✓	-
Freireich et al. (2015)	✓	-	✓	✓

Freireich et al. (2011) investigated an approach in which a population balance model (PBM) is used together with a DEM simulation. To couple the two models, they developed a compartment model (which includes a spray, passive and active bed zones). The spray-zone residence time and cycle time were estimated by post-processing the data taken from the DEM simulations with a tablet movement-tracing algorithm.

The quality of the coating can be described by the inter-particle coating variability (Kumar et al., 2015). This variability refers to the variation in solid coating mass that pharmaceutical tablets receive during the process. During film coating, the coating deposited on the tablets has a statistical distribution. One can define the inter-particle coating variability ( $CoV_{inter}$ ) as the coefficient of variation of this coating mass distribution which is equal to the ratio of the standard deviation ( $\sigma_{coat}$ ) and the mean ( $\mu_{coat}$ ) of the total polymer mass distribution:

$$CoV_{inter} = \sigma_{coat} / \mu_{coat} \quad (2.7)$$

It is obvious that the smaller the  $CoV_{inter}$ , the better the coating uniformity.

Kumar et al. (2015) extended the approach of Freireich et al. (2011) and predicted the tablet residence time under the spray more accurately by eliminating the time thresholds applied in previous works to avoid short duration residence time correlations. According to Kumar et al. (2015), these thresholds result in significant differences in time distributions (lower predictions of residence time under spray) and affect the final uniformity results.

Ketterhagen (2011) investigated the effect of tablet shape in the movement of particles inside the coating drum and managed to calculate not only the spray-zone residence time of the tablets but also the orientation of the tablets in the spray zone. The model predictions for the intra-tablet coating uniformity were validated by experimental data obtained using a machine vision system. Freireich et al. (2015) expanded the work of Ketterhagen (2011) to predict coating thickness distributions. They concluded that with increasing tablet sphericity, the intra-tablet coating uniformity improves.

Freireich et al. (2015) used DEM together with an image-based method to track the tablet exposure to a simulated spray of small area panels and to calculate the variation in coating mass over a single tablet surface (intra-tablet uniformity). They considered tablet orientation and shadowing effects to get more precise results. They attempted to validate their numerical results but unfortunately only qualitative comparisons could be made due to the limited number of tablets sampled experimentally and differences in spray zone areas and coating liquid flux distributions.

Using models (Table 2.3) that predict the motion of tablets in the rotating drum and the time they spend under the spray allows the estimation of the coating variability. The insight can be used to optimize coating uniformity and thus enhance tablet appearance. In this thesis, information from tablet motion models is used to estimate the time tablets spend under spray and the amount of coating applied per unit time. The spray-zone residence time and amount of applied coating are inputs in the model developed in this work.

Table 2.4: Overview of models that predict droplet behavior on pharmaceutical tablets.

References	Model output		
	Wetting rate	Absorption rate	Evaporation rate
Aulton and Twitchell (1995)	✓	✓	-
Shaari (2007)	✓	-	-
Bolleddula et al. (2010)	✓	-	-
Niblett et al. (2017)	✓	-	✓
Current work	✓	✓	✓

#### 2.1.4 Single droplet behavior on solid substrates

During pharmaceutical film-coating, wetting takes place when spray droplets impinge on the surface of a tablet core. After impingement, the coating spread over the surface and penetrate into the tablet core (Twitchell et al., 1995). Coating spreading and absorption into tablets can affect film surface roughness and adhesion (Aulton and Twitchell, 1995). Table 2.4 highlights the most important available models in the literature that concern droplet behavior on pharmaceutical tablet cores.

In the literature, one can find a few predictive theoretical models that simulate pure liquid spreading, receding, splashing and rebounding after droplet impingement on a dry wall. These models, even if they are not specific to pharmaceutical coating liquids, can provide useful insight into the droplet impact behavior after impingement on a rigid substrate - such as a pharmaceutical tablet.

Shaari (2007) investigated both experimentally and numerically the impact and spreading of a pure liquid water droplet on pharmaceutical tablets. He divided the process into two sub-processes: short-term and long-term. The former involved the first milliseconds after impact when spreading, splashing and rebounding occur, whereas the latter included penetration and/or wetting. He conducted a series of experiments to investigate the impact behaviour of a droplet on tablet surfaces with different roughness. Using a Volume-Of-Fluid (VOF) CFD model, he described quantitatively the short-term phenomena, but he did not develop any numerical model to describe the long-term phenomena, in particular coating absorption.

Pasandideh et al. (1995) developed a model that estimates the maximum spreading diameter of a pure liquid droplet after impact on a solid substrate. They managed to determine the condition at which capillary effects are negligible and inertia governs the spreading. Moreover, Roisman et al. (2002) mathematically described the spreading and receding behaviour of a lamella (liquid film that forms after high velocity impingement). More recently, Park et al. (2003) developed a mathematical model to estimate the maximum spreading factor at low impact velocity. They defined the spreading factor ( $\beta$ ) as the ratio of the cyclical wetted area diameter at time  $t$  to the initial droplet diameter of the spherical droplet just before impingement.

Attane et al. (2007) developed an analytical 1-D spreading model for pure liquid droplets based upon the energy equation. By assuming the shape of a droplet (either spherical cap or cylindrical), Attane et al. (2007) reduced the unknown variables in the energy balance equation. They compared their model with others from the literature (Kim and Chun, 2001; Bechtel et al, 1981), getting better predictions of the maximum spreading factor.

The extent of the wetting of a pharmaceutical tablet can be most generally assessed with the equation for the wetting contact angle  $\vartheta$  (Muliadi and Sojka, 2010; Aulton and Twitchell, 1995; Twitchell et al., 1995):

$$\cos \vartheta = \frac{\gamma_{sv} - \gamma_{sl}}{\gamma_{lv}} \quad (2.8)$$

where  $\gamma_{sv}$ ,  $\gamma_{sl}$ ,  $\gamma_{lv}$  are the solid-vapor, solid-liquid and liquid-vapor interfacial free energies, respectively. The angle  $\vartheta$  ranges from 0 to 180°: when  $\vartheta = 0^\circ$  the solid substrate is “fully wetted” and when  $\vartheta = 180^\circ$  the solid is “not wetted”. In-between values indicate “partial wetting”.

Three types of wetting (Fig. 2.2) take place during film-coating (Muliadi, 2010):

- adhesional
- immersional
- spreading

The rate of pharmaceutical tablet wetting (spreading wetting) has been found to follow Tanner’s law (Rafai and Bonn, 2005):

$$R(t) \propto t^{1/10} \quad (2.9)$$

where  $R$  is the wetted area radius and  $t$  is time. Rafai and Bonn (2005) proved that Tanner’s law holds for Newtonian and non-Newtonian coating liquids.

Adhesional wetting provides the bond (adhesion) between the polymer film and the tablet core (Aulton and Twitchell, 1995; Muliadi, 2010). During adhesional wetting, the liquid spreads on the surface and the wetting front moves inside the porous substrate as well (Aulton and Twitchell, 1995). Adhesional wetting occurs immediately after droplet impact and spreading.

Immersional wetting is different from adhesional wetting because there is no spreading on the surface of the tablet i.e. the liquid-vapor interface remains the same (Aulton and Twitchell 1995). Aulton and Twitchell suggested that immersional wetting takes place after adhesional wetting and that immersional wetting is directly related to film adhesion.

Recently, Niblett et al. (2017) developed a detailed mathematical model that predicts pure droplet spreading (spreading wetting) on pharmaceutical tablets. They assumed that the droplets have a cylindrical shape as they spread on the tablet surface and that complete drying occurs when all the solvent evaporates. They did not account for droplet absorption into the tablet core (neglected immersional and adhesional wetting).

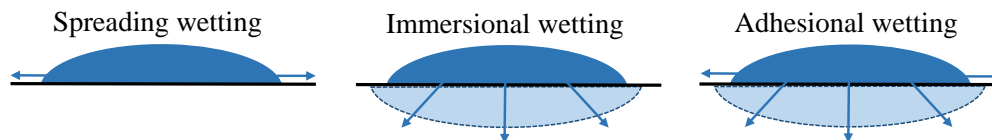


Figure 2.2: Types of wetting on pharmaceutical tablets.

Several researchers have developed models which estimate the absorption rate of pure liquid droplets (Reis et al., 2003; Alleborn and Raszillier, 2004) into porous substrates (immersional and adhesional wetting). Most of the previous work on liquid absorption by substrates is based on the Lucas-Washburn or Darcy's equations to predict liquid penetration depth in porous media (Siregar, 2012). To the best of our knowledge, these models have never been used for the pharmaceutical film-tablet system so far.

Denesuk et al. (1994) investigated capillary penetration of droplets into porous substrates, assuming essentially two dewetting scenarios during droplet absorption: the "constant drawing area", which assumes a fixed contact line during absorption and the "decreasing drawing area", which assumes a moving contact line with constant contact angle. The porous medium was modelled as a solid with an array of parallel cylindrical pores with constant radius. They assumed that absorption is driven by capillarity. Additionally, Davis and Hocking (2000) investigated the spreading and absorption of two-dimensional pure liquid droplets on permeable substrates. They also modelled the substrate as an array of vertical pores of constant width.

All of the above work neglected the presence of particles inside the coating suspension droplet. Bolleddula et al. (2010) studied the impact and spreading behavior of viscous suspensions on the surface of pharmaceutical tablets. They concluded that coating suspension spreading wetting after impact can be divided into two distinct regimes: the inertia and capillarity driven regimes. During the inertia driven regime, the diameter reaches an asymptotic value referred to as the maximum spreading factor. Following the inertia driven regime the droplet continues to spread by capillarity.

In this work (Chapter 3), a mathematical model that describes the spreading, absorption and evaporation of water-based pharmaceutical coating suspensions after impingement on porous substrates, e.g. pharmaceutical tablets, is developed. The approach followed for the initial droplet impact spreading period takes into consideration the high shear viscosities of pharmaceutical coating suspensions, enhancing models found in the literature (Attane et al., 2007) that only predict the behavior of low viscosity liquids (water, ethanol). The current model can account for the specific operating conditions inside a pharmaceutical pan-coater (high temperature, high air flow, high relative humidity).

Even if the single droplet models are simplistic and do not account for the entire film which covers the tablet surface they can provide useful insight regarding the behavior of coating formulations on permeable substrates such as solid dosage forms. In this thesis (Chapter 3), a novel model that predicts droplet spreading, absorption and evaporation is presented.

Table 2.5: Overview of models that predict spray impact on rigid substrates.

References	Model	Model output		
		Film spreading	Film thickness	Splashing
Yarin and Weis (1995)	Theoretical	-	-	✓
Tropea and Marengo (1998)	Empirical	-	✓	-
Lee and Ryou (2001)	Empirical	✓	✓	-
Cossali et al. (2005)	Empirical	-	✓	✓
Roisman et al. (2006)	Theoretical	-	-	✓
Kalantari and Tropea (2007)	Empirical	-	✓	-
Current work	Theoretical	✓	✓	-

### 2.1.5 Spray impingement on solid substrates

The application of coating films is an important step in the manufacture of pharmaceutical tablets. Understanding the phenomena taking place during coating spray application provides important information that can be used to reduce the number of defective tablets and select the optimal conditions for the coating process. This section deals with models available in the open literature that predict spray (arrays of droplets) impingement on rigid surfaces (Table 2.5). To the best of the author's knowledge there are currently no spray impingement models specific to the film-coating process reported in the literature.

Previous work aiming to numerically simulate pure liquid spray impingement on impermeable solid substrates mainly relied on models that were derived from single droplet impact studies (Tropea and Marengo, 1998; Cossali et al., 2005). Models following this approach described the spray impingement as a superposition of single droplet impacts. According to Roisman et al. (2006), these models have shortcomings, because they cannot consider interactions between neighbouring spreading droplets, and so they are insensitive to spray density. Nevertheless, information about the single droplet impact (Section 2.1.4) can provide useful insight into the complex spray impingement process (Moreira et al., 2010).

The models concerning spray impingement can be divided into two categories: models simulating impact on a dry substrate and models describing spray impact on a wetted surface or liquid film. There are several outcomes following the spray impingement on a dry solid substrate. A droplet of the spray may deposit onto a cylindrical or spherical-cap film, disintegrate (splash) into secondary droplets, or recede and potentially rebound (Roisman et al., 2006; Moreira et al., 2010).

Roisman et al. (2006) and Yarin and Weis (1995) experimentally and theoretically investigated the impingement of spray droplets on liquid films that already cover rigid substrates. They found that droplets with low impact velocity and small size can deposit on the film surface or coalesce, whereas droplets with moderate and high impact velocities tend to form a crater at the impingement region that leads to splashing and even to film disintegration. Only few researchers have proposed empirical splashing and disintegration criteria or developed models for predicting the outcome of droplet impact on liquid films of different thickness (Kalantari and Tropea, 2007; Roisman et al., 2006).

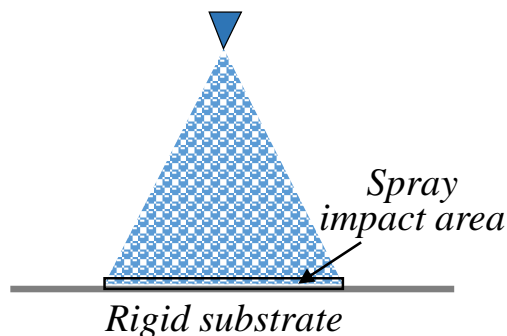


Figure 2.3: Spray impingement on a rigid substrate.

Obtaining accurate and detailed information about spray impingement through experiments is challenging (Cossali et al., 2005). In the literature, one can find experimental work concerning the interaction of spray droplets on a wall, as well as splashing and breakup (Yarin and Weiss, 1995; Barnes et al., 1999; Kalb et al., 2000; Cossali et al., 2005). Moreira et al. (2010) reviewed the aforementioned studies that were mainly focused on simultaneous and subsequent impacts of two droplets of similar sizes and initial velocities. Moreover, Roisman et al. (2002) developed a detailed model to estimate the velocity and shape of the uprising liquid film, accounting for droplet collisions on the substrate and the influence of droplet spacing, but not including predictions for possible break-up of the uprising film.

Concerning the prediction of film thickness after spray impact, Lee and Ryou (2001) developed an empirical model that aims to predict the outcome of diesel spray impingement on a rigid wall. Recently, Kalantari and Tropea (2007) conducted experiments and derived a semi-empirical relation for the film thickness. Their experimental data were used for validation of the model developed in this work.

Generally, research for pharmaceutical sprays is focused on droplet atomization and evaporation (Muliadi and Sojka, 2010), and therefore no previous work that deals in detail with coating spray impact on tablets was found. To conclude, most spray impact models available in the literature are either based on empirical equations or on CFD computationally expensive simulations (Moreira et al., 2010) and are not directly applicable to the pharmaceutical film-coating process. In this thesis (Chapter 4), spray impact and film spreading on a pharmaceutical tablet while this passes through the spray-zone in a rotating coating drum is investigated and a novel model is developed.

Table 2.6: Overview of models that predict film behavior on porous substrates.

References	Liquid type	Model simulates		
		Film flow	Absorption	Evaporation
Schwartz (1999)	Pure liquid	✓	-	-
O'brien & Schwartz (2001)	(non-)Newtonian suspension	✓	-	-
Alleborn & Razhilier (2004)	Pure liquid	-	✓	-
Siregar (2012)	Newtonian solution	-	✓	✓
Pham and Kumar (2019)	Newtonian suspension	-	✓	✓
Current work	(non-)Newtonian suspension	✓	✓	✓

### 2.1.6 Thin film flow and absorption onto and into porous substrates

As mentioned earlier in this chapter, investigating only the behavior of a single droplet on a tablet surface cannot provide all the necessary information required to describe in detail the phenomena taking place at the point of contact between the coating liquid and a tablet during the film-coating process. This is because after spray impingement (Section 2.1.5) a thin film is formed. In this section, models from the literature which describe film behavior on a solid substrate are presented (Table 2.6).

The wetting and spreading phenomena of pure liquid thin films on impermeable, non-porous substrates have been investigated employing the “lubrication approximation” theory (Schwartz, 1999). By exploiting the negligible vertical film dimensions compared to the in-plane extension of the coating, one can derive a set of simplified continuity and Navier-Stokes equations which describe the flow of a film over a substrate when inertia is negligible.

This idea has been expanded by Alleborn and Razhillier (2004) who also investigated spreading and absorption of pure liquid thin films in the framework of lubrication approximation theory. Siregar et al. (2010) developed a similar model for ink-jet printing process. They assumed that pure liquid absorption takes place after the droplet impinges and spreads on the substrate and modeled spray impact and absorption independently. In this thesis (Chapter 5), a model which builds on the previous work of Alleborn and Razhillier (2004) and Siregar (2012) is developed. The current model is based on the lubrication approximation theory approach and predicts coating film absorption into a porous tablet while it accounts for film drying.

Most pharmaceutical coating formulations utilized by the pharmaceutical industry are aqueous polymer suspensions and not pure liquids. To model their flow on the surface of a pharmaceutical tablet, one can adopt the “mixture modeling” approach. This is valid for fluid-particle systems in which the mean velocity fields of the continuous and disperse phases rapidly relax to local dynamical equilibrium, a condition that is often met in liquid-particle suspensions (Jackson, 2000; Jamshidi et al., 2019). Weidner et al. (1996) and O’Brien and Schwartz (2002) combined the mixture modeling approach and lubrication approximation method to simulate the drying of suspension films and their flow over impermeable substrates.

Pham and Kumar (2019) studied the appearance of the coffee-ring pattern when a very thin droplet (which can be regarded a cylindrical film) containing particles is deposited on a porous substrate. They developed a lubrication theory approach model to predict the behavior of colloidal suspensions on porous media. They accounted for carrier fluid evaporation and assumed that the droplet solidifies when the solid concentration in the droplet reaches the random-packing limit. Their detailed model predicted that substrate permeability can suppress the appearance of coffee-rings and enhance solid particle deposition uniformity.

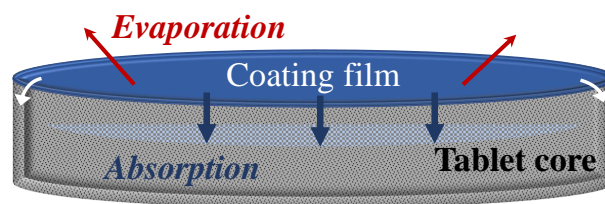


Figure 2.4: Coating film behavior on porous tablets.

Models for suspension flow in porous media should take into account particle retention (attachment) in the pores (Bradford et al., 2002). Yoon et al. (2004), Civan (2011) and Holloway et al. (2011) investigated theoretically and experimentally particle retention during absorption of suspensions into porous media and capillary tubes. Even though the above contributions are not specific to pharmaceutical coating suspensions they provide a background that can be used to develop models which predict polymer retention inside tablets. According to Holloway et al. (2011), the critical particle diameter/pore diameter ratio at which a concentrated suspension clogs a capillary tube is 0.06. During the film-coating process, clogging of the tablet pores with polymer particles can hinder coating suspension absorption into the tablets thus influencing their final water content.

Modeling the suspension thin film behavior onto and into tablets (Fig. 2.4) can be useful to the pharmaceutical industry. The relevant mathematical models found in the literature do not consider at the same time film spreading, absorption and drying and thus are not appropriate to be used for the pharmaceutical film-coating process. In this thesis, the above issues are addressed and a novel model that can estimate the behavior of a pharmaceutical thin film on a tablet, as well as the water and solid content inside the tablet during film-coating, is developed (Chapter 5).

### 2.1.7 Tablet drying and film adhesion

As the coating (suspension) film flows and absorbs into the porous tablet (Section 2.1.6) the carrier fluid evaporates during film coating. In Chapter 1, it is mentioned that it is desirable that some of the coating liquid does dry inside the tablet core in order to enhance film adhesion. In this section, tablet and film drying (Fig. 2.5) and adhesion studies found in the literature are presented (Table 2.7).

The drying of aqueous suspensions and the formation of solid films is of great importance to the investigation of the film-coating process (Felton, 2013). Dry film formation is commonly divided into three stages, which are (Kiil, 2006):

- the unhindered evaporation of the solvent (water) from the film surface
- the diffusion of the solvent through a dry layer (crust) at the film surface
- the particle-particle coalescence

Table 2.7: Overview of the main studies regarding film and tablet drying and film adhesion.

References	Investigation of		
	Film drying	Porous medium (tablet) drying	Film adhesion
Roberts and Griffiths (1999)	-	✓	-
Kiil (2006)	✓	-	-
Muliadi and Sojka (2010)	-	-	✓
Siregar et al. (2013)	✓	-	-
Niblett et al. (2017)	✓	-	-
Current work	✓	✓	-

Vanderehoff et al. (1973), Croll (1987) and Kiil (2006) have developed mechanistic models which describe the first two stages and take into account heat and mass transfer in films during drying. These models consider that as the coating dries (water evaporates unhindered from the film surface) the volume fraction of the solids approaches a critical value. When this value is reached, a solid layer (crust) develops at the film surface. At this stage the solvent diffuses through the solid crust.

More recently, Niblett et al. (2017) studied the application and complete drying of coating liquids on pharmaceutical tablets. The mathematical model presented in their work predicts the drying of a single coating droplet - not of a film - which is deposited on the surface of a tablet. They performed experiments that validated their mathematical model.

Even though several researchers attempted to investigate coating film coalescence, there is no clear convergence with respect to the underlying mechanisms (Kiil, 2006; Felton, 2013). Thus, the term “coalescence” in most theoretical studies refers to the entire process of compaction, deformation, cohesion, and polymer chain inter-diffusion of the individual solid (coating polymer) particles (Kiil, 2006).

If water penetrates into the tablet during coating application, then tablet drying is only complete when all the water evaporates from within the tablet core (Fig. 2.5). Therefore, evaporation from within a porous medium is of interest in pharmaceutical coating processes. Understanding the dynamics of evaporation from within the tablet cores during the coating process can help reduce the water content of the final product. Excess water in the core may lead to reduction of the shelf-life of the coated tablet.

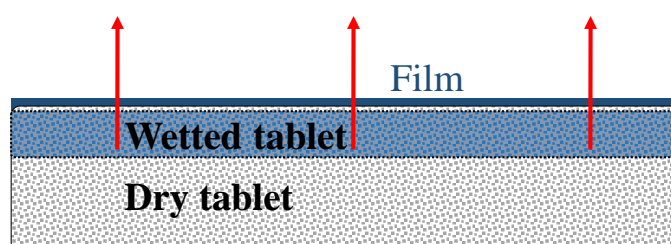


Figure 2.5: Tablet drying during film-coating.

Earlier work reviewed (Roberts and Griffiths, 1995; Hu and Larson, 2004; Siregar et al., 2013) was mostly concerned with evaporation of droplets on non-porous surfaces. Roberts and Griffiths (1999) first developed a mathematical model for droplet evaporation from building materials. They validated their numerical results with field and wind tunnel experiments.

Sahota and Pagni (1979) have studied the heat and mass transfer in porous media with an emphasis on fire safety. They developed an implicit numerical scheme to study the time dependent solution of two-phase, two-component flow in porous concrete structures. They also considered the pressure build up inside the porous medium (concrete) due to the presence of water. Their experimental and theoretical results agreed quite well. Yortsos and Stubos (2001) presented a detailed review of multiple phase change processes including drying in porous media.

Experimental studies that investigate the rate of liquid depletion from within the porous matrix are available in the literature (Reis et al., 2003; Tag et al., 2010). Reis et al. performed their experiments with glass beads, while Tag et al. worked with pharmaceutical tablets. For both studies, all their experimental data were derived from experiments conducted at room ambient temperature. In this thesis, the experimental data of Reis et al. and Tag et al. are used for the validation of the developed novel evaporation model (Chapter 6).

To enhance film adhesion onto the tablet core, part of the coating liquid needs to dry inside the tablet (wetted region, Fig. 2.5). According to Cole et al. (1995), it is challenging for experimental work to provide a quantitative relationship between the coating-tablet surface energetics and the resulting adhesive strength. Coating-tablet contact angle measurements can also provide an indication of film adhesion (Felton, 2013). Muliadi and Sojka (2010) reported that the amount of coating that dries into the core affects adhesion. Therefore, tablet permeability can influence the quality of the coating.

Adhesion between a drying coating film and a solid surface is essential to avoid tablet defects (Muliadi and Sojka, 2010) such as peeling and flaking. Loss of adhesion may cause an accumulation of moisture at the film-tablet interface, potentially affecting the stability of drugs susceptible to hydrolytic degradation (Amidon, 1999). Moreover, inadequate adhesion can compromise the enhanced mechanical properties that the coating provides to the substrate (Aulton and Twitchell, 1995).

The binding of a polymer with a porous tablet can be estimated using an adsorption model. Adsorption of the coating polymer molecules leads to the immobilization of some of the spreading or diffusing solute, which reduces the driving forces and diffusion rate, until adsorption reaches equilibrium with the free solute concentration at each position of the porous medium. Siregar et al. (2013) developed an adsorption model to account for the binding of the solute with the impermeable surface during evaporation.

Models in the literature that describe film drying and adhesion are not specific to the pharmaceutical industry and the conditions of the film-coating process. This thesis aims to provide an understanding of the drying dynamics of coating films in order to avoid over-wetting, which lead to pharmaceutical tablet defects.

## 2.2 Concluding remarks

In this chapter, mathematical models presented in the open literature to date considering the overall pharmaceutical film-coating process were reviewed. The reviewed models are useful to the pharmaceutical industry but cannot provide information regarding coating film flow and absorption onto and into a tablet nor solvent evaporation from within a tablet core. Thus, it is now apparent that accurate prediction of the water or solid coating content inside a tablet with the aforementioned models is not possible. One of the main thesis objectives is therefore to provide this missing insight into the process and to assist the pharmaceutical industry in optimizing the performance of the tablet coating process.

Moreover, previous work that is not specific to film-coating but concerns physical phenomena that take place during coating (spray impingement, film spreading, absorption and drying) was also analyzed in this chapter. These previous studies serve as a background for the novel mathematical models developed in the current thesis. Additionally, some experimental results of the above work were used to validate models developed in the framework of this project.

The literature review in this chapter aims to give an idea of the level of understanding of the film-coating process up to this day. The studies reviewed in this chapter concerning droplet behavior on porous media are used in Chapter 3 to develop a model that predicts coating droplet impact, spreading and absorption into pharmaceutical tablets. Furthermore, the models developed in Chapters 4 and 5 build on the studies reviewed in this chapter regarding spray impingement on rigid substrates and thin film flow, respectively. Finally, the novel model described in Chapter 6 uses as a starting point the work presented in this review-chapter that concerns liquid evaporation from within a porous medium.

# CHAPTER 3

## Single droplet behavior on a tablet

---

This chapter deals with single droplet impact, spreading, evaporation and absorption onto and into tablets. A mathematical model that predicts the behavior of single droplets after impact on tablets is developed and validated with experimental results from the literature. The model output can provide insight into the phenomena at the point of contact between the tablet and the coating droplet.

---

Publication which has arisen from this work: Christodoulou, C., Sorensen, E., García-Muñoz, S. and Mazzei, L., 2018. Mathematical modelling of water absorption and evaporation in a pharmaceutical tablet during film coating. *Chemical Engineering Science*, 175, pp.40-55.

### 3.1 Introduction

It is well understood that during the pharmaceutical aqueous film-coating process the amount of liquid water that interacts with the porous tablet core can affect the quality of the final product (Muliadi and Sojka, 2010; Chapter 2). Therefore, understanding and simulating the mechanisms of water droplet spreading, absorption and evaporation is crucial in order to control the process and optimize the shelf-life of the tablets.

The purpose of the work presented in this chapter is to describe the spreading, absorption and evaporation phenomena after a single droplet impacts onto a porous tablet. In the next chapters, this work is broadened to study the behavior of a thin coating film on a tablet after spray impingement. Note that in this chapter, the coating formulation is regarded as Newtonian. Non-Newtonian behavior is studied in Chapter 5.

The droplet behavior was divided into two phases of different dynamics and duration: the kinematic phase and the capillary phase. The kinematic phase describes the first milliseconds after impact during which inertial forces are significant and govern droplet spreading. Shaari (2007) showed experimentally that droplet absorption into the tablet is negligible during the first milliseconds of spreading. The subsequent capillary phase concerns the droplet flow, evaporation and absorption into the tablet when the inertial forces become negligible. Figure 3.1 summarizes the approach followed in order to simulate the droplet behavior.

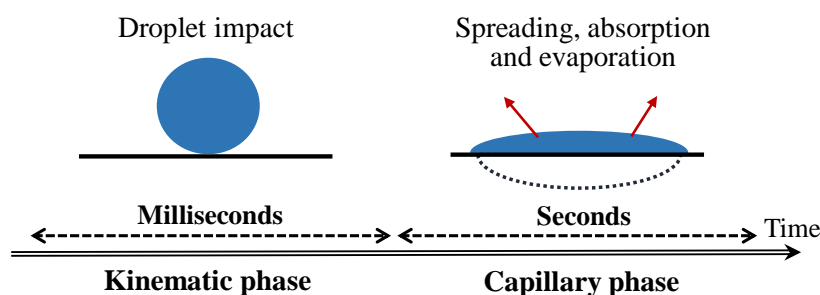


Figure 3.1: Mathematical modelling approach.

### 3.2 Mathematical model

The kinematic phase model describes the first milliseconds after impact during which inertial forces are significant and should not be neglected. Roisman et al. (2002) showed experimentally that the characteristic time of the kinematic phase is of order  $t_i \equiv D_0/U_0$ , with  $D_0$  and  $U_0$  being the initial diameter of the droplet and the droplet vertical velocity before impact, respectively. In this work, it was assumed that during the kinematic phase the absorption phenomena are negligible. Indeed, in experiments conducted by Shaari (2007), the spreading behavior of a droplet on a metal surface was identical to the one on porous substrates for the first milliseconds after impact thus indicating that absorption phenomena can be neglected during this phase.

The capillary phase concerns the droplet behavior when the inertial forces become negligible ( $t > t_i$ ). A model based on the lubrication approximation method was developed to simulate droplet motion during the capillary phase (Section 3.2.2). The model additionally accounts for evaporation during absorption. Previous work (Alleborn and Razhiller, 2004) neglected droplet evaporation because the evaporation dynamics are significantly slower at the conditions which they studied. However, the temperature, humidity and air flow conditions inside a coating drum accelerate evaporation and make its effect not negligible.

#### 3.2.1 Kinematic phase

To rigorously determine the motion of a droplet during the kinematic phase ( $t \leq t_i$ ), one would have to solve the mass and linear momentum balance equations, which is mathematically complex and can be computationally demanding. In this work, an approach based on the mechanical energy balance equation was adopted to develop a model that can quickly and accurately estimate droplet spreading during the kinematic phase. The integral mechanical energy balance equation, which was derived (see Appendix) from the generalized transport theorem (Slattery et al., 2007), reads:

$$\begin{aligned} & \frac{d}{dt} \left[ \int_{\mathcal{R}_1} \left( \frac{1}{2} \rho_1 \mathbf{u}_1 \cdot \mathbf{u}_1 + f_1 \right) d\mathbf{x} + \int_{\mathcal{S}_{12}} \left( \frac{1}{2} \rho_{12} \mathbf{u}_{12} \cdot \mathbf{u}_{12} + f_{12} \right) d\mathbf{s} \right. \\ & \quad \left. + \int_{\mathcal{S}_{13}} \left( \frac{1}{2} \rho_{13} \mathbf{u}_{13} \cdot \mathbf{u}_{13} + f_{13} \right) d\mathbf{s} + \gamma_{12} (A_{12} - A_{13} \cos \vartheta) \right] \\ & = \int_{\mathcal{S}_{12}} \mathbf{n}_{21} \cdot \boldsymbol{\sigma}_2 \cdot \mathbf{u}_{12} d\mathbf{s} + \int_{\mathcal{S}_{13}} \mathbf{n}_{31} \cdot \boldsymbol{\sigma}_3 \cdot \mathbf{u}_{13} d\mathbf{s} + \int_{\mathcal{R}_1} \boldsymbol{\tau}_1 : \partial_{\mathbf{x}} \mathbf{u}_1 d\mathbf{x} \end{aligned} \quad (3.1)$$

where  $\mathcal{S}_{12}$  is the interface between the liquid coating (phase 1) and the gas (phase 2) and  $\mathcal{S}_{13}$  is the interface between the liquid and the solid (phase 3) as seen in Figure 3.2. The spatial region bounded by the dividing surfaces  $\mathcal{S}_{12}$  and  $\mathcal{S}_{13}$  is denoted by  $\mathcal{R}_1$ . Moreover,  $\mathbf{n}_{rs}$  denotes the unit vector normal to  $\mathcal{S}_{rs}$  pointing from phase  $r$  into phase  $s$ , and  $A_{rs}$  denotes the area of  $\mathcal{S}_{rs}$ . In Equation (3.1),  $\rho_1$ ,  $f_1$  and  $\mathbf{u}_1$  are the fluid density, the gravitational potential energy (per unit volume) and the fluid velocity for phase 1, respectively, whereas  $\rho_{rs}$ ,  $f_{rs}$  and  $\mathbf{u}_{rs}$  are the fluid density, the gravitational potential energy (per unit surface) and the fluid velocity over the dividing surface  $\mathcal{S}_{rs}$ , respectively. The stress tensor of phase  $r$  is denoted by  $\boldsymbol{\sigma}_r$  and its deviatoric part by  $\boldsymbol{\tau}_r$ , whereas  $\gamma_{12}$  is the surface tension on the surface  $\mathcal{S}_{12}$  and  $\vartheta$  is the dynamic contact angle of the three phases.

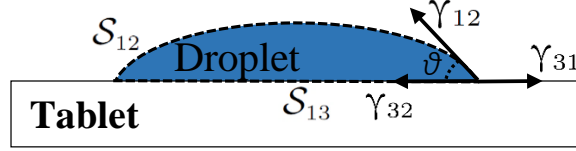


Figure 3.2: Spherical cap droplet on a tablet.  $\vartheta$  is the dynamic contact angle and  $\mathcal{S}_{rs}$  and  $\gamma_{rs}$  are the interface and the interfacial tension between phases  $r$  and  $s$ , respectively.

The left-hand side of Equation (3.1) features the rate of change of the total energy of the droplet, which comprises kinetic energy, potential energy of the gravitational field and surface energy, while the right-hand side features the rate of work performed by phases 2 and 3 (surrounding gas and solid tablet) on the coating and the rate of conversion of mechanical energy into internal energy due to viscous dissipation within the liquid. Equation (3.1) can be written more concisely as:

$$\frac{dE_K}{dt} + \frac{dE_G}{dt} + \frac{dE_S}{dt} = W_S - \Phi \quad (3.2)$$

where  $E_K$ ,  $E_G$  and  $E_S$  are the kinetic, gravitational and surface energies of the droplet, respectively;  $\Phi$  (which is positive) is the rate of viscous dissipation of the droplet kinetic energy and  $W_S$  denotes the rate of work done on the droplet by the droplet surroundings.

In the case of a single droplet impingement on a rigid substrate, the rate of work done by the surroundings can be neglected. Indeed, Equation (3.2), without the term  $W_S$ , has been repeatedly reported in the literature (Attane et al. 2007; Bolleddula et al., 2010). However, to the best of the author's knowledge, no rigorous derivation has been offered. The derivation of the mechanical energy balance equation for a droplet impinging on a solid substrate is therefore presented in the Appendix of this chapter.

To estimate the rate of change of the droplet gravitational potential energy ( $dE_G/dt$ ), one can neglect the gravitational potential energy per unit surface ( $f_{rs}$ ) over the liquid-air ( $\mathcal{S}_{12}$ ) and liquid-tablet ( $\mathcal{S}_{13}$ ) dividing surfaces. Thus, considering significant only the gravitational potential energy of the coating droplet per unit volume,  $f_1$ , one can write:

$$\frac{dE_G}{dt} \approx \frac{d}{dt} \int_{\mathcal{R}_1} f_1 d\mathbf{x} = \frac{d}{dt} \left( \frac{\pi}{6} D_0^3 \rho_1 \mathbf{g} h_m \right) \quad (3.3)$$

where  $\mathbf{g}$  is the gravitational field,  $D_0$  is the droplet diameter before impact and  $h_m$  is the distance from the tablet surface to the droplet center of mass. The gravitational potential energy of an impinging droplet is usually neglected (Bolleddula et al., 2010) if the droplet Bond number is small ( $\text{Bo} \equiv \rho_1 g D_0 / \gamma_{12} \ll 1$ ).

The rate of change of the droplet surface energy appears on the left-hand side of Equation (3.1):

$$\frac{dE_S}{dt} = \frac{d}{dt} \left[ \gamma_{12} (A_{12} - A_{13} \cos \vartheta) \right] \quad (3.4)$$

where  $A_{12}$  and  $A_{13}$  are the areas of the liquid-gas and liquid-solid interfaces, respectively. In this work, it is assumed that the surface tension ( $\gamma_{12}$ ) is constant and uniform. In Equations

(3.1) and (3.4),  $\vartheta$  is the dynamic contact angle which is assumed to be approximately equal to the equilibrium contact angle (Attane et al., 2007).

To calculate the kinetic energy of the droplet and the rate of viscous dissipation of kinetic energy, one needs to know the velocity field  $\mathbf{u}_1$  inside the control volume (coating droplet of volume  $V$ ). To obtain this, the mass and linear momentum balance equations need to be solved; in this work, we decided not to do so, favoring a less computationally demanding modeling approach. The consequence of this choice is that in order to proceed a functional form for the velocity field needs to be assumed.

The form of the velocity field can vary considerably inside the droplet. For droplet impact conditions of interest in most spray impingement processes ( $U_0 \sim 10$  m/s;  $D_0 \sim 10^{-4}$  m;  $\text{Re} > 100$ ; Kalantari and Tropea, 2007), one can assume that the droplet presents two regions in which the velocity field is substantially different (Kim and Chun, 2001); the first region spans almost the entire droplet and in this region the flow can be approximated as inviscid, while the second region is a boundary layer of thickness  $\delta$  near the tablet surface ( $\mathcal{S}_{13}$ ) where viscous dissipation is significant. Batchelor (2000) estimated the boundary layer thickness for the type of flow described above, showing that:

$$\frac{\delta}{h_m} \sim \left( \frac{\mu_1}{\rho_1 U_m h_m} \right)^{1/2} \sim \left( \frac{\mu_1}{\rho_1 U_0 D_0} \right)^{1/2} \sim \frac{1}{\sqrt{\text{Re}}} \quad (3.5)$$

where  $\text{Re} \equiv \rho_1 U_0 D_0 / \mu_1$  is the impact Reynolds number,  $U_m$  is the velocity of the droplet center of mass ( $dh_m/dt$ ) and  $\mu_1$  is the liquid coating formulation viscosity. According to Bolleddula et al. (2010), in most coating spray impact conditions,  $\text{Re} > 100$  and so  $\delta/h_m < 0.1$ ; the boundary layer is thus much thinner than the inviscid-flow bulk region. Later in this chapter, the droplet behavior when the impact Reynolds number is low ( $\text{Re} \sim 10$ ) is also investigated.

First, droplet impacts where  $\text{Re} > 100$  are studied. For these cases, the velocity field in the inviscid-flow region of the coating droplet can be used to estimate the total kinetic energy of the droplet, since the boundary layer, being thin, does not contribute significantly to this quantity. In contrast, the velocity field in the boundary layer should be used to calculate the rate of viscous dissipation of the droplet kinetic energy, since the contribution of the inviscid-flow region to this quantity is negligible.

To calculate the kinetic energy, it was assumed that the flow field in the bulk of the droplet is axisymmetric near a stagnation point (O), which is located on the tablet surface where the droplet impinges (Fig. 3.3). This type of flow is known as ‘‘stagnation point flow’’ (Batchelor, 2000). The motion of the droplet is then described in terms of a stream function  $\psi(r, z, t)$ , where  $r$  and  $z$  are the radial and vertical cylindrical coordinates, respectively. In particular, the radial ( $u_{1r}$ ) and vertical ( $u_{1z}$ ) velocity components are given by:

$$u_{1r} = -(1/r) \partial_z \psi \quad ; \quad u_{1z} = (1/r) \partial_r \psi \quad (3.6)$$

while the angular velocity component is zero.

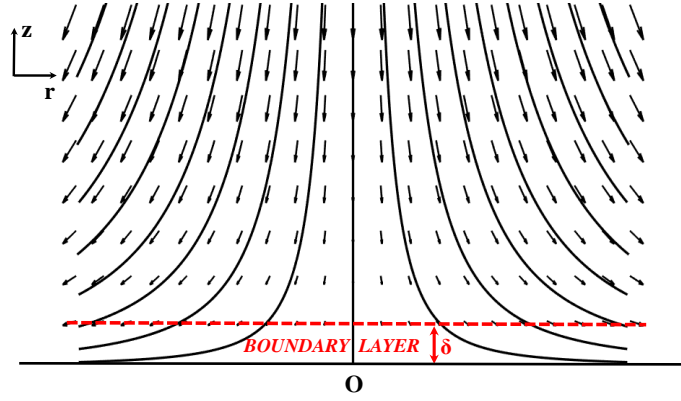


Figure 3.3: Axisymmetric stagnation point flow. The lines denote the flow streamlines.

The stream function for irrotational flow near a stagnation point is well documented in the literature and is given by  $\psi = (k/2)zr^2$ , where  $k$  is a constant (Batchelor et al., 2000). Substituting this function in Equation (3.6) gives:

$$u_{1r} = -\frac{1}{2}kr \quad ; \quad u_{1z} = kz \quad (3.7)$$

For an impinging droplet, the value of the parameter  $k$  can be calculated by considering the relations (3.7) at the droplet center of mass:

$$u_{1r}(0, h_m, t) = 0 \quad ; \quad u_{1z}(0, h_m, t) = \frac{dh_m}{dt} = kh_m \quad \Rightarrow \quad k = \frac{U_m}{h_m} \quad (3.8)$$

Substituting  $k$  into Equation (3.7) yields:

$$u_{1r} = -\frac{1}{2} \frac{r}{h_m} U_m \quad (3.9)$$

$$u_{1z} = \frac{z}{h_m} U_m \quad (3.10)$$

The above equations satisfy the continuity equation for an incompressible fluid. Expressing the kinetic energy ( $E_K$ ) of the droplet in terms of the velocity components for the “stagnation point flow” (Equations 3.9, 3.10), and neglecting the kinetic energy associated with the dividing surfaces  $\mathcal{S}_{12}$  and  $\mathcal{S}_{13}$  yields:

$$\begin{aligned} E_K &\approx \frac{1}{2} \rho_1 \int_{\mathcal{R}_1} \mathbf{u}_1 \cdot \mathbf{u}_1 \, d\mathbf{x} = \frac{1}{2} \rho_1 \int_{\mathcal{R}_1} (u_{1r}^2 + u_{1z}^2) \, d\mathbf{x} \\ &\approx \frac{1}{2} \rho_1 \int_{\mathcal{R}_1} \left[ \left( -\frac{1}{2} \frac{r}{h_m} U_m \right)^2 + \left( \frac{z}{h_m} U_m \right)^2 \right] d\mathbf{x} \end{aligned} \quad (3.11)$$

Here one can integrate over the entire region  $\mathcal{R}_1$  occupied by the impinging droplet instead of restricting the integration to the inviscid-flow region. This simplification does not affect the result significantly, since in the current conditions the boundary layer is thin. To calculate the above integral, it was assumed that the droplet has a spherical cap shape, so that the following geometrical relations hold:

$$R_d^2 = \frac{D_0^2}{3} \left( \frac{D_0}{h_{max}} - \frac{h_{max}^2}{D_0^2} \right) \quad ; \quad h_m = \frac{1}{6} \left( 2h_{max} + \frac{h_{max}^4}{D_0^3} \right) \quad (3.12)$$

In the geometrical relations (3.12),  $R_d$  and  $h_{max}$  are the time-dependent droplet wetted area radius and maximum droplet height, respectively.

Integrating Equation (3.11) over the volume of a spherical cap described by the geometrical relations (Eq. 3.12), and taking the time derivative, yields:

$$\frac{dE_K}{dt} = \frac{d}{dt} \left[ \frac{\rho_1 \pi U_m^2}{2h_m^2} \left( \frac{R_d^4 h_{max}}{16} + \frac{13R_d^2 h_{max}^3}{72} + \frac{h_{max}^5}{10} \right) \right] \quad (3.13)$$

Viscous dissipation during droplet impingement occurs in the boundary layer and the bulk of the droplet. Since the boundary layer is thin, one can calculate the rate of viscous dissipation in the latter region by integrating over  $\mathcal{R}_1$  as follows:

$$\begin{aligned} \Phi_b &= - \int_{\mathcal{R}_1} \boldsymbol{\tau}_1 : \partial_{\mathbf{x}} \mathbf{u}_1 d\mathbf{x} = 2\mu_1 \int_{\mathcal{R}_1} \left[ (\partial_r u_{1r})^2 + (u_{1r}/r)^2 + (\partial_z u_{1z})^2 + \frac{1}{2} (\partial_z u_{1r} + \partial_r u_{1z})^2 \right] d\mathbf{x} \\ &= 3\mu_1 \int_{\mathcal{R}_1} \left( \frac{1}{h_m} U_m \right)^2 d\mathbf{x} = \frac{\mu_1 \pi U_m^2 h_{max}}{2 h_m^2} (3R_d^2 + h_{max}^2) \end{aligned} \quad (3.14)$$

In the boundary layer close to the surface viscous dissipation is significant (Kim and Chun, 2001). Since in this region a functional form for the velocity field  $\mathbf{u}_1$  is not known, one cannot solve the volume integral rigorously as in Equations (3.11) and (3.14); however, the value of the rate of viscous dissipation in the boundary layer ( $\Phi_\delta$ ) can be estimated using scaling analysis.

In the Appendix of this thesis, it is shown that the  $\Phi_\delta$  estimate can be obtained as follows:

$$\begin{aligned} \Phi_\delta &= - \int_{\mathcal{R}_\delta} \boldsymbol{\tau}_1 : \partial_{\mathbf{x}} \mathbf{u}_1 d\mathbf{x} \sim \frac{\mu_1}{\delta^2} \int_{\mathcal{R}_\delta} u_{1r}^2 d\mathbf{x} \sim \frac{\mu_1}{\delta} \int_{\mathcal{S}_{13}} u_{1r}^2 ds \\ &\sim \frac{\mu_1}{h_m} \left( \frac{\rho_1 U_m h_m}{\mu_1} \right)^{1/2} \int_{\mathcal{S}_{13}} \left( -\frac{1}{2} \frac{r}{h_m} U_m \right)^2 ds \end{aligned} \quad (3.15)$$

where  $\mathcal{R}_\delta$  is the boundary layer region and  $\mathcal{S}_{13}$  is the droplet-tablet dividing surface that corresponds to the wetted area. This expression estimates correctly the order of magnitude of  $\Phi_\delta$ ; however, to obtain a more accurate result an empirical dissipation factor, denoted as  $F_d$ , is introduced. The estimation of its value is discussed later in this chapter.

With the introduction of the dissipation factor, the expression yields:

$$\Phi_\delta \approx \frac{F_d \mu_1 U_m^2}{4h_m^3} \left( \frac{\rho_1 U_m h_m}{\mu_1} \right)^{1/2} \int_0^{2\pi} \int_0^{R_d} r^3 dr d\phi = \frac{F_d \mu_1 U_m^2 \pi R_d^4}{8h_m^3} \left( \frac{\rho_1 U_m h_m}{\mu_1} \right)^{1/2} \quad (3.16)$$

Because the velocity field inside the bulk of the droplet is essentially inviscid, estimating the rate of viscous dissipation only from Equation (3.14), when the impact Reynolds number is high, would grossly underestimate the value of the viscous dissipation rate. Indeed, since in these conditions it is  $\text{Re} > 100$  and  $h_{max} \sim R_d$ , and using scaling to compare  $\Phi_b$  and  $\Phi_\delta$  yields:  $\Phi_b/\Phi_\delta \sim \delta/h_m \ll 1$ . Thus,  $\Phi \approx \Phi_\delta$  needs to be considered in the mechanical energy balance Equation (3.2).

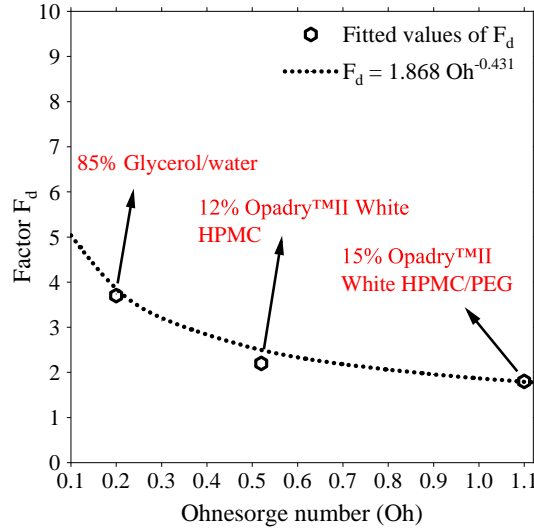


Figure 3.4:  $F_d$  factor estimation. The experimental data are from Bolleddula et al. (2010).

To estimate the rate of viscous dissipation, an expression for the factor  $F_d$  is needed. Empirical equations for the dissipation factor have been derived by Bechtel et al. (1981) and Kim and Chun (2001), who fitted their experimental data for water droplets impact to obtain  $F_d = 5.3 \text{ Oh}^{-1/2}$  and  $F_d = \sqrt{\pi} \text{ Oh}^{-1/2}$ , respectively. Here, Oh denotes the Ohnesorge number ( $\text{Oh} \equiv \mu / \sqrt{\rho \gamma D_0}$ ).

As the focus of this work is on pharmaceutical coatings,  $F_d$  is fitted to match the experimental data of Bolleddula et al. (2010) for the spreading of various coating droplets impinging on tablets with different Ohnesorge (Oh) number values. In all case studies chosen for the fitting  $\text{Re} \sim 100$ . In this work, gPROMS Modelbuilder was used to estimate the values of  $F_d$  introduced in the kinematic phase model to approximate the wetted area radius after impact of OpadryII White coating droplets (with ranging solid concentrations) and a glycerol/water solution droplet. By plotting the values of  $F_d$ , against the corresponding ones of the Ohnesorge number (Fig. 3.4) and by using regression, the following expression was derived:

$$F_d = 1.868 \text{ Oh}^{-0.431} \quad (3.17)$$

Equation (3.17) holds for the coating droplets used in the experiments by Bolleddula et al. (2010) against which the results of the current model were validated. Note that in the validation section the model is predictive, and not fitted, since it is used to analyze case studies different from those used in the derivation of Equation (3.17). The dissipation factor proposed in this work could also be used to estimate viscous dissipation of various other coating formulations for moderate droplet Re and Oh numbers ( $\text{Re} \sim 100$ ,  $\text{Oh} \sim 0.1$ ).

During film-coating, the Re number of the droplet might be low ( $\text{Re} \sim 10$ ). This can occur when the coating is very viscous, the droplet is small or the impact velocity is low. When  $\text{Re} \sim 10$ , viscous dissipation is significant in the entire droplet, and not only in a thin boundary layer close to the tablet surface. To find an appropriate velocity field form for the droplet, Volume-Of-Fluid simulations of droplet impact on a rigid surface were performed. The methodology for these VOF simulations is described in detail by Shaari (2007).

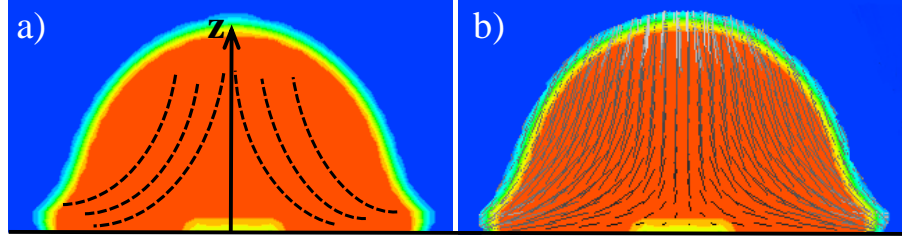


Figure 3.5: VOF simulation of droplet impact ( $Re = 10$ ). a) The assumed axisymmetric stagnation point flow, b) the calculated flow streamlines from the VOF simulation.

From the VOF simulations, it can be seen (Fig. 3.5) that the flow in the droplet when  $Re = 10$  ( $D_0 = 10^{-5}m$ ,  $U_0 = 10$  m/s,  $\mu_1 = 0.01$  Pa s,  $\rho_1 = 10^3$  kg/m<sup>3</sup>) resembles (qualitatively) the stagnation point flow assumed for the bulk of the droplet in the case of high  $Re$ . Based on the above, the total kinetic energy of the droplet (Eq. 3.13) was again estimated using the stagnation point flow velocity field (Eqs. 3.9, 3.10). Nonetheless, according to Batchelor et al. (2000), Equations (3.9, 3.10) suggest that the flow in the droplet is essentially inviscid. Since the actual flow in the droplet is not described exactly by the prescribed velocity field, a correction factor ( $\Lambda$ ) was introduced to estimate the rate of viscous dissipation:

$$\Phi = \frac{\Lambda \mu_1 \pi U_m^2 h_{max}}{2 h_m^2} (3R_d^2 + h_{max}^2) \quad (3.18)$$

The factor  $\Lambda$  was fitted (Fig. 3.6) so that the predicted droplet spreading matches the experimental data of Bolleddula et al. (2010) for the impact of various droplets impinging on tablets with low Reynolds number ( $Re \sim 10$ ). The correction factor  $\Lambda$  is given by:

$$\Lambda = (3/2) \sqrt{\pi} Oh^{-2/3} \quad (3.19)$$

Note that the results for the OpadryII White 15% PEG and glycerol/water solutions were not used for validation as they were used for the fitting of  $\Lambda$ .

To solve the mechanical energy balance equation one can now substitute the expressions for the gravitational, surface and kinetic energies given by Equations (3.3), (3.4) and (3.13), respectively. If the droplet impact Reynolds number is high ( $Re > 100$ ), it can be assumed that a boundary layer forms and that the rate of viscous dissipation in this boundary layer is calculated using Equation (3.16). If the droplet has a low impact Reynolds number before impact ( $Re \sim 10$ ), the rate of viscous dissipation in the entire droplet can be estimated using Equation (3.18).

The initial conditions required to solve the mechanical energy balance equation are:

$$\left. \frac{dh_m}{dt} \right|_{t=0} = -U_0 \quad ; \quad h_{max} \Big|_{t=0} = D_0 \quad (3.20)$$

The mechanical energy balance equation was written in terms of just one independent variable ( $h_m$ ). To do so, the expressions for the droplet potential (gravitational + surface) energy, kinetic energy and rate of viscous dissipation were substituted into Equation (3.2) and then the geometrical relations (3.12) were used to eliminate the variables  $R_d$  and  $h_{max}$ .

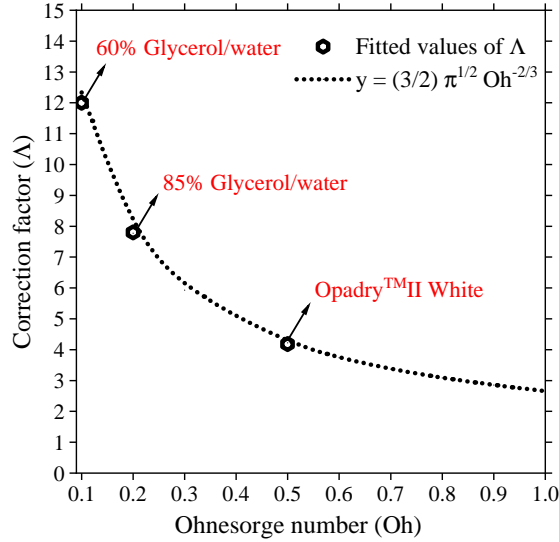


Figure 3.6:  $\Lambda$  factor estimation. The experimental data are from Bolleddula et al. (2010).

The output of the kinematic phase model (droplet geometry at  $t = t_i$ ) is used as an initial condition in the subsequent ( $t > t_i$ ) capillary phase model where droplet evaporation and absorption into the tablet are taken into account. The model for the capillary phase is presented in the next section of this chapter.

### 3.2.2 Capillary phase

In this section, a mathematical model that describes the flow, evaporation and absorption of the droplet into the tablet when the capillary effects become dominant (capillary phase:  $t > t_i$ ) is presented. The model developed in this work employs the lubrication approximation method (Alleborn and Razhillier, 2004; Siregar et al., 2010) to calculate droplet behavior on the tablet surface while accounting for coating solvent (water) evaporation under pharmaceutical coating operating conditions.

The flow of the droplet on the tablet surface (Fig. 3.7) is governed by the continuity and Navier-Stokes equations:

$$\partial_x \cdot \mathbf{u}_1 = 0 \quad (3.21)$$

$$\rho_1 (\partial_t \mathbf{u}_1 + \mathbf{u} \cdot \partial_x \mathbf{u}_1) = -\partial_x p + \mu_1 \partial_x^2 \mathbf{u}_1 + \rho_1 \mathbf{g} \quad (3.22)$$

where  $\rho_1$  and  $\mu_1$  are the density and viscosity of the liquid that forms the droplet, respectively, and  $\mathbf{u}_1$  denotes the velocity vector. The fluid was assumed to be incompressible.

Solving Equations (3.21) and (3.22) is complex and computationally expensive. A simplification is made possible by the lubrication approximation method due to the geometry of the droplet once the kinematic phase is over (Szeri, 2010): under normal conditions the in-plane dimension of the film is greater than its thickness. The lubrication approximation theory uses scaling to estimate the order of magnitude of the terms of the continuity and Navier-Stokes equations. The equations are then simplified by deleting those terms that are judged to be too small to have significant effect.

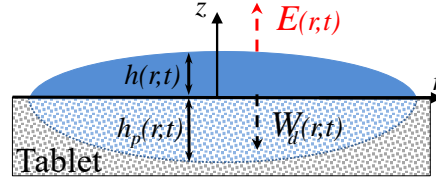


Figure 3.7: Droplet evaporation and absorption into the tablet. The model calculates the droplet height  $h$  and the wetting front depth  $h_p$  into the tablet.

Alleborn and Raszillier (2004) and Siregar (2012) both used the lubrication approximation method in cylindrical coordinates ( $r, z$  coordinates shown in Figure 3.7) to solve the Navier-Stokes equations and derived the following equation that calculates the height profile  $h(r, t)$  of the droplet after it is deposited onto a porous substrate:

$$\partial_t h = \frac{1}{3\mu_1} \frac{1}{r} \partial_r (rh^3 \partial_r p) - W_d \quad (3.23)$$

where  $W_d$  is a sink term (absorption velocity) that accounts for the droplet absorption within the porous substrate. Previous models (Alleborn and Razhillier, 2004; Siregar et al., 2010) assumed that evaporation phenomena are negligible during the spreading and absorption of a droplet. That is because the dynamics of evaporation are considerably slower than the dynamics of spreading and absorption. According to experiments performed by Hu and Larson (2005) and Siregar et al. (2010), the characteristic time for the absorption of a  $\mu\text{l}$  droplet is of the order of seconds, while the evaporation of the same droplet, at room temperature, from within a porous medium takes a considerable length of time (100–150 min). By using Equation (3.23), one can accurately describe the behavior of a spherical cap-shaped coating droplet after its initial spreading on a rigid substrate during the kinematic phase, thus simplifying the problem and reducing the computational effort.

Nonetheless, inside a coating drum, the temperature, relative humidity and air flow conditions accelerate evaporation. Therefore, one should not neglect the evaporation of the droplet from the surface of the tablet during the capillary phase. In the current work, equation (3.23) is modified to account for the evaporation velocity ( $E$ ) during the absorption process:

$$\partial_t h = \frac{1}{3\mu_1} \frac{1}{r} \partial_r (rh^3 \partial_r p) - W_d - E \quad (3.24)$$

Equation (3.24) predicts the droplet height (thickness) profile  $h$  above the surface of a porous tablet in pharmaceutical coating process conditions. In Chapter 5, a general evolution equation for the thickness of a coating dispersion film or droplet on a tablet surface is rigorously derived. Equation (3.24) is a special form of that equation for a Newtonian coating liquid of constant density and viscosity.

To derive an equation for the evaporation velocity  $E$ , it was assumed that the droplet shape is a spherical cap with a wetted area radius  $R_d$  (calculated at the end of the kinematic phase). Following Popov (2005), who investigated the evaporation of sessile droplets, one gets:

$$E(r, t) = \frac{\dot{m}_e}{\pi\rho_1} \left[ 1 - \left( \frac{r}{R_d} \right)^2 \right]^{-1/2} \quad (3.25)$$

The evaporation mass flux  $\dot{m}_e$  can be estimated by the expression (Kiil, 2006):

$$\dot{m}_e = \frac{k_m \mathcal{M}_w}{\mathfrak{R}} \left[ \frac{p_v^*(T_d)}{T_d} - \frac{RH p_v^*(T_{2\infty})}{T_{2\infty}} \right] \quad (3.26)$$

where  $k_m$  is the mass transfer coefficient,  $\mathcal{M}_w$  is the molecular weight of water,  $RH$  is the relative humidity in the air bulk,  $\mathfrak{R}$  is the universal gas constant, and  $p_v^*$  is the saturated vapor pressure calculated at the droplet surface temperature  $T_d$  and the bulk air temperature  $T_{2\infty}$ . The mass transfer coefficient  $k_m$  was estimated using the Ranz-Marshall correlation for the Sherwood (Sh) number:

$$\text{Sh} \equiv \frac{k_m R_d}{\mathcal{D}_v} = 2 + 0.65 \cdot \text{Re}_g^{1/2} \text{Pr}_g^{1/3} \quad (3.27)$$

For a drying process under atmospheric pressure, the diffusion coefficient of water vapor in air  $\mathcal{D}_v$  can be calculated as (Mezhericher et al., 2008):

$$\mathcal{D}_v = 3.564 \cdot 10^{-10} (T_d + T_{2\infty})^{1.75} \quad (3.28)$$

where  $T_d$  and  $T_g$  are the droplet and air temperatures in Kelvin, respectively. In this chapter, the temperature of the droplet is assumed to be constant. Changes in coating liquid temperature after its application on a tablet are investigated in Chapter 5. In the Ranz-Marshall correlation,  $\text{Re}_g$  and  $\text{Pr}_g$  are the Reynolds and Prandtl dimensionless numbers, defined as:

$$\text{Re}_g \equiv \frac{R_d \rho_2 u_2}{\mu_2} ; \text{Pr}_g \equiv \frac{c p_2 \mu_2}{k_2} \quad (3.29)$$

where  $u_2$ ,  $\mu_2$ ,  $c p_2$ ,  $\rho_2$ ,  $k_2$  are the velocity, viscosity, specific heat, density and thermal conductivity of air, respectively.

According to Schwartz and Weidner (1995), the pressure ( $p$ ) source in small droplets is the pressure jump at the free surface due to surface tension  $\gamma_{12}$ :

$$p = \gamma_{12} \partial_s \cdot \mathbf{n}_{12} \quad (3.30)$$

where  $\partial_s$  is the surface gradient operator and  $\mathbf{n}_{12}$  is the unit vector pointing from the droplet to the air. To calculate the term  $\partial_s \cdot \mathbf{n}_{12}$  for a thin droplet, the expression of Siregar (2012) can be employed:

$$\partial_s \cdot \mathbf{n}_{12} = -\frac{1}{r} \partial_r \left( \frac{r \partial_r h}{\sqrt{1 + (\partial_r h)^2}} \right) \quad (3.31)$$

When a droplet flows on the tablet, liquid flows over a dry surface. Such contact-line motions do not agree with the no-slip boundary condition at the film-tablet interface which were employed to derive the droplet motion equation (Eq. 3.23, Alleborn and Raszillier, 2004). To overcome this problem, the approach of Schwartz and Eley (1998) was followed. They assumed that a submicroscopic layer (precursor film) of liquid covers the dry substrate region directly adjacent to the droplet edges. Inside this submicroscopic film, a “disjoining” pressure ( $\pi_c$ ) arises (Slattery et al., 2007). This pressure component takes into account the Van der Waals forces between droplet and tablet and is significant at the contact line.

Based on the work by Schwartz (1999) the disjoining pressure was calculated as follows:

$$\pi_c = \beta \left[ \left( \frac{\hat{h}}{h} \right)^N - \left( \frac{\hat{h}}{h} \right)^M \right] ; \quad \beta = \frac{1}{\hat{h}} \frac{(N-1)(M-1)}{2(N-M)} \gamma_{12} (1 - \cos \vartheta) \quad (3.32)$$

where  $N$  and  $M$  are positive constants with  $N > M > 1$  and  $\vartheta$  is the equilibrium contact angle. Following Schwartz (2001),  $N$  and  $M$  are taken to be equal to 3 and 2, respectively. The precursor film thickness  $\hat{h}$  is much smaller compared to the droplet height ( $\hat{h} \approx 0.1 \mu\text{m}$ ). Modeling the disjoining pressure using Equation 3.32 allowed the prescription of an equilibrium contact angle.

The final equation, which is used in the current mathematical model, for the calculation of the pressure in the droplet reads:

$$p = -\gamma_{12} \frac{1}{r} \partial_r \left[ \frac{r \partial_r h}{\sqrt{1 + (\partial_r h)^2}} \right] - \pi_c \quad (3.33)$$

To use Equation (3.24) one needs an expression for the droplet absorption velocity ( $W_d$ ). The equation that calculates  $W_d$  is:

$$W_d = \begin{cases} \varphi w_p|_{z=0} & \text{if } h > \hat{h} \\ 0 & \text{if } h < \hat{h} \end{cases} \quad (3.34)$$

where  $w_p$  is the (volume averaged) mixture velocity in the vertical direction inside the tablet which is discussed below. With the above relation, the precursor film is not allowed to be absorbed into the porous substrate. The absorption velocity becomes effectively zero when the droplet height  $h$  reaches the characteristic height of the precursor film  $\hat{h}$ .

To calculate the liquid vertical ( $w_p$ ) and radial ( $v_p$ ) velocity components inside the tablet, the Darcy's equation (simplified momentum balance equation) was used, neglecting gravity:

$$w_p = -\frac{\mathcal{K}_p}{\varphi \mu_1} \partial_z p_p \quad (3.35)$$

$$v_p = -\frac{\mathcal{K}_p}{\varphi \mu_1} \partial_r p_p \quad (3.36)$$

where  $p_p$  is the pressure inside the tablet and  $\mathcal{K}_p$  is the tablet permeability which was estimated from the Kozeny-Carman equation:

$$\mathcal{K}_p = \frac{d_p^2 \varphi^3}{180(1-\varphi)^2} \quad (3.37)$$

where  $d_p$  and  $\varphi$  are the tablet average pore diameter and porosity, respectively.

To calculate the pressure inside the tablet core ( $p_p$ ) the Laplace equation  $\partial_{\mathbf{x}} \cdot \partial_{\mathbf{x}} p_p = 0$  was used. In cylindrical coordinates it reads:

$$(1/r) \partial_r (r \partial_r p_p) + \partial_z (\partial_z p_p) = 0 \quad (3.38)$$

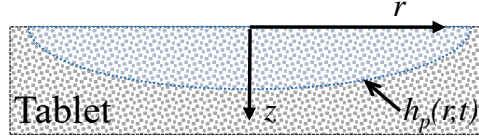


Figure 3.8: Wetting front depth ( $h_p$ ) inside the tablet.

For the pressure  $p_p$ , one can write two boundary conditions; one at the tablet core surface ( $z = 0$ ) and one at the wetting front depth ( $z = h_p$ ; Fig. 3.8):

$$p_p = p \text{ at } z = 0 \quad ; \quad p_p = p_c \text{ at } z = h_p \quad (3.39)$$

where  $p_c$  is the capillary pressure. The capillary pressure depends on the dimensions of the average pore and the solid-liquid contact angle ( $\vartheta$ ), and it equals the Laplace pressure in a capillary given by:

$$p_c = - (4/d_p) \gamma_{12} \cos \vartheta \quad (3.40)$$

Equations (3.35) and (3.36) give the velocity field of the liquid inside the porous tablet core. To calculate the wetting front depth inside the tablet ( $h_p$ ), the wetting front profile as:  $F_p(r, z, t) \equiv h_p(r, t) - z$  was defined. The substantial derivative of  $F_p$  is zero and this allows one to write:

$$\frac{DF_p}{Dt} = \partial_t F_p + (1/\varphi) \mathbf{u}_p \cdot \partial_x F_p = 0 \Rightarrow \partial_t h_p = - \left( v_p \Big|_{z=h_p} \partial_r h_p - w_p \Big|_{z=h_p} \right) \quad (3.42)$$

Following the work of Alleborn and Razhillier (2004), the below conditions at the boundaries of the computational domain ( $0, R_{max}$ ) were implemented:

$$\partial_r h = \partial_r h_p = 0 \text{ at } r = 0 \text{ and } r = R_{max} \quad (3.43)$$

where  $R_{max}$  was chosen to be significantly greater than the maximum wetting area radius  $R_d$ . These boundary conditions suggest that the slope of the droplet surface and the liquid flux vanish across the boundaries of the computational domain. For  $r = 0$ , the above relations (3.43) can also be acknowledged as symmetry conditions that are derived from the droplet spherical cap shape assumption.

Equations (3.24) to (3.43) constitute the mathematical model for the capillary phase that is proposed coupled with the kinematic phase model presented earlier in Section 3.2.1 to predict the behavior of a pharmaceutical coating droplet after impingement on a tablet.

### 3.2.3 Numerical solution

To predict the behavior of a coating droplet after impact onto a tablet the kinematic (Section 3.2.1) and capillary (Section 3.2.2) phase models were combined. The outputs of the kinematic phase model (droplet height and wetted area diameter) were used as initial conditions (at  $t = t_i$ ) for the capillary phase equations which were then made dimensionless using the following dimensionless variables:

$$r^* \equiv \frac{r}{R_0}, h^* \equiv \frac{h}{H_0}, z^* \equiv \frac{z}{H_0}, h_p^* \equiv \frac{h_p}{H_0}, t^* \equiv \frac{\gamma_{12} H_0^3}{\mu_1 R_0^4} t, W_d^* \equiv \frac{\mu_1 R_0^4}{\gamma_{12} H_0^4} W_d$$

$$p^* \equiv \frac{H_0}{\gamma_{12}} p, w_p^* \equiv \frac{\mu_1}{\gamma_{12}} w_p, v_p^* \equiv \frac{\mu_1}{\gamma_{12}} v_p, p_p^* \equiv \frac{H_0}{\gamma_{12}} p_p, \pi_c^* \equiv \frac{H_0}{\gamma_{12}} \pi_c$$

where  $R_0$  is a characteristic droplet radius and  $H_0$  is a characteristic droplet height. Here,  $R_0$  and  $H_0$  were defined to be the wetted area radius ( $R_d$ ) and the maximum droplet height ( $h_{max}$ ) after the completion of the kinematic phase, respectively.

For the behavior of the droplet above the surface i.e. for  $0 < r^* < 1$ , after substituting the dimensionless variables in Equations (3.24, 3.33), it was obtained:

$$\partial_{t^*} h^* = \frac{R_0^2}{3H_0^2} \frac{1}{r^*} \partial_{r^*} \left( r^* h^{*3} \partial_{r^*} p^* \right) - W_d^* - E^* \quad (3.44)$$

$$E^* = \frac{\mu_1 R_0^4}{\pi \rho_1 \gamma_{12} H_0^4} \dot{m}_v \left( 1 - r^{*2} \right)^{-1/2} \quad (3.45)$$

$$p^* = - \left( \frac{H_0}{R_0} \right)^2 \frac{1}{r^*} \partial_{r^*} \left[ \frac{r^* \partial_{r^*} h^*}{\sqrt{1 + [(H_0/R_0) \partial_{r^*} h^*]^2}} \right] - \pi_c^* \quad (3.46)$$

Equation (3.44) calculates the droplet height profile  $h$ , while Equations (3.45) and (3.46) provide information on the evaporation velocity  $E$  of the droplet and the pressure inside the liquid  $p$ , respectively.

The Equations (3.35, 3.36, 3.38 and 3.45) that describe the movement of the liquid inside the porous medium (for  $0 < r^* < 1$  and  $0 < z^* < h_p^*$ ) become in dimensionless form:

$$w_p^* = - \frac{\mathcal{K}_p}{H_0^2 \varphi} \partial_{z^*} p_p^* \quad (3.47)$$

$$v_p^* = - \frac{\mathcal{K}_p}{H_0 R_0 \varphi} \partial_{r^*} p_p^* \quad (3.48)$$

$$\left( \frac{H_0}{R_0} \right)^2 \frac{1}{r^*} \partial_{r^*} \left( r^* \partial_{r^*} p_p^* \right) + \partial_{z^*} (\partial_{z^*} p_p^*) = 0 \quad (3.49)$$

$$\partial_{t^*} h_p^* = - \frac{R_0^4}{H_0^4} \left[ \frac{H_0}{R_0} \frac{\partial_{r^*} h_p^*}{v_p^*} \Big|_{(z^*=h_p^*)} - w_p^* \Big|_{(z^*=h_p^*)} \right] \quad (3.50)$$

Equations (3.47 to 3.49) calculate the velocity and pressure profile, respectively of the fluid that is absorbed into the porous medium, while Equation (3.50) predicts the wetting front.

This model consists of equations that are defined in a moving domain (Eq. 3.47 - Eq. 3.49). The wetting front depth changes with time and therefore every variable that is defined between 0 and  $h_p$  has no fixed boundaries. Since the moving boundaries are a function of time, and their location needs to be determined to derive the solution, this model is non-linear. In general, the non-linearity associated with the moving boundary usually makes the analysis of this class of problems challenging. A common example of this category of problems is the model of the melting of ice that was first developed by Stefan (Kutluay et al., 1997).

It is possible to fix the moving boundaries of a problem by using a fixed coordinate system in space for the moving boundary condition. The transformation proposed by Landau (1950) is:

$$\xi \equiv \frac{z^*}{h_p^*} \quad (3.51)$$

With the help of this transformation, the moving interface  $z^* = h_p^*$  was fixed at  $\xi = 1$ . The above transformation was implemented to the partial differential equations (Eq. 3.47 - Eq. 3.49) that are defined in the  $z$ -direction between 0 and  $h_p^*$ . Implementing the above transformation in the dimensionless equation for the vertical velocity component of the liquid inside the porous medium  $w_p$  yields:

$$w_p^* = -\frac{\mathcal{K}_p}{H_0^2 h_p^*} \partial_\xi p_p^* \quad (3.52)$$

By using Landau's transformation the moving boundary in the above equation is fixed at  $\xi = 1$ . The rest of the equations defined in a moving domain were treated in the same way as Eq. (3.52), but are not reported here for the sake of brevity.

To conclude, Equations (3.44-3.50) constitute the model for the capillary phase. In this chapter, it is proposed that the capillary phase and the kinematic phase (Section 3.2.1) models are coupled in order to predict the behavior of a pharmaceutical coating droplet after impingement on a porous substrate. The capillary phase model input parameters are the wetted area diameter  $D_d = 2R_d$  and the maximum height of the droplet  $h_{max}$ , which are calculated from the kinematic phase model. As an output from the capillary phase model, the droplet height profile  $h$ , the wetting front depth  $h_p$  and the absorption time  $\tau_a$  can be calculated.

### 3.3 Numerical results and validation

The numerical results from the model described in Section 3.2 were validated with experiments from the literature. Because the experimental data were taken from multiple sources, this chapter was not limited to a single case study, instead the current model predictions were compared with independent experimental studies of different researchers. In the following sections, the numerical results for the kinematic and capillary phase models are analyzed and validated. All the numerical calculations were performed in gPROMS (Process Systems Enterprise Ltd., 2019), employing the Modelbuilder modelling platform.

Some of the input parameters of the model presented in Section 3.2 were difficult to determine precisely from the experimental data presented in the literature. To account for this, the experimental measurement errors of the input parameters were propagated to the numerical results following the stochastic sampling method of Cacuci (2003). First, the probability distributions (measurement error) of the input parameters were defined based on experimental data found in the literature. Subsequently, these distributions were used to generate a sample (Sobol sampling) using gPROMS Modelbuilder in order to create multiple scenarios of the single-droplet model developed and presented in Section 3.2. Lastly, a series of simulations were performed and the standard deviation of the response variables (Cacuci,

2003) was calculated. The calculated propagated errors of the numerical results appear as error bars or lines in the figures of Section 3.3.

### 3.3.1 Kinematic phase results

In the following subsection, the numerical results of the kinematic phase model (wetted area diameter  $D_d$  and maximum height  $h_{max}$  of the droplet) are presented and compared to the experimental data from Bolleddula et al. (2010). They investigated the spreading of viscous pharmaceutical coatings (Table 3.1) that contained different percentages of solids. The experimental measurement error of the coating properties (density, surface tension and viscosity measured at shear rate  $1000\text{ s}^{-1}$ ) was estimated to be 5% (Bolleddula et al., 2010).

The values of the dissipation factors  $F_d$  and  $\Lambda$  were estimated by solving Equations (3.17) and (3.19). The first factor was used for the estimation of the rate of viscous dissipation when the impact Reynolds number was relatively high ( $\text{Re} > 100$ ), whereas the second factor when the Reynolds number was low ( $\text{Re} \sim 10$ ), as proposed in Section (3.2.1). Note that the model presented in this chapter is predictive. Therefore, the numerical results for the coating formulations OpadryII White 12%, 15% PEG and glycerol/water solutions are not presented here as they were used for the fitting of the dissipation factors  $F_d$  and  $\Lambda$  and are considered biased.

In Figure 3.9.a), the model predictions are compared with the experimental data obtained by Bolleddula et al. (2010) for coating droplet impingement (20% OpadryII White PVA). The impact velocity and droplet diameter in both the experiments and numerical simulations are  $2.47\text{ m/s}$  and  $2.5\text{ mm}$  ( $\text{Re} = 168$ ), respectively. The normalized maximum droplet height ( $h_{max}/D_0$ ) and wetted area diameter ( $D_d/D_0$ ) reach a plateau when the end of the inertia-driven regime is approached (after a time  $t_i \equiv D_0/U_0 \approx 1\text{ ms}$ ). Figure 3.9.a) shows that the model predictions agree well with the experimental data found in the literature.

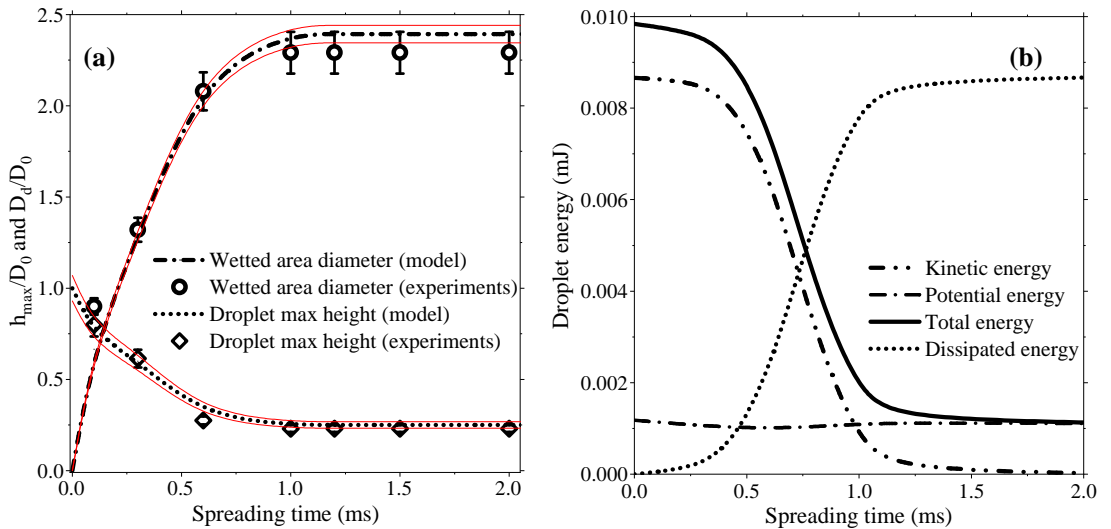


Figure 3.9: Kinematic phase model results. a) Normalized wetted area diameter and droplet max height (experiments by Bolleddula et al., 2010) and, b) Kinetic energy dissipation during spreading.

Table 3.1: Coating droplets rheology properties. Taken from Bolleddula et al. (2010).

Coating	Density ( $\text{kg/m}^3$ )	Surface tension (N/m)	Viscosity (mPa s)
OpadryII White 10% HPMC	1020	0.04822	98
OpadryII White 12% HPMC	1030	0.04766	175
OpadryII White 15% HPMC	1040	0.04667	377
OpadryII White 20% PVA	1070	0.04393	39

In Figure 3.9.b), it is shown how the kinetic energy of the coating droplet is dissipated after impingement. The droplet kinetic energy approaches zero when the inertia-driven regime is completed at  $t = t_i$ . This means that for longer times ( $t > t_i$ ) spreading owing to inertial forces would be negligible, if the droplet impinged alone. During spray application, however, the work done on the surface of the applied coating by subsequent droplets makes the film spread further. The spreading owing to successive droplet impacts is discussed in Chapter 4.

Figure 3.10.a) shows the numerical prediction for the diameter of the wetted area together with experimental results of Bolleddula et al. (2010) for the coating OpadryII White 10% HPMC. The droplet diameter before impact was taken to be 2.4 mm and three impact velocity scenarios were investigated: 0.41 m/s, 0.93 m/s and 2.47 m/s ( $\text{Re} = 10 - 60$ ). In Figure 3.10.a), the red error lines for the numerical results are the propagated measurement errors of the model input parameters (coating properties), whereas for the validation data, the error bars stand for the droplet height measurement error that was estimated based on the graphs presented by Bolleddula et al. (2010).

The numerical solutions closely predict the droplet spreading behavior for all impact velocities considered. The results illustrate that the kinematic phase takes place in the characteristic time  $t_i \equiv D_0/U_0$ . After that characteristic time (1 ms, 2 ms and 5 ms, respectively, for the three impact velocities examined), the spreading affected by inertial forces seems to be negligible as the wetted area and spreading factor reach a plateau.

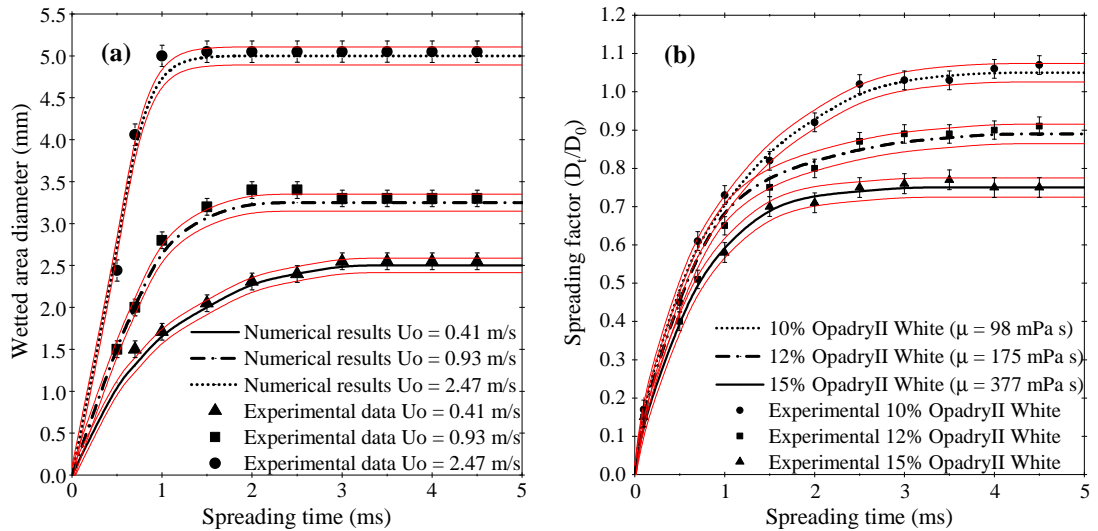


Figure 3.10: Validation of the kinematic phase model with experimental data from Bolleddula et al. (2010): a) Wetted area diameter of OpadryII 10% droplets for different impact velocities. b) Spreading factor of droplets of different viscosity after deposition.

Table 3.2: Comparison of the current model with the model from Roisman et al. (2002) in terms of the final spreading factor. Experiments from Bolleddula et al. (2010).

Coating liquid	Final spreading factor		Experiment	%  Error	
	This work	Roisman et al.		This work	Roisman et al.
Opadry 10%	1.31	1.42	1.30	0.8 %	9.2 %
Opadry 12%	1.23	1.33	1.20	2.5 %	10.8 %
Opadry 15%	1.03	1.17	1.10	3.0 %	17.0 %

In the literature, most of the experimental results are presented in terms of a spreading factor (Bolleddula et al., 2010). The spreading factor is the ratio of the diameter of the wetted area ( $D_d$ ) to the initial diameter of the droplet ( $D_0$ ). Figure 3.10.b) compares the numerical results for the spreading factor of different coating droplets that impinge on a tablet surface ( $U_0 = 2.5$  m/s) with the experimental data available (Bolleddula et al., 2010). The numerical results are in good agreement with the experimental data for all three viscous coating formulations.

Bolleddula et al. (2010) mentioned in their conclusions that the model from the literature which best predicted their experimental data for large droplets was the one from Roisman et al. (2002) who regarded that the impinging droplet has a lamella shape bounded by a rim. The numerical results of the kinematic phase model, and those of the model of Roisman et al. (2002), are compared with the experimental data for the three Opadry WhiteII HPMC coatings (impact velocity = 0.93 m/s) obtained by Bolleddula et al. (2010). The percentage errors of the spreading factor at the end of the inertia driven regime for both models are reported in Table 3.2. This shows that the model presented in this work predicts the behavior of the coating droplets (investigated by Bolleddula et al., 2010) better than the model from Roisman et al. (2002).

The numerical results presented in this section are in good agreement with experimental data obtained from several pharmaceutical coating droplets. The numerically calculated wetted area diameters and maximum droplet heights for different impact scenarios (impact velocity  $U_0$  and droplet diameter  $D_0$ ) and for different coating formulations are all in good agreement with the corresponding experimental measurements of Bolleddula et al. (2010).

### 3.3.2 Capillary phase results

In this subsection, the results for the capillary phase model are presented and compared to experimental data from the literature. The initial time for the numerical results of the capillary phase model is taken to be the time when the inertial forces become negligible at the end of the kinematic phase ( $t_0 = t_i$ ). The experimental data were taken from the recent paper of Lee et al. (2016). They used high-speed imaging and neutron radiography to quantify water absorption in porous materials from droplet deposition until depletion. For the validation of the capillary phase model it was assumed that the behavior of the absorbed droplet does not change significantly if the substrate is a pharmaceutical tablet of similar porosity and pore diameter.

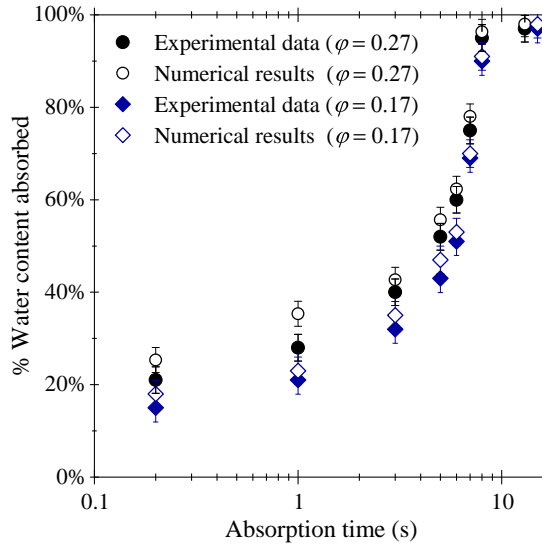


Figure 3.11: Capillary phase model results. Percentage of liquid content absorbed inside porous substrate of different porosities. Experimental data from Lee et al. (2016).

Figure 3.11 shows the capillary phase model predictions together with experimental data regarding the percentage of water content that is absorbed inside porous substrates (Savonnières and Meule stones) after impact of a 4.3 mg droplet on their surface. The numerical results and experimental data regarding the Savonnières and Meule stones are denoted in Figure 3.11 with circles and diamonds, respectively. The small over-prediction during the first seconds is likely due to the inability of the current model to account for the air trapped between the droplet and the substrate. The trapped air can impede the absorption of the droplet (Lee et al., 2016). The numerical results of the current model presented in this chapter follow the trend of the experimental data with a mean percentage error of 5.1%.

The ability of the model to predict the depth of the maximum wetting front distance from the surface is illustrated in Table 3.3 which compares this work with experimental data for Meule stones ( $\varphi = 16.6 \pm 0.3\%$  and  $d_p = 9.1 \pm 1.5 \mu\text{m}$ ). The measurement errors for the input parameters (porosity, pore diameter) were taken from the paper of Lee et al. (2016). This initial uncertainty for the porous matrix properties was propagated using the stochastic sampling method (Cacuci and Cacuci, 2003). The model predictions, along with their propagated error, are compared with experimental data whose error bars were estimated from the graphs presented by Lee et al. (2016).

Table 3.3: Validation of the numerical results and experimental data for the maximum wetting front depth during the capillary phase. Experiments by Lee et al. (2016).

Time (s)	Maximum wetting front depth (mm)		%  Error
	Numerical results	Experimental data	
0	0.00	0.00	0.0 %
3	-1.03	-1.00	3.0 %
6	-1.52	-1.50	1.3 %
9	-1.70	-1.65	3.0 %
12	-1.78	-1.70	4.7 %

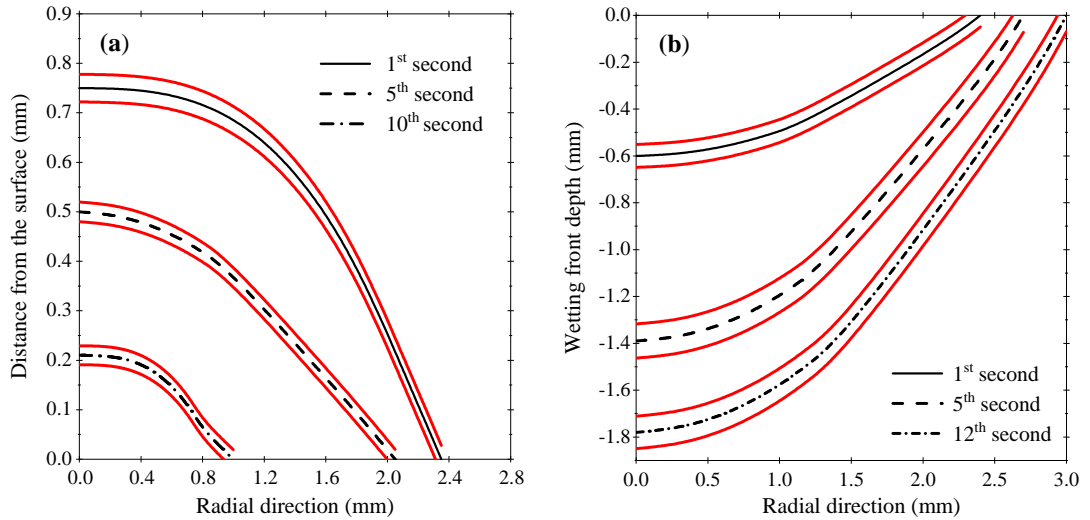


Figure 3.12: a) Droplet height profile on the surface after 1, 5 and 10 s, and b) wetting front profile in the substrate after 1, 5 and 12 s. The red lines denote the propagated error of the model input parameters

The model presented in this work for the capillary phase allows the dynamic simulation of spreading and absorbing of water droplets into porous tablets. Figures 3.12.a) and 3.12.b) illustrate the numerical results for the liquid movement above and below a porous substrate surface, respectively. The porous matrix ( $\varphi = 16.6 \pm 0.3\%$ ,  $d_p = 9.1 \pm 1.5 \mu\text{m}$ ) was assumed completely dry before the deposition of the droplet (droplet volume =  $4.3 \mu\text{l}$ ). Figures 3.12.a) and 3.12.b) show the depletion of the liquid from the surface and the evolution of the wetting front in the porous matrix. The red lines in Figure 3.12 represent the propagated measurement errors of the model input parameters. The absorption time calculated by the capillary model (12 s) is the same as that reported in the work of Lee et al. (2016).

Figures 3.13.a) and 3.13.b) compare capillary phase model results with experimental data for water droplet absorption in Savonnières porous stones (Lee et al., 2016). The error bars for the numerical results are estimated by propagating the uncertainty for the porosity and pore diameter of the Savonnières stones. Both the numerical results for the maximum droplet height (Fig. 3.13.a), and the distance of the wetting front from the surface of the porous substrate (Fig. 3.13.b), are in good agreement with the experimental data.

Previous models in the literature assume that the evaporation phenomena are negligible during the capillary phase (Alleborn and Raszillier, 2004; Siregar, 2012). This is because only the liquid absorption at room temperature and humidity conditions was considered. However, inside a coating drum, the temperature, relative humidity and air flow conditions accelerate evaporation. Therefore, in this work the evaporation velocity (Eq. 3.25) was taken into account since it affects the amount of liquid that is absorbed into the porous substrate. Figures 3.14.a) and 3.14.b) illustrate the difference in the absorption process between a model that neglects evaporation and the current approach. For the current approach, operating conditions that resemble those inside a pharmaceutical pan-coater were chosen ( $T_B = 50^\circ\text{C}$ ,  $RH = 50\%$ ), whereas for the model that neglects evaporation, the evaporation term on the right-hand side of Equation (3.24) was neglected.

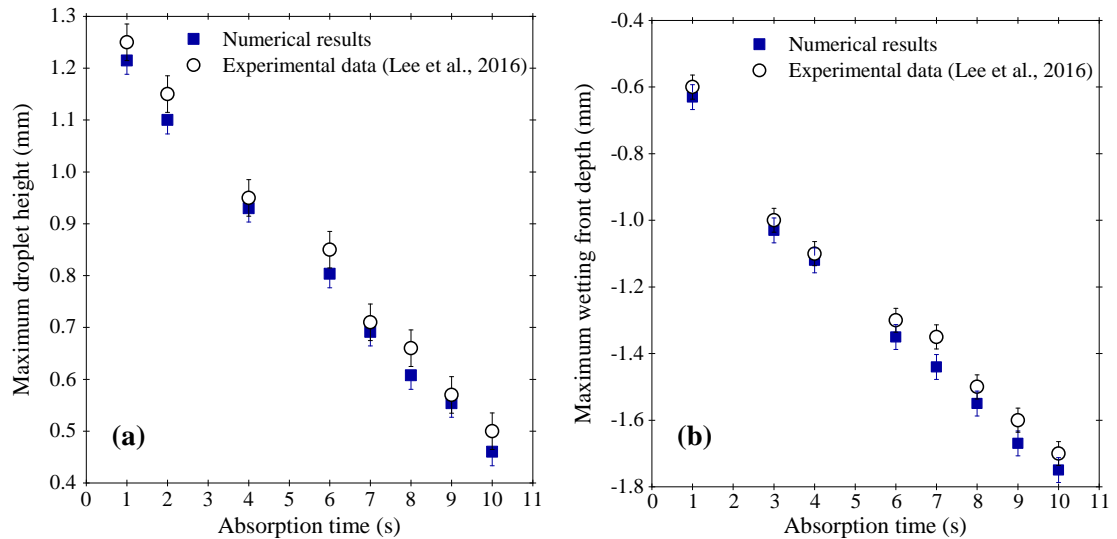


Figure 3.13: Comparison between simulation and experimental data for a) the maximum droplet height on the substrate surface, and b) the maximum wetting depth in the substrate. Experimental data from Lee et al. (2016).

The numerical results show that the effect of evaporation during the capillary phase is significant when the ambient conditions are similar to those in a pharmaceutical pan-coater. The droplet height profile in Figure 3.14.a) is significantly lower ( $\approx 0.5$  mm), after 3 s of absorption, when one accounts for the evaporation from the surface. Similarly, the final wetting front depth (distance from the surface) in Figure 3.14.b) is higher when one includes the evaporation from the surface velocity in the calculations.

Overall, the ability of the mathematical model, presented in this chapter, to predict the height profile of a single droplet above a porous substrate, and at the same time calculate the depth of the liquid (wetting) front inside this substrate, can be used to predict the water content on the surface and inside a pharmaceutical tablet during the film coating process.

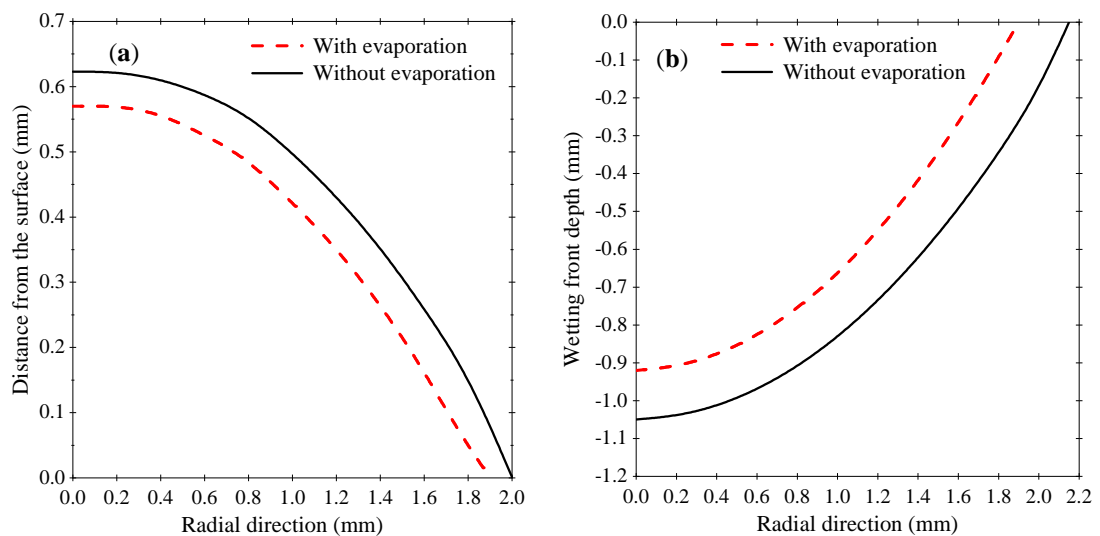


Figure 3.14: Effect of evaporation in liquid absorption during the capillary phase, a) Droplet height profiles after 3 s. b) Final wetting front profile inside the porous matrix.

### 3.4 Concluding remarks

The mathematical model presented in this chapter aimed to numerically simulate the behavior of a single droplet after impingement on a porous tablet in pharmaceutical film-coating process conditions. The 1D droplet spreading model for the initial impact period was combined successfully with the lubrication approximation method for the capillary phase model which describes the droplet evaporation and absorption into the tablet. The combination of the two models that were presented in this chapter is a novel approach that can provide an estimate for the water content of a pharmaceutical tablet after droplet impingement during the film-coating process.

The validation with experimental data from different studies showed that the numerical model presented in Section 2 of this chapter is predictive and can be used to simulate droplet impact, spreading, absorption and evaporation from porous pharmaceutical tablets. The 1D mechanical energy balance equation model that was presented, accurately simulated the spreading of the droplet during the first milliseconds after impact when the inertial forces are significant. Moreover, the capillary phase model based on the lubrication approximation was successfully coupled with the initial impact model and enhanced to include a prediction for evaporation during absorption. The numerical results for spreading and absorption were validated with experimental data from Bolleddula et al. (2010) and Lee et al. (2016).

The work presented in this chapter aims to provide information about the aqueous film-coating process that is widely utilized within the pharmaceutical industry. The insight from the single-droplet model can help to understand the phenomena that take place at the point of impact between tablet and coating. However, during film-coating multiple droplets (spray) impinge simultaneously on the same tablet. Thus, in the next chapter, a detailed model that deals with spray impingement on tablets is developed. Additionally, the modification of the existent models in the next chapters is useful in order to be able to simulate the spreading and absorption of whole coating films on tablet surfaces. In Chapter 5, thin film absorption and drying is studied while also taking into account the presence of solid particles in the coating formulation.

### 3.5 Appendix of Chapter 3

In this Appendix, the mechanical energy equation used in the model presented in this chapter is derived (Subsection 3.5.1) and the main assumptions regarding viscous dissipation in the boundary layer are further justified (Subsection 3.5.2).

#### 3.5.1 Mechanical energy balance equation derivation

The mechanical energy balance equation in the form of Equation (3.2) in Chapter 3 - without the term for the rate of work done by the droplet surroundings - has been used several times in the literature (Attane et al., 2007). However, to the best of the author's knowledge, no rigorous derivation has ever been reported.

Consider as control volume the entire droplet. The two surfaces that bound the droplet are dividing surfaces. The first, denoted by  $\mathcal{S}_{12}$ , is the interface between the liquid and the gas, while the second, denoted by  $\mathcal{S}_{13}$ , is the interface between the liquid and the solid. The interface  $\mathcal{S}_{23}$  between the gas and the solid is not included in the control volume. The three dividing surfaces meet at the common line  $\mathcal{C}$ . The three-dimensional spatial region bounded by the dividing surfaces  $\mathcal{S}_{12}$  and  $\mathcal{S}_{13}$  is denoted by  $\mathcal{R}_1$ . The derivation of the integral mechanical energy balance equation over the control volume is presented here. The derivation is based here on the generalized transport theorem, following the approach of Slattery et al. (2007). Let us consider:

$$D_t \int_{\mathcal{R}_1} e_1 d\mathbf{x} + D_t \int_{\mathcal{S}_{12}} e_{12} d\mathbf{s} + D_t \int_{\mathcal{S}_{13}} e_{13} d\mathbf{s} \quad (\text{a1})$$

where

$$e_1 \equiv (1/2) \rho_1 \mathbf{u}_1 \cdot \mathbf{u}_1 \quad ; \quad e_{12} \equiv (1/2) \rho_{12} \mathbf{u}_{12} \cdot \mathbf{u}_{12} \quad ; \quad e_{13} \equiv (1/2) \rho_{13} \mathbf{u}_{13} \cdot \mathbf{u}_{13} \quad (\text{a2})$$

Here  $\rho_r$  and  $\mathbf{u}_r$  are the fluid density and velocity fields within the region  $\mathcal{R}_r$ , whereas  $\rho_{rs}$  and  $\mathbf{u}_{rs}$  are the fluid density and velocity fields over the surface  $\mathcal{S}_{rs}$ . Using the generalized transport theorem, one can manipulate each term individually. First, it is:

$$D_t \int_{\mathcal{R}_1} e_1 d\mathbf{x} = \int_{\mathcal{R}_1} \partial_t e_1 d\mathbf{x} + \int_{\mathcal{S}_{12}} \mathbf{n}_{12} \cdot \mathbf{u}_{12} e_1 d\mathbf{s} + \int_{\mathcal{S}_{13}} \mathbf{n}_{13} \cdot \mathbf{u}_{13} e_1 d\mathbf{s} \quad (\text{a3})$$

where  $\mathbf{n}_{rs}$  denotes the unit vector normal to  $\mathcal{S}_{rs}$  pointing from phase  $r$  into phase  $s$  (therefore, it is outwardly directed for region  $\mathcal{R}_r$ ). For the second integral in Equation (a1):

$$D_t \int_{\mathcal{S}_{12}} e_{12} d\mathbf{s} = \int_{\mathcal{S}_{12}} \left( \dot{\nabla} e_{12} - 2 \mathcal{H}_{12} \mathbf{n}_{12} \cdot \mathbf{u}_{12} e_{12} \right) d\mathbf{s} + \int_{\mathcal{C}} \mathbf{m}_{12} \cdot \mathbf{u}_{\mathcal{C}} e_{12} d\mathbf{s} \quad (\text{a4})$$

Here  $\mathcal{H}_{rs}$  is the mean curvature of the surface  $\mathcal{S}_{rs}$ , whereas  $\mathbf{m}_{rs}$  is the unit vector tangent to the surface  $\mathcal{S}_{rs}$ , normal to the line  $\mathcal{C}$  and outwardly directed. Moreover,  $\mathbf{u}_{\mathcal{C}}$  is the fluid velocity field over  $\mathcal{C}$  and  $\dot{\nabla}$  denotes the invariant time derivative operator (Grinfeld, 2013) defined as:

$$\dot{\nabla} e_{rs} \equiv \partial_t e_{rs} - \mathbf{v}_{rs} \cdot \partial_{\mathbf{s}} e_{rs} \quad (\text{a5})$$

In this equation,  $\partial_t e_{rs}$  is calculated while holding the surface coordinates constant; therefore, this derivative depends on the parametrization, that is, on the choice of surface coordinates. Also  $\mathbf{v}_{rs}$ , which represents the coordinate velocity of the surface (that is, the time rate of change of spatial position following a surface point with fixed surface coordinates), depends on the parametrization. Conversely, the surface gradient  $\partial_s e_{rs}$  and the time derivative  $\dot{\nabla} e_{rs}$  are invariants and do have a clear physical meaning.

Finally, for the third integral in Equation (a1), one can write a similar expression:

$$D_t \int_{S_{13}} e_{13} ds = \int_{S_{13}} \left( \dot{\nabla} e_{13} - 2 \mathcal{H}_{13} \mathbf{n}_{13} \cdot \mathbf{u}_{13} e_{13} \right) ds + \int_C \mathbf{m}_{13} \cdot \mathbf{u}_C e_{13} ds \quad (\text{a6})$$

These equations can be manipulated further using the divergence theorem. Let us start with Equation (a3); by applying this theorem to the region  $\mathcal{R}_1$ , the following relation is obtained:

$$\int_{\mathcal{R}_1} \partial_x \cdot (\mathbf{u}_1 e_1) dx = \int_{S_{12}} \mathbf{n}_{12} \cdot \mathbf{u}_1 e_1 ds + \int_{S_{13}} \mathbf{n}_{13} \cdot \mathbf{u}_1 e_1 ds \quad (\text{a7})$$

Notice that while in the generalized surface transport theorem the surface integrals feature the velocity of the bounding surface (in Equation a3 these velocities are  $\mathbf{u}_{12}$  and  $\mathbf{u}_{13}$ ), in the divergence theorem the surface integrals feature the velocity of the fluid evaluated at the boundary of the region - but within the region (in Equation a7 this velocity is  $\mathbf{u}_1$ ).

So, Equation (a3) can be written as follows:

$$\begin{aligned} D_t \int_{\mathcal{R}_1} e_1 dx &= \int_{\mathcal{R}_1} [\partial_t e_1 + \partial_x \cdot (\mathbf{u}_1 e_1)] dx - \int_{S_{12}} \mathbf{n}_{12} \cdot (\mathbf{u}_1 - \mathbf{u}_{12}) e_1 ds \\ - \int_{S_{13}} \mathbf{n}_{13} \cdot (\mathbf{u}_1 - \mathbf{u}_{13}) e_1 ds &= \int_{\mathcal{R}_1} [\partial_t e_1 + \partial_x \cdot (\mathbf{u}_1 e_1)] dx - \int_{S_{12}} \dot{V}_{12} e_1 ds - \int_{S_{13}} \dot{V}_{13} e_1 ds \end{aligned} \quad (\text{a8})$$

where:

$$\dot{V}_{12} \equiv \mathbf{n}_{12} \cdot (\mathbf{u}_1 - \mathbf{u}_{12}) \quad ; \quad \dot{V}_{13} \equiv \mathbf{n}_{13} \cdot (\mathbf{u}_1 - \mathbf{u}_{13}) \quad (\text{a9})$$

For Equation (a4):

$$\int_{S_{12}} \partial_s \cdot (\mathbf{u}_{12} e_{12}) ds = \int_C \mathbf{m}_{12} \cdot \mathbf{u}_{12} e_{12} ds - \int_{S_{12}} 2 \mathcal{H}_{12} \mathbf{n}_{12} \cdot \mathbf{u}_{12} e_{12} ds \quad (\text{a10})$$

So, one obtains:

$$\begin{aligned} D_t \int_{S_{12}} e_{12} ds &= \int_{S_{12}} \left[ \dot{\nabla} e_{12} + \partial_s \cdot (\mathbf{u}_{12} e_{12}) \right] ds - \int_C \mathbf{m}_{12} \cdot (\mathbf{u}_{12} - \mathbf{u}_C) e_{12} ds \\ &= \int_{S_{12}} \left[ \dot{\nabla} e_{12} + \partial_s \cdot (\mathbf{u}_{12} e_{12}) \right] ds - \int_C \dot{V}_{12,C} e_{12} ds \end{aligned} \quad (\text{a11})$$

With similar passages, one can also obtain:

$$D_t \int_{S_{13}} e_{13} ds = \int_{S_{13}} \left[ \dot{\nabla} e_{13} + \partial_s \cdot (\mathbf{u}_{13} e_{13}) \right] ds - \int_C \dot{V}_{13,C} e_{13} ds \quad (\text{a12})$$

where:

$$\dot{V}_{12,C} \equiv \mathbf{n}_{12} \cdot (\mathbf{u}_{12} - \mathbf{u}_C) \quad ; \quad \dot{V}_{13,C} \equiv \mathbf{n}_{13} \cdot (\mathbf{u}_{13} - \mathbf{u}_C) \quad (\text{a13})$$

The results derived permit us to write:

$$\begin{aligned} & D_t \int_{\mathcal{R}_1} e_1 d\mathbf{x} + D_t \int_{S_{12}} e_{12} d\mathbf{s} + D_t \int_{S_{13}} e_{13} d\mathbf{s} \\ &= \int_{\mathcal{R}_1} [\partial_t e_1 + \partial_{\mathbf{x}} \cdot (\mathbf{u}_1 e_1)] d\mathbf{x} + \int_{S_{12}} [\dot{\nabla} e_{12} + \partial_{\mathbf{s}} \cdot (\mathbf{u}_{12} e_{12})] d\mathbf{s} \\ & \quad + \int_{S_{13}} [\dot{\nabla} e_{13} + \partial_{\mathbf{s}} \cdot (\mathbf{u}_{13} e_{13})] d\mathbf{s} - \int_{S_{12}} e_1 \dot{V}_{12} d\mathbf{s} \\ & \quad - \int_{S_{13}} e_1 \dot{V}_{13} d\mathbf{s} - \int_C (e_{12} \dot{V}_{12,C} + e_{13} \dot{V}_{13,C}) d\mathbf{s} \end{aligned} \quad (\text{a14})$$

In the specific problems investigated in Chapter 3, there is no mass transfer between the phases; the equation above, consequently, may be simplified. In particular, the last line vanishes, because the velocities of the material particles, of the surface particles and of the common line particles are all equal at the boundaries. Hence, the volume and surface flow rates introduced in Equations (a9) and (a13) are zero.

Equation (a14) then becomes:

$$\begin{aligned} & D_t \int_{\mathcal{R}_1} e_1 d\mathbf{x} + D_t \int_{S_{12}} e_{12} d\mathbf{s} + D_t \int_{S_{13}} e_{13} d\mathbf{s} = \int_{\mathcal{R}_1} [\partial_t e_1 + \partial_{\mathbf{x}} \cdot (\mathbf{u}_1 e_1)] d\mathbf{x} \\ & \quad + \int_{S_{12}} [\dot{\nabla} e_{12} + \partial_{\mathbf{s}} \cdot (\mathbf{u}_{12} e_{12})] d\mathbf{s} + \int_{S_{13}} [\dot{\nabla} e_{13} + \partial_{\mathbf{s}} \cdot (\mathbf{u}_{13} e_{13})] d\mathbf{s} \end{aligned} \quad (\text{a15})$$

To manipulate this equation further, one needs to integrate over the region  $\mathcal{R}_1$  the mechanical energy balance equation holding for single-phase fluids (Bird et al., 2007). This gives:

$$\int_{\mathcal{R}_1} [\partial_t e_1 + \partial_{\mathbf{x}} \cdot (\mathbf{u}_1 e_1)] d\mathbf{x} = - \int_{\mathcal{R}_1} [\partial_{\mathbf{x}} \cdot (\boldsymbol{\sigma}_1 \cdot \mathbf{u}_1) - \boldsymbol{\tau}_1 : \partial_{\mathbf{x}} \mathbf{u}_1 - \rho_1 \mathbf{u}_1 \cdot \mathbf{g}] d\mathbf{x} \quad (\text{a16})$$

where it has been assumed that the fluid is incompressible, so that the field  $\mathbf{u}_1$  is solenoidal. Here  $\boldsymbol{\sigma}_1$  is the fluid stress tensor field within region  $\mathcal{R}_1$  and  $\boldsymbol{\tau}_1$  is its deviatoric part; and  $\mathbf{g}$  is the gravitational field. The first term on the right-hand side can be expressed as:

$$\int_{\mathcal{R}_1} \partial_{\mathbf{x}} \cdot (\boldsymbol{\sigma}_1 \cdot \mathbf{u}_1) d\mathbf{x} = \int_{S_{12}} \mathbf{n}_{12} \cdot \boldsymbol{\sigma}_1 \cdot \mathbf{u}_1 d\mathbf{s} + \int_{S_{13}} \mathbf{n}_{13} \cdot \boldsymbol{\sigma}_1 \cdot \mathbf{u}_1 d\mathbf{s} \quad (\text{a17})$$

Moreover

$$\int_{\mathcal{R}_1} \rho_1 \mathbf{u}_1 \cdot \mathbf{g} d\mathbf{x} = - \int_{\mathcal{R}_1} \mathbf{u}_1 \cdot \partial_{\mathbf{x}} f_1 d\mathbf{x} = - D_t \int_{\mathcal{R}_1} f_1 d\mathbf{x} \quad (\text{a18})$$

where  $f_1$  is the potential energy per unit volume of the gravitational field in the region considered (as pointed out, this region identifies a material body because no mass transfer between the phases is present).

The last two equations allow Equation (a16) to be written in the following form:

$$\begin{aligned} \int_{\mathcal{R}_1} [\partial_t e_1 + \partial_{\mathbf{x}} \cdot (\mathbf{u}_1 e_1)] d\mathbf{x} = & - D_t \int_{\mathcal{R}_1} f_1 d\mathbf{x} - \int_{\mathcal{S}_{12}} \mathbf{n}_{12} \cdot \boldsymbol{\sigma}_1 \cdot \mathbf{u}_1 ds \\ & - \int_{\mathcal{S}_{13}} \mathbf{n}_{13} \cdot \boldsymbol{\sigma}_1 \cdot \mathbf{u}_1 ds + \int_{\mathcal{R}_1} \boldsymbol{\tau}_1 : \partial_{\mathbf{x}} \mathbf{u}_1 d\mathbf{x} \end{aligned} \quad (\text{a19})$$

The last two terms on the right-hand side of Equation (a15) can be treated by adopting a similar strategy. Let us integrate over the surface  $\mathcal{S}_{12}$  the jump mechanical energy balance equation (Slattery et al., 2007, Delhaye, 1974). Doing so yields the following integral equation:

$$\begin{aligned} \int_{\mathcal{S}_{12}} [\dot{\nabla} e_{12} + \partial_{\mathbf{s}} \cdot (\mathbf{u}_{12} e_{12})] ds = & \int_{\mathcal{S}_{12}} [\mathbf{n}_{12} \cdot (\boldsymbol{\sigma}_1 - \boldsymbol{\sigma}_2) \cdot \mathbf{u}_{12} + 2 \mathcal{H}_{12} \mathbf{n}_{12} \cdot \mathbf{u}_{12} \gamma_{12}] ds \\ & + \int_{\mathcal{S}_{12}} [\mathbf{u}_{12} \cdot \partial_{\mathbf{s}} \gamma_{12} + \rho_{12} \mathbf{u}_{12} \cdot \mathbf{g}] ds \end{aligned} \quad (\text{a20})$$

Here  $\boldsymbol{\sigma}_2$  is the fluid stress tensor within the region occupied by phase 2, which in this case is the gas, and  $\gamma_{12}$  is the surface tension on  $\mathcal{S}_{12}$ . In writing the equation above, it is assumed that the surface stress tensor is isotropic, so that no viscous part is present. Assuming that  $\gamma_{12}$  is uniform (that is, independent of position), the first term on the second line of Equation (a20) vanishes. Moreover, if the surface densities are assumed constant and uniform, then:

$$\begin{aligned} \int_{\mathcal{S}_{12}} \rho_{12} \mathbf{u}_{12} \cdot \mathbf{g} ds = & - \int_{\mathcal{S}_{12}} \mathbf{u}_{12} \cdot \partial_{\mathbf{x}} f_{12} ds = - \int_{\mathcal{S}_{12}} \mathbf{u}_{12} \cdot (\mathbf{I} \cdot \partial_{\mathbf{x}} f_{12}) ds \\ = & - \int_{\mathcal{S}_{12}} \mathbf{u}_{12} \cdot [(\mathbf{n}_{12} \mathbf{n}_{12} + \mathbf{P}) \cdot \partial_{\mathbf{x}} f_{12}] ds = - \int_{\mathcal{S}_{12}} [\mathbf{u}_{12} \cdot (\mathbf{n}_{12} \mathbf{n}_{12} \cdot \partial_{\mathbf{x}} f_{12}) + \mathbf{u}_{12} \cdot (\mathbf{P} \cdot \partial_{\mathbf{x}} f_{12})] ds \\ = & - \int_{\mathcal{S}_{12}} (\dot{\nabla} f_{12} + \mathbf{u}_{12} \cdot \partial_{\mathbf{s}} f_{12}) ds = - \int_{\mathcal{S}_{12}} [\dot{\nabla} f_{12} + \partial_{\mathbf{s}} \cdot (\mathbf{u}_{12} f_{12})] ds \\ = & - \int_{\mathcal{S}_{12}} (\dot{\nabla} f_{12} - 2 \mathcal{H}_{12} \mathbf{n}_{12} \cdot \mathbf{u}_{12} e_{12}) ds - \int_{\mathcal{C}} \mathbf{m}_{12} \cdot \mathbf{u}_{12} e_{12} ds = - D_t \int_{\mathcal{S}_{12}} f_{12} ds \end{aligned} \quad (\text{a21})$$

where  $\mathbf{I}$  and  $\mathbf{P}$  are the identity tensor and the projection tensor, respectively, and  $f_{12}$  is the potential energy per unit surface of the gravitational field over the surface considered.

Above, in the passage on the third line, the term  $\mathbf{u}_{12} \cdot \partial_{\mathbf{s}} f_{12}$  has been replaced with  $\partial_{\mathbf{s}} (\mathbf{u}_{12} \cdot f_{12})$ . In general, the two terms differ by the amount  $f_{12} \partial_{\mathbf{s}} \cdot \mathbf{u}_{12}$ . However, because no mass transfer takes place between the phases, and because the surface density has been assumed to be constant and uniform, the surface velocity field  $\mathbf{u}_{12}$  is solenoidal. To show this, the jump mass balance equation is employed, which reads:

$$\dot{\nabla} \rho_{12} = \rho_1 \dot{V}_{12} + \rho_2 \dot{V}_{21} - \partial_{\mathbf{s}} \cdot (\rho_{12} \mathbf{u}_{12}) \quad (\text{a22})$$

In this equation, because of the assumptions just reported, the invariant time derivative and the mass transfer terms are zero; therefore, so is the divergence of  $\rho_{12} \mathbf{u}_{12}$ . But since the density is uniform, this implies that the velocity field is divergence-free. This completes the proof.

To manipulate the term in Equation (a20) involving the mean curvature of the surface, it is assumed that the shape of the droplet is that of a spherical cap. This means that  $\mathcal{S}_{13}$  is a disk, whose radius is denoted by  $R_d$ , while the common line is a circle. Exploiting the radial symmetry, one can then write:

$$\begin{aligned}
\int_{\mathcal{S}_{12}} 2\mathcal{H}_{12} \mathbf{n}_{12} \cdot \mathbf{u}_{12} \gamma_{12} ds &= \int_{\mathcal{C}} \mathbf{m}_{12} \cdot \mathbf{u}_{12} \gamma_{12} ds - D_t \int_{\mathcal{S}_{12}} \gamma_{12} ds \\
&= \gamma_{12} \left( \mathbf{m}_{12} \cdot \mathbf{u}_{12} \int_{\mathcal{C}} ds - D_t \int_{\mathcal{S}_{12}} ds \right) \\
&= \gamma_{12} \left[ |\mathbf{u}_{12}| (2\pi R_d) \cos \vartheta - D_t A_{12} \right] = \gamma_{12} \left[ D_t R_d (2\pi R_d) \cos \vartheta - D_t A_{12} \right] \\
&= \gamma_{12} \left[ D_t (\pi R_d^2) \cos \vartheta - D_t A_{12} \right] = \gamma_{12} D_t (A_{13} \cos \vartheta - A_{12}) \tag{a23}
\end{aligned}$$

where it has been assumed that the surface tension is constant (in addition to being uniform). Moreover,  $\vartheta$  is the dynamic contact angle - which is not expected to be equal to the equilibrium contact angle, even if one often replaces the former with the latter - whilst  $A_{r_s}$  denotes the area of  $\mathcal{S}_{r_s}$ . Equation (a23) holds for the case of a cylindrical droplet or film where the surface  $\mathcal{S}_{13}$  is a disk of radius  $R_f$ .

The relations derived above allow us to write Equation (a20) in the following form:

$$\begin{aligned}
\int_{\mathcal{S}_{12}} [\dot{\nabla} e_{12} + \partial_s \cdot (\mathbf{u}_{12} e_{12})] ds &= -D_t \left[ \int_{\mathcal{S}_{12}} f_{12} ds + \gamma_{12} (A_{12} - A_{13} \cos \vartheta) \right] \\
&\quad + \int_{\mathcal{S}_{12}} \mathbf{n}_{12} \cdot (\boldsymbol{\sigma}_1 - \boldsymbol{\sigma}_2) \cdot \mathbf{u}_{12} ds \tag{a24}
\end{aligned}$$

The last term on the right-hand side of Equation (a15) can be treated similarly; however, since the surface  $\mathcal{S}_{13}$  is flat, the term involving the mean curvature vanishes and the final result is:

$$\int_{\mathcal{S}_{13}} [\dot{\nabla} e_{13} + \partial_s \cdot (\mathbf{u}_{13} e_{13})] ds = -D_t \int_{\mathcal{S}_{13}} f_{13} ds + \int_{\mathcal{S}_{13}} \mathbf{n}_{13} \cdot (\boldsymbol{\sigma}_1 - \boldsymbol{\sigma}_3) \cdot \mathbf{u}_{13} ds \tag{a25}$$

One can now introduce the last two equations and Equation (a19) into (a15) and doing this yields the integral mechanical energy balance equation:

$$\begin{aligned}
D_t \left[ \int_{\mathcal{R}_1} (e_1 + f_1) d\mathbf{x} + \int_{\mathcal{S}_{12}} (e_{12} + f_{12}) ds + \int_{\mathcal{S}_{13}} (e_{13} + f_{13}) ds + \gamma_{12} (A_{12} - A_{13} \cos \vartheta) \right] \\
= \int_{\mathcal{S}_{12}} \mathbf{n}_{21} \cdot \boldsymbol{\sigma}_2 \cdot \mathbf{u}_{12} ds + \int_{\mathcal{S}_{13}} \mathbf{n}_{31} \cdot \boldsymbol{\sigma}_3 \cdot \mathbf{u}_{13} ds + \int_{\mathcal{R}_1} \boldsymbol{\tau}_1 : \partial_x \mathbf{u}_1 d\mathbf{x} \tag{a26}
\end{aligned}$$

The left-hand side features the rate of change of the total energy of the droplet, which comprises kinetic energy, potential energy and surface energy, while the right-hand side features the rate of work performed by phases 2 and 3 on the droplet and the rate of conversion of mechanical energy into internal energy due to the action of the viscous stress within the droplet.

### 3.5.2 Estimation of the rate of viscous dissipation in the droplet-film boundary layer

In this section, the rate of viscous dissipation of the droplet kinetic energy in the boundary layer of thickness  $\delta$  near the tablet surface (Fig. 3.3; Section 3.2.1), where viscous dissipation is significant, is estimated.

In the boundary layer, a functional form for the velocity field  $\mathbf{u}_1$  is not available. Thus, one cannot solve the following volume integral rigorously:

$$\Phi_\delta = - \int_{\mathcal{R}_\delta} \boldsymbol{\tau}_1 : \partial_{\mathbf{x}} \mathbf{u}_1 d\mathbf{x} \quad (\text{a27})$$

However, the value of the rate of viscous dissipation in the boundary layer  $\Phi_\delta$  can be estimated using scaling analysis. The rate of viscous dissipation of kinetic energy in the boundary layer region  $\mathcal{R}_\delta$  is given by:

$$\begin{aligned} \Phi_\delta &= - \int_{\mathcal{R}_\delta} \boldsymbol{\tau}_1 : \partial_{\mathbf{x}} \mathbf{u}_1 d\mathbf{x} = \int_{\mathcal{R}_\delta} \left[ \tau_{rr} \frac{\partial u_{1r}}{\partial r} + \tau_{rz} \frac{\partial u_{1r}}{\partial z} + \tau_{\theta\theta} \left( \frac{u_{1r}}{r} \right) + \tau_{zr} \frac{\partial u_{1z}}{\partial r} + \tau_{zz} \frac{\partial u_{1z}}{\partial z} \right] d\mathbf{x} \\ &= \int_{\mathcal{R}_\delta} \left[ 2\mu_1 \left( \frac{\partial u_{1r}}{\partial r} \right)^2 + \mu_1 \left( \frac{\partial u_{1r}}{\partial z} + \frac{\partial u_{1z}}{\partial r} \right) \frac{\partial u_{1r}}{\partial z} \right. \\ &\quad \left. + \mu_1 \left( \frac{u_{1r}}{r} \right)^2 + \mu_1 \left( \frac{\partial u_{1r}}{\partial z} + \frac{\partial u_{1z}}{\partial r} \right) \frac{\partial u_{1z}}{\partial r} + 2\mu_1 \left( \frac{\partial u_{1z}}{\partial z} \right)^2 \right] d\mathbf{x} \end{aligned} \quad (\text{a28})$$

To estimate  $\Phi_\delta$  the following local scales are introduced:

$$\frac{\partial u_{1r}}{\partial r} \sim \frac{v_r}{R_d} ; \quad \frac{\partial u_{1r}}{\partial z} \sim \frac{v_r}{\delta} ; \quad \frac{\partial u_{1z}}{\partial z} \sim \frac{v_z}{\delta} \quad (\text{a29})$$

where  $v_r$  and  $v_z$  are local scales of the radial and vertical velocity in the boundary layer of thickness  $\delta$ , and  $R_d$  is the radius of the area of the tablet wetted by the droplet.

In this work, it was considered that  $\partial_r u_{1z}$  is negligible since the changes of the vertical velocity ( $u_{1z}$ ) in the radial direction are expected to be very small inside the boundary layer. The boundary layer thickness  $\delta$  is given by Equation (3.5) in Section 3.2.1.

Substituting the scales above into Equation (a28) gives:

$$\Phi_\delta \sim \int_{\mathcal{R}_\delta} \left[ 3\mu_1 \left( \frac{v_r}{R_d} \right)^2 + \mu_1 \left( \frac{v_r}{\delta} \right)^2 + 2\mu_1 \left( \frac{v_z}{\delta} \right)^2 \right] d\mathbf{x} \quad (\text{a30})$$

The first term in the integral on the right-hand side of Equation (a30) can be neglected since  $R_d \gg \delta$ . To relate the scales of the radial and vertical velocities, the continuity equation is used:

$$\frac{1}{r} \left( r \frac{\partial u_{1r}}{\partial r} + u_{1r} \right) + \frac{\partial u_{1z}}{\partial z} = 0 \Rightarrow \frac{v_r}{R_d} \sim \frac{v_z}{\delta} \Rightarrow v_z \sim \frac{\delta}{R_d} v_r \quad (\text{a31})$$

Substituting Equation (a31) into (a30) yields:

$$\Phi_\delta \sim \int_{\mathcal{R}_\delta} \left[ \mu_1 \left( \frac{v_r}{\delta} \right)^2 + 2 \mu_1 \left( \frac{v_r}{R_d} \right)^2 \right] d\mathbf{x} \sim \int_{\mathcal{R}_\delta} \mu_1 \left( \frac{v_r}{\delta} \right)^2 d\mathbf{x} \sim \frac{\mu_1}{\delta^2} \int_{\mathcal{R}_\delta} v_r^2 d\mathbf{x} \quad (\text{a32})$$

Since the scale of a dependent variable is its maximum value in the region of interest, in the boundary layer one can take  $u_{1r}$  to be equal to  $v_r$ , where  $u_{1r}$  is given by Equation (3.9). Using the relation  $d\mathbf{x} = \delta d\mathbf{s}$ , denoting the wetted area under the droplet by  $\mathcal{S}_{13}$ , Equation (a32) becomes:

$$\Phi_\delta \sim \frac{\mu_1}{\delta} \int_{\mathcal{S}_{13}} u_{1r}^2 d\mathbf{s} \quad (\text{a33})$$

Equation (a33) was employed in the model presented in Chapter 3 (Section 3.2.1) to estimate the rate of viscous dissipation of the droplet kinetic energy in the boundary layer of thickness  $\delta$  near the tablet surface.

# CHAPTER 4

## Spray impingement onto a tablet

---

This chapter deals with coating spray impingement onto pharmaceutical tablets. A mathematical model that predicts liquid coating spreading on the surface of a tablet while it passes under a spray is developed. The output of the model provides useful insight into the coating film formation, thickness and spreading rate on dry tablet cores during the film-coating process.

---

Publication which has arisen from this work: Christodoulou, C., Sorensen, E., García-Muñoz, S. and Mazzei, L., 2019. Mathematical modeling of spray impingement and film formation on pharmaceutical tablets during coating. Submitted.

### 4.1 Introduction

Understanding the phenomena taking place during coating application on a solid dosage form provides important information that can be used to reduce the number of defective tablets and select the optimal conditions for the film-coating process. This chapter aims to provide insight into the process of spray impingement onto pharmaceutical tablets which can assist in the selection of the appropriate values for the process parameters required to enhance the quality of the final product.

In this chapter, coating spray impingement and film spreading on a tablet core while the tablet passes through the area under the spray in a rotating coating drum is investigated. A mathematical model that can describe spray impact on tablets during film-coating is developed. The current model does not require prior knowledge of the process via empirical relations or experimental data, and it is based on the mechanical energy equation as in the single droplet impact case (Chapter 3).

The spray-impingement model presented here accurately predicts the time required for the wetting of the entire tablet surface that faces the spray as well as the liquid film thickness, while taking into account coating (viscosity, density, surface tension) and spray (droplet size, velocity, mass flow rate) properties. Furthermore, sensitivity analysis was performed to study the effect of coating properties and process parameters on the film spreading rate and on the final liquid film thickness.

In comparison with commercial CFD simulations, which take hours or days to give results, the model presented here provides solutions considerably faster (CPU time < 5s) without sacrificing accuracy significantly. This computational efficiency allows one to perform variance-based sensitivity analysis to study the influence of process parameters on the coating spreading behavior. The mathematical model was implemented employing the gPROMS Modelbuilder platform (Process Systems Enterprise Ltd., 2019) and the numerical results were validated with experimental data from the literature.

## 4.2 Mathematical model

Film coatings are generally applied on tablets by spraying a coating formulation on their surface (Felton, 2003). After impingement onto the tablet, the droplets spread on its dry surface and form a thin film. Based on the experimental work of Bolleddula et al. (2010) for pharmaceutical coating droplets, we assumed that the droplets spread without disintegrating or rebounding after impact. As discussed in the previous chapter, the spreading of a single droplet that impacts on a dry rigid substrate can be divided into two consecutive regimes: during the first the spreading is inertia-driven (kinematic phase), while during the second it is capillarity-driven (capillary phase).

Continuous droplet impingement leads to the expansion of the wetted area and the formation of a liquid film that eventually covers the entire surface of the tablet. Following the liquid film formation, the solvent (normally water) both evaporates, and concurrently absorbs into the porous core of the tablet, leaving behind a dry polymeric film on the tablet surface (Fig. 4.1). In this chapter, multiple droplet impact and spreading on a pharmaceutical tablet while it passes through the area under the spray of a rotating coating drum is investigated.

To model spray impingement, it was assumed that the spray is uniform and it is divided into arrays of droplets that impinge successively onto the substrate orthogonally to its surface (Fig. 4.2.a). To simplify the problem, it was also considered that over a time interval of magnitude  $t_i = D_0/U_0$ , where  $D_0$  and  $U_0$  represent the average diameter and velocity of the droplets before impact, respectively, the droplets in the first array impinge and spread without being affected by the subsequent droplets. The value of  $t_i$  has the same order of magnitude as the time scale of the inertia-driven spreading regime reported in the literature (Bolleddula et al., 2010). Since the capillarity spreading is much slower, becoming significant only after several seconds, this type of spreading can be neglected. At any given time  $t < t_i$ , the wetted area can be estimated by calculating the spreading of a single droplet of initial diameter  $D_0$  and impact velocity  $U_0$  (Fig. 4.2.b), and by assuming that all the droplets of the first array behave independently and identically as they impact on the dry tablet surface. To check the validity of the above assumptions the model was validated against experimental data from the literature. The reasonably good agreement of the model predictions with the experiments showed that the aforementioned assumptions are acceptable.

After the impact of the first array (initial tablet wetting), it was assumed that the wetted area is made up of disconnected films, one associated with each droplet. The impingement of subsequent droplets on the surface of these films increases their volume, making them spread further and raising their thickness.



Figure 4.1: Outline of the coating application process during pharmaceutical coating.

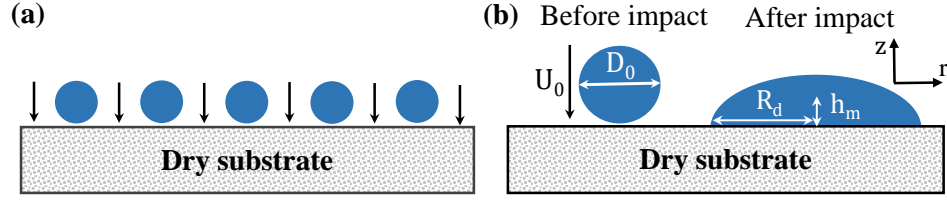


Figure 4.2: a) Droplet array, and b) single droplet impact on a dry tablet.

The spreading was considered to be completed when the wetted area becomes equal to the area of the tablet surface that is facing the spray, i.e. when the table surface has been completely covered. Here, it was assumed that coating liquid evaporation and absorption into the tablet core become significant after the tablet is no longer under the spray, and therefore drying and absorption phenomena are neglected. This assumption was based on experimental observations which show that film absorption and drying are significantly slower than coating spreading after spray impact (Niblett et al., 2017; Shaari, 2007).

In this section, the mathematical model is presented in two subsections: Subsection 4.2.1 concerns the impact of the first array of droplets onto the dry tablet core surface (initial wetting stage), and Subsection 4.2.2 deals with subsequent droplet impingement and spreading (impingement on wetted surface stage).

#### 4.2.1 Initial wetting

In this subsection, multiple droplet impingement onto dry surfaces of tablets entering the spray-zone is studied. All the droplets of the first array were assumed to behave identically after impact since they are similarly sized (droplets of average volume  $V$ ) and have similar impact velocities. This assumption allows one to simulate the spreading of a single droplet impacting the tablet with the average velocity and diameter of the spray droplets, and then calculate, at any time  $t < t_i$ , the total wetted area on the tablet by multiplying the wetted area of a single droplet by the number of droplets in the horizontal array ( $N_d$ ).

Since all the droplets of the first array behave independently and identically, the equivalent radius  $R_{eq}$  of the wetted area at any given time  $t < t_i$  can be calculated as:

$$\pi R_{eq}^2 = N_d (\pi R_d^2) \quad (4.1)$$

$$N_d = (\dot{Q}_t / V \rho_1) t_i \quad (4.2)$$

where  $N_d$  is the number of droplets in each array, which depends on the spray mass flow rate applied to the tablet  $\dot{Q}_t$  and on the characteristic time  $t_i$ . The mass flow rate of coating applied on a single tablet can be calculated from the overall spray mass flow rate  $\dot{Q}$ , which is a process parameter, if the ratio of tablet-bed to single-tablet surface area ( $L \equiv A_{bed}/A_t$ ) is known, since  $\dot{Q}_t = \dot{Q}/L$ . To calculate the wetted area radius  $R_d$  of an individual droplet (of density  $\rho_1$ ) in the first array, the mechanical energy balance equation written below was solved (in the same way as in Chapter 3):

$$\frac{dE_K}{dt} + \frac{dE_G}{dt} + \frac{dE_S}{dt} = W_S - \Phi \quad (4.3)$$

In Equation (4.3),  $E_K$ ,  $E_G$  and  $E_S$  are the kinetic, gravitational and surface energies of the droplet, respectively;  $\Phi$  is the rate of viscous dissipation of the droplet kinetic energy and  $W_S$  denotes the rate of work done by the droplet surroundings. The expressions for the estimation of the above terms are presented in Chapter 3. Assuming that after impact the droplet has a spherical-cap shape allowed us to solve the mechanical energy balance equation and to predict the wetted area diameter ( $D_d = 2R_d$ ) for  $t < t_i$ .

Equation (4.1) neglects droplet-droplet interactions on the tablet surface. However, it is reported in the literature that droplet interaction on a rigid substrate can affect film spreading and lead to secondary droplet generation (Kalantari and Tropea, 2007). In this work, Volume-Of-Fluid simulations (Fig. 4.3) were performed to compare the spreading of two droplets interacting versus a single droplet spreading alone. The droplets in the VOF simulation were 2.5 mm in diameter ( $D_0$ ) and the points of impact were  $2D_0$  apart. In experiments performed by Barnes et al. (1999), it was observed that droplet spacing  $2D_0$  results in maximum probability for secondary splashing during droplet-droplet interaction.

The VOF results presented in Table 4.1 show that the droplets interaction did not have a significant effect on the overall spreading since the wetted area diameter of the interacting droplets is very close to twice the wetted area diameter of a single spreading droplet at the same characteristic time  $t_i$ . The above results indicate that droplet-droplet interactions can be neglected without significantly sacrificing accuracy in the pharmaceutical coating spraying conditions investigated in this work.

Table 4.1: Droplet-droplet interaction effect on the wetted area diameter at  $t_i = D_0/U_0$ .

Coating liquid	Impact velocity (m/s)	Liquid viscosity (cP)	Wetted area diameter (mm)		% Error
			2×Single droplet	Two droplets	
Glycerol/Water	1.0	35.5	10.10 (2×5.05)	10.05	0.5%
Opadry 15%	2.5	73.6	11.50 (2×5.75)	11.15	3.0%
Opadry 10%	5.0	98.0	11.80 (2×5.90)	11.35	3.8%

To summarize, the single-droplet model, presented in Chapter 3, together with Equations (4.1) and (4.2), allows describing the spreading of the first array of droplets impinging on a dry tablet until the second array of droplets impacts on top of them at  $t = t_i$ . The subsequent droplets of the spray will impact on the initial wetted surface, leading to further spreading and thickening of the coating film. Successive droplet impacts on the wetted surface are discussed in the next section.

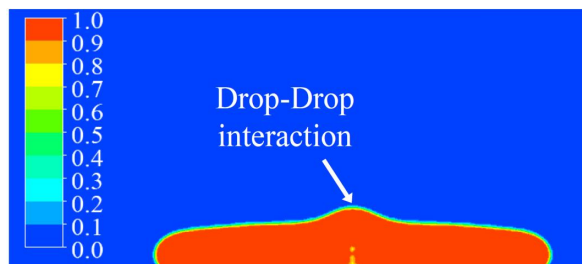


Figure 4.3: Droplet-droplet interaction on a rigid surface. Volume-Of-Fluid simulation.

### 4.2.2 Droplet impingement on wetted surface - Film spreading

Droplets of the spray which follow directly behind the first array will impinge on the wetted area (calculated in Subsection 4.2.1) and will contribute to its spreading. It was assumed that at this stage, the wetted area is made up of disconnected identical cylindrical films (Fig. 4.4) that expand axisymmetrically. Over a time interval  $dt$ , the impingement of a droplet on the surface of a film increases its volume by  $dV_f = (\dot{Q}_i/\rho_1) dt$ , where  $\dot{Q}_i$  is the droplet mass flow rate applied to each disconnected film ( $\dot{Q}_i = \dot{Q}_t/N_d$ ). Thus, the volume of each film at any given time  $t+dt > t_i$  can be calculated by  $V_f(t+dt) = V_f(t) + dV_f$ . The coating application is assumed to be complete when the wetted area reaches the area of the tablet surface facing the spray ( $A_t$ ).

Similar to the single droplet case (Section 4.2.1), it was assumed that the spreading of each disconnected cylindrical film of volume  $V_f$  is governed by the mechanical energy balance equation:

$$\frac{dE_{Kf}}{dt} + \frac{dE_{Gf}}{dt} + \frac{dE_{Sf}}{dt} = W_{Sf} - \Phi_f \quad (4.4)$$

where  $E_{Kf}$ ,  $E_{Gf}$  and  $E_{Sf}$  are the kinetic, gravitational and surface energies of each film, respectively,  $\Phi_f$  is the rate of viscous dissipation of the kinetic energy of the film and  $W_{Sf}$  denotes the rate of work done on the film surface by the surroundings. The key difference compared to the single-droplet case, is that the first term on the right-hand side, which denotes the rate of work done by the surroundings on the film surface, cannot be neglected. The part of the work done by the surroundings, that in particular needs to be accounted for, is that carried out by the droplets that impinge onto the surface of the film.

Similarly to the single droplet case, the rate of change of the gravitational and surface energies of each cylindrical film was calculated as follows:

$$\frac{dE_{Gf}}{dt} = \frac{d}{dt} (V_f \rho_1 g H_m) \quad (4.5)$$

$$\frac{dE_{Sf}}{dt} = \frac{d}{dt} [2\gamma_{12}\pi R_f H_f + \gamma_{12}\pi R_f^2 (1 - \cos\vartheta)] \quad (4.6)$$

where  $H_f$ ,  $H_m$  and  $R_f$  represent the film thickness, center of mass height and wetted area radius, respectively. Here, the height of the center of mass of the coating film is equal to half of the film thickness ( $H_m = H_f/2$ ). In Equation (4.6),  $\gamma_{12}$  and  $\vartheta$  are the coating film surface tension and contact angle on the tablet surface, respectively.

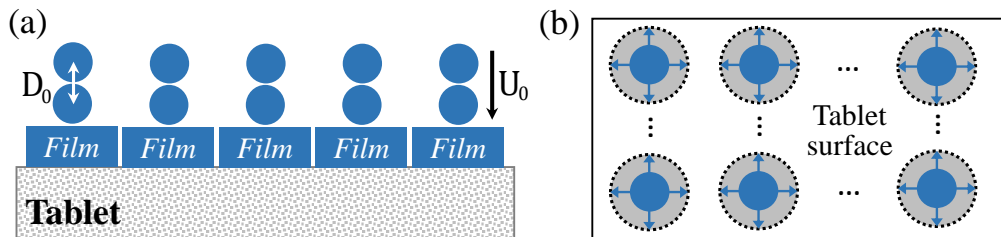


Figure 4.4: Successive droplet impact onto the tablet. a) Side and b) top view of the tablet.

To calculate the kinetic energy rate of change and the rate of viscous dissipation terms in Equation (4.4), one needs to assume a functional form for the velocity field inside the spreading films. Here, the approach of Madejski (1976), who proposed the following shear flow velocity field (Fig. 4.5), was followed:

$$u_{1r} = Crz ; u_{1z} = -Cz^2 \quad (4.7)$$

where  $r$  and  $z$  are the radial and vertical cylindrical coordinates. The prescribed velocity field accounts for the no-slip condition at the solid surface.

By assuming that the wetted area expansion ( $dR_f/dt$ ) is equal to the average radial velocity at  $r = R_f$ , one can write:

$$\frac{dR_f}{dt} = \frac{1}{H_f} \int_0^{H_f} u_{1r}(R_f, z) dz = \frac{CR_f}{H_f} \int_0^{H_f} z dz \Rightarrow C = \frac{2}{R_f H_f} \frac{dR_f}{dt} \quad (4.8)$$

Substituting  $C$  into Equation (4.7) gives:

$$u_{1r} = \frac{2rz}{R_f H_f} \frac{dR_f}{dt} \quad (4.9)$$

$$u_{1z} = -\frac{2z^2}{R_f H_f} \frac{dR_f}{dt} \quad (4.10)$$

Using scaling arguments it is proved below that the above velocity components are considerably smaller than the impact velocity  $U_0$ . From Equations (4.9) and (4.10):

$$u_{1r} = \frac{2rz}{R_f H_f} \frac{dR_f}{dt} \sim \frac{R_f H_f}{R_f H_f} \frac{dR_f}{dt} \sim \frac{dR_f}{dt} \quad (4.11)$$

$$u_{1z} = -\frac{2z^2}{R_f H_f} \frac{dR_f}{dt} \sim \frac{H_f^2}{R_f H_f} \frac{dR_f}{dt} \sim \frac{H_f}{R_f} \frac{dR_f}{dt} \quad (4.12)$$

To estimate the spreading rate ( $dR_f/dt$ ), one can assume that when a droplet impinges on the film surface, the change in thickness is negligible compared to the wetted area radius increase. Thus:

$$dV_f = 2\pi R_f H_f dR_f = 2\pi R_f H_f \frac{dR_f}{dt} t_i = (1/6) \pi D_0^3 \quad (4.13)$$

where  $dV_f$  is the change of film volume when a droplet impinges on its surface.

Since in the simulation case studies investigated in this thesis  $H_f \sim D_0$  and  $t_i \sim D_0/U_0$ , one can write:

$$R_f D_0 \frac{dR_f}{dt} \frac{D_0}{U_0} \sim D_0^3 \Rightarrow \frac{dR_f}{dt} \sim \frac{D_0}{R_f} U_0 \ll U_0 \quad (4.14)$$

Substituting Equation (4.14) into (4.11) and (4.12) yields:

$$\frac{u_{1r}}{U_0} \sim \frac{D_0}{R_f} \ll 1 \quad (4.15)$$

$$\frac{u_{1z}}{U_0} \sim \left(\frac{D_0}{R_f}\right)^2 \ll 1 \quad (4.16)$$

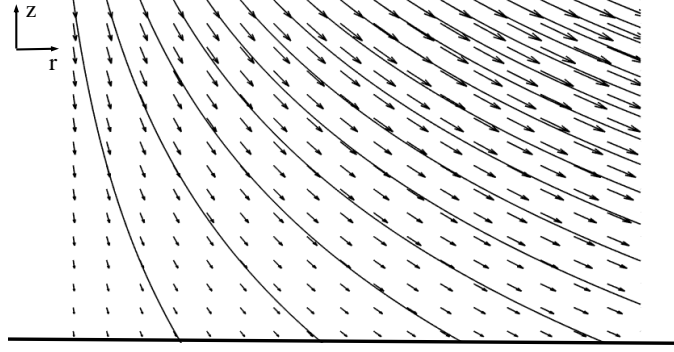


Figure 4.5: Shear flow velocity field. The dotted lines denote the streamlines.

By comparing the vertical and radial velocity components inside each spreading film, one gets:

$$u_{1z} \ll u_{1r} \ll U_0 \quad (4.17)$$

Note that at the very first stages of the spray application,  $R_f \sim H_f \sim D_0$ , and thus the velocity inside the spreading film and the droplet impact velocity  $U_0$  have the same order of magnitude. In the simulations carried out for this work, the time interval over which this condition holds is very short compared to that over which the tablet is sprayed. For most of the time  $D_0/R_f \ll 1$  and consequently the order of magnitude of the droplet impact velocity is significantly larger than that of the velocity field  $\mathbf{u}_1$  inside each cylindrical film.

Based on the above, the form of the velocity field inside each spreading film does not vary considerably during droplet impact onto the film surface. Thus, the velocity components (Eqs. 4.11, 4.12) were used to calculate the rate of change of kinetic energy ( $dE_{Kf}/dt$ ) and viscous dissipation loss rate ( $\Phi_f$ ) of each cylindrical film of volume  $V_f$  as follows:

$$\begin{aligned} \frac{dE_{Kf}}{dt} &= \frac{d}{dt} \left( \frac{1}{2} \rho_1 \int_{\mathcal{R}_f} \mathbf{u}_1 \cdot \mathbf{u}_1 d\mathbf{x} \right) = \frac{1}{2} \rho_1 \frac{d}{dt} \left[ \int_{\mathcal{R}_f} (u_{1r}^2 + u_{1z}^2) d\mathbf{x} \right] \\ &\approx \frac{d}{dt} \left[ \frac{\rho_1 \pi H_f}{60} (6H_f^2 + 5R_f^2) \left( \frac{dR_f}{dt} \right)^2 \right] \end{aligned} \quad (4.18)$$

$$\begin{aligned} \Phi_f &= - \int_{\mathcal{R}_f} \boldsymbol{\tau}_1 : \partial_{\mathbf{x}} \mathbf{u}_1 d\mathbf{x} = 2\mu_1 \int_{\mathcal{R}_f} \left[ (\partial_r u_{1r})^2 + (u_{1r}/r)^2 + (\partial_z u_{1z})^2 + \frac{1}{2} (\partial_z u_{1r} + \partial_r u_{1z})^2 \right] d\mathbf{x} \\ &\approx \frac{2\mu_1 \pi}{H_f} (R_f^2 + 8H_f^2) \left( \frac{dR_f}{dt} \right)^2 \end{aligned} \quad (4.19)$$

In Equation (4.18), the kinetic energy associated with the liquid-air ( $\mathcal{S}_{12}$ ) and liquid-tablet ( $\mathcal{S}_{13}$ ) dividing surfaces is neglected.

The rate of work done by the surroundings on the surface of each film is given by:

$$W_{Sf} = \int_{\mathcal{S}_{12}} \mathbf{n}_{21} \cdot \boldsymbol{\sigma}_2 \cdot \mathbf{u}_{12} ds + \int_{\mathcal{S}_i} \mathbf{n}_{df} \cdot \boldsymbol{\sigma}_1 \cdot \mathbf{u}_1 ds + \int_{\mathcal{S}_{13}} \mathbf{n}_{31} \cdot \boldsymbol{\sigma}_3 \cdot \mathbf{u}_{13} ds \quad (4.20)$$

where  $\mathcal{S}_i$  is the droplet-film dividing surface (Fig. 4.6) and  $\mathbf{n}_{df}$  is the unit vector normal to  $\mathcal{S}_i$  pointing from the droplet to the film.

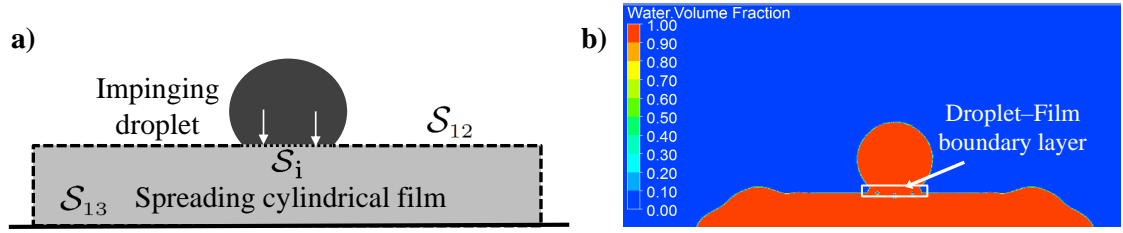


Figure 4.6: a) Droplet impact on a film, b) Volume-Of-Fluid CFD simulation of droplet-film impingement.

In Equation (4.20), one can neglect the first term on the right-hand side which denotes the rate of work done on the surface  $S_{12}$  by the surrounding gas. This is the same approximation used in Chapter 3, where a single droplet impinging on a dry substrate was treated. Since the fluid velocity at the tablet-film interface  $S_{13}$  is zero ( $\mathbf{u}_{13} = 0$ ; no-slip boundary condition), the third term on the right-hand side is zero.

The rate of work done by the impinging droplets on the surface of each cylindrical film can be repartitioned into two contributions:

$$W_{sf} \approx \int_{S_i} \mathbf{n}_{df} \cdot \boldsymbol{\sigma}_1 \cdot \mathbf{u}_1 ds = \int_{S_i} p_1 \mathbf{n}_{df} \cdot \mathbf{u}_1 ds + \int_{S_i} \mathbf{n}_{df} \cdot \boldsymbol{\tau}_1 \cdot \mathbf{u}_1 ds \quad (4.21)$$

where  $p_1$  is the pressure in the coating liquid. The two terms on the right-hand side represent the rates of work done by the pressure and viscous forces, respectively, on the surface of the film.

First the pressure term on the right-hand side of Equation (4.21) is considered. To calculate the work done by the pressure forces on  $S_i$ , one needs an expression for the pressure field. To derive it, it was assumed that the region of the droplet near the interface (droplet-film boundary layer, Fig. 4.6.b) decelerates significantly upon impact, as in this region the velocity field magnitude is far less than  $U_0$ . In fact, using scaling arguments, one can write:

$$\frac{u_{1z}}{U_0} \sim \frac{CH_f^2}{U_0} \sim \frac{H_f}{R_f U_0} \frac{dR_f}{dt} \sim \left(\frac{H_f}{R_f}\right)^2 \sim \left(\frac{D_0}{R_f}\right)^2 \ll 1 \quad (4.22)$$

where  $C$  is given by Equation (4.8). In the last passage (Eq. 4.22), it has been assumed that the thickness of the film has the same order of magnitude as  $D_0$  which is true in the current conditions, and that  $dR_f/dt \sim (H_f/R_f)U_0$ , which is previously in this chapter shown to be true (Eq. 4.14).

Note that at the very beginning of the spray application,  $R_f \sim H_f$ , and so the velocity in the droplet-film boundary layer and the impact velocity of the droplet have the same order of magnitude. The time interval over which this condition holds is very short compared to that over which the tablet is sprayed ( $\sim 0.1$  s; Kumar et al., 2015). For most of the time,  $H_f/R_f \ll 1$  and consequently the droplet impact velocity is significantly larger than the vertical velocity in the film. To further support this, CFD VOF simulations (Fig. 4.7) were performed. The results show that there is at least an order of magnitude difference between  $U_0$  ( $\approx 1$  m/s) and the vertical velocity close to the droplet-film interface ( $u_{1z} < 0.1$  m/s).

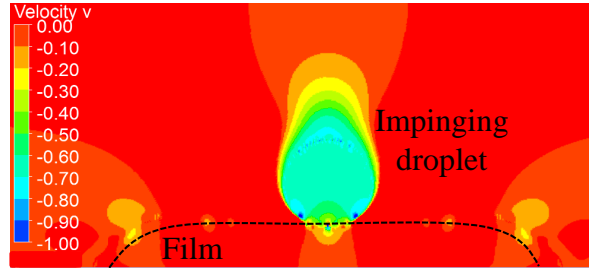


Figure 4.7: Vertical to the solid substrate velocity component during droplet impingement on a film ( $Re = 250$ ,  $U_0 = 1\text{m/s}$ ,  $D_0 = 2.5\text{ mm}$ ,  $\mu_1 = 10\text{ cP}$ ,  $\rho_1 = 1000\text{ kg/m}^3$ ).

It is concluded here that in the droplet-film boundary layer, the kinetic energy of the fluid turns almost entirely into pressure energy, so that in this region  $p_1 \approx (1/2) \rho_1 U_0^2$ . Thus, one can write:

$$\int_{S_i} p_1 \mathbf{n}_{df} \cdot \mathbf{u}_1 ds \sim (1/2) \rho_1 U_0^2 \int_{S_i} \mathbf{n}_{df} \cdot \mathbf{u}_1 ds = (1/2) U_0^2 \dot{m}(t) \quad (4.23)$$

where  $\dot{m}$  is the droplet mass entering in/merging with the film per unit time. This quantity is time-dependent, but its order of magnitude is given by the ratio between the droplet mass  $M_D$  and the time  $t_i$  required by the droplet to fully merge with the film. Based on the above one obtains:

$$\int_{S_i} p_1 \mathbf{n}_{df} \cdot \mathbf{u}_1 ds \equiv W_p \sim (1/2) U_0^2 M_D / t_i = (1/2) U_0^2 \dot{Q}_i \quad (4.24)$$

where  $\dot{Q}_i$  denotes the droplet mass flow rate applied to each disconnected cylindrical film. This is equal to the ratio  $\dot{Q}_t / N_d$ , in which the values of both quantities can be regarded as known (refer to the previous section).

To calculate the rate of work done by viscous forces on each film ( $W_V$ ), the no-slip boundary condition at the tablet-film interface was considered. The rate of work done on  $S_{12}$  was neglected and the rate of work done by the viscous forces only inside the droplet region that decelerates upon impact (droplet-film boundary layer) was considered significant. Pasandideh-Fard et al. (1996) reported that the droplet-film boundary layer thickness is  $\ell \sim D_0 / \sqrt{Re}$ . Since the velocity field inside the boundary layer is unknown, scaling analysis was used to estimate the rate of work done by the viscous forces. The local scales of the fluid velocity  $\mathbf{u}_1$  and shear stress  $\boldsymbol{\tau}_1$  in the boundary layer are taken to be  $U_0$  and  $\mu_1 U_0 / \ell$ , respectively. One can then write:

$$\begin{aligned} \int_{S_i} \mathbf{n}_{df} \cdot \boldsymbol{\tau}_1 \cdot \mathbf{u}_1 ds &\sim -\frac{\mu_1 U_0^2}{\ell} A_i \sim -\frac{\mu_1 U_0^2}{\ell} \frac{\dot{Q}_i}{U_0 \rho_1} \\ &\sim -\frac{U_0^2 \dot{Q}_i D_0}{Re \ell} \sim -\left(\frac{1}{\sqrt{Re}}\right) U_0^2 \dot{Q}_i \end{aligned} \quad (4.25)$$

where  $A_i$  denotes the area of the surface  $S_i$  (Fig. 4.6). Consequently, if  $1/\sqrt{Re} \ll 1$ , the rate of work done by the viscous forces is negligible compared to that done by the pressure forces. This is because:

$$\left(\frac{1}{\sqrt{Re}}\right) U_0^2 \dot{Q}_i \ll U_0^2 \dot{Q}_i \quad \Rightarrow \quad \int_{S_i} \mathbf{n}_{df} \cdot \boldsymbol{\tau}_1 \cdot \mathbf{u}_1 ds \ll \int_{S_i} p_1 \mathbf{n}_{df} \cdot \mathbf{u}_1 ds \quad (4.26)$$

For sprays where  $1/\sqrt{\text{Re}} \sim 1$ , the mechanical energy balance equation (Equation 4.4) needs to account for the rate of work done by the viscous forces on each cylindrical film:

$$\int_{S_i} \mathbf{n}_{df} \cdot \boldsymbol{\tau}_1 \cdot \mathbf{u}_1 ds \equiv W_V \sim \left( \frac{1}{\sqrt{\text{Re}}} \right) W_P \quad (4.27)$$

So, by substituting Equations (4.24) and (4.27) into (4.21), one can calculate the overall rate of work done by the surrounding fluid (impinging droplets and air) on the surface of each cylindrical film ( $W_S \equiv W_P + W_V$ ).

To calculate the thickness ( $H_f$ ) of each disconnected film, one needs to solve the mechanical energy balance equation. To do so, the expressions for the rate of work done by the surrounding fluid on the film surface ( $W_{Sf}$ ), the rate of change of gravitational, surface and kinetic energies of the film ( $E_{Gf}$ ,  $E_{Sf}$ ,  $E_{Kf}$ ), as well as the rate of kinetic energy viscous dissipation ( $\Phi_f$ ), given by Equations (4.20), (4.5), (4.6), (4.18) and (4.19), respectively, were substituted into Equation (4.4).

Since the shape of each film is assumed to be cylindrical [ $V(t) = \pi R_f^2(t) H_f(t)$ ;  $H_m = H_f/2$ ], the number of unknown variables in the mechanical energy balance equation was reduced to one (the variable being  $H_f$ ). The equation was solved by adopting the following initial conditions:

$$\left. \frac{dR_f}{dt} \right|_{t=t_i} = \left. \frac{dR_d}{dt} \right|_{t=t_i} \quad (4.28)$$

$$R_f|_{t=t_i} = R_d|_{t=t_i} \quad (4.29)$$

where  $t_i = D_0/U_0$ . When the equivalent wetted area ( $A_{eq} = N_d \pi R_f^2$ ) reaches the area of the tablet surface, it was assumed that the coating application process is completed. In this work, it was considered that the final film thickness is equal to the thickness of each individual disconnected film  $H_f$ .

The model equations presented in this section describe the spreading of disconnected cylindrical coating films under a spray. To simplify the problem the model considers that the droplets merge with the film as they impact (Fig. 4.8) and hence the crown formation and splashing were neglected (Subsection 4.2.3). This means that the current model might not yield accurate predictions when these phenomena are relevant. However, it is expected that the effect of these phenomena will be negligible in the case studies investigated in this thesis. This validity of the above assumption is discussed in the next section.

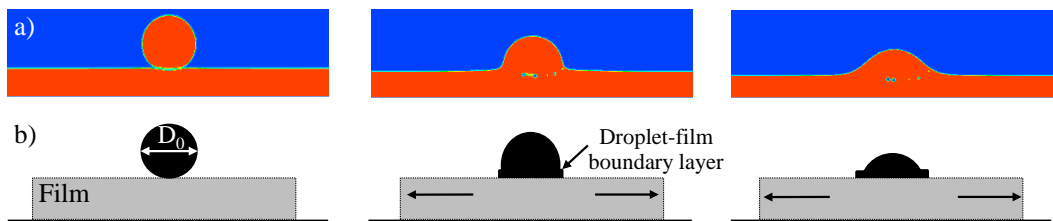


Figure 4.8: Droplet impingement on a film and merging. a) Volume-Of-Fluid CFD simulation, and b) current modeling approach.

### 4.2.3 Splashing of impinging droplets

In this chapter, it is considered that when a droplet impacts on a film it merges with the film without crown formation and subsequent splashing. It was also assumed that no splashing occurs when droplets impinge on a dry surface. Here the validity of these assumptions is discussed.

In their work, Mundo et al. (1998) and Bolleddula et al. (2010) considered that splashing occurs when  $\text{Oh Re}^{1.25} > 57$  where Oh and Re are the Ohnesorge and Reynolds numbers of the droplet upon impact, respectively. In the literature, this empirical criterion has been used to predict whether splashing occurs when Opadry coating droplets impact on dry tablets (Bolleddula et al., 2010).

In cases where droplets impact on thin films, the criterion is different (Cossali et al., 2005):  $\text{Oh}^{-0.4} \text{We} > 2100 + 5880 h^{1.44}$  where  $h \equiv H_f/D_0$  and We is the droplet Weber number at impact. The criteria for droplet impact on both solid and wetted surfaces are both met for the case studies investigated in this work. Thus, it is justified to neglect droplet splashing in the current model.

To summarize, the model presented in Section 4.2 allows estimating of the time  $\tau_F$  required for the surface of a tablet to become fully covered by a thin coating film. Predicting this “application” time is important, because if the tablet is sprayed for a shorter time, it will only become partially coated, while if it is sprayed for a longer time, the coating will spread to adjacent tablets possibly leading to inter-tablet coating non-uniformity. In the next section, the results of the model are presented and validated with experimental data from the literature.

## 4.3 Numerical results and validation

The numerical results from the model described in Section 4.2 were validated with experimental data from the literature. In Subsection 4.3.1, the model predictions for the final film thickness were compared with the corresponding experimental results of Kalantari and Tropea (2007). They investigated water spray impingement on rigid surfaces while varying impact conditions such as the spray droplet average size and velocity.

It is well documented in the literature that film formation after spray impact on a rigid surface is influenced by the spray mass flow rate, the droplet mean size and velocity, and the liquid properties (Cossali et al., 2005). In Subsection 4.3.2, variance-based sensitivity analysis was performed employing the gPROMS global sensitivity analysis tool to study the effect of these parameters on the coating film thickness ( $H_f$ ) and application time ( $t_F$ ). This analysis indicated how the model output variances depend on the input factors that are subject to uncertainty (Saltelli et al., 2010) and allowed the identification of the model parameters.

### 4.3.1 Validation of spray impingement numerical results

In this section, the numerical results of the current model concerning liquid film spreading after spray impact are presented and validated with experimental data found in the literature. Kalantari and Tropea (2007) conducted a thorough experimental investigation of water ( $\rho_1 = 998 \text{ kg/m}^3$ ,  $\mu_1 = 1 \text{ cP}$ ,  $\gamma_{12} = 0.072 \text{ N/m}$ ) spray impact onto a rigid surface. They used a high-speed camera to measure the average film thickness ( $\bar{H}_f$ ) after the “target” surface was completely wetted. It should be noted that in their experiments the thickness did not vary significantly during continuous spraying. In the numerical simulations, presented in this section, the thickness of each disconnected film increases initially until it reaches a maximum value (Fig. 4.12). After this point, the thickness does not change significantly and each film continues only to spread. The moment the films come into contact, the “target” surface (tablet surface) was considered to be completely wetted and consequently  $\bar{H}_f$  was calculated at this point.

In Figure 4.9.a), the experimental data (Kalantari and Tropea, 2007) for the normalized film thickness ( $\bar{H}_f/D_0$ ) as a function of the impact Reynolds number are compared with the corresponding numerical results of the model presented in this chapter. In the numerical simulations as well as in the experiments, the film thickness  $\bar{H}_f$  is calculated after the entire target surface is wetted (application time,  $t = \tau_F$ ). The water spray volumetric flow rate in both experiments and simulations is set equal to 11/h ( $\dot{Q}_t = 16.8 \text{ g/min}$ ) over a cyclical target 5 mm in diameter (in the current modeling approach this represents the tablet) and the impact Reynolds number is set to range from 300 to 600 ( $U_0 = 7 - 18 \text{ m/s}$  and  $D_0 = 30 - 75 \mu\text{m}$ ).

Kalantari and Tropea (2007) reported that the experimental error of the  $\bar{H}_f$  measurements ranged from  $5 \mu\text{m}$  to  $22 \mu\text{m}$  but they did not mention the corresponding error at each impact condition (impact Re) they investigated. Thus, in Figure 4.9.a),  $\pm 10\%$  error bars were introduced to assess the agreement between numerical and experimental results. Figure 4.9.a) shows that the numerical results agree well with the experimental data.

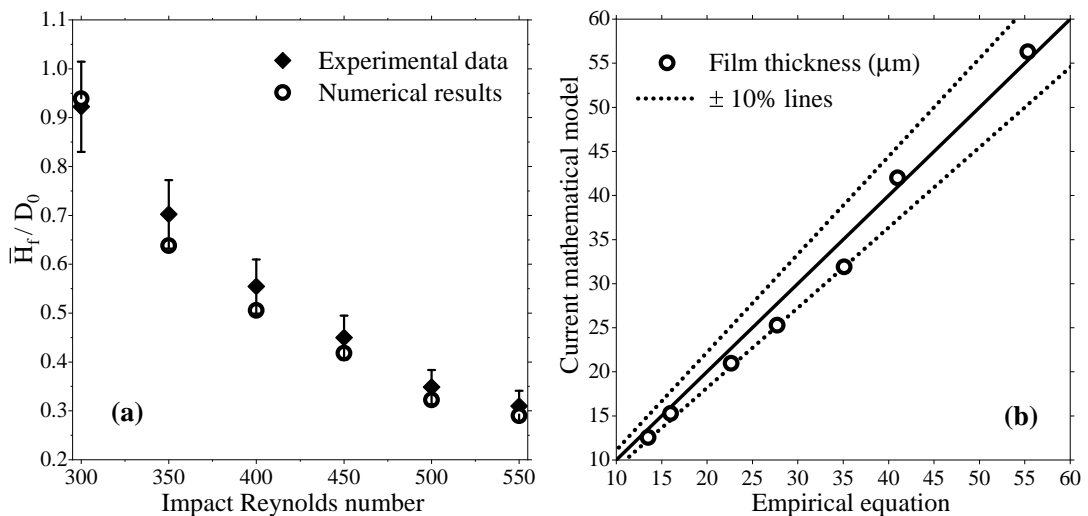


Figure 4.9: Film height as a function of the droplet impact Reynolds number. Comparison with a) experimental data, and b) empirical equation by Kalantari and Tropea (2007).

Table 4.2: Film thickness at the moment when the entire target surface is wetted ( $t = \tau_F$ ). Validation of the spray model against the empirical equation by Kalantari and Tropea (2007).

Droplet diameter ( $\mu\text{m}$ )	Impact velocity (m/s)	Impact Re number	Film thickness ( $\mu\text{m}$ )		% Error  $\mu\text{m}$
			Model	Empirical equation	
60	10.0	599	16.65	16.24	2.5
65	8.0	519	24.20	22.66	6.8
55	9.0	494	19.62	20.92	6.2
30	15.0	449	12.54	13.50	7.1
50	8.0	399	24.97	27.72	9.9

Figure 4.9.b) compares the predictions of the model presented in Section 4.2 with the predictions of the empirical equation  $\bar{H}_f = 22149 \cdot D_0 \text{Re}^{-1.769}$  which was derived by Kalantari and Tropea (2007) by fitting their experimental data. As seen in Figure 4.9.b), the results of the current model are in reasonable agreement with the values of the empirical equation ( $|\% \text{Error}| < 10\%$ ).

The good agreement with experimental data is also shown in Table 4.2, where the percentage error of the film thickness model predictions for different impact Reynolds numbers ( $|\% \text{Error}| < 9.1\%$ ) is calculated. Even though the current model results are close to the empirical equation predictions, the small deviation might be caused by the inability of the model to account for possible splashing and crater formation during droplet-film impact. According to the literature (Bisighini et al., 2010), however, the effect of these phenomena should be small for the impact conditions during film-coating. This is consistent with the model predictions being good.

The results presented here can be used to predict the thickness of the liquid film applied on a tablet after passing through the spray zone in a rotating coating drum. If the solvent evaporates evenly from the tablet surface then the final film thickness can be estimated.

### 4.3.2 Sensitivity analysis

It is well documented in the literature that film spreading under spray is affected by many parameters (Cossali et al., 2005). These parameters include the size and velocity of the spray droplets before impact, the spray flow rate and liquid viscosity. Variance-based sensitivity analysis (Saltelli et al., 2010) is performed next to assess the influence of these parameters on the main outputs from the model presented in this chapter: the film thickness ( $\bar{H}_f$ ) when the entire tablet surface is wetted, and the application time ( $\tau_F$ ).

The global sensitivity tool (GSA) of gPROMS Modelbuilder (Process Systems Enterprise Ltd., 2019) was used, and the method of Saltelli et al. (2010) was followed to calculate the first order and total sensitivity indices. The first order sensitivity index, also known as the ‘‘importance’’ measure, represents the main effect of the parameter (factor) on the output. The total index additionally accounts for all higher-order effects to the output due to interactions between parameters. A large numerical value indicates a significant effect.

From the sensitivity indices in Table 4.3 one can rank the model parameters based on their effect on the model output (response). It can be seen that the droplet viscosity, velocity and diameter before impact are the parameters that affect the final film thickness ( $H_f$ ) the most. The overall spray mass flow rate ( $\dot{Q}$ ) only has significant secondary effects on the film thickness, but influences significantly the application time ( $\tau_F$ ). A small first order effect does not necessarily mean that a factor does not affect the response, since it might still be important through its interactions with other factors. For this reason, the total effect was also considered. The rest of the model parameters (not shown in Table 4.3) have small sensitivity indices and do not significantly affect the film thickness and application time.

Figure 4.10.a), shows the influence of the droplet impact velocity ( $U_0$ ) on the thickness ( $H_f$ ) of the cylindrical films. Three scenarios for different impact velocities are presented: 4, 5 and 6 m/s. In all scenarios, the droplet mean diameter, the spray mass flow rate and the coating viscosity were set equal to 150  $\mu\text{m}$ , 200 g/min and 10 cP, respectively. The model predicts that the final value of the film thickness increases when the impact velocity decreases.

The simulations also show that the thickness of each film does not vary significantly after it reaches a maximum value. This prediction agrees with experimental observations (Moreira et al., 2010). At this point, each film continues to spread with the same thickness until the entirety of the tablet surface is wetted. In Figure 4.10.a), the application time  $\tau_F$  is taken equal to 100 ms (typical for the tablet film-coating process; Kumar et al., 2015) for all case studies.

In Figure 4.10.b), the influence of the spray droplets mean diameter ( $D_0$ ) on the film thickness ( $H_f$ ) is studied. The velocity of the droplets and the spray rate were set equal to 5 m/s and 200 g/min, respectively. The numerical model predicts that larger droplets form thicker films. Similar behavior is observed experimentally for the single coating droplet impact case; larger droplet diameters result in higher  $h_{max}$  values (Shaari, 2007).

The importance of the spray liquid properties has often been mentioned in the literature (Moreira et al., 2010). Figure 4.10.c) highlights the effect of coating viscosity ( $\mu_1$ ) on film thickness ( $H_f$ ). The droplet velocity was set at 5 m/s and the flow rate at 200 g/min. As expected, more viscous liquids form thicker films that also spread more slowly. The rate of work done by the viscous forces during droplet-film impact ( $W_V$ ), which is included in the energy balance, is of high significance for highly viscous coatings.

Table 4.3: Sensitivity analysis. Variance-based method by Saltelli et al. (2010).

Factor	First order ( $\bar{H}_f$ )	Total effect ( $\bar{H}_f$ )	First order ( $\tau_F$ )	Total effect ( $\tau_F$ )
Droplet diameter, $D_0$	0.201	0.254	0.077	0.088
Impact velocity, $U_0$	0.467	0.526	0.170	0.189
Spray mass flow rate, $\dot{Q}$	0.001	0.059	0.635	0.641
Liquid viscosity, $\mu_1$	0.276	0.326	0.106	0.113

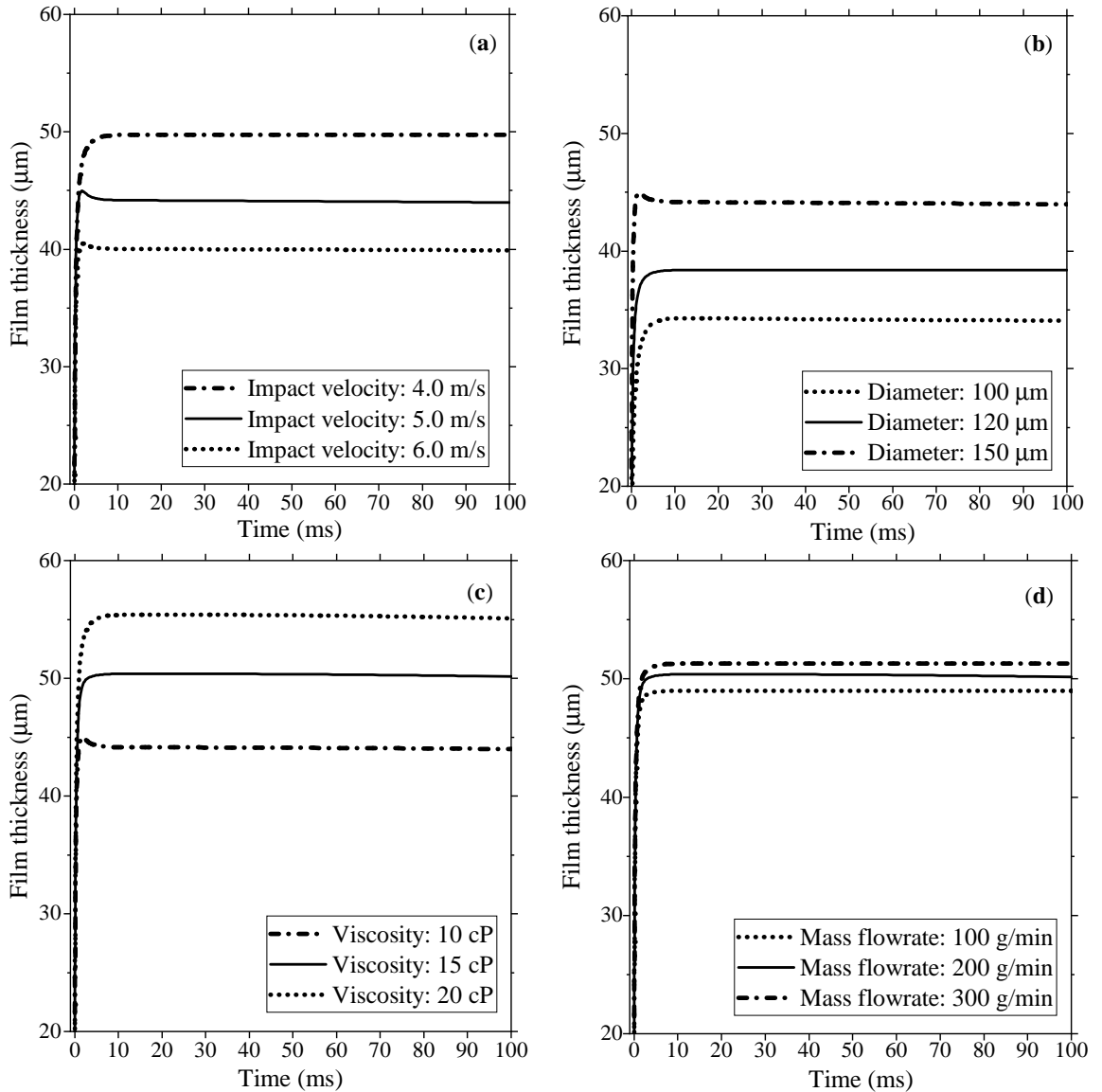


Figure 4.10: Film thickness variation with changing: a) droplet velocity ( $D_0 = 150\mu\text{m}$ ,  $\mu_1 = 10\text{ cP}$ ,  $\dot{Q} = 200\text{ g/min}$ ), b) droplet diameter ( $U_0 = 5\text{ m/s}$ ,  $\mu_1 = 10\text{ cP}$ ,  $\dot{Q} = 200\text{ g/min}$ ), c) viscosity ( $D_0 = 150\mu\text{m}$ ,  $\dot{Q} = 200\text{ g/min}$ ,  $U_0 = 5\text{ m/s}$ ), d) spray rate ( $D_0 = 150\mu\text{m}$ ,  $\mu_1 = 15\text{ cP}$ ,  $U_0 = 5\text{ m/s}$ ).

Figure 4.10.d) shows the effect of spray mass flow rate ( $\dot{Q}$ ) on the film thickness ( $H_f$ ). The droplet diameter ( $150\mu\text{m}$ ) and impact velocity ( $5\text{ m/s}$ ) were kept constant, and only the number of droplets impinging per unit time (spray density) was changed. The numerical simulations show that higher spray densities result in slightly thinner films. The model prediction agrees with the behavior observed in the experiments by Kalantari and Tropea (2007).

To summarize, the sensitivity analysis shows that the mean droplet diameter ( $D_0$ ) and velocity ( $U_0$ ) are the parameters that significantly affect the film thickness and the time required for the coating film to cover the tablet surface which is facing the spray. Moreover, the spray mass flow rate mainly influences the application time, and liquid properties, such as the coating viscosity ( $\mu_1$ ) and density ( $\rho_1$ ), play a less significant role.

#### 4.4 Concluding remarks

The spraying of coating liquids is a complex process that is difficult to simulate accurately with reasonable computational cost. In the work presented in this chapter, a novel mathematical model that can very quickly calculate the film thickness and the coating formulation spreading rate on the surface of a tablet that passes through the spray zone was developed. The results of the developed model, which was implemented in gPROMS Modelbuilder, were validated with experimental data found in the literature. In Subsection 4.3.1, it is shown that the model predictions agree with the experiments.

Liquid coating film formation during spray impingement is affected by many parameters. To find out which parameters affect the model outputs (such as the film thickness and application time) variance-based sensitivity analysis was performed. An advantage of the current model when compared to traditional CFD simulations is the computational speed. Implementing this accurate method for sensitivity analysis is possible because of the limited time required by a single run of the model ( $< 5$  s). In Subsection 4.3.2, it was found that the mean droplet diameter and velocity before impact significantly affect the film thickness and the application time. Additionally, it was concluded that the spray mass flow rate significantly influences only the time required to cover the tablet with the coating film, whereas liquid properties such as the coating viscosity and density are not as important.

As discussed in the introduction of this thesis, spray properties such as the atomizing air pressure, the design and configuration of the guns/nozzles and the spray mass flow rate, all influence the droplet mean size and velocity, as well as the spray density and spray zone area, quantities that play a key role in controlling the process and enhancing the quality of the tablets. High spray mass flow rates may cause coating defects (most common being tablet sticking and logo bridging), whereas significantly low spray mass flow rates may lead to spray drying phenomena which affect the duration and efficiency of the coating process. Using information derived from the model presented in this chapter, one can predict the film thickness and application time for a given coating formulation, spray flow rate and droplet mean size and velocity before impact. This insight can be used by the pharmaceutical industry to adopt the appropriate spray properties and to optimize the final product.

# CHAPTER 5

## Suspension film behavior on a tablet

---

In this chapter, a model that can quickly estimate the flow, evaporation and absorption of coating suspension films into porous tablets is developed. The main outputs of the model are the amount of water and coating particles which penetrate into the tablet porous core as well as the film drying rate. Knowledge of the amount of water and solids in a solid dosage form can be used to optimize tablet shelf-life and adhesion of the dry coating film.

---

### 5.1 Introduction

Film coatings are generally applied on pharmaceutical tablets by spraying the coating formulation on their surface. Most coating formulations employed by the pharmaceutical industry are aqueous polymer suspensions. To investigate the behavior of a coating suspension on a pharmaceutical tablet during the film-coating process, one needs to simultaneously consider the flow of the suspension on the surface of the tablet; the evaporation of the suspension continuous phase; and the absorption of the suspension into the porous matrix of the tablet core. Previous work concerning the simulation of thin film behavior on rigid substrates dealt with either pure liquids, or neglected the absorption of the suspension or the evaporation of the carrier fluid. This work aims to address all the above concurrent phenomena.

The model developed in this chapter aims to describe the behavior of a coating formulation after this has been applied on a tablet and is no longer under a spray; that is, after the initial inertia-driven spreading process (described in Chapter 4) has completed. The “mixture modeling” approach and the “lubrication approximation” method were used to simplify the equations describing the behavior of the coating liquid-particle system and to develop a mathematical model for simulating film motion and drying on tablet surfaces. The influence of solvent evaporation on important physical properties of the coating suspension, such as the density and viscosity, is taken into consideration. The model also simulates the absorption of the coating suspension inside the porous tablet core, since predicting the wetting front profile inside the core provides important information about the tablet water content during the film-coating process.

Recent models which simulate coating application on tablets have focused on single droplet impact cases and/or have neglected coating absorption into the tablet (Bolleddula et al., 2010; Niblett et al., 2017). The main outputs of the model presented in this chapter are the amount of the applied suspension (water and coating particles) which penetrates into the tablet core as well as the prediction of the film drying time. Predicting the amount of water and solid polymer inside the tablet during the film-coating process can be used by the pharmaceutical industry to enhance tablet shelf-life and adhesion of the dry film as discussed in Chapter 2.

## 5.2 Mathematical model

During the coating process, thin film coatings are applied on tablets by spraying a polymer-based suspension onto their surface. After impingement onto the tablet, the droplets spread on its dry surface (Felton, 2013). Continuous droplet impingement (spray impact) leads to the expansion of the wetted area and the formation of a liquid (suspension) film/layer that eventually covers part or the entire surface of the tablet facing the spray. According to the work of Bolleddula et al. (2010), this initial spreading of a coating suspension over a tablet surface is a process that is inertia-driven and much faster ( $t_i \sim 10^{-3}$ s) than the suspension drying and absorption into the tablet processes, which take place during the film-coating process (Felton, 2013) and whose duration is of the order of seconds.

Following the formation of a liquid layer that covers the tablet surface, the coating suspension penetrates into the porous tablet core and flows over adjacent dry parts of the tablet surface (Fig. 5.1). The carrier fluid also evaporates from the film surface. Suspension drying significantly influences the motion of the film (absorption into the tablet and spreading over the tablet dry surface) as it affects its density and viscosity. In fact, the suspension viscosity diverges when the particle volume fraction approaches a critical value (Mueller et al., 2009). At this critical volume fraction, the particles come into close contact, start to coalesce and form a porous wetted solid (Taylor and Winnik, 2004). At this point, the film absorption into the tablet and flow over the adjacent dry surfaces are negligible and the carrier fluid evaporates through the pores of the wetted solid or “crust” (Kiil, 2006).

This chapter considers the behavior of a pharmaceutical coating suspension (consisting of water and particles) after this has been applied on a tablet and is no longer under a spray; that is, after the initial spreading process (Chapter 4) has completed. Following Niblett et al., (2017), it was assumed in this work that the coating suspension film initially covers part of the “upper” surface of a cylindrical tablet (Fig. 5.1) leaving all adjacent areas dry. It was also taken into account that the coating film can penetrate into the tablet, while the coating suspension carrier fluid can evaporate. The model accounts for the particle retention in the pores, since the retention may hinder suspension absorption into the tablet. The simulation was regarded as completed when the particle concentration of the suspension becomes high enough ( $\phi = \phi^*$ ) that the coating film can no longer be considered as a liquid, but as a wetted solid - at this moment the formation of a porous wetted crust in the entire film takes place (Kiil, 2006). The time required for the crust formation is considered as the “crust formation time”  $t_{cr}$  in the model. For  $t > t_{cr}$ , water evaporates from within the porous crust. Note that water evaporation from within a porous medium is not investigated here but is studied in the next chapter.

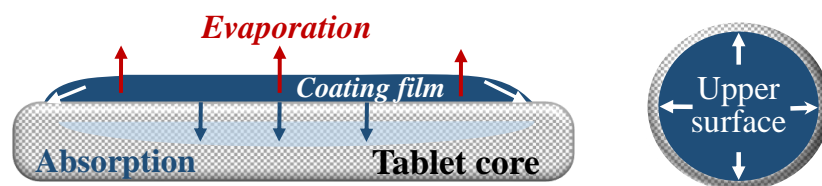


Figure 5.1: Coating film applied on the surface of a porous tablet core.

To summarize, the model presented here can accurately calculate the time required for crust (wetted solid) formation in the entire coating film; the amount of coating suspension absorbed into the tablet core; the thickness of the film while it evaporates, flows over the tablet and penetrates into the tablet; and the profile of the solid particle volume fraction on the tablet surface and inside the tablet after coating suspension application. In this section, the mathematical model is described and is presented in two subsections: Subsection 5.2.1 concerns the behavior of the coating thin film on the tablet surface and Subsection 5.2.2 deals with coating suspension penetration into the dry porous tablet. In Subsection 5.2.3, the steps needed to numerically solve the model are explained.

### 5.2.1 Coating behavior on the tablet surface

After the coating suspension film has been applied on the tablet, it can spread over adjacent dry parts of the tablet surface, absorb into the porous tablet core, and dry while the coating carrier fluid (water) evaporates (Fig. 5.1). In this subsection, the part of the model which deals with non-Newtonian suspension film drying and flow over the surface of the tablet is presented. This work extends the model presented in Chapter 3, which concerns the behavior of single Newtonian droplets on a tablet.

Pharmaceutical coatings are multiphase media (liquid-particle suspensions). To simplify the problem, it was assumed that the coating film consists of only one carrier liquid (liquid phase; water) and identical coating particles (solid phase). This assumption is acceptable for most aqueous-based coating formulations which contain very similarly sized particles (Cole et al., 1995). It was also considered that there is rapid relaxation between the fluid and solid velocity fields. This is true in the simulations performed in this study since the Stokes number is small ( $St \ll 1$ ; see appendix). The last assumption allows one to use the mixture modeling approach (Manninen et al., 1996). This approach is based on a set of four balance equations which can be reduced to three by expressing the slip velocity between the phases with a constitutive equation. The three remaining balance equations are two continuity equations (one for the mixture, treated as an effective fluid, and one for the solid phase) and one linear momentum balance equation for the mixture.

To obtain the continuity equation for the mixture, one has to sum the continuity equations for the solid and liquid phases. Doing so yields:

$$\partial_t \rho = -\partial_x \cdot (\rho \mathbf{u}) \quad (5.1)$$

where  $\rho$  and  $\mathbf{u}$  are the density and velocity field of the mixture (that is, of the coating suspension), respectively, and are defined as follows:

$$\rho \equiv \varepsilon \rho_e + \phi \rho_s ; \quad \rho \mathbf{u} \equiv \varepsilon \rho_e \mathbf{u}_e + \phi \rho_s \mathbf{u}_s \quad (5.2)$$

where  $\varepsilon$  and  $\rho_e$  are the volume fraction and density of the liquid phase, respectively, and  $\phi$  and  $\rho_s$  are the volume fraction and density of the solid phase, respectively. Moreover,  $\mathbf{u}_e$  and  $\mathbf{u}_s$  are the velocities of the liquid and solid phases, respectively.

To derive a linear momentum balance equation for the mixture one needs to follow the same procedure as with the continuity equation. Summing the dynamical equations for the fluid and solid phases yields the equation of motion for the coating suspension:

$$\partial_t(\rho\mathbf{u}) = -\partial_x \cdot (\rho\mathbf{u}\mathbf{u}) - \partial_x \cdot \boldsymbol{\sigma}_m + \rho\mathbf{g} \quad (5.3)$$

where  $\mathbf{g}$  is the gravitational field and  $\boldsymbol{\sigma}_m$  is the mixture stress tensor. The equation above is unclosed; to make it solvable, one needs to provide a constitutive equation for the mixture stress tensor. This equation is discussed below.

As mentioned before, an additional continuity equation for the solid phase (particles in the suspension) is needed to model the behavior of the coating film. Since the solid particles are incompressible, this equation reads:

$$\partial_t\phi = -\partial_x \cdot (\phi\mathbf{u}) - \partial_x \cdot \mathbf{j} \quad (5.4)$$

The term  $\partial_x \cdot \mathbf{j}$  arises because the particles do not move at the same velocity as the mixture. Therefore, one can regard the quantity  $\mathbf{j}$  as a particle migration flux. The derivation of an expression for the particle migration flux is discussed in Subsection 5.2.1.

By solving Equations (5.1), (5.3) and (5.4) together with the appropriate expressions for the mixture stress tensor  $\boldsymbol{\sigma}_m$  and particle migration flux  $\mathbf{j}$ , one can calculate the velocity field of the mixture. However, solving the above system of equations in three dimensions is computationally demanding. To deal with this, the lubrication approximation assumptions (Szeri, 2010) were employed to simplify the problem and reduce the computational effort without sacrificing accuracy.

Coating suspension films are very thin compared to the characteristic length of the tablet surface they cover. Having two greatly differing length scales enables one to use the lubrication approximation method to simplify the three-dimensional linear momentum balance and continuity equations. Using scaling, the order of magnitude of the various terms of the governing equations (Eqs. 5.1, 5.3 and 5.4) were estimated and then the equations of the model were simplified by deleting the terms that are judged to be too small to have significant effect (see appendix).

In the framework of the lubrication approximation, inertia and gravity were assumed to be negligible in the thin suspension film applied onto the tablet (Szeri, 2010). It is reported in the literature that thin pharmaceutical suspension films formed by droplet impingement have approximately cylindrical shape (Niblett et al., 2017). In this work, by considering that the film covering the tablet surface has a cylindrical shape, the simplified linear momentum balance equation was derived; in component form, when expressed in cylindrical coordinates, this yields:

$$\partial_r p = \partial_z \tau_{zr} \quad ; \quad \partial_z p = 0 \quad (5.5)$$

where  $r$  and  $z$  are the radial and vertical cylindrical coordinates, respectively (see Fig. 5.2) and  $p$  is the pressure in the film.

From Equation (5.5) one can conclude that the pressure  $p$  is a function of the radial coordinate and of the time only. In the appendix of this chapter, Equation (5.5) is derived using the lubrication approximation method. Note that in using cylindrical coordinates, all changes in the azimuthal coordinate were neglected. This is consistent with the assumption for the axisymmetric shape of the film and the tablet.

In the literature, pharmaceutical coating suspensions have been reported to exhibit either Newtonian or slight shear thinning behavior (Bolleddula et al., 2010; Ketterhagen et al., 2017; Niblett et al., 2017) over a range of shear rates ( $10^{-3} - 10^3 \text{ s}^{-1}$ ) which is of interest for the coating-application process. The rheological behavior depends on their composition (type of polymer) and their solid volume fraction (Cole et al., 1995). In this work, the general case of a coating suspension that behaves as a power law fluid was considered. Thus, one can capture both the Newtonian and the non-Newtonian shear thinning behavior by specifying appropriate values for the flow and consistency indexes that feature in the constitutive equation for the stress tensor.

Assuming that the coating mixture behaves as a power law fluid for a specific shear rate range gives the following constitutive equation:

$$\tau_{zr} = m_0 |\partial_z v|^{n-1} \partial_z v \quad (5.6)$$

where  $v$  is the radial velocity component of the mixture,  $m_0$  is the consistency index and  $n$  is the flow index. Substituting Equation (5.6) into (5.5) gives:

$$\partial_r p = \partial_z \left[ m_0 |\partial_z v|^{n-1} \partial_z v \right] \quad (5.7)$$

Integrating Equation (5.7) twice over the film (that is, between  $z = 0$  and  $z = h(r, t)$ ) yields:

$$v = \frac{n}{n+1} \left( -\frac{\partial_r p}{m_0} \right)^{1/n} \left[ h^{\frac{n+1}{n}} - (h-z)^{\frac{n+1}{n}} \right] \quad (5.8)$$

Setting  $n = 1$  gives the expression for a Newtonian fluid. For Equation (5.8), boundary conditions were set for no-shear stress at the liquid-film interface ( $z = h$ ) and no-slip at the tablet-film interface ( $z = 0$ ):

$$\partial_z v \Big|_{z=h} = 0 \quad ; \quad v \Big|_{z=0} = 0 \quad (5.9)$$

To use Equation (5.8) an expression for the pressure  $p$  must be specified. Following Schwartz et al. (2001), who investigated the flow of thin films over impermeable substrates, one writes:

$$p = -\gamma_s \partial_x \cdot \partial_x h - \pi_c \quad (5.10)$$

where  $\gamma_s$  is the surface tension at the film-air interface and  $\pi_c$  is the disjoining pressure. According to Schwartz et al. (2001), the curvature of the film-air interface when the film lies on a flat surface is approximately equal to  $\partial_x \cdot \partial_x h(r, t) = (1/r) \partial_r (r \partial_r h)$ . This approximation is valid only when the film is very thin compared to its length. Thus, the above estimation of the film curvature is reasonable for the case studies investigated in this work.

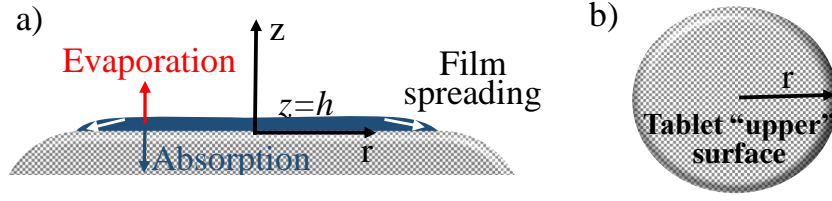


Figure 5.2: a) Coating film on a tablet surface, b) Tablet top view.

The disjoining pressure was calculated in the same way as in Chapter 3, using the Frumkin-Derjaguin model (Schwartz, 1999):

$$\pi_c = \beta \left[ \left( \frac{\hat{h}}{\bar{h}} \right)^N - \left( \frac{\hat{h}}{\bar{h}} \right)^M \right] ; \quad \beta = \frac{1}{\hat{h}} \frac{(N-1)(M-1)}{2(N-M)} \gamma_s (1 - \cos \vartheta) \quad (5.11)$$

where  $\hat{h}$  is the precursor film thickness,  $N$  and  $M$  are positive constants with  $N > M > 1$  and  $\vartheta$  is the equilibrium contact angle of the film on the tablet. Following Schwartz et al. (2001),  $N$  and  $M$  were taken to be equal to 3 and 2, respectively. In all simulation performed in this work, the precursor film thickness  $\hat{h}$  is much smaller than the coating film thickness ( $\hat{h} = 0.1 \mu\text{m}$ ).

Using the lubrication approximation theory, a film thickness evolution equation was derived from the continuity equation written for the mixture. In cylindrical coordinates, Equation (5.1) reads:

$$\partial_t \rho = -(1/r) \partial_r (r \rho v) - \partial_z (\rho w) \quad (5.12)$$

where  $w$  is the vertical velocity component inside the film.

Integrating Equation (5.12) over the vertical direction  $z$ , from  $z = 0$  to  $z = h$ , gives:

$$\partial_t (\rho h) = -(1/r) \partial_r (\rho r Q_s) - \rho W_a - \dot{m}_e \quad (5.13)$$

The derivation of the above equation is given in appendix of this chapter; in this equation,  $W_a$  is the absorption velocity,  $\dot{m}_e$  is the evaporation mass flux and:

$$Q_s \equiv \int_0^h v dz \quad (5.14)$$

Equation (5.13) was used to calculate the thickness  $h$  of the film. However, to solve it, one needs expressions for the absorption velocity and the evaporation mass flux. The former was calculated from the boundary condition at the film-tablet interface:

$$W_a = \varphi w_p \quad \text{at } z = 0 \quad (5.15)$$

where  $w_p$  is the (volume averaged) mixture velocity in the vertical direction inside the tablet which is discussed in Subsection 2.2, and  $\varphi$  is the porosity of the tablet.

To calculate the evaporation mass flux  $\dot{m}_e$  it was assumed that during film drying and before wetted crust formation, the coating carrier fluid can find its way to the film-air

interface without being hindered by the particles (Kiil, 2006). In the literature, the carrier fluid evaporation flux from a thin film is reported to be constant over the film-air interface (Weidner et al. 1996; Kiil, 2006) and given by:

$$\dot{m}_e = \frac{k_m \mathcal{M}_w}{\mathfrak{R}} \left[ \frac{p_\nu^*(T_s)}{T_s} - \frac{RH p_\nu^*(T_{2\infty})}{T_{2\infty}} \right] \quad (5.16)$$

where  $k_m$  is the mass transfer coefficient,  $\mathcal{M}_w$  is the molecular weight of the evaporating liquid phase (water),  $RH$  is the relative humidity in the air bulk,  $\mathfrak{R}$  is the universal gas constant, and  $p_\nu^*$  is the saturated vapor pressure calculated at the film-air interface temperature  $T_s$  and the bulk air temperature  $T_{2\infty}$ . Notice that in the current work, concerning pharmaceutical tablet coating, the film curvature effect on the evaporation rate (negligible Kelvin effect) was neglected. Previous work also neglected this effect (Weidner et al., 1996; O'brien and Schwartz, 2002).

The mass transfer coefficient  $k_m$  can be estimated with the Ranz-Marshall correlation for the Sherwood number Sh:

$$\text{Sh} \equiv \frac{k_m L_s}{\mathcal{D}_\nu} \equiv 2 + 0.65 \text{Re}_g^{1/2} \text{Sc}_g^{1/3} \quad (5.17)$$

where  $\mathcal{D}_\nu$  is the vapor diffusivity and  $L_s$  is the characteristic length of the film. In the simulations,  $L_s$  was taken to be equal to the diameter of the wetted area of the cylindrical coating film covering the surface of the tablet.

In Equation (5.17), the Reynolds ( $\text{Re}_g$ ) and Schmidt ( $\text{Sc}_g$ ) numbers are defined as follows:

$$\text{Re}_g \equiv \frac{\rho_2 v_2 L_s}{\mu_2} \quad ; \quad \text{Sc}_g \equiv \frac{\mu_2}{\rho_2 \mathcal{D}_\nu} \quad (5.18)$$

where  $\rho_2$ ,  $\mu_2$  and  $v_2$  are the density, viscosity and characteristic velocity of the gas above the tablet, respectively.

The vapor diffusivity  $\mathcal{D}_\nu$  was obtained using the following empirical relation (Mezhericher et al. 2008):

$$\mathcal{D}_\nu = 3.564 \cdot 10^{-10} (T_s + T_{2\infty})^{1.75} \quad (5.19)$$

where  $T_{2\infty}$  is the bulk air temperature in the coating drum in Kelvin.

To calculate the evaporation flux  $\dot{m}_e$  (Eq. 5.16), one needs to estimate the temperature at the film surface  $T_s$ . Following Kiil (2006), it was assumed that the temperature ( $T_1$ ) is uniform throughout the film since this is very thin. Thus,  $T_s = T_1$  was calculated from an energy equation for the thin film:

$$\langle \rho c_{p1} \rangle V_1 \partial_t T_1 = -\dot{m}_e \Delta H_e A_{12} - h_H (T_1 - T_{2\infty}) A_{12} - k_3 \partial_z T_3 \Big|_{z=0} A_{13} \quad (5.20)$$

where  $A_{12}$  and  $A_{13}$  are the areas of the film-air and film-tablet interfaces, respectively,  $V_1$  is the volume of the film,  $c_{p1}$  is the heat capacity of the film,  $T_3$  is the temperature field within the tablet,  $h_H$  is the heat transfer coefficient,  $k_3$  is the thermal conductivity of the tablet

and  $\Delta H_e$  is the enthalpy of vaporization. The above expression was derived from the general equation of change of internal energy in the appendix of this chapter. The calculation of the heat conduction from the substrate (tablet) to the coating film is also analyzed in the appendix.

Estimating the particle concentration in the film during coating can provide important information about intra-tablet coating uniformity. An evolution equation for the solid volume fraction inside the film was derived from the continuity equation written for the solid phase in the coating mixture. This in cylindrical coordinates reads:

$$\partial_t \phi = -(1/r) \partial_r (r\phi v) - \partial_z (\phi w) - (1/r) \partial_r (rj_r) - \partial_z j_z \quad (5.21)$$

The quantities  $j_r$  and  $j_z$  denote the components of the particle migration flux in the radial and vertical directions, respectively. Using the “well mixed” approximation, Weidner et al. (1996) neglected particle migration across the film thickness. This approximation is based on the fact that the vertical migration term is negligible compared to the radial migration term, because in the vertical direction of the thin film the solid volume fraction variations are mild.

The “well mixed” approximation was adopted and Equation (5.21) was simplified as follows:

$$\partial_t \phi = -(1/r) \partial_r (r\phi v) - \phi \partial_z w - (1/r) \partial_r (rj_r) \quad (5.22)$$

Following similar steps as those presented in the derivation of the film thickness evolution equation (see appendix of the chapter) and making the necessary simplifications yields the following equation:

$$\partial_t \phi = -\frac{\rho Q_s}{h} \partial_r (\phi/\rho) + \frac{\phi \dot{m}_e}{\rho h} - \frac{1}{hr} \partial_r (rhj_r) + \frac{\phi}{\rho} \partial_t \rho \quad (5.23)$$

To solve Equation (5.23) one needs expressions for the particle migration flux  $j_r$ . To derive such expression one first needs to estimate the Peclet number  $Pe \equiv a^2 \dot{\gamma} / \mathcal{D}$  where  $\mathcal{D}$  is the particle Brownian diffusion coefficient,  $a$  is the particle radius (assuming they resemble a sphere) and  $\dot{\gamma}$  is the shear rate scale. For the cases considered in this work,  $Pe \sim 10^{-6}$  (see appendix). Because the particle Peclet number is much smaller than unity, the coating suspensions of interest in this work can be considered Brownian. So, the main cause for particle migration can be regarded to be the Brownian motion.

Thus, the radial component of the particle migration was calculated from:

$$j_r = -\mathcal{D} \partial_r \phi \quad (5.24)$$

The Brownian diffusivity ( $\mathcal{D}$ ) is a function of the solid volume fraction (Batchelor, 2000). Following Russel et al. (1989), the following expression was used:

$$\mathcal{D}(\phi) = K(\phi) \frac{d}{d\phi} [\phi Z(\phi)] \mathcal{D}_0 \quad (5.25)$$

where  $K(\phi) \equiv (1 - \phi)^{6.55}$  is the particle sedimentation coefficient,  $Z(\phi) = 1.85/(\phi^* - \phi)$  is the compressibility factor (Yiantsios and Higgins, 2006) and  $\mathcal{D}_0 = (k_B T_w)/(6\pi\mu_w a)$  is the Einstein diffusivity, where  $k_B$  is the Boltzmann coefficient, while  $T_w$  and  $\mu_w$  are the carrier fluid temperature and viscosity, respectively. In the expression for the compressibility factor,  $\phi^*$  is the close packing volume fraction. According to Rutgers (1962a), this is 0.67 for hard spheres.

As mentioned before, pharmaceutical coatings can exhibit either Newtonian or slight shear thinning behavior (Bolledulla et al., 2010; Ketterhagen et al., 2017). Since the coating mixture viscosity is affected by the solid particle concentration, in the case of the shear thinning behavior, one can write a constitutive equation in the form:

$$\eta(\dot{\gamma}, \phi) = m_0(\phi) |\partial_z v|^{n(\phi)-1} \quad (5.26)$$

where  $m_0(\phi)$  and  $n(\phi)$  need to be calculated from experimental data concerning the rheology of different pharmaceutical suspensions (Mueller et al., 2010).

For coating formulations that behave as Newtonian fluids, the mixture viscosity is a function of the volume fraction of particles. A constitutive equation that allows calculating it is that of Krieger and Dougherty (1959), which reads:

$$\eta(\phi) = \mu_w (1 - \phi/\phi^*)^{-1.82} \quad (5.27)$$

Equation (5.27) can be used to accurately predict the Newtonian viscosity of a Brownian suspension for particle volume fractions ranging from 0 to 0.55 (Buyevich and Kapbsov, 1999).

For higher volume fractions than 0.55, and up to the closed-packed limit of  $\phi \rightarrow \phi^*$ , one can use the expression derived by Brady (1993):

$$\eta(\phi) = \mu_w 1.3 (1 - \phi/\phi^*)^{-2} \quad (5.28)$$

Equation (5.28) was obtained by Brady (1993) for low shear rates and close to the limit of  $\phi \rightarrow \phi^*$ . It was considered that the simulation is completed when the particle volume fraction becomes equal to  $\phi^*$  and the suspension film can no longer be regarded as a liquid (the viscosity becomes infinite) but as a wetted solid. At this stage the formation of a wetted crust takes place in the entire thin film. The time required for the crust formation is considered as the ‘‘crust formation time’’  $t_{cr}$  in the model.

Ketterhagen et al. (2017) reported that an increase in the film temperature would decrease the viscosity of the coating suspension. This effect can be captured with an empirical equation of the form  $\eta(\dot{\gamma}, \phi, T) = \eta(\dot{\gamma}, \phi)|_{20^\circ\text{C}} \cdot \exp[A_c/(T_1 - T_c)]$ , where  $A_c$  ( $^\circ\text{C}$ ) and  $T_c$  ( $^\circ\text{C}$ ) are coefficients determined by experimental data (Civan, 2008b), and  $\eta(\dot{\gamma}, \phi)|_{20^\circ\text{C}}$  is calculated from Equations (5.26-5.28).

In Subsection 5.2.1, the part of the model which deals with the suspension flow and drying over the surface of the tablet was presented. With Eqs. (5.13) and (5.23), one can predict the film thickness and the particle volume fraction profiles over the surface of the tablet. However, solving them requires an expression for the absorption velocity ( $W_a$ ) at the film-tablet boundary (see Equation 5.15). In Subsection 5.2.2, the coating suspension absorption into the tablet is investigated and an expression for  $W_a$  is derived.

### 5.2.2 Coating absorption into the tablet core

As mentioned before, the coating suspension penetrates into the porous tablet at the same time as it dries and flows over the surface of this tablet. Since the characteristic size of the particles of a coating suspension ( $a = 10^{-8}$  m; Cole et al., 1995) is much smaller than the diameter of the tablet pores ( $d_p = 10^{-6}$  m; Collins et al., 2007), no pore clogging occurs. However, particle retention on the pore walls takes place, and reduces the porosity and permeability of the tablet. When the coating suspension dries at the surface of the tablet, the imbibition stops. In this subsection, the part of the model which predicts the wetting front profile of a coating suspension inside the tablet core is presented. To estimate the suspension velocity field inside the tablet, the mixture model balance equations were solved while taking into account the effect of particle retention on the porosity and the permeability of the porous tablet.

The mass balance for the suspension over a differential control volume containing only the bulk volume of the pores, but not the pore wall, reads:

$$\partial_t(\varphi\rho) = -\partial_{\mathbf{x}} \cdot (\varphi\rho\mathbf{u}_p) - \rho_s\Gamma \quad (5.29)$$

where  $\mathbf{u}_p$  is the volume-averaged velocity of the suspension inside the porous tablet and  $\Gamma$  represents the volume rate of particles deposited per unit bulk volume of porous medium. The constitutive equation for  $\Gamma$  is discussed below in this section.

The tablet porosity  $\varphi$  is given by:

$$\varphi = \varphi_0 - \epsilon_p \quad (5.30)$$

where  $\varphi_0$  is the tablet porosity before any suspension gets absorbed and  $\epsilon_p$  is the volume fraction of the particles deposited on the walls of the pores.

The mass balance equation for the mixture over a differential volume containing only the pore walls is:

$$\rho_s\partial_t\epsilon_p = \rho_s\Gamma \quad (5.31)$$

The mass balance equation for the suspended particles (solid phase) over a differential control volume containing only the bulk volume of the pores is given by:

$$\partial_t(\varphi\phi_p) = -\partial_{\mathbf{x}} \cdot (\varphi\phi_p\mathbf{u}_p) - \partial_{\mathbf{x}} \cdot \mathbf{j}_p - \rho_s\Gamma \quad (5.32)$$

where  $\phi_p$  is the particle volume fraction in the suspension in the tablet pores and  $\mathbf{j}_p$  is the particle migration flux which is discussed later in this section.

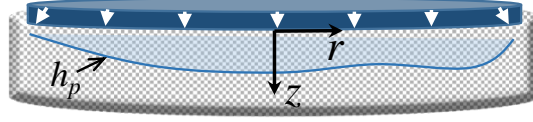


Figure 5.3: Wetting front depth inside the tablet.

To calculate the suspension velocity field inside the porous tablet  $\mathbf{u}_p$ , Darcy's equation was used:

$$\mathbf{u}_p = -\frac{1}{\varphi} \frac{\mathcal{K}_p}{\eta} \partial_{\mathbf{x}} p_p \quad (5.33)$$

where  $p_p$  is the pressure inside the tablet and  $\mathcal{K}_p$  is the tablet permeability which was estimated from the modified Kozeny-Carman equation (Civan, 2011):

$$\mathcal{K}_p = \frac{d_p^2 \varphi_0^3}{180 (1 - \varphi_0)^2} \left(1 - \frac{\epsilon_p}{\varphi_0}\right)^2 \quad (5.34)$$

where  $d_p$  is the average pore diameter of the tablet.

To calculate the mixture pressure inside the tablet  $p_p$ , Darcy's equation was substituted into the mass balance Equation (5.29):

$$\partial_t (\varphi \rho) = \partial_{\mathbf{x}} \cdot [(\mathcal{K}_p / \eta) \rho \partial_{\mathbf{x}} p_p] - \rho_s \Gamma \quad (5.35)$$

For the pressure  $p_p$ , one can write two boundary conditions; one at the tablet core surface and one at the wetting front depth:

$$p_p = p, \text{ at } z = 0 \quad ; \quad p_p = p_c, \text{ at } z = h_p \quad (5.36)$$

where  $p_c$  is the capillary pressure and  $h_p$  is the wetting front depth inside the tablet (Fig. 4). The capillary pressure depends on the dimensions of the average pore and the solid-liquid contact angle ( $\vartheta$ ) and it equals the Laplace pressure in a capillary, given by:

$$p_c = -(4/d_p) \gamma_s \cos \vartheta \quad (5.37)$$

Equation (5.33) gives the velocity field of the coating mixture inside the porous tablet. To calculate the wetting front depth inside the tablet  $h_p$ , the wetting front profile can be defined as  $F_p(r, z, t) \equiv h_p(r, t) - z$  (Leal, 2007). The substantial derivative of  $F_p$  is zero and this allows one to write:

$$\begin{aligned} \frac{DF_p}{Dt} = 0 &\Rightarrow \partial_t F_p + \mathbf{u}_p \cdot \partial_{\mathbf{x}} F_p = 0 \\ &\Rightarrow \partial_t h_p + v_p \Big|_{h_p} \partial_r h_p - w_p \Big|_{h_p} = 0 \end{aligned} \quad (5.38)$$

where  $v_p$  and  $w_p$  are the radial and vertical velocity components of the mixture inside the porous medium, respectively. To calculate these velocity components, one needs to express Darcy's equation (Eq. 5.33) in cylindrical coordinates which is reported in the appendix for the sake of brevity.

Iwasaki (1937) derived an expression for the particle retention rate assuming it proportional to the total particle flux:

$$\Gamma = \mathcal{F}_p (\varphi \phi_p \mathbf{u}_p + \mathbf{j}_p) \cdot \mathbf{n}_p \quad (5.39)$$

where  $\mathbf{n}_p \equiv \partial_{\mathbf{x}} F_p / |\partial_{\mathbf{x}} F_p|$  denotes the outwardly pointing unit vector normal to the wetting front and  $\mathcal{F}_p$  is the particle “filter” coefficient. Following Elimelech et al. (2013), the particle filter coefficient was estimated from:

$$\mathcal{F}_p = (3/2) [(1 - \varphi_0) / d_p] \beta_k r_k (1 - \epsilon_p / \epsilon_p^*)^2 \quad (5.40)$$

where  $r_k$  denotes the single-collector contact efficiency which represents the rate of collisions between the tablet pores and the solid particles within the coating suspension,  $\epsilon_p^*$  is the maximum deposited volume fraction at which the filter coefficient becomes zero and  $\beta_k$  is the attachment efficiency coefficient that represents the fraction of particle collisions leading to particle attachment to the pores (Fig. 5.4).

According to Elimelech et al. (2013), the attachment efficiency coefficient is of order 1 and can be determined experimentally. In this work, since there is no information available in the open literature regarding pharmaceutical suspensions, the attachment coefficient was set  $\beta_k = 1$  as in Civan (2011). For different porous media (e.g. tablets)  $\epsilon_p^*$  is determined by experiments ( $\epsilon_p^* = 0.95 \varphi$ ; Civan, 2011).

Finally, the single-collector contact efficiency coefficient can be calculated from the empirical equation (Tufenkji and Elimelech, 2004):

$$r_k = (3/2) \mathcal{A}_s \left( \frac{a}{d_p} \right)^2 ; \quad \mathcal{A}_s = \frac{2(1 - \lambda_p^5)}{2 - 3\lambda_p + 3\lambda_p^5 - 2\lambda_p^6} ; \quad \lambda_p = (1 - \varphi)^{1/3} \quad (5.41)$$

Notice that the above equations are valid for particles of small radius  $a$  ( $10^{-8}$  m to  $10^{-9}$  m) and in the absence of external forces.

To solve Equation (5.39) one needs an expression for the particle migration flux  $\mathbf{j}_p$ . Following Civan (2011), the flux of suspended particles in a mixture which flows into a porous medium is given by:

$$\mathbf{j}_p = -\varphi \mathcal{D}_p \partial_{\mathbf{x}} \phi_p \quad (5.42)$$

where  $\mathcal{D}_p$  is the coefficient of dispersion of suspended particles migrating in the mixture.

According to Civan (2011), an appropriate empirical relation that relates the particle dispersion coefficient inside a porous medium with the Brownian diffusion coefficient was derived by Hiby (1962):

$$\frac{\mathcal{D}_p}{\mathcal{D}} = 0.67 + \frac{0.65 \text{Pe}_d}{1 + 6.7 \text{Pe}_d^{-1/2}} \quad (5.43)$$

where  $\text{Pe}_d$  is the Peclet number based on the porous medium pore diameter defined as  $\text{Pe}_d \equiv u_p d_p / \mathcal{D}$  where  $u_p$  denotes the order of magnitude of the velocity field of the mixture into the pores.

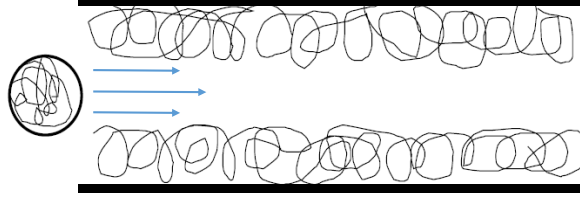


Figure 5.4: Particle passing through a tablet pore. The random lines denote the retained solid coating.

To calculate the particle volume fraction inside the porous tablet, Equations (5.29) and (5.32) were combined to obtain in cylindrical coordinates:

$$\begin{aligned} \rho\varphi \partial_t(\phi_p/\rho) = & -\rho\varphi [(v_p/r) \partial_r(r\phi_p/\rho) + w_p \partial_z(\phi_p/\rho)] - (1/r)\partial_r(rj_{pr}) \\ & -\partial_z j_{pz} - [1 - (\rho_s/\rho) \phi_p] \Gamma \end{aligned} \quad (5.44)$$

where the particle retention rate  $\Gamma$  and the radial and vertical components of the particle migration flux ( $j_{pr}$  and  $j_{pz}$ , respectively) are given by Equations (5.39) and (5.42), respectively, written in cylindrical coordinates (not reported here for the sake of brevity; see appendix of this chapter).

To conclude, in Subsection 5.2.2, the part of the model which deals with the coating film flow inside the tablet was presented. From Equations (5.38) and (5.44), one can predict the wetting front profile and the particle volume fraction inside the porous tablet. Together with Equations (5.38) and (5.44), the expressions for the mixture velocity (Eq. 5.33), pressure (Eq. 5.35), particle retention rate (Eq. 5.39) and migration flux (Eq. 5.42) were solved. These equations expressed in cylindrical coordinates are reported in the appendix of this chapter.

### 5.2.3 Numerical solution

In this subsection, the steps needed to numerically solve the model are shown. The equations that calculate the behavior of the coating suspension film on the surface of the tablet were made dimensionless using the following variables:

$$\begin{aligned} h &\equiv H_0 h^* ; \quad W_a \equiv (\gamma_s/\mu_w) W_a^* ; \quad \dot{m}_e \equiv \rho_e (\gamma_s/\mu_w) \dot{m}_e^* ; \quad Q_s \equiv Q_s^* (\gamma_s/\mu_w) R_0 \\ t &\equiv H_0 (\mu_w/\gamma_s) t^* ; \quad j_r \equiv (\gamma_s/\mu_w) j_r^* ; \quad p \equiv (\gamma_s/R_0) p^* ; \quad \rho \equiv \rho_e \rho^* \\ \eta &\equiv \mu_w \eta^* ; \quad r \equiv R_0 r^* ; \quad z \equiv H_0 z^* \end{aligned}$$

where  $H_0$  and  $R_0$  denote the initial maximum film thickness and the characteristic length of the tablet surface, respectively. Using the above, one can make dimensionless and solve the equations for the film thickness profile (Eq. 5.13) and the solid volume fraction profile (Eq. 5.23), together with the necessary closure equations for the suspension density, velocity, pressure, evaporation flux and viscosity, and particle migration flux (Eqs. 5.2, 5.8, 5.10, 5.16, 5.26 and 5.24, respectively).

Moreover, the evolution equations that calculate the coating suspension wetting front depth (Eq. 5.38) and polymer volume fraction inside the porous tablet (Eq. 5.44) were made dimensionless together with the necessary closure equations for the suspension velocity and pressure, and the particle retention and migration flux inside the tablet (Eqs. 5.33, 5.35, 5.39 and 5.42, respectively) using the following dimensionless variables:

$$h_p \equiv H_0 h_p^* ; w_p \equiv (\gamma_s/\mu_w) w_p^* ; v_p \equiv (\gamma_s/\mu_w) v_p^*$$

$$j_{pr} \equiv (\gamma_s/\mu_w) j_{pr}^* ; j_{pz} \equiv (\gamma_s/\mu_w) j_{pz}^* ; p_p \equiv (\gamma_s/R_0) p_p^*$$

The equations describing the behavior of the coating mixture inside the tablet are defined in a moving domain ( $0 < z^* < h_p^*$ , Fig. 5.3). This is because the wetting front position changes with time. It is possible to turn the integration domain into one with fixed boundaries through a suitable change of independent variables. This was done, in the same way as in Chapter 3, by employing the transformation proposed by Landau (1950). By using Landau's transformation the moving boundary in Eqs. (5.33, 5.35, 5.38, 5.39, 5.42, 5.44) is fixed (Kutluay et al. 1997).

In Section 5.2, the main evolution equations of the model were presented. This model can predict the film thickness, imbibition depth and coating particle volume fraction onto and into a pharmaceutical tablet. The model can also estimate the crust formation time  $t_{cr}$  required for the polymer concentration to reach a critical value  $\phi^*$  at which point the coating suspension film can no longer be considered as liquid but as a solid (the mixture viscosity diverges).

### 5.3 Numerical results and validation

In this section, the numerical results from the model described in Section 5.2 are presented. Because the experimental data were taken from multiple sources, a single case study was not investigated; instead parts of the model were validated separately with experimental and theoretical studies of different researchers.

In Subsection 5.3.1, experimental and numerical data from the work of Niblett et al. (2017) are used to validate the numerical predictions concerning the drying rate of pharmaceutical coating suspension films (Subsection 5.3.1). In Subsection 5.3.2, the predictions of the model for the absorption of pure liquid films into porous media are compared with the corresponding experimental results of Léang et al. (2019). Léang et al. (2019) investigated the absorption of liquids of different viscosity into porous media of different permeabilities.

Experimental data which are suitable to validate the part of the model that accounts for the effect of particles on pharmaceutical coating suspension absorption into a tablet were not available in the open literature. However, in Subsection 5.3.3, numerical results that showcase the influence of different model parameters on coating suspension flow and absorption into the tablet are presented. All the numerical calculations were performed in gPROMS (PSE, 2019), employing the Modelbuilder modeling platform.

### 5.3.1 Coating film drying rate

In this work, a model was developed that can predict the drying rate of a coating suspension on a tablet surface. The model calculates the concentration of particles into the coating suspension as it dries and takes into account that when the particle volume fraction becomes equal to  $\phi^*$  the coating film can no longer be considered as a liquid with suspended solids, but behaves as a wetted solid (Kiil, 2006).

The model developed in this work can calculate the wetted crust formation time  $t_{cr}$ , given the film-coating process conditions (temperatures, relative humidity and air flow rate). According to Niblett et al., (2017), calculating the time required for the coating film to solidify on the surface of a tablet is important, since after that time ( $t > t_{cr}$ ), no coating suspension can be exchanged between tablets as they move (rotate) in the drum and thus no tablet defects (inter-tablet coating variability) can be created.

In this subsection, the ability of the current model to calculate the drying rate of an aqueous pharmaceutical coating suspension (Aquarius Prime, 10% w/w solid particles,  $\rho_s = 1438 \text{ kg/m}^3$ ,  $\gamma_s = 0.046 \text{ N/m}$ ) is shown. The results of the model are compared with the equivalent numerical results reported by Niblett et al. (2017), who performed experiments to study the drying rate of pharmaceutical suspensions and its effect on tablet appearance. Based on their experimental observations, they developed a model that can estimate the drying rate of the coating suspensions used in the experiments. They reported that the experiments and their model are in good agreement, but did not explicitly report the experimental values for the evaporation flux or the overall drying time.

The tablet in both this study and the one by Niblett et al. (2017) was taken to be cylindrical (7 mm in diameter). The suspension film was also considered to be cylindrical and cover only the “upper” round surface of the tablet (see Fig. 5.2). Since Niblett et al. (2017) did not report initial temperatures of the tablet or of the suspension after application, it was considered that the tablets are preheated close to the temperature of the bulk air (Möltgen et al., 2012) and that the suspension is sprayed at 25°C.

Finally, because Niblett et al. (2017) studied the coating suspension behavior on flat, impermeable substrates and did not investigate the coating suspension flow or absorption into the tablet, these processes were also neglected in the simulations (for this case study only), and the part of the model related to coating suspension drying presented in Subsection 5.2.1 was validated here.

In Table 5.1, the solvent evaporation flux  $\dot{m}_e$  predictions of the model are compared to those estimated by the model of Niblett et al. (2017). The conditions of the coating runs and simulations performed by Niblett et al. appear in Table 5.1 as well. These conditions were used in the validation simulations.

Table 5.1: Current model predictions for coating solvent evaporation mass flux  $\dot{m}_e$ . Validation with numerical results by Niblett et al. (2017).

Bulk air temperature ( $^{\circ}\text{C}$ )	Relative humidity	Air flow rate ( $\text{m}^3\text{s}^{-1}$ )	Evaporation mass flux ( $\text{kg}/\text{m}^2\text{s}$ )	
			Niblett et al., 2017	Model
60	0.50	0.090	0.0075	0.0074
70	0.42	0.100	0.0139	0.0134
60	0.58	0.075	0.0065	0.0060
65	0.40	0.070	0.0084	0.0092
65	0.40	0.070	0.0096	0.0101

From the model output, one can deduct that higher temperature and air flow rate in the coating drum, as well as lower relative humidity, lead to faster evaporation rates. The model is in good agreement with the data by Niblett et al. (2017) as seen also in Figure 5.5 ( $|\% \text{Error}| < 12\%$ ). In Figure 5.5, the dotted lines represent the 10% error lines.

### 5.3.2 Pure solvent absorption rate

Here, the model (Subsection 5.2.1) predictions for the absorption of pure liquids into porous media with the corresponding experimental results of Léang et al. (2019) are validated. Léang et al. investigated the absorption of different solvents into porous media of different permeabilities. During this research project, it was not possible to find experimental data regarding concentrated suspension penetration into porous media which are suitable to validate the part of the model that accounts for coating suspension film absorption and particle retention inside the pores of a pharmaceutical tablet. Thus, only the ability of the model to simulate the absorption of pure liquid films (of ranging viscosity) into different porous substrates while the films evaporate is shown here. Coating suspension penetration into porous media and the influence of particle retention on the absorption rate are discussed in Subsection 5.3.3.

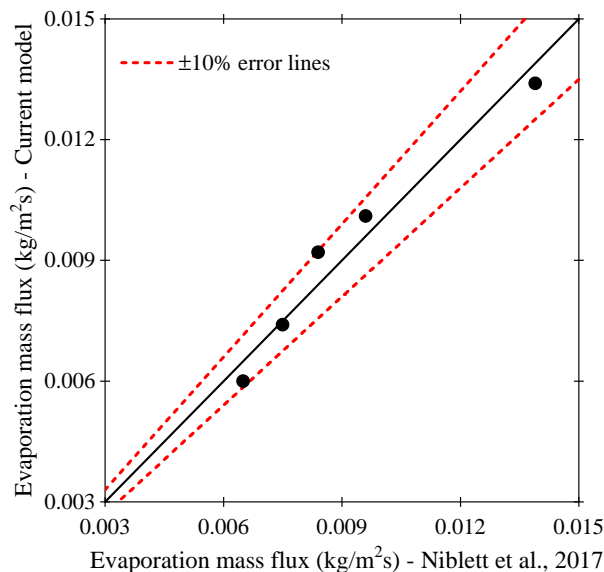


Figure 5.5: Validation of numerical results for pharmaceutical coating (Aquarius Prime) drying rate. Comparison with data by Niblett et. al. (2017).

In Figure 5.6.a), the model predictions for the maximum water ( $M_w = 18$  g/mol,  $\rho = 998$  kg/m<sup>3</sup>,  $\mu_w = 1$  cP,  $\gamma_s = 0.072$  N/m) film penetration depth into a porous medium are compared with the corresponding experimental data of Léang et al. (2019). In the simulation and experiment, the initial film thickness, the porosity and the pore radius of the substrate were set to  $h = 200$   $\mu$ m,  $\varphi = 0.33 \pm 0.02$  and  $r_p = 4.8 - 5$  nm, respectively. The water contact angle  $\vartheta$  with the porous substrate was measured by Léang et al. (2019) to be  $31 \pm 2^\circ$ . The values of the relative humidity ( $RH = 54 \pm 2\%$ ) and the air, film and substrate temperatures ( $20^\circ$ C) used in the simulations in this work were the same as those used in the experiments. The water evaporation mass flux reported by Léang et al. ( $\dot{m}_e = 4.9 \cdot 10^{-5}$  kg/m<sup>2</sup>s) was very close to the one calculated by the model ( $\dot{m}_e = 5.01 \cdot 10^{-5}$  kg/m<sup>2</sup>s).

Figure 5.6.b) shows the validation of the model predictions for viscous liquid absorption into a porous medium (glycerol,  $M_w = 92$  g/mol,  $\rho = 1260$  kg/m<sup>3</sup>,  $\mu = 1500$  cP,  $\gamma_s = 0.063$  N/m). In the simulation and experiment, the initial film thickness, the porosity and the pore radius of the substrate were set to  $h = 200$   $\mu$ m,  $\varphi = 0.31 \pm 0.03$  and  $r_p = 7.9 - 8$  nm, respectively. The glycerol contact angle  $\vartheta$  with the porous substrate was measured by Léang et al. (2019) to be  $20 \pm 2^\circ$ . Again, the values of the relative humidity ( $RH = 54 \pm 2\%$ ) and the air, film and substrate temperatures ( $20^\circ$ C) used in the simulations were the same as those used in the experiments. The results in Figures 5.6.a) and 5.6.b) are in reasonable agreement with the experimental data ( $|\%Error| < 15\%$ ) given the uncertainty of the model input/experimental parameters.

The red dotted lines in Figure 5.6 represent the propagated error due to input parameter uncertainty. Some of the input parameters of the model were difficult to determine precisely from the experimental results reported in the literature. To account for this, the experimental measurement errors (reported by Léang et al., 2019) of the input parameters were propagated to the numerical results of the model following the stochastic sampling method of Cacuci and Cacuci (2003). First, the probability distributions (measurement error) of the input parameters were defined based on experimental data found in the literature. Subsequently, these distributions were used to generate a sample and create multiple scenarios using gPROMS Modelbuilder. Lastly, a series of simulations were performed and the standard deviation of the response variable, which in this case is the maximum wetting front depth (penetration depth), was calculated (Cacuci and Cacuci, 2003). The above method is made possible by the ability of the current model to provide predictions for the wetting front in a reasonably short time ( $< 1$  min). Such analysis would not be possible with more computationally expensive CFD simulations.

In the case of pharmaceutical coating dispersions, the solid particles can hinder solvent absorption by clogging the pores and reducing the tablet permeability. It is reported in the literature that water penetrates into the porous core (Möltgen et al., 2012) and that coating suspension absorption into the tablet promotes film adhesion (Muliadi and Sojka, 2010). Thus, the effect of particle retention on coating absorption is investigated qualitatively in Subsection 5.3.3.

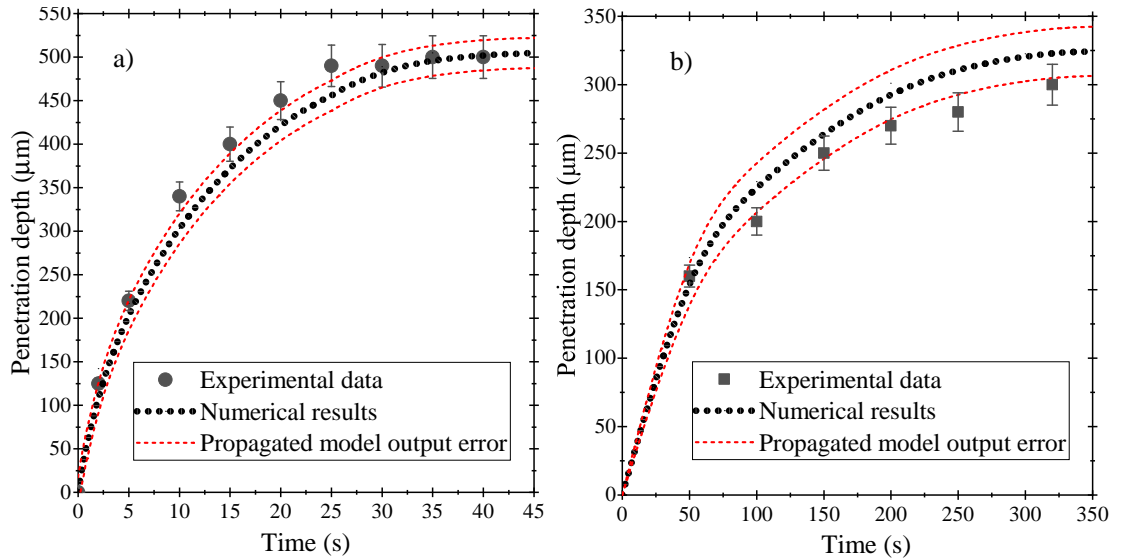


Figure 5.6: Validation of numerical results for pure liquid (a. water, b. glycerol) absorption rate into porous substrates. Comparison with experimental data reported by Léang et al. (2019).

### 5.3.3 Coating flow, absorption and evaporation

In this subsection, numerical results of the overall model are presented. These results highlight the influence of different process and suspension parameters on film flow and absorption into the tablet. This work aims to assist the pharmaceutical industry understand how different parameters affect the amount of water and solid particles entering the tablet. Excess water inside the tablet may lead to shorter tablet shelf-life, whereas lack of particle penetration into the pores can lead to poor film adhesion (Cole et al., 1995).

Figure 5.7 shows the model (Section 5.2) predictions for the thickness and particle volume fraction profiles of a suspension film which is applied onto a tablet. In the simulation, the thin film (100 μm) was considered to cover part of the upper surface of a cylindrical tablet 1 cm in radius (the wetted area radius is 0.8 cm). The coating suspension drying, flow over the dry parts of the tablet surface, and penetration into the tablet were simulated. The temperature and relative humidity of the air above the film were set  $T = 50^\circ\text{C}$  and  $RH = 0.50$ , respectively. These conditions are representative of the conditions in a coating process.

The coating suspension was considered to have an initial volume fraction of particles of 0.20, an initial temperature of  $25^\circ\text{C}$ , and to exhibit a shear thinning behavior. For the range of shear rates in this simulation, it was regarded that the coating suspension behaves as a power law fluid. The consistency and flow indices were calculated from the experimental data of Bolleddula et al. (2010) for OpadryII White pharmaceutical suspensions  $n(\phi) = 0.85\phi^{-0.04}$ ,  $m_0(\phi) = \hat{m}_0(1 - \phi/0.67)^{-2}$  where  $\hat{m}_0 = 10 \text{ Pa}\cdot\text{s}^n$  and  $\phi \geq 0.20$ . Finally, the initial tablet porosity and temperature were set to 0.3 and  $50^\circ\text{C}$ , respectively, and the suspension particle size is set to be smaller than the pore radius ( $a = 10^{-9}\text{m} \ll d_p = 10^{-6}\text{m}$ ).

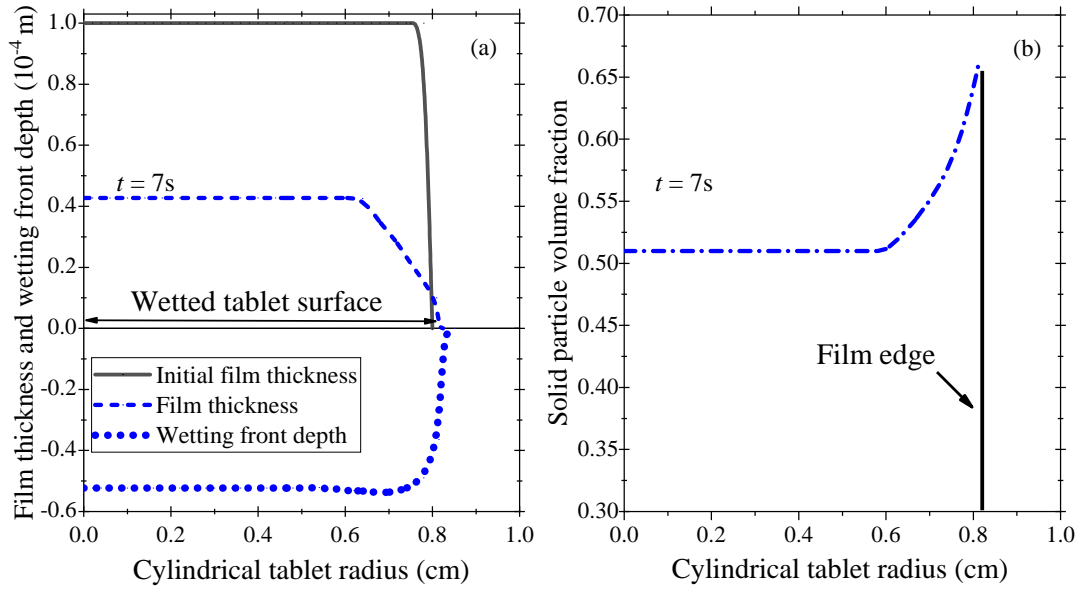


Figure 5.7: a) Suspension film thickness and penetration depth profiles, and b) particle volume fraction distribution, in the film after 7 s.

As seen in Figure 5.7.a), after 7 s the coating suspension has spread over the dry parts of the tablet. The model predicted that the wetted area radius expands over the dry surface by 0.015 cm. Moreover, the model calculated that after 7 s the maximum coating suspension penetration is  $55 \mu\text{m}$ . Figure 5.7.b) shows the solid particle volume fraction inside the suspension film after 7 s. The concentration of particles is higher towards the film contact line where there is less carrier fluid (water) as the coating flows over the surface of the tablet. This was expected based on the work of Pham and Kumar (2019) who investigated the formation of coffee-ring patterns during the evaporation and imbibition of droplets containing solutes.

In Figure 5.8.a), the influence of the water evaporation velocity ( $E \equiv \dot{m}_e/\rho_e$ ) on the suspension wetting front depth is studied. Different process conditions (temperatures, drying air flux and relative humidity) were set so that the evaporation velocity ranges from  $5 \cdot 10^{-6}$  m/s to  $5 \cdot 10^{-8}$  m/s. The initial particle volume fraction of the suspension and the initial porosity and pore radius of the tablet were the same in all simulations ( $\phi_0 = 0.15$ ,  $\varphi_0 = 0.33$ ,  $d_p = 10^{-6}$  m). In all case studies presented in Figure 5.8, the particle size was taken to be smaller than the pore radius ( $a/d_p < 10^{-2}$ ) and the initial film thickness was taken to be  $100 \mu\text{m}$ . The results suggest that higher evaporation velocities lead to less suspension in the tablet. This is expected since more coating dries on the surface when the evaporation rate is high. Notice that when the evaporation velocity is significantly lower than the absorption (calculated here:  $W_a \sim 10^{-6}$  m/s), the effect of evaporation is small.

The pharmaceutical industry utilizes coating suspensions (formulations) of different solid volume fraction. Figure 5.8.b) shows the effect of the initial solid volume fraction on the wetting front depth. The coating suspension was considered to be Newtonian and the initial porosity and pore diameter of the tablet as well as the evaporation velocity were the same in all simulations ( $\varphi_0 = 0.33$ ,  $d_p = 10^{-6}$  m,  $E = 5 \cdot 10^{-6}$  m/s).

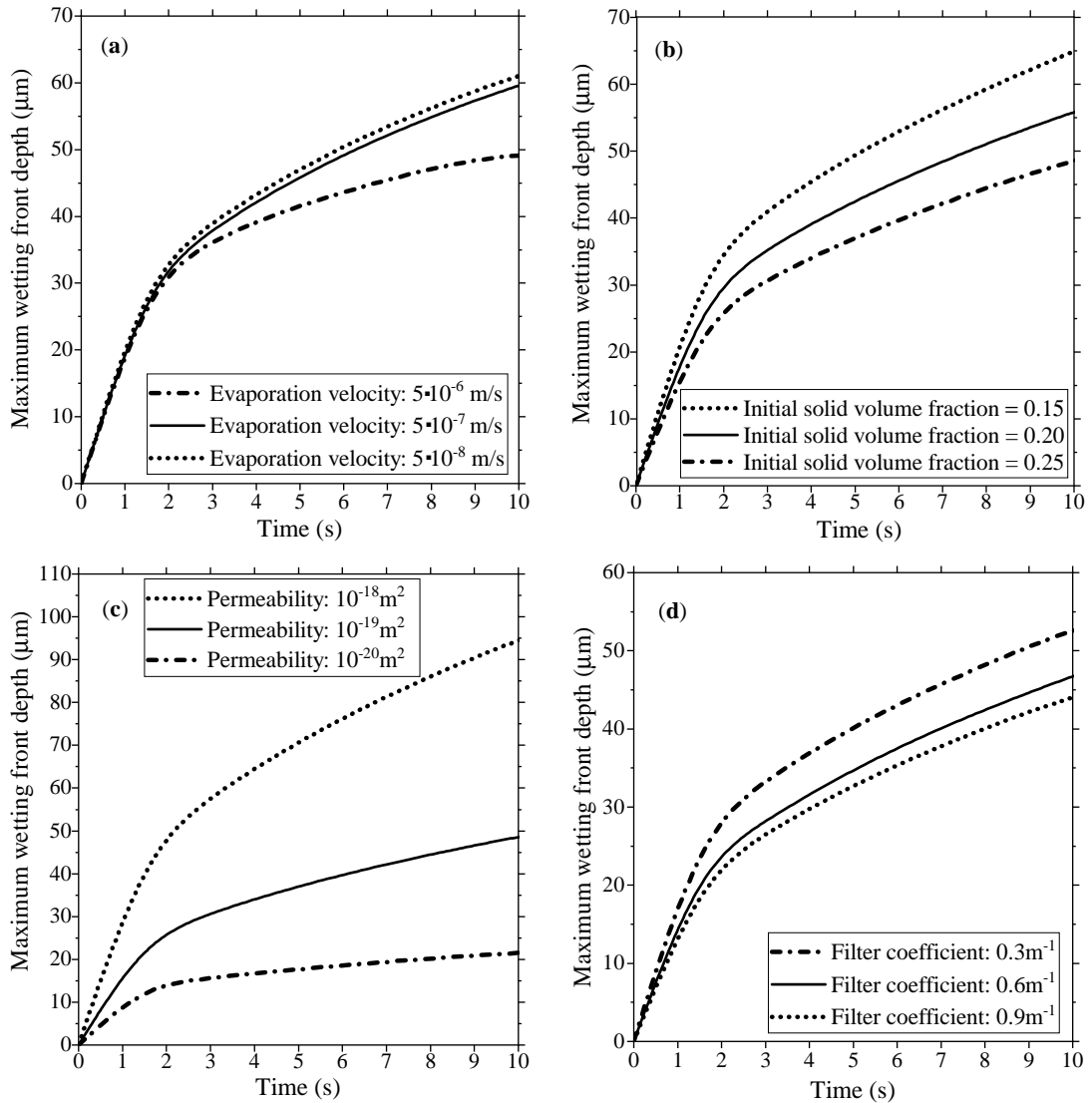


Figure 5.8: Effect of the a) evaporation velocity, b) initial solid volume fraction, c) tablet initial permeability, and d) filter coefficient on the coating suspension absorption rate.

As seen in Figure 5.8.b), since the volume fraction of particles is connected to the viscosity of the coating suspension, higher initial concentration of particles leads to higher viscosity and thus the film spreads and penetrates into the tablet more slowly. Slower absorption means that more coating dries on the surface of the tablet and therefore the final wetting front depth is lower in the case of high initial particle volume fraction in the suspension.

In Figure 5.8.c), numerical results of the model that highlight the influence of the initial tablet permeability on coating suspension absorption into the tablet are presented. In these simulations, the evaporation velocity was calculated to be  $E = 5 \cdot 10^{-6}$  m/s and the particle radius and initial volume fraction were taken to be  $10^{-8}$  m and 0.15, respectively. It is observed that lower initial permeability makes the effect of particle retention on the absorption rate stronger. As expected, the model predicts that higher initial permeability leads to more suspension into the tablet. Tablet permeability can be manipulated during tablet formation in order to reduce the amount of water penetrating into the core.

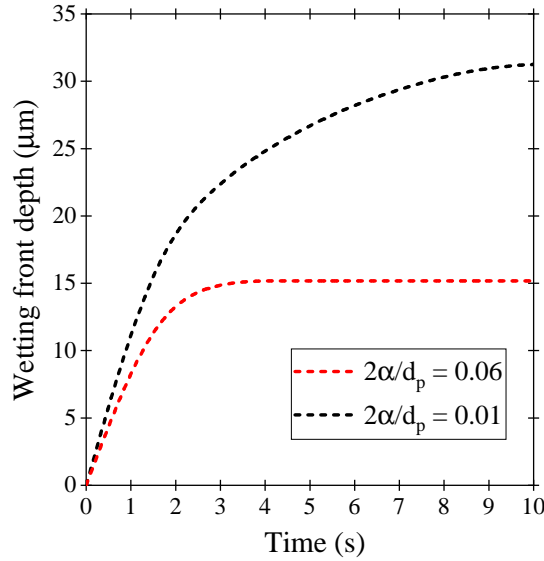


Figure 5.9: Effect of the particle diameter/pore diameter ratio on the suspension wetting front depth.

Particle retention can affect coating absorption by blocking tablet pores and reducing permeability. The filter coefficient  $\mathcal{F}_p$  used in all case studies presented before was estimated from Equation (5.40). Since Equation (5.40) is not validated for the specific case concerning this work, the effect of the initial filter coefficient on the suspension penetration depth prediction was investigated. In Figure 5.8.d), it is shown that increasing the filter coefficient increases the volume fraction of retained particles ( $\epsilon_p$ ) and thus hinders coating absorption. The coating suspension was considered to have an initial particle volume fraction of  $\phi_0 = 0.15$  and the initial porosity and pore diameter of the tablet as well as the evaporation velocity were the same in all simulations ( $\varphi_0 = 0.33$ ,  $d_p = 10^{-6}$  m,  $E = 5 \cdot 10^{-6}$  m/s). Accurately estimating the filter coefficient is important because it will allow more accurate prediction of the particle volume fraction in the tablet.

Figure 5.9 shows how the particle diameter/pore diameter ratio affects coating absorption. In the first case,  $2a/d_p = 0.06$ , whereas in the second  $2a/d_p = 0.01$ . The initial tablet porosity and pore diameter of the tablet as well as the water evaporation velocity were the same in both simulations ( $\varphi_0 = 0.30$ ,  $d_p = 10^{-7}$  m,  $E = 5 \cdot 10^{-6}$  m/s). From the figure, one can deduce that if  $2a/d_p \geq 0.06$ , significant particle retention can hinder absorption after 3 s. After this stage, the particle volume fraction in the pores is too high and the tablet becomes almost impermeable ( $\varphi = \varphi_0 - \epsilon_p \rightarrow 0$ ). According to Holloway et al. (2011), the critical particle diameter/pore diameter ratio at which a concentrated suspension clogs a capillary tube is 0.06. Indeed, the model predicts that in this case clogging occurs after a few seconds of absorption (3 s). Having low water content and at least some solid particles retained close to the tablet surface (as in the case study where  $2a/d_p = 0.06$ ) is preferred by the pharmaceutical industry in order to increase the tablet shelf-life and avoid defects such as peeling of the dry coating film (Cole et al., 1995; Muliadi and Sojka, 2010).

## 5.4 Concluding remarks

This work considers the film-coating process that is widely utilized within the pharmaceutical industry. Film-coating is a complex process that is difficult to simulate accurately with reasonable computational cost. In this chapter, a model that extends the work presented in Chapter 3 was developed. This model can quickly simulate the coating suspension film flow and drying over tablet surfaces, and the coating suspension absorption into porous tablets. This information allows predicting the evolution of the film penetration depth inside the porous structure of the tablets and the time required for the formation of a porous crust around the tablets. The detailed derivations of the main equations of the mathematical model are presented in the chapter and its appendix. The numerical results of the model, which was implemented in the gPROMS Modelbuilder platform, were validated with experimental and numerical data found in the literature. In Section 5.3, it is shown that the current model predictions are in good agreement with the experimental data from the open literature.

Pharmaceutical coating film behavior on a tablet surface is affected by many parameters. To determine which parameters affect the process more, multiple runs of the model were performed. An advantage of the model developed in this chapter when compared to traditional CFD simulations is the computational speed. Simulating many scenarios with the model presented here is possible because of the limited time required by a single run (CPU time < 1 min). The numerical results of the model suggested that an increase in the drying rate and initial particle concentration of the coating suspension leads to reduced coating penetration into the tablet and thus less water content into the pores. Finally, the influence of the particle retention rate on the tablet permeability was investigated numerically. It was found that particles can hinder the absorption of the coating suspension into the tablet and thus affect the amount of water and solid polymer that penetrates into the tablet. Knowledge of the amount of water and solids inside a pharmaceutical solid dosage form can be used to optimize tablet shelf-life and adhesion of the dry coating film (Felton, 2013).

## 5.5 Appendix of Chapter 5

In this appendix, the derivations of important equations of the model presented in the main chapter are presented. These equations are the simplified linear momentum balance equation written for the coating suspension which forms a thin film onto the tablet (Eq. 5.5), the film thickness evolution equation (Eq. 5.13), the energy equation that yields the coating film temperature (Eq. 5.20) and the particle volume fraction evolution equation (Eq. 5.23). Additionally, the estimation of the Peclet and Stokes numbers for the flows investigated in the main article is shown and the main equations of Subsection 5.2.2 are presented in cylindrical coordinates.

### 5.5.1 Simplified momentum balance equation

In the main article, the lubrication approximation theory is used to simplify the linear momentum balance equation written for the coating formulation (Eq. 5.3). The main assumption of the lubrication approximation is that, if  $R$  designates the length scale of the film in the radial direction on a round tablet surface, and  $H$  designates its length scale across its thickness in the direction normal to the tablet surface, then:  $H/R \ll 1$ . Having two greatly differing length scales allows simplifying the three-dimensional problem. According to Szeri (2010), one can also neglect inertial and gravitational effects in most lubricant thin films.

Here, the simplified the linear momentum balance equation (Eq. 5.5) of the main article is derived in cylindrical coordinates using the lubrication approximation theory assumptions. Note that in the above derivation all changes in the azimuthal coordinate were neglected. This is because one can take advantage of the axisymmetric shape of the coating film covering the tablet surface. To the best of this author's knowledge, the following analysis has never been reported for a suspension (pharmaceutical coating formulation) whose density and viscosity change in time.

In the radial cylindrical coordinate Equation (5.3) becomes:

$$\rho \partial_t v = -\rho v \partial_r v - \rho w \partial_z v - \partial_r p + (1/r) \partial_r (r \tau_{rr}) + \partial_z \tau_{zr} - \tau_{\theta\theta}/r \quad (\text{a1})$$

By scaling Equation (a1) one gets:

$$\partial_{\bar{t}} \bar{v} = -\frac{V t_c}{R} \bar{v} \partial_{\bar{r}} \bar{v} - \frac{W t_c}{H} \bar{w} \partial_{\bar{z}} \bar{v} - \frac{p_c t_c}{\rho V R} \partial_{\bar{r}} \bar{p} + \frac{\mu t_c}{\rho R^2} \frac{1}{\bar{r}} \partial_{\bar{r}} (\bar{r} \bar{\tau}_{rr}) + \frac{\mu t_c}{\rho H^2} \partial_{\bar{z}} \bar{\tau}_{zr} - \frac{\mu t_c}{\rho R^2} \frac{\bar{\tau}_{\theta\theta}}{\bar{r}} \quad (\text{a2})$$

where the following scales were used:

$$\begin{aligned} \bar{r} &\equiv r/R ; & \bar{z} &\equiv z/H ; & \bar{w} &\equiv w/W ; & \bar{v} &\equiv v/V ; & \bar{p} &\equiv p/p_c ; & \bar{t} &\equiv t/t_c \\ \bar{\tau}_{zr} &\equiv (H/\mu V) \tau_{zr} ; & \bar{\tau}_{rr} &\equiv (R/\mu V) \tau_{rr} ; & \bar{\tau}_{zz} &\equiv (H/\mu V) \tau_{zz} ; & \bar{\tau}_{\theta\theta} &\equiv (R/\mu V) \tau_{\theta\theta} \end{aligned} \quad (\text{a3})$$

where where  $\rho$  and  $\mu$  are the density and viscosity of the suspension, respectively (which, for simplicity, are taken to be constants), while  $t_c$  and  $p_c$  are the characteristic time and pressure scales of the flow.

In Equation (a2), various time scales arise:

$$\tau_{c,1} \equiv R/V ; \quad \tau_{c,2} \equiv H/W ; \quad \tau_{d,1} \equiv \rho R^2/\mu ; \quad \tau_{d,2} \equiv \rho H^2/\mu$$

From the continuity equation one concludes that  $\tau_{c,1} = \tau_{c,2}$ . Additionally, comparing  $\tau_{d,1}$  and  $\tau_{d,2}$  yields:  $\tau_{d,2} = (H/R)^2 \tau_{d,1} \ll \tau_{d,1}$ . Finally, one can note that:

$$\tau_{d,2}/\tau_{c,1} = \frac{H^2 V \rho}{\mu R} = \frac{H}{R} \frac{\rho H V}{\mu} = \frac{H}{R} \text{Re} \quad (\text{a4})$$

Knowing that  $H/R \ll 1$  and also  $\text{Re} \ll 1$  it is concluded that the shortest characteristic time is  $\tau_{d,2}$ . Substituting  $t_c \equiv \tau_{d,2}$  into Equation (a2) gives:

$$\begin{aligned} \partial_{\bar{t}} \bar{v} = & -\frac{H}{R} \text{Re} \bar{v} \partial_{\bar{r}} \bar{v} - \frac{H}{R} \text{Re} \bar{w} \partial_{\bar{z}} \bar{v} - \frac{H}{R} \frac{p_c H}{\mu V} \partial_{\bar{r}} \bar{p} \\ & + \left(\frac{H}{R}\right)^2 \frac{1}{\bar{r}} \partial_{\bar{r}} (\bar{r} \bar{\tau}_{rr}) + \partial_{\bar{z}} \bar{\tau}_{zr} - \left(\frac{H}{R}\right)^2 \frac{\bar{\tau}_{\theta\theta}}{\bar{r}} \end{aligned} \quad (\text{a5})$$

Assuming that the pressure term is as important as the viscous term, one obtains  $p_c \equiv (R/H)(\mu V/H)$ . Substituting the pressure term in Equation (a5) and eliminating the negligible terms yields:

$$\partial_{\bar{t}} \bar{v} = -\partial_{\bar{r}} \bar{p} + \partial_{\bar{z}} \bar{\tau}_{zr} \quad (\text{a6})$$

Let us assume that the system evolves toward steady state. This assumption is valid for a thin suspension film that is deposited on the surface of a tablet. At steady state, the pressure term is equal in magnitude to the viscous term, and their combination vanishes. Before this happens, the convective terms cease to be negligible. In fact, they start dictating the time scale. This is no longer  $\tau_{d,2}$ , but becomes  $\tau_{c,1}$ . In this part of the time domain, a new approximation holds, which one gets by rescaling the equation of motion. By choosing  $t_c \equiv \tau_{c,1}$  Equation (a2) becomes:

$$\begin{aligned} \frac{H}{R} \text{Re} \partial_{\bar{t}} \bar{v} = & -\frac{H}{R} \text{Re} (\bar{v} \partial_{\bar{r}} \bar{v} + \bar{w} \partial_{\bar{z}} \bar{v}) - \frac{H}{R} \frac{p_c \text{Re}}{\rho V^2} \partial_{\bar{r}} \bar{p} \\ & + \left(\frac{H}{R}\right)^2 \frac{1}{\bar{r}} \partial_{\bar{r}} (\bar{r} \bar{\tau}_{rr}) + \partial_{\bar{z}} \bar{\tau}_{zr} - \left(\frac{H}{R}\right)^2 \frac{\bar{\tau}_{\theta\theta}}{\bar{r}} \end{aligned} \quad (\text{a7})$$

which reduces to:

$$\frac{H}{R} \frac{p_c \text{Re}}{\rho V^2} \partial_{\bar{r}} \bar{p} = \partial_{\bar{z}} \bar{\tau}_{zr} \quad (\text{a8})$$

Since the left-hand side must have unit order of magnitude, one obtains  $p_c \equiv (R/H)(1/\text{Re})\rho V^2$  and the final leading order equation is:

$$\partial_{\bar{r}} \bar{p} = \partial_{\bar{z}} \bar{\tau}_{zr} \quad (\text{a9})$$

Written in dimensional form this yields Equation (5.5.a) of the main article.

In the vertical cylindrical coordinate Equation (5.3) becomes:

$$\rho \partial_t w = -\rho v \partial_r w - \rho w \partial_z w - \partial_z p + (1/r) \partial_r (r \tau_{rz}) + \partial_z \tau_{zz} \quad (\text{a10})$$

Scaling Equation (a10) with the scales appearing in Equation (a3) and considering again that the system evolves toward steady state and that the characteristic time is the convection characteristic time ( $\tau_{c,1} \equiv H/W \equiv R/V$ ) gives:

$$\frac{H}{R} \text{Re} \partial_{\bar{t}} \bar{w} = -\frac{H}{R} \text{Re} (\bar{v} \partial_{\bar{r}} \bar{w} + \bar{w} \partial_{\bar{z}} \bar{w}) - \frac{p_c \text{Re} R}{\rho V^2 H} \partial_{\bar{z}} \bar{p} + \frac{1}{\bar{r}} \partial_{\bar{r}} (\bar{r} \bar{\tau}_{rz}) + \partial_{\bar{z}} \bar{\tau}_{zz} \quad (\text{a11})$$

which reduces to:

$$\frac{p_c \text{Re} R}{\rho V^2 H} \partial_{\bar{z}} \bar{p} = \frac{1}{\bar{r}} \partial_{\bar{r}} (\bar{r} \bar{\tau}_{rz}) + \partial_{\bar{z}} \bar{\tau}_{zz} \quad (\text{a12})$$

Substituting in Equation (a12) the scale of the pressure  $p_c$  obtained above for the case when the system evolves towards steady state, yields:

$$\partial_{\bar{z}} \bar{p} = \left( \frac{H}{R} \right)^2 \left[ \frac{1}{\bar{r}} \partial_{\bar{r}} (\bar{r} \bar{\tau}_{rz}) + \partial_{\bar{z}} \bar{\tau}_{zz} \right] \quad (\text{a13})$$

In the limit of  $H/R \ll 1$ , the term  $\partial_{\bar{z}} \bar{p}$  can be regarded equal to zero. This yields Equation (5.5.b) of the main chapter.

### 5.5.2 Film thickness evolution equation

In this section, the film thickness evolution equation is derived from the continuity equation written for the mixture. The latter in cylindrical coordinates reads:

$$\partial_t \rho = -(1/r) \partial_r (r \rho v) - \partial_z (\rho w) \quad (\text{a14})$$

Integrating Equation (a14) over the vertical direction  $z$ , from  $z = 0$  to  $z = h$ , gives:

$$\int_0^h \partial_t \rho dz = -(1/r) \int_0^h \partial_r (r \rho v) dz - \int_0^h \partial_z (\rho w) dz \quad (\text{a15})$$

The term on the left-hand side can be written as:

$$\int_0^h \partial_t \rho dz = \partial_t \int_0^h \rho dz - \rho \Big|_{z=h} \partial_t h = \partial_t \int_0^h \rho dz - \rho_e \partial_t h \quad (\text{a16})$$

where it has been assumed that the mixture (coating suspension) density at the film-air interface is the density of the water that evaporates.

The first and second terms on the right-hand of Equation (a15) side can be expanded as follows:

$$-(1/r) \int_0^h \partial_r (r \rho v) dz = -(1/r) \partial_r \int_0^h \rho r v dz + (\rho v) \Big|_{z=h} \partial_r h \quad (\text{a17})$$

$$-\int_0^h \partial_z (\rho w) dz = -(\rho w) \Big|_0^h = -(\rho w) \Big|_{z=h} + (\rho w) \Big|_{z=0} \quad (\text{a18})$$

Substituting Equations (a18) to (a20) into Equation (a17) yields:

$$\partial_t \int_0^h \rho dz - \rho_e \partial_t h = -(1/r) \partial_r \int_0^h \rho r v dz + (\rho v) \Big|_{z=h} \partial_r h - (\rho w) \Big|_{z=h} + (\rho w) \Big|_{z=0} \quad (\text{a19})$$

At  $z = 0$  the boundary does not move. So, the last term on the right hand side represents the mass that leaves the control volume. This term represents the mass loss owing to absorption. In the main article, this term is taken equal to  $-\rho W_a$ , where  $W_a$  is the absorption velocity at the film-tablet interface. The term immediately preceding the absorption flux in Equation (a19) cannot be regarded as the mass loss owing to evaporation ( $\dot{m}_e$ ). This is because the interface (or equivalently the boundary of the control volume) moves. However, one can use the mass jump condition and write:

$$\dot{m}_e = \mathbf{n} \cdot (\mathbf{u} - \mathbf{u}_s) \rho \Big|_{z=h} \quad (\text{a20})$$

where  $\mathbf{n}$  is the unit vector normal to the interface pointing from the mixture into the air,  $\mathbf{u}$  is the mixture velocity,  $\mathbf{u}_s$  is the velocity of the interface and  $\rho$  is the mixture density. At the interface ( $z = h$ ), the latter is equal to the density of the pure liquid (water) that evaporates. In cylindrical coordinates Equation (a20) becomes:

$$\dot{m}_e = [n_r(v_i - u_{sr}) + n_z(w_i - u_{sz})] \rho_e \quad (\text{a21})$$

where  $v_i$  and  $w_i$  are the radial and vertical velocity components of the mixture at the film-air interface, respectively, and  $\rho_e$  is the density of the suspension at the interface. To proceed  $n_r$  and  $n_z$  need to be related to the film thickness  $h(r, t)$ . To do this, one writes:

$$F = z - h(r, t) \quad ; \quad \mathbf{n} = \frac{\partial_x F}{|\partial_x F|} \quad (\text{a22})$$

From Equation (a22) one obtains:

$$\mathbf{n} = -\frac{\partial_r h}{\sqrt{1 + (\partial_r h)^2}} \hat{\mathbf{r}} + \frac{1}{\sqrt{1 + (\partial_r h)^2}} \hat{\mathbf{z}} \quad (\text{a23})$$

where  $\hat{\mathbf{r}}$  and  $\hat{\mathbf{z}}$  denote the unit vector in the radial and vertical direction, respectively.

The vector of unit magnitude tangent to the film and normal to  $\mathbf{n}$  is given by:

$$\mathbf{t} = \frac{1}{\sqrt{1 + (\partial_r h)^2}} \hat{\mathbf{r}} + \frac{\partial_r h}{\sqrt{1 + (\partial_r h)^2}} \hat{\mathbf{z}} \quad (\text{a24})$$

Assuming that the velocity of the mixture tangent to the interface is equal to the velocity of the interface yields:

$$\mathbf{u}_i \cdot \mathbf{t} = \mathbf{u}_s \cdot \mathbf{t} \Rightarrow v_i t_r + w_i t_z = u_{sr} t_r + u_{sz} t_z \quad (\text{a25})$$

and since  $t_r = n_z$  and  $t_z = -n_r$ :

$$(v_i - u_{sr}) n_z = (w_i - u_{sz}) n_r \quad (\text{a26})$$

Substituting Equation (a26) into the jump condition yields:

$$\dot{m}_e = \left[ \frac{n_r^2}{n_z} (w_i - u_{sz}) + n_z (w_i - u_{sz}) \right] \rho_e = \frac{1}{n_z} (w_i - u_{sz}) \quad (\text{a27})$$

The vertical velocity of the interface  $u_{sz}$  is given by:

$$u_{sz} = \partial_t h + u_{sr} \partial_r h \quad (\text{a28})$$

Combining Equations (a26) and (a28) gives:

$$u_{sz} = \frac{\partial_t h + [v_i + (n_r/n_z) w_i] \partial_r h}{1 - (n_r/n_z) \partial_r h} \quad (\text{a29})$$

Since it is  $n_z = 1/\sqrt{1 + (\partial_r h)^2}$  and  $n_r/n_z = -\partial_r h$ , substituting Equation (a29) into the jump condition (a27) yields:

$$\rho_e w_i = \frac{1}{\sqrt{1 + (\partial_r h)^2}} \dot{m}_e + \rho_e \frac{\partial_t h + (v_i + w_i \cdot \partial_r h) \partial_r h}{1 + (\partial_r h)^2} \quad (\text{a30})$$

In this work, thin films where  $\partial_r h \ll 1$  are of interest. Thus, Equation (a30) becomes:

$$\rho_e w_i = \dot{m}_e + \rho_e [\partial_t h + v_i \partial_r h] \quad (\text{a31})$$

Substituting the above equation into the mass balance equation (Eq. a19) gives:

$$\partial_t \int_0^h \rho dz = -(1/r) \partial_r \int_0^h r \rho v dz - \dot{m}_e - \rho W_a \quad (\text{a32})$$

Assuming that the mixture density is uniform over (most of) the film thickness (Weidner et al., 1996), one can see that Equation (a32) reduces to Equation (5.13) of Chapter 5.

### 5.5.3 Energy equation

To derive the energy Equation (5.20) one can start from the equation of change for temperature reported in Bird et al. (2007). This equation reads:

$$\rho_1 c_{p1} D_t T_1 = -\partial_x \cdot \mathbf{q}_1 + \boldsymbol{\tau}_1 : \partial_x \mathbf{u}_1 - \left( \frac{\partial \ln \rho_1}{\partial \ln T_1} \right)_p D_t p_1 \quad (\text{a33})$$

where  $D_t$  is the substantial time derivative and  $c_p$ ,  $\mathbf{q}$ ,  $\mathbf{u}$  and  $\boldsymbol{\tau}$  denote the heat capacity, heat flux, velocity field, and deviatoric stress tensor, respectively. Here the subscript 1 is used to identify the mixture. The last term on the right-hand side is zero for fluids with constant density. The mixture has not constant density, but it is expected to vary very little, in particular with the temperature. The generation term (conversion of kinetic energy into internal energy) is very small and can be neglected as well. Thus, Equation (a33) becomes:

$$\rho_1 c_{p1} D_t T_1 = -\partial_x \cdot \mathbf{q}_1 \quad (\text{a34})$$

Integrating over the region  $\mathcal{R}_1$  occupied by the film, which is bounded by the surfaces  $\mathcal{S}_{12}$  (film-air interface) and  $\mathcal{S}_{13}$  (film-tablet interface), gives:

$$\int_{\mathcal{R}_1} \rho_1 c_{p1} D_t T_1 d\mathbf{x} = - \int_{\mathcal{R}_1} \partial_x \cdot \mathbf{q}_1 d\mathbf{x} \quad (\text{a35})$$

To manipulate the term on the right-hand side, the divergence theorem is used:

$$\int_{\mathcal{R}_1} \partial_{\mathbf{x}} \cdot \mathbf{q}_1 d\mathbf{x} = \int_{\mathcal{S}_{12}} \mathbf{q}_1 \cdot \mathbf{n}_{12} d\mathbf{x} + \int_{\mathcal{S}_{13}} \mathbf{q}_1 \cdot \mathbf{n}_{13} d\mathbf{x} \quad (\text{a36})$$

where  $\mathbf{n}_{ij}$  denotes the unit vector normal to  $\mathcal{S}_{ij}$  pointing from phase  $i$  into phase  $j$ .

Since the film is very thin, to manipulate the term on the left-hand side, it is assumed that  $T_1$  is uniform. Note that this assumption cannot be used for the term on the right-hand side, because if one did, the term would vanish. So, one obtains:

$$D_t T_1 \int_{\mathcal{R}_1} \rho_1 c_{p1} d\mathbf{x} = - \int_{\mathcal{S}_{12}} \mathbf{q}_1 \cdot \mathbf{n}_{12} d\mathbf{x} - \int_{\mathcal{S}_{13}} \mathbf{q}_1 \cdot \mathbf{n}_{13} d\mathbf{x} \quad (\text{a37})$$

Since  $T_1$  is uniform it is  $D_t T_1 = \partial_t T_1$ .

Moreover, the term  $\rho_1 c_{p1}$  is given by:

$$\rho_1 c_{p1} = \rho_e (1 - \phi) c_{pe} + \rho_s \phi c_{ps} \quad (\text{a38})$$

and is therefore a function of the  $\phi$ , which in turn is a function of  $r$  and  $t$ .

Let us now define:

$$\langle \rho_1 c_{p1} \rangle \equiv \frac{1}{V_1} \int_{\mathcal{R}_1} \rho_1 c_{p1} d\mathbf{x} \quad (\text{a39})$$

where  $V_1$  is the volume of the film.

The simplified enthalpy jump condition at the film-gas interface  $\mathcal{S}_{12}$ , reads (Delhaye, 1974):

$$\dot{m}_e (\hat{H}_1 - \hat{H}_2) = -\mathbf{n}_{12} \cdot (\mathbf{q}_1 - \mathbf{q}_2) \quad (\text{a40})$$

To derive an expression for  $\mathbf{q}_1$  it was considered that  $\Delta H_e \equiv \hat{H}_2 - \hat{H}_1$  and  $\mathbf{n}_{12} \cdot \mathbf{q}_2 \equiv h_H (T_1 - T_{2\infty})$ , where  $\Delta H_e$ ,  $h_H$  and  $T_{2\infty}$  denote the enthalpy of vaporization, heat transfer coefficient and bulk air temperature. Equation (a40) finally becomes:

$$\mathbf{n}_{12} \cdot \mathbf{q}_1 = \dot{m}_e \Delta H_e + h_H (T_1 - T_{2\infty}) \quad (\text{a41})$$

The simplified enthalpy jump condition written for the film-tablet interface  $\mathcal{S}_{13}$  yields an expression for the heat conduction from the tablet to the film:

$$\mathbf{n}_{13} \cdot \mathbf{q}_1 = \mathbf{n}_{13} \cdot \mathbf{q}_3 = k_3 \partial_z T_3 \Big|_{z=0} \quad (\text{a42})$$

where  $k_3$  is the heat conductivity of the tablet core and  $T_3$  is the tablet core temperature.

Substituting Equations (a39), (a41) and (a42) into (a37) gives:

$$\langle \rho_1 c_{p1} \rangle V_1 \partial_t T_1 = - \int_{\mathcal{S}_{12}} \dot{m}_e \Delta H_e d\mathbf{s} - \int_{\mathcal{S}_{12}} h_H (T_1 - T_{2\infty}) d\mathbf{s} - \int_{\mathcal{S}_{13}} k_3 \partial_z T_3 \Big|_{z=0} d\mathbf{s} \quad (\text{a43})$$

On the right-hand side all the integrated functions are uniform over the surfaces. Thus:

$$\langle \rho_1 c_{p1} \rangle V_1 \partial_t T_1 = -\dot{m}_e \Delta H_e A_{12} - h_H (T_1 - T_{2\infty}) A_{12} - k_3 \partial_z T_3 \Big|_{z=0} A_{13} \quad (\text{a44})$$

where  $A_{12}$  and  $A_{13}$  are the areas of the film-air and film-tablet interfaces respectively. The above energy equation (Eq. 5.20) was used in the model presented in Chapter 5 to calculate the coating film temperature.

#### 5.5.4 Heat conduction from the tablet to the film

The last term in Equations (5.20) and (a44) denotes the heat conduction from the tablet core to the coating film. To estimate this term one needs to calculate the temperature profile in the tablet ( $T_3$ ) using the following equation of energy conservation:

$$c_{p3} \rho_3 \partial_t T_3 = k_3 \partial_{zz}^2 T_3 \quad (\text{a45})$$

with boundary conditions:

$$T_3 = T_1 \quad \text{at } z = 0 \quad (\text{a46})$$

$$\partial_t T_3 = 0 \quad \text{at } z = -\ell \quad (\text{a47})$$

where  $\ell$  is taken to be the distance between the tablet-film interface and the tablet core center. The tablet density, heat capacity and heat conductivity were taken from the literature ( $\rho_3 = 1300 \text{ kg/m}^{-3}$ ,  $c_{p3} = 1000 \text{ J kg}^{-1} \text{ K}^{-1}$ ,  $k_3 = 0.7 \text{ J s}^{-1} \text{ m}^{-1} \text{ K}^{-1}$ ; Krok et al., 2017).

From Equations (a48-a50), one can calculate the heat conduction from the tablet to the coating suspension:  $k_3 \partial_z T_3$  at  $z = 0$  and solve the energy Equation (5.20) in the main chapter.

#### 5.5.5 Particle volume fraction evolution equation

In this section, a particle volume fraction evolution equation (Eq. 5.23) is rigorously derived from the continuity equation written for the solid phase inside the coating film. Integrating Equation (5.22) over  $z$  gives:

$$\int_0^h \partial_t \phi dz = -(1/r) \int_0^h \partial_r (r\phi v) dz - \int_0^h \partial_z (\phi w) dz - (1/r) \int_0^h \partial_r (r j_r) dz \quad (\text{a48})$$

The term on the left-hand side can be written as:

$$\int_0^h \partial_t \phi dz = \partial_t \int_0^h \phi dz - \phi \Big|_{z=h} \partial_t h \quad (\text{a49})$$

The first term on the right-hand side can be expanded as:

$$(1/r) \int_0^h \partial_r (r\phi v) dz = (1/r) \partial_r \int_0^h r\phi v dz - (\phi v) \Big|_{z=h} \partial_r h \quad (\text{a50})$$

The second term on the right-hand side becomes:

$$\int_0^h \partial_z (\phi w) dz = (\phi w) \Big|_{z=h} - (\phi w) \Big|_{z=0} \quad (\text{a51})$$

Performing the same analysis as in the Section (5.5.2) and assuming that no particles evaporate allows one to write:

$$(\phi w) \Big|_{z=h} - (\phi w) \Big|_{z=0} = \phi \Big|_{z=h} \partial_t h + (\phi v) \Big|_{z=h} \partial_r h + \phi \Big|_{z=0} W_a \quad (\text{a52})$$

Finally, the third on the right-hand side becomes:

$$(1/r) \int_0^h \partial_r (r j_r) dz = (1/r) \partial_r \int_0^h r j_r dz - j_r \Big|_{z=h} \partial_r h \quad (\text{a53})$$

Substituting Equations (a52), (a53), (a55) and (a56) into (a51) yields:

$$\begin{aligned} \partial_t \int_0^h \phi dz - \phi \Big|_{z=h} \partial_t h &= -(1/r) \partial_r \int_0^h r \phi v dz + (\phi v) \Big|_{z=h} \partial_r h \\ -\phi \Big|_{z=h} \partial_t h - (\phi v) \Big|_{z=h} \partial_r h - \phi \Big|_{z=0} W_a - (1/r) \partial_r \int_0^h r j_r dz &+ j_r \Big|_{z=h} \partial_r h \end{aligned} \quad (\text{a54})$$

Making use of the “well mixed” approximation (uniform  $\phi$  across the thickness of the film) and that the migration flux at the film-air interface are zero one gets:

$$\partial_t (\phi h) = -(1/r) \partial_r \left( r \phi \int_0^h v dz \right) - \phi W_a - (1/r) \partial_r (r h j_r) \quad (\text{a55})$$

Using the film thickness evolution equation the first term on the right-hand side of the above equation can be expanded:

$$\begin{aligned} (1/r) \partial_r \left( r \phi \int_0^h v dz \right) &= (1/r) \partial_r \left[ (\phi/\rho) \rho r Q_s \right] = (1/r) \left[ \rho r Q_s \partial_r (\phi/\rho) + (\phi/\rho) \partial_r (\rho r Q_s) \right] \\ &= \rho Q_s \partial_r (\phi/\rho) - (\phi/\rho) \partial_t (\rho h) - \phi W_a - \phi (\dot{m}_e/\rho) \end{aligned} \quad (\text{a56})$$

where  $Q_s$  is the surface flux given by Equation (5.14). Equation (a57) then becomes:

$$\partial_t (\phi h) = -\rho Q_s \partial_r (\phi/\rho) + (\phi/\rho) \partial_t (\rho h) + \phi (\dot{m}_e/\rho) - (1/r) \partial_r (r h j_r) \quad (\text{a59})$$

which simplifies to Equation (5.23) of the main chapter.

### 5.5.6 Estimation of the Peclet and Stokes numbers

To derive an expression for the particle migration flux in the main article, it is important to first estimate the Peclet number  $Pe \equiv a^2 \dot{\gamma} / \mathcal{D}$  where  $\mathcal{D}$  is the Brownian diffusion coefficient of the particles in the suspension,  $a$  is the particle radius (assuming the particles are spherical) and  $\dot{\gamma}$  is the shear rate scale. In the simulations performed in Chapter 5, it is  $\dot{\gamma} \sim 1 \text{ s}^{-1}$  and  $a \sim 10^{-8} \text{ m}$ .

The particle Brownian diffusion coefficient  $\mathcal{D}$  is estimated by Equations (5.25) of the main article. The term in front of the Einstein diffusivity  $\mathcal{D}_0$  is of order 1 for all the values of  $\phi$  of interest in the simulations of Chapter 5 ( $\phi < \phi^*$ ). Thus, for the Brownian diffusion coefficient it is  $\mathcal{D} \sim \mathcal{D}_0 = (k_B T_w)/(6\pi\mu_w a)$  where  $k_B = 10^{-23}$  J/K is the Boltzmann constant, and  $T_w \approx 320$  K and  $\mu_w = 0.001$  Pa.s are the carrier fluid temperature and viscosity, respectively. Thus, the Brownian diffusion is estimated:  $\mathcal{D} \sim 10^{-10}$  m<sup>2</sup>.

The Peclet number can be estimated:

$$\text{Pe} \equiv \frac{a^2 \dot{\gamma}}{\mathcal{D}} \sim \frac{(10^{-8})^2}{10^{-10}} \sim 10^{-6} \quad (\text{a61})$$

Since in this work  $\text{Pe} \ll 1$ , the dispersions can be considered Brownian.

To determine if the motion of the particles of the coating suspensions investigated in the main article is dictated by that of the carrier fluid, the Stokes number ( $\text{St}$ ) was calculated. This is defined as the ratio of the particle relaxation time ( $\tau_a$ ) to the characteristic flow time scale ( $\tau_c$ ).

For a concentrated suspension the particle relaxation time is defined as (Jackson, 2000):

$$\tau_a \equiv \frac{(1 - \phi)^{2.65}}{1 + (\phi\rho_p)/[(1 - \phi)\rho_e]} \frac{\rho_p a^3}{K_a \mu} \quad (\text{a62})$$

where  $\rho_s$  and  $\rho_e$  are the densities of the particle and carrier fluid, respectively ( $\sim 10^3$  kg/m<sup>3</sup>),  $a$  is the particle radius,  $\mu$  is the carrier fluid viscosity ( $\sim 10^{-3}$  Pa.s) and  $K_a$  is a coefficient that depends on the shape, size and orientation of the particle (Coussot and Ancey, 1999). The characteristic flow time scale, as discussed in Section 5.5.1 the convection characteristic time  $\tau_c = R/V$ . Based on the above, for the values of  $\phi$  of interest in the simulations, one gets:

$$\text{St} \equiv \frac{\tau_a}{\tau_c} = \frac{(1 - \phi)^{2.65}}{1 + (\phi\rho_p)/[(1 - \phi)\rho_e]} \frac{\rho_p a^3 V}{K_a \mu R} \sim 10^{-11} \quad (\text{a63})$$

In the above equation it is  $K_a \sim a \sim 10^{-8}$  m,  $V \sim 10^{-3}$  m/s and  $R \sim 10^{-2}$  m which is true in the simulations performed in the current study.

Since  $\text{St} \ll 1$  the motion of the particles in the suspension is mainly dictated by that of the carrier fluid. Therefore, employing the mixture modeling approach is valid for the case studies investigated in this work.

### 5.5.7 Main equations of Section 5.2.2 expressed in cylindrical coordinates

In this section, Equations (5.33), (5.35), (5.39) and (5.42) of the main article are written in cylindrical coordinates. These equations were solved together with Eqs. (5.38) and (5.44) to calculate the wetting front profile and the particle volume fraction inside the tablet pores.

Equation (5.33) becomes:

$$v_p = -\frac{1}{\varphi} \frac{\mathcal{K}_p}{\eta} \partial_r p_p \quad ; \quad w_p = -\frac{1}{\varphi} \frac{\mathcal{K}_p}{\eta} \partial_z p_p \quad (\text{a64})$$

Equation (5.35) becomes:

$$\partial_t (\varphi \rho) = (1/r) \partial_r [r (\mathcal{K}_p/\eta) \rho \partial_r p_p] + \partial_z [(\mathcal{K}_p/\eta) \rho \partial_z p_p] - \rho_s \Gamma \quad (\text{a65})$$

Equation (5.39) becomes:

$$\Gamma = \mathcal{F}_p \left[ -\frac{\partial_r h_p}{\sqrt{1 + (\partial_r h_p)^2}} (\varphi \phi_p v_p + j_{pr}) + \frac{1}{\sqrt{1 + (\partial_r h_p)^2}} (\varphi \phi_p w_p + j_{pz}) \right] \quad (\text{a66})$$

Equation (5.41) becomes:

$$j_{pr} = -\varphi \mathcal{D}_p \partial_r \phi_p \quad ; \quad j_{pz} = -\varphi \mathcal{D}_p \partial_z \phi_p \quad (\text{a67})$$

Note that in using cylindrical coordinates all changes in the azimuthal coordinate were neglected. This is consistent with the assumptions made in Chapter 5.

# CHAPTER 6

## Water evaporation from within a porous tablet

---

This chapter deals with water evaporation from within porous media. A mathematical model that predicts the evaporation rate of water which has been absorbed into a pharmaceutical tablet during the film-coating process is developed. The output of the current model provides insight into the final water content of a tablet core during the film-coating process.

---

Publication which has arisen from this work: Christodoulou, C., Sorensen, E., García-Muñoz, S. and Mazzei, L., 2018. Mathematical modelling of water absorption and evaporation in a pharmaceutical tablet during film coating. *Chemical Engineering Science*, 175, pp.40-55.

### 6.1 Introduction

Droplet evaporation from within a porous medium is of interest in pharmaceutical coating processes. Understanding the dynamics of evaporation phenomena can help minimize the water content inside the tablet that may lead to disintegration of the active ingredients and short shelf-life. The novel evaporation model presented in this chapter aims to predict the evaporation front movement inside a porous medium (tablet) and to provide information about the water content of the tablet during the film-coating process.

Previous work (Roberts and Griffiths, 1995; Pakala et al., 2012) considered evaporation from porous materials that are not used by the pharmaceutical industry (concrete, sand). These models are empirical and specific to their case studies, thus they cannot be considered for the film-coating process considered in this thesis. Therefore, in this work a different approach was followed: A method that simulates the process of slurry-droplet drying was adopted and a new model was developed. In this introductory section, the modeling approach of the slurry-droplet drying process is briefly discussed. This approach inspired the current modeling approach for water evaporation from within a porous matrix.

Spray drying is utilized today in the food, pharmaceutical, chemical and biochemical industries. According to the morphology of individual droplets, the drying process can be divided and modeled in two stages: in the 1<sup>st</sup> stage, a droplet, containing solids dispersed in the liquid, exchanges heat with the drying air and therefore evaporates and shrinks. The 2<sup>nd</sup> stage commences at the point when the solid volume fraction in the droplet reaches its critical value. When this happens, the droplet can no longer be considered as a liquid with dissolved solids but must be regarded as a wet particle with a wet core and a porous “dry” region close to its surface that does not contain any liquid, as seen in Figure 6.1.

Mezhericher et al. (2008) developed a model for the two stages of the slurry-droplet drying process. They took into account the time-dependent characteristics of the process, the temperature profile within both the dry and wet regions of a particle, the heat absorption by the dried region and the temperature dependence of droplet physical properties.

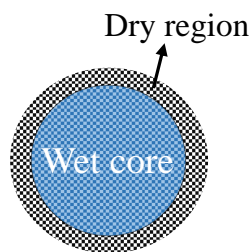


Figure 6.1: Second stage of a spray drying process.

Golman and Julklang (2013) also developed and validated a mathematical model for the 2<sup>nd</sup> stage of the drying process. They specifically investigated the effect of the porosity of the dried layer on the drying kinetics of the slurry-droplet. They assumed that the evaporation takes place in the droplet at the boundary that separates the dried and wet core regions. The evaporation surface recedes inside the droplet, the wet core shrinks and the dried layer grows as the drying progresses. The droplet radius remains constant during this stage.

In the next section, a novel model that was developed in this work to predict the evaporation from within a porous substrate is described. As mentioned before, a modeling approach for the drying of slurry-droplets was adopted. The dry region formed on the surface of the droplet represents the dried part of the tablet, whereas the wet core represents the still wetted part of the tablet (Fig. 6.2). The current evaporation model aims to analyze the effect of the film-coating process conditions on the water evaporation from within a tablet.

## 6.2 Mathematical model

After a coating suspension (water and particles) is applied on the surface of a tablet, it starts to dry and to penetrate into the tablet (see Chapters 4 and 5). As the carrier fluid evaporates, the solid volume fraction in the suspension increases and after some time it reaches a critical value ( $\phi^*$ ). At this critical value, the particles come into contact and the coating film can no longer be considered as a liquid with suspended solids, but behaves as a wetted solid. This wetted solid was regarded to be a wetted porous crust that covers the surface of the tablet (Kiil, 2006). After the crust formation, the water continues to evaporate from within the crust and the tablet until the pores are dry.

In this work, to develop a model that predicts water evaporation from within the porous matrix comprising of the tablet and the crust covering its surface, it was assumed that the volume close to the porous matrix surface can be divided into two regions: the wetted region - where liquid water fills the pores - and the dried region - from where the water has already evaporated - as seen in Figure 6.2. The dried region is not completely dry since vapor diffuses through it; however, no liquid water is present inside the pores of this region.

The dried region volume was assumed to be initially negligible, whereas the wetted region was considered to include the wetted tablet (were the coating suspension has penetrated) and the wetted crust. The current model assumes that evaporation takes place at the boundary that separates the dried and wetted regions. As the evaporation progresses (Fig. 6.2), the dried region increases in size whereas the wetted region reduces. Complete water content evaporation is achieved if the wetted region disappears.

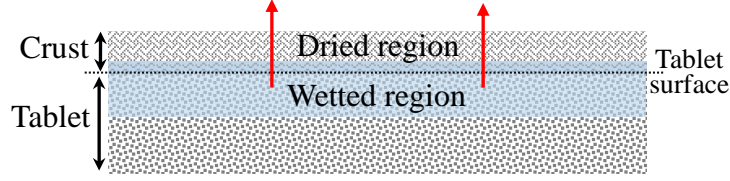


Figure 6.2: Liquid evaporation from within a porous matrix.

To predict the evaporation rate from within the wetted porous matrix consisting of the wetted porous tablet and the crust (Fig. 6.2), one needs to calculate the temperature profile inside its dried and wetted regions using the following equations of energy conservation:

$$\left[ \varphi \rho_1 c_{p1} + (1 - \varphi) \rho_s c_{ps} \right] \partial_t T_{TW} = k_{TW} \partial_z (\partial_z T_{TW}), \quad -H_{pm} \leq z \leq -H_p \quad (6.1)$$

$$\left[ \varphi \rho_2 c_{p2} + (1 - \varphi) \rho_s c_{ps} \right] \partial_t T_{TD} = k_{TD} \partial_z (\partial_z T_{TD}), \quad -H_p(t) < z \leq 0 \quad (6.2)$$

where  $\varphi$  is the porosity of the porous matrix,  $T_{TD}$  and  $T_{TW}$  are the temperatures in the dried and wetted regions of the porous matrix, respectively, and  $c_{ps}$ ,  $c_{p1}$ ,  $c_{p2}$ ,  $\rho_s$ ,  $\rho_1$ ,  $\rho_2$  and  $k_{TD}$ ,  $k_{TW}$  are the heat capacities and densities of the solid, liquid and gas phases, respectively, and the conductivities of the wetted and dry porous matrix, respectively. Here, for  $-H_c < z \leq 0$  (where  $H_c$  is the crust thickness), the porous matrix porosity and the solid density and heat capacity are those of the porous polymer crust, whereas for  $-H_{pm} < z \leq -H_c$ , the same properties refer to the tablet core.

Equation (6.1) holds for the wetted region which lies between the evaporation front depth  $H_p(t)$  and maximum wetted depth  $H_{pm}$  (Fig. 6.3), whereas Equation (6.2) holds for the dried region that is located between the porous matrix surface and the evaporation front depth. As the evaporation process progresses, the evaporation front advances and the dried region increases in size whereas the wetted region reduces.

The thermal conductivities of the dried ( $k_{TD}$ ) and wetted ( $k_{TW}$ ) regions were estimated using the Woodside and Messmer model (Woodside and Messmer, 1961). They combined empirical equations for series and parallel distributions of solid, liquid and vapor phases in a porous medium:

$$k_{TD} = \frac{\alpha_p k_s k_v}{k_s (1 - \beta_p) + \beta_p k_v} + \gamma_p k_v \quad (6.3)$$

$$k_{TW} = \frac{\alpha_p k_s k_l}{k_s (1 - \beta_p) + \beta_p k_l} + \gamma_p k_l \quad (6.4)$$

where  $k_s$  is the thermal conductivity of the porous substrate (tablet or crust), and  $k_v$  and  $k_l$  are the thermal conductivities of the vapor and water, respectively. Following Kiil (2006), it was assumed that the thermal conductivities of the dried and wetted regions are constant.

The parameters  $\alpha_p$ ,  $\beta_p$  and  $\gamma_p$  were estimated using the following equations (Woodside and Messmer, 1961):

$$\alpha_p = 1 - \gamma, \quad \beta_p = (1 - \varphi)/\alpha_p, \quad \gamma_p = \varphi - 0.03 \quad (6.5)$$

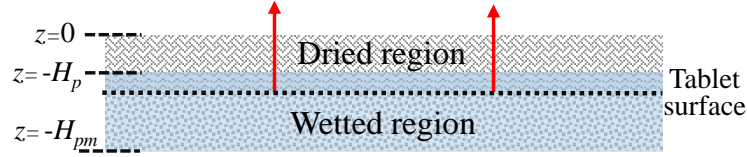


Figure 6.3: Evaporation front within a tablet.

Following Kadja and Bergeles (2003), the porosity of the crust above the tablet surface ( $-H_c < z \leq 0$ ) can be considered to be equal to the water volume fraction at the critical point where the particles come into contact ( $\varphi_c = 0.33$ ). Finally, it was assumed that no further coalescence takes place as the water evaporates through the crust and thus the porous crust porosity remains constant during the evaporation process (Kiil, 2006).

To solve the energy conservation equations (Eqs. 6.1 and 6.2), the following boundary conditions were adopted:

$$\partial_z T_{TW} = 0, \quad z = -H_{pm} \quad (6.6)$$

$$T_{TW} = T_{TD}, \quad z = -H_p \quad (6.7)$$

$$\varphi \rho_1 \Delta H_e \frac{dH_p}{dt} = k_{TD} \partial_z T_{TD} - k_{TW} \partial_z T_{TW}, \quad z = -H_p \quad (6.8)$$

$$h_H (T_2 - T_{TD}) = k_{TD} \partial_z T_{TD}, \quad z = 0 \quad (6.9)$$

where  $\Delta H_e$  is the heat of vaporization,  $T_2$  is the temperature of the air above the tablet and  $h_H$  is the heat transfer coefficient. The calculation of the heat transfer coefficient is presented below in this section.

In Equation (6.6), the temperature  $T_{TW}$  gradient in the z-direction at the wetting front boundary ( $z = -H_{pm}$ ) was set equal to zero. This is a symmetry condition justified by the fact that the line  $z = -H_{pm}$  is regarded as a symmetry line between the part of the tablet shown in Figure 6.3 and the specular part that is not shown. This is true since both sides of the tablet are similarly wetted and experience the same changes in temperature. The boundary condition (6.7) states that the dried and wetted region temperatures are equal at the evaporation front ( $z = -H_p$ ).

Equations (6.8) and (6.9) represent the enthalpy jump conditions at the evaporation front and at the tablet surface, respectively. The simplified enthalpy jump condition at the liquid-air interface inside a porous tablet reads (Delhaye, 1974):

$$\dot{m}_e (\hat{H}_1 - \hat{H}_2) = -\mathbf{n}_{12} \cdot (\mathbf{q}_1 - \mathbf{q}_2) \quad (6.10)$$

where  $\mathbf{n}_{12}$  is the unit vector normal to the interface pointing from continuous medium 1 (liquid) to continuous medium 2 (air/vapor inside the porous medium),  $\mathbf{q}$  is the heat flux and  $\dot{m}_e$  is the evaporation mass flux. To derive Equation (6.8), one can define at the liquid-gas interface inside a porous matrix:

$$\hat{H}_1 - \hat{H}_2 \equiv \Delta H_e \quad ; \quad \dot{m}_e \equiv \varphi \rho_1 dH_p/dt \quad (6.11)$$

and then get:

$$-\mathbf{n}_{12} \cdot (\mathbf{q}_1 - \mathbf{q}_2) = k_{TD} \partial_z T_{TD} \Big|_{z=-H_p} - k_{TW} \partial_z T_{TW} \Big|_{z=-H_p} \quad (6.12)$$

Substituting Equations (6.11) and (6.12) into (6.10) yields the enthalpy jump condition (6.8).

To derive Equation (6.9), one writes:

$$-\mathbf{n}_{12} \cdot (\mathbf{q}_1 - \mathbf{q}_2) = -h_H \left( T_2 - T_{TD} \Big|_{z=0} \right) + k_{TD} \partial_z T_{TD} \Big|_{z=0} \quad (6.13)$$

which is true at the surface of the crust (Kiil, 2006). Substituting Equation (6.13) into (6.10) and assuming that, in this case, the left-hand side of Equation (6.10) is zero, yields the enthalpy jump condition (6.9).

The vapor concentration in the dried region of the porous matrix was obtained from the mass balance:

$$\varphi \partial_t \mathcal{C}_v = \mathcal{D}_{TD} \partial_z (\partial_z \mathcal{C}_v) \quad (6.14)$$

where  $\mathcal{D}_{TD}$  is the effective vapor diffusivity. Equation (6.14) was formulated assuming that the accumulation of vapor in the pores balances the transfer of water vapor to the particle surface by a diffusive mechanism. The effective vapor diffusivity in the porous medium ( $\mathcal{D}_{TD}$ ) was estimated using the empirical equation found in Golman and Julklang (2013):

$$\mathcal{D}_{TD} = \mathcal{D}_{TW} \varphi^{1.9} \quad (6.15)$$

$$\mathcal{D}_{TW} = 0.22 \cdot 10^{-4} \left( \frac{T_2}{273.15} \right)^{1.75} \quad (6.16)$$

where  $T_2$  should be given in Kelvin.

One can write the Neumann boundary conditions for the mass balance equation (Equation 6.14) at the crust surface ( $z = 0$ ) and the evaporation front ( $z = -H_p$ ) as follows:

$$-\mathcal{D}_{TD} \partial_z \mathcal{C}_v = k_m \left( \mathcal{C}_v \Big|_{z=0} - \mathcal{C}_{v_{air}} \right), \quad z = 0 \quad (6.17)$$

$$\varphi \rho_1 \frac{dH_p}{dt} = -\mathcal{D}_{TD} \mathcal{M}_w \partial_z \mathcal{C}_v, \quad z = -H_p \quad (6.18)$$

where  $\mathcal{C}_{v_{air}}$  is the vapor concentration in the surrounding (bulk) air and  $\mathcal{M}_w$  is the molecular weight of the liquid (water) that evaporates. Equations (6.17) and (6.18) are the mass jump conditions at the crust surface and at the evaporation front, respectively.

According to Golman and Julklang (2013), one can calculate the vapor concentration in the air bulk  $\mathcal{C}_{v_{air}}$  from the following equation:

$$\mathcal{C}_{v_{air}} = \frac{RH \rho_v^*}{\mathcal{M}_w} \quad (6.19)$$

where  $\rho_v^*$  is the saturated vapor density in the air and  $RH$  is the bulk air relative humidity.

In this work, the mass ( $k_m$ ) and heat ( $h_H$ ) transfer coefficients were evaluated by the Ranz-Marshall correlations for the Nusselt (Nu) and Sherwood (Sh) numbers:

$$\text{Nu} \equiv \frac{h_H S_{ep}}{k_2} = 2 + 0.65 \cdot \text{Re}^{1/2} \text{Pr}^{1/3} \quad (6.20)$$

$$\text{Sh} \equiv \frac{k_m S_{ep}}{\mathcal{D}_{TW}} = 2 + 0.65 \cdot \text{Re}^{1/2} \text{Sc}^{1/3} \quad (6.21)$$

where  $S_{ep}$  denotes the characteristic length of the evaporation interface of the absorbed liquid. The evaporation interface can be approximated to be circular since coating films and droplets that absorb into a tablet have approximately cylindrical or spherical cap shapes when they are initially applied on the surface of the tablet. This assumption was experimentally validated by Niblett et al. (2017) for the film-coating process.

In Equations (6.20) and (6.21), Re, Pr and Sc are the Reynolds, Prandtl and Schmidt numbers, respectively, defined as:

$$\text{Re} \equiv \frac{u_2 \rho_2 S_{ep}}{\mu_2}, \quad \text{Pr} \equiv \frac{c_{p2} \mu_2}{k_2}, \quad \text{Sc} \equiv \frac{\mu_2}{\rho_2 \mathcal{D}_{TW}} \quad (6.22)$$

where  $u_2$ ,  $\mu_2$ ,  $c_{p2}$ ,  $\rho_2$  are the velocity, viscosity, specific heat and density of the air surrounding the tablet, respectively.

The wetted region volume inside the porous tablet can be estimated from the evaporation depth  $H_p$  (Fig. 6.3). The evaporation mass flux of the water from within the porous matrix is estimated from Equation (6.11.b). To calculate the evolution of the evaporation front, Equations (6.1, 6.2, 6.14) and their boundary conditions must be solved together.

### 6.3 Numerical solution

To numerically solve Equations (6.1, 6.2, 6.14) and their boundary conditions, one needs to first make them dimensionless, and then apply Landau's boundary immobilisation technique for the equations that involve the moving evaporation front. This is because the evaporation front position changes with time. It is possible to turn the integration domain into one with fixed boundaries through a suitable change of independent variables (Kutluay et al., 1997).

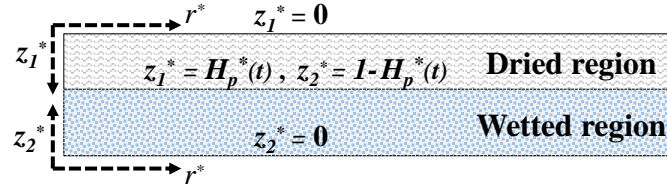
The equations were made dimensionless using the following variables:

$$z^* \equiv \frac{z}{H_{pm}}, \quad H_p^* \equiv \frac{H_p}{H_{pm}}, \quad t^* \equiv \frac{\mathcal{D}_{TD}}{H_{pm}} t, \quad T^* \equiv \frac{c_{ps}}{\Delta H_e} T, \quad C_v^* \equiv \frac{\mathcal{M}_w}{\rho_1} C_v$$

To perform the Landau's transformation, the  $z^*$  domain was divided into two sub-domains  $z_1^*$  and  $z_2^*$  as seen in Figure 6.4. The transformed variables are:

$$\xi \equiv \frac{z_1^*}{H_p^*(t^*)}, \quad \xi' \equiv \frac{z_2^*}{H_{pl}^*(t^*)} \quad (6.23)$$

where  $H_{pl} = H_{pm} - H_p$ . The Landau transformation modifies the model domains from  $0 < (z_1^*, z_2^*) < (H_p^*, H_{pl}^*)$  to  $0 < (\xi, \xi') < 1$ .

Figure 6.4: Domains  $z_1^*$  and  $z_2^*$ .

The dimensionless equations for the temperature profile inside the tablet are:

$$\left[ \varphi M_{1l} + (1 - \varphi) M_{1s} \right] \left( \partial_{t^*} T_{TW}^* + \frac{\xi'}{1 - H_p^*} \frac{dH_p^*}{dt^*} \partial_{\xi'} T_{TW}^* \right) = \frac{\partial_{\xi'} (\partial_{\xi'} T_{TW}^*)}{(1 - H_p^*)^2}, \quad 0 \leq \xi' \leq 1 \quad (6.24)$$

$$\left[ \varphi M_{2g} + (1 - \varphi) M_{2s} \right] \left( \partial_{t^*} T_{TD}^* - \frac{\xi}{H_p^*} \frac{dH_p^*}{dt^*} \partial_{\xi} T_{TD}^* \right) = \frac{\partial_{\xi} (\partial_{\xi} T_{TD}^*)}{H_p^{*2}}, \quad 0 \leq \xi \leq 1 \quad (6.25)$$

For the concentration profile:

$$\varphi \left( \partial_{t^*} C_v^* - \frac{\xi}{H_p^*} \frac{dH_p^*}{dt^*} \partial_{\xi} C_v^* \right) = \frac{\partial_{\xi} (\partial_{\xi} C_v^*)}{H_p^{*2}}, \quad 0 \leq \xi \leq 1$$

where:

$$M_{1l} \equiv \frac{\rho_1 c_{p1} \mathcal{D}_{TW}}{k_{TW}}, \quad M_{1s} \equiv \frac{\rho_s c_{ps} \mathcal{D}_{TW}}{k_{TW}}, \quad M_{2g} \equiv \frac{\rho_2 c_{p2} \mathcal{D}_{TD}}{k_{TD}}, \quad M_{2s} \equiv \frac{\rho_s c_{ps} \mathcal{D}_{TD}}{k_{TD}}$$

The boundary conditions (Eqs. 6.6 to 6.9 and 6.17, 6.18) become in dimensionless form:

$$\partial_{\xi'} T_{TW}^* = 0, \quad \xi' = 0 \quad (6.26)$$

$$T_{TW}^* = T_{TD}^*, \quad \xi = \xi' = 1 \quad (6.27)$$

$$(T_2^* - T_{TD}^*) = \frac{M_{TD}}{H_p^*} \partial_{\xi} T_{TD}^*, \quad \xi = 0 \quad (6.28)$$

$$\frac{M_{b,TD}}{H_p^*} \partial_{\xi} T_{TD}^* - \frac{M_{b,TW}}{1 - H_p^*} \partial_{\xi'} T_{TW}^* = \varphi \frac{dH_p^*}{dt^*}, \quad \xi = \xi' = 1 \quad (6.29)$$

$$M_{mb} (C_{v_{z=0}}^* - C_{v_2}^*) = \frac{1}{H_p^*} \partial_{\xi} C_v^*, \quad \xi = 0 \quad (6.30)$$

$$\frac{dH_p^*}{dt^*} = -\frac{\partial_{\xi} C_v^*}{H_p^*}, \quad \xi = 1 \quad (6.31)$$

where:

$$M_{TD} \equiv \frac{k_{TD}}{H_{pm} h_H}, \quad M_{mb} \equiv \frac{H_{pm} k_m}{\mathcal{D}_{TD}}, \quad M_{b,TD} \equiv \frac{k_{TD}}{\rho_1 c_{ps} \mathcal{D}_{TD}}, \quad M_{b,TW} \equiv \frac{k_{TW}}{\rho_1 c_{ps} \mathcal{D}_{TW}}$$

By solving Equations (6.24) to (6.31), it is possible to simulate water evaporation from within porous substrates. This model can be used to simulate tablet drying inside a coating drum and thereby predict the water content in the final product. The validation of the model developed in this chapter is presented in the following section.

## 6.4 Numerical results and validation

In this section, the numerical results of the evaporation model are presented. The evaporation model was presented in Section 6.2 and describes the rate of liquid depletion from within a porous matrix. For validation, the numerical results were compared with experimental data taken from the work of Reis et al. (2003) and Tag et al. (2010). Reis et al. performed their water evaporation experiments with glass beads, while Tag et al. worked with pharmaceutical tablets of uniform porosity. All the experimental data reported in this work were derived from experiments conducted at room ambient temperature.

### 6.4.1 Water evaporation from porous media

Figure 6.5.a) compares the numerical results with the experimental ones for water evaporation from within a  $\text{CaCO}_3$  porous tablet (Tag et al., 2010) at conditions of low temperature ( $T_B = 20^\circ\text{C}$ ) and high relative humidity ( $RH = 50\%$ ). The  $\text{CaCO}_3$  tablets ( $\rho_s = 1300 \text{ kg/m}^3$ ,  $c_{ps} = 1000 \text{ J kg}^{-1}\text{K}^{-1}$ ,  $k_s = 0.7 \text{ J s}^{-1}\text{m}^{-1}\text{K}^{-1}$ ) had a porosity of 0.08 and the wetted region had a maximum wetted front depth ( $H_{pm}$ ) of 1.2 mm. The liquid evaporation from within the porous matrix is quite slow due to the relatively low ambient temperature, high relative humidity, low porosity and the lack of air flow on the surface of the tablet. As can be seen from Figure 6.5, the numerical results from the solution of the model are in good agreement with the experimental data as the mean relative error is 0.76%.

In Figure 6.5.b), the evaporation model is validated with experimental data for glass beads ( $\rho_s = 2300 \text{ kg/m}^3$ ,  $c_{ps} = 840 \text{ J kg}^{-1}\text{K}^{-1}$ ,  $k_s = 1.05 \text{ J s}^{-1}\text{m}^{-1}\text{K}^{-1}$ ). The experiments were conducted by Reis et al. (2003) at ambient conditions ( $20^\circ\text{C}$ ) with no air flow over the porous matrix (stagnant air). The glass beads had a size of  $50 \mu\text{m}$  and the overall porous matrix had a porosity  $\varphi$  of 0.42. The evaporation rate in the experiments conducted by Reis et al. (2003) is higher than that observed by Tag et al. (2010). This is due to the higher porosity of the glass beads that allows the evaporating water vapor to diffuse easier through the pores. The numerical results are very close to the corresponding experimental data with a mean relative error of 2% and the model thus also predicts these results well.

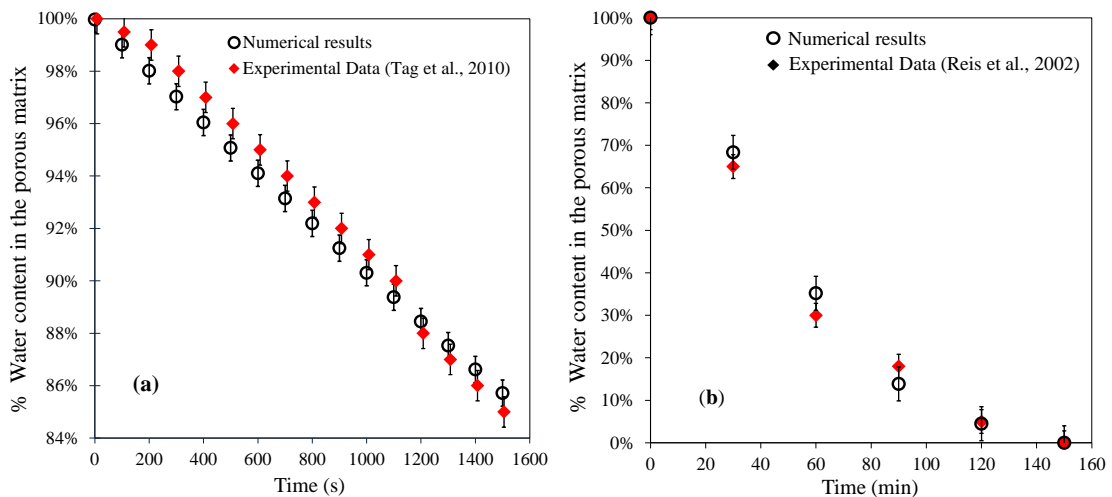


Figure 6.5: Evaporation of water inside a)  $\text{CaCO}_3$  tablets and b) glass beads during the evaporation phase. Experiments from a) Tag et al. (2010) and b) Reis et al. (2003).

The error bars of the numerical results presented in Figures 6.5.a) and 6.5.b) were estimated in this work by propagating the experimental measurement errors for the porosity and pore diameter which are assumed to be the same as in the capillary phase (taken from Lee et al., 2016). Tag et al. (2010) also mentioned a deviation in the room temperature (20-27°C) which was taken into account in the calculations of this work. The experimental data errors were estimated from the figures presented in the paper of Tag et al. (2010) and Reis et al. (2002).

The wetted region profile inside the porous matrix during water evaporation can be calculated by subtracting the advancing evaporation front depth  $H_p$  from the wetted region depth. Figure 6.6 presents the numerical results for the wetted region profile inside a porous matrix ( $\text{CaCO}_3$  tablet;  $\varphi = 0.30$ ,  $d_p = 10\ \mu\text{m}$ ) after 60 and 120 minutes, respectively. The origin of the  $z$ -coordinate represents the evaporation front depth  $H_p$  which increases as the water evaporation process progresses. In the simulations performed to calculate the results presented in Figure 6.6, the initial maximum wetting region depth was set to be 1.8 mm and the air temperature and relative humidity were taken to be 20°C and 50%, respectively.

Figure 6.7 shows the model prediction for the wetted region position inside a porous tablet. For the numerical simulation, operating conditions that resemble those inside a pan-coater during the pharmaceutical film-coating process were chosen ( $T_2 = 50^\circ\text{C}$ ,  $RH = 70\%$ ,  $u_2 = 1\ \text{m/s}$ ). The initial wetted region depth was the same as in the case study presented in Figure 6.6. No experimental data, available in the open literature, could be found for the validation of this simulation. The origin of the  $z$ -coordinate represents the evaporation front depth  $H_p$  which progresses as more water evaporates. The model presented in this work suggests that the complete evaporation of a  $4.3\ \mu\text{L}$  water droplet absorbed into a tablet ( $\varphi = 0.30$ ) takes 2 minutes.

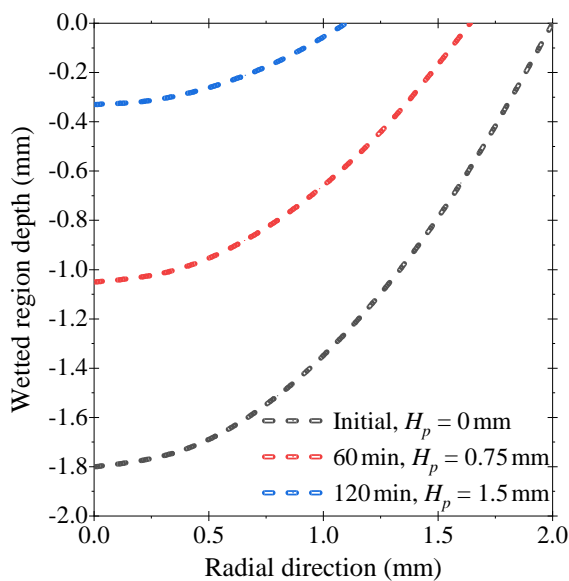


Figure 6.6: Wetted region profile in glass beads during evaporation. (Substrate porosity = 0.30; initial water droplet volume =  $4.3\ \mu\text{L}$ ).

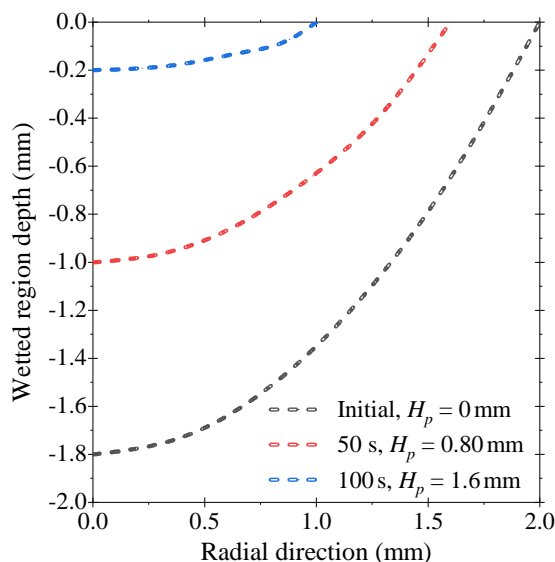


Figure 6.7: Wetting front depth profile during the evaporation phase under coating process conditions. (Substrate porosity = 0.30; initial water droplet volume = 4.3  $\mu\text{L}$ ).

The validation of the numerical results with the experimental data from the two separate papers (Reis et al., 2003; Tag et al., 2010) shows that the evaporation model proposed is able to accurately predict the water evaporation from different porous materials in different process conditions.

#### 6.4.2 Case study: Prediction of the water content of a tablet during film-coating

In this case study, the evaporation of water from a tablet, under coating process conditions, is investigated. This case study illustrates the ability of the models developed in this thesis to calculate the water content of the tablet from the moment of initial aqueous coating suspension impact onto a tablet until the moment it completely evaporates from within this porous tablet. To derive the results reported here, the model presented in this chapter was combined with models developed in previous chapters of this thesis. These models describe spray impingement (Chapter 4) and film absorption and drying (Chapter 5).

The case study simulation begins at the moment the tablet enters the area under the spray inside a rotating drum (spray zone) and the first coating suspension droplets impinge onto its surface. The coating suspension then spreads on the surface of the tablet forming a thin film. This inertia-driven spreading is simulated by the model equations presented in Chapter 4. The output of this model is the thickness and the wetted area of the film at the moment the tablet leaves the spray zone. This output serves as an input for the model that simulates suspension film drying and absorption into the tablet which follow the inertia-driven suspension spreading (Chapter 5). Solving the model equations presented in Chapter 5 yields the profile of water content and solid particle content inside and outside the tablet during suspension drying and absorption. When the particle volume fraction of the suspension becomes sufficiently high, a wetted crust forms in the entirety of the film. At this stage, the profile of the water content inside the tablet is calculated and used as an initial condition for the evaporation model presented in this chapter. The simulation is completed when the water is completely evaporated from within the coated tablet.

Table 6.1: Process parameters for the case studies.

Process conditions	Scenario 1	Scenario 2
Temperature of bulk air	60°C	65°C
Temperature of tablet surface	35°C	40°C
Relative humidity	50%	45%
Drying air flow rate	0.10 m <sup>3</sup> /s	0.15 m <sup>3</sup> /s

The conditions of the process were chosen to match typical conditions inside a pharmaceutical coating drum (am Ende et al., 2005) and are shown in Table 6.1 (Scenario 1). The coating suspension spray mean droplet diameter and velocity before impact was taken to be 100  $\mu\text{m}$  and 10 m/s, respectively. The spray mass flow rate was set to be 200 g/min. The coating suspension was assumed to be formed of water and polymer particles of 10 nm in size. The suspension properties appear in Table 6.2. The volume fraction of solid particles before impact was taken to be 0.10.

The tablet was assumed to be cylindrical with a radius of 1 cm. The porosity of the substrate-tablet was taken equal to 0.33 and the mean pore diameter was considered equal to 10  $\mu\text{m}$  (Krok et al., 2017). Finally, the time a tablet spends under the spray (spray zone) was set to be 0.06 s, whereas the cycle time until it enters the spray zone again was taken equal to 5 s (Kumar et al., 2015). Generally, the motion of the tablets in a coating drum can be calculated by DEM-based models discussed in Chapter 2.

Using the droplet impact conditions mentioned above as inputs, the spray impingement model estimated the thickness of the coating film when the tablet leaves the spray zone and the inertia-driven spreading ceases to be significant. The film thickness is calculated to be  $H_f = 40 \mu\text{m}$ . The spray impingement model also predicted that the entire surface facing the spray is covered with the suspension film. For the impact conditions (droplet size and velocity) chosen above, no splashing was assumed to take place during spray impingement.

When the tablet leaves the spray zone after 0.06 s, the model presented in Chapter 5 can calculate the coating suspension absorption into the porous tablet and the film drying on its surface. The model predicted that the maximum coating suspension penetration depth into the tablet was 28  $\mu\text{m}$  and that the time required for the suspension viscosity to become infinite when the particle volume fraction approaches a critical value ( $\phi = \phi^* = 0.67$ ) was 3 s (as seen in Figure 6.9). As mentioned in Chapter 5, at this critical volume fraction, the particles coalesce and form a porous crust. At this point, the film absorption and capillary spreading is negligible and the solvent evaporates through the pores of the crust.

Table 6.2: Coating suspension properties for the case studies (from: Amidon et al., 1999).

Coating properties	Value
Surface tension	0.040 N/m
Initial particle volume fraction	0.10
Particle density	1200 kg/m <sup>3</sup>
Carrier fluid density	998 kg/m <sup>3</sup>
Carrier fluid viscosity	0.001 Pa s

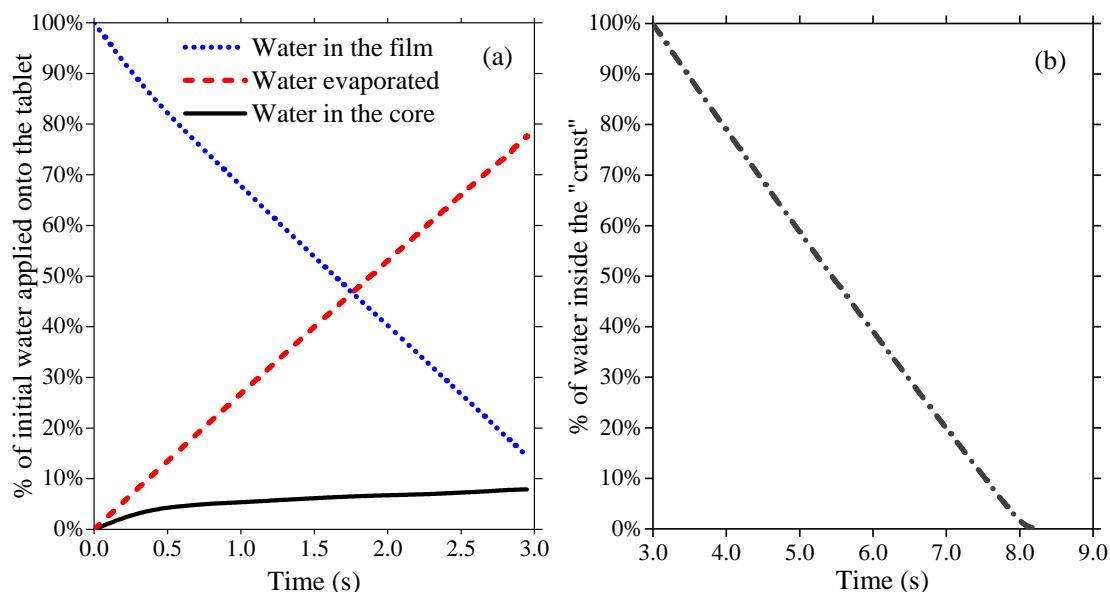


Figure 6.8: a) Water that has evaporated or is inside the film or inside porous tablet core.  
 b) Water evaporation rate from within the suspension film crust.

Figure 6.8.a) shows the predictions for the amount of water that is evaporated, absorbed into the tablet, or remains on the surface of the tablet as the liquid phase of the suspension coating. The initial water volume applied on the tablet was calculated to be  $11.25 \mu\text{L}$ . After 3 seconds, the particle volume fraction approaches the critical value of 0.67 and the solid crust forms at the surface of the suspension film. At this moment, the model presented in Chapter 5 predicts that 79% of the initial water is evaporated, whereas 9% is absorbed into the tablet as a suspension (Fig. 6.8.a).

Using the information about the amount of water inside the porous crust, the model presented in this chapter (Section 6.2) calculates the rate of water evaporation from within a porous medium. The porosity of the porous crust was taken to be 0.33 (Kiil, 2006), whereas the porosity of the tablet is reduced due to polymer particle deposition on its surface (see Chapter 5). The final average tablet core porosity was calculated by the model presented in Chapter 5 (Eq. 5.30) to be 0.20. The initial dried region is considered to be the crust at the surface of the coating film which initially has infinitesimal thickness. As the water evaporates, the dried region increases in size (see Fig. 6.3).

In Figure 6.8.b), the reduction in water content from within the crust is shown. The model predicts that it takes 8 seconds for all the water contained in the crust and the tablet to completely evaporate. Figure 6.9 (scenario 1; blue line) combines Figures 6.8.a) and 6.8.b) and presents the rate at which the water contained in the tablet (applied while crossing the spray-zone) evaporates. Since the cycle time is taken to be 5s (typical value found in Kumar et al., 2015), the tablet will have 15% of the initial water content ( $1.69 \mu\text{L}$ ) applied to it during its first pass under the spray zone when it enters the spray zone for the second time. The time required for the complete drying of the tablet is 8s. If the cycle time is longer than 8s then the liquid water content inside the tablet at the end of the process will be negligible.

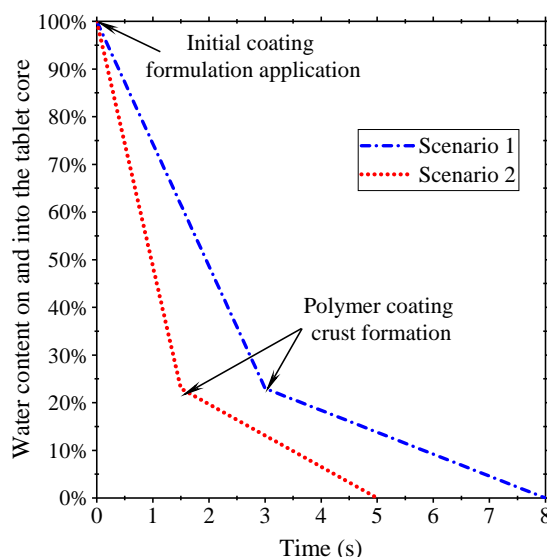


Figure 6.9: Reduction of the water content of the tablet after it leaves the spray zone.

Choosing the process conditions of scenario 1 (Table 6.1) does not allow all the water to evaporate from the tablet before this re-enters the spray zone. In this work, appropriate film-coating process conditions (scenario 2; Table 6.1) that lead to complete water evaporation during the tablet cycle time in the coating drum were found by simulating many different scenarios. Simulating many scenarios with the model presented in this thesis is possible because of the limited time required by a single run (CPU time < 5 min).

Figure 6.9 (red line) shows the reduction of the water content of the tablet when the process conditions of scenario 2 are chosen. According to the numerical results, the water content when the tablet re-enters the spray zone is negligible. From the results of this case study, it can be seen that choosing suboptimal process conditions (scenario 1; Table 6.1) can lead to water remaining inside the tablet that can potentially affect its quality and its shelf-life due to active ingredient and excipient disintegration (see Chapter 1).

## 6.5 Concluding remarks

The model developed in this chapter considers water evaporation from within a porous substrate under film-coating operating conditions. The current approach allows the consideration of elevated temperature, humidity level and ambient air flow and more accurately predicts the tablet water content during the coating process. The validation of the numerical results with the experimental data from the two separate papers shows that the evaporation model is able to efficiently predict the water evaporation from different materials in different conditions. The experimental results of both Reis et al. (2003) and Tag et al. (2010) are successfully estimated by the evaporation model, showing that the depletion of water from within a porous matrix can take a significant amount of time. Tablets in coating process operating conditions will dry notably faster due to higher temperatures and air flow. This was illustrated in the case study presented in this chapter. To conclude, the numerical results for the water content inside a porous matrix, and the distance of the wetted front from the surface, can be used to predict the water content inside a pharmaceutical tablet during the film-coating process.

# CHAPTER 7

## Conclusions and directions for future research

---

This chapter summarizes the main contributions and findings that have been presented in this thesis. In the final section, some possible directions for future work are outlined.

---

The work presented in this thesis is concerned with investigating the fundamental phenomena taking place at the point of contact between a tablet and the coating formulation during a pharmaceutical film-coating process. This study involves the development of models that predict the behavior of an aqueous coating suspension from the moment it is sprayed onto a tablet surface until the moment all the water evaporates, leaving a dry solid film behind. The main goal of this thesis is to provide insight into the film-coating process in an effort to increase the quality of the coated tablets.

Overall, the work is characterized by several novel features which differentiate it from previous studies found in the open literature regarding the film-coating process. These features include: the modeling of the impingement of an entire array (spray) of droplets onto a single tablet; the simulation of simultaneous coating suspension drying and absorption into a tablet under film-coating process conditions; the consideration of the effect of the polymer solids on the coating formulation motion; and the modeling of water evaporation from within a porous pharmaceutical tablet.

During this project, detailed models were developed that simulate single droplet behavior on a tablet (Chapter 3), spray impingement onto a tablet (Chapter 4), suspension film drying, capillary spreading and absorption into a tablet (Chapter 5) and water evaporation from within the tablet (Chapter 6). Each one of these four models is described in a different chapter of this thesis. A summary of the main contributions and findings of the work presented in these chapters are reviewed and discussed in the following sections.

### 7.1 Single droplet behavior on a tablet

The first contribution of this thesis is the modeling of the spreading, absorption and evaporation phenomena after a single droplet impinges onto a pharmaceutical tablet. Previous work either neglected droplet absorption into the tablet or did not account for droplet evaporation as they considered only room ambient conditions (where evaporation is negligible). In this work, the droplet behavior was divided into two phases of different dynamics and duration: the kinematic phase and the capillary phase. The kinematic phase described the first milliseconds after impact during which inertial forces are significant, while the capillary phase concerned the behavior of the droplet when the capillary effects become dominant. To model the kinematic phase, a 1D spreading model was developed. This model was based on the mechanical energy balance equation written for the droplet during the first milliseconds of spreading. For the capillary phase, the continuity and Navier-Stokes equations were solved using the lubrication approximation method.

The 1D droplet spreading model for the initial impact period was combined successfully with the lubrication approximation method for the droplet capillary flow, evaporation and absorption into the tablet. The combination of the two models presented in this chapter is a novel approach that can estimate the water content of a pharmaceutical tablet after droplet impact during the film-coating process.

Even if the single droplet models are simplistic, and do not account for the entire film which covers the tablet surface, they can provide useful insight regarding the behavior of water and other coating solvents on permeable substrates such as pharmaceutical tablets. The validation with experimental data from different studies showed that the numerical model presented in Chapter 3 is predictive and can be used to simulate single pure liquid droplet impact, spreading, evaporation and absorption into pharmaceutical tablets.

## 7.2 Spray impingement onto a tablet

An important contribution of this work is the development of a model that accurately simulates coating spray impingement and film spreading on a tablet while this passes through the area under the spray in a rotating coating drum (Chapter 4). This model does not require prior knowledge of the process via empirical relations or experimental data and it is based on the mechanical energy balance equation as for the single droplet case (Chapter 3).

In Chapter 4, the results of the model were compared with experimental data found in the literature (Kalantari and Tropea, 2007) and it was shown that the model predictions agree with the experiments. The output of the model can provide useful insight into the coating formulation film thickness and spreading rate on dry tablets during the coating process.

In comparison with commercial CFD software simulations - which take hours or days to output results - the model presented in Chapter 4 provides solutions considerably faster (< 5s) without making significant sacrifices in accuracy. This computational efficiency allowed the execution of variance-based sensitivity analysis to study the influence of process parameters on the coating spreading behavior. In Chapter 4, it was found that the mean droplet diameter and velocity before impact are the parameters that significantly affect the film thickness and the application time. Additionally, it was concluded that the spray mass flow rate significantly influences only the time required to cover the tablet with the coating, whereas liquid properties such as the coating viscosity and density are not as important.

## 7.3 Suspension film behavior on a tablet

Another contribution of this thesis is the development of a model that describes the behavior of a coating suspension (water and particles) film on the surface of a porous tablet during the pharmaceutical film-coating process (Chapter 5). In Chapter 5, the work presented in Chapter 3 is extended to predict the behavior of non-Newtonian coating suspensions and to account for the influence of particle concentration on the film flow on the surface of the tablet and on the coating suspension absorption into the tablet.

The mixture modeling approach and the lubrication approximation method were used to simplify the equations describing the behavior of the coating liquid-particle system and to develop a model for simulating film motion and drying on tablet surfaces. The influence of water evaporation on important physical properties of the coating suspension, such as the density and viscosity, was taken into consideration. The model presented in Chapter 5 also simulates the absorption of the coating suspension inside the porous tablet, since predicting the wetting front profile inside the tablet provides important information about the tablet water content during the film-coating process.

Previous models which simulate coating suspension application on tablets focused on single droplet impact cases and/or neglected suspension absorption into the tablet. On the contrary, the main outputs of the model are the amount of the applied suspension which penetrates into the tablet core and the prediction of the film drying time. Knowledge of the amount of water and solid polymer inside the tablet can be used by the pharmaceutical industry to enhance tablet shelf-life and adhesion of the dry film. In Chapter 5, it is shown that the numerical results of the developed model agree well with experimental data taken from the literature and with Volume-Of-Fluid CFD simulations. An advantage of the current model when compared to traditional CFD simulations is the computational speed as mentioned previously.

In the results section of Chapter 5, it was found that a decrease in the drying rate and initial solid volume fraction of the coating suspension lead to higher coating suspension absorption rates into the tablet and thus more water penetrating the tablet. The influence of the particle retention on the penetration depth was also investigated. It was found that at the particle diameter/pore diameter ratio ( $2a/d_p$ ) of 0.06 the tablet pores are clogged by particles. This result agrees with experimental observations (Holloway et al., 2011). Having low water content and solid particles retained close to the tablet surface (as in the case study where  $2a/d_p = 0.06$ ) is preferred by the pharmaceutical industry in order to increase the tablet shelf-life and avoid defects such as peeling of the dry coating film (Cole et al., 1995; Muliadi and Sojka, 2010).

#### 7.4 Water evaporation from within a porous tablet

Chapter 6 deals with water evaporation from within porous media (tablets). The main contribution presented in this chapter is a novel model that predicts the evaporation rate of water which has been absorbed into a pharmaceutical tablet during the film-coating process. A method that simulates the process of slurry-droplet drying was adopted and a novel model was developed. The output of this evaporation model provides useful insight into the final water content of a tablet core during the film-coating process.

The validation of the numerical results presented in Chapter 6 with the experimental data from two separate papers shows that the current evaporation model is able to efficiently predict the water content evaporation from different materials in different conditions. The experimental results which were successfully estimated by the current evaporation model show that the depletion of water from within a porous matrix can take a significant amount

of time. Pharmaceutical tablets in coating process operating conditions will dry notably faster due to higher temperatures and air flow. This was illustrated in the case study presented in this chapter.

From the results of the case study, it was concluded that choosing suboptimal process conditions (e.g. spray rate, drum rotation speed, inlet air temperature) can lead to water remaining inside the tablet that can potentially affect its quality and its shelf-life due to active ingredient and excipient disintegration.

## 7.5 Summary of main contributions

The main contributions of this work are:

- A mathematical model that can simulate the behavior of a single pure liquid droplet after it is applied on a pharmaceutical tablet was developed. The mathematical model was validated with experimental data from the open literature. The information from the single-droplet model can help to gain a basic understanding of liquid water behavior on a pharmaceutical tablet.
- A model that can predict spray impingement (not only a single droplet) onto a tablet during the film-coating process was developed. The mathematical model was validated with experimental data from the open literature. Variance-based sensitivity analysis was performed to study the influence of process parameters on the coating formulation spreading behavior on the surface of a pharmaceutical tablet.
- A model that simulates coating suspension film (water and coating particles) flow, drying and absorption into a tablet was developed. Parts of the model were validated with experimental data and CFD Volume-Of-Fluid simulations. The main outputs of this model are the calculation of the amount of water and coating particles which penetrate into the tablet porous core and the film drying time on the tablet surface. Knowledge of the amount of water and solids in a solid dosage form can be used to optimize tablet shelf-life and adhesion of the dry coating film.
- A model that considers water evaporation from within a porous substrate under pharmaceutical film-coating operating conditions was developed. The approach allows considering elevated temperature, humidity level and ambient air flow and more accurately predicts the tablet water content during the film-coating process. The model was validated with experimental data from the open literature.
- The numerical results of the developed models were analyzed in order to understand the phenomena at the point of contact between a pharmaceutical coating formulation and a tablet during the film-coating process. This insight can assist the pharmaceutical industry in choosing the appropriate process conditions which maximize the quality of the final product.

## 7.6 Directions for future research

In this last section, a few recommendations for future work are discussed. Some broader directions for future research are also outlined.

### 7.6.1 Extending this research

In this work, models considering single impact and spray impact onto a pharmaceutical tablet were developed (Chapters 3 and 4). These models were validated with experimental data from the literature. The agreement of the numerical results with the experiments was good in all cases. To enhance the predictive ability of the impingement models a few modifications can be proposed:

Oblique droplet impact on the tablet surface can increase the probability of splashing and affect the coating formulation spreading rate. Additionally, since the tablet moves inside the rotating drum, the tablet velocity can influence the droplet impact outcome. The current model accounts only for vertical droplet impact on stationary tablets. Enhancing the current model by accounting for oblique droplet impact and tablet movement can lead to even better agreement with the experimental data.

In Chapter 5, a model that predicts the behavior of coating suspensions on tablets was developed. Based on limited information found in the literature, it was assumed that the coating suspension behaves as a power law fluid. Moreover, general semi-empirical relations for the effect of particle volume fraction on the viscosity of the suspension were used in the model. Experiments should be performed to determine the rheology of coating formulations and the relation between the particle volume fraction and the viscosity of the suspension.

The model presented in Chapter 5 accounts for particle retention in the tablet pores. Validation of the model predictions of the particle retention rate and the changes in tablet porosity is needed. Unfortunately, no experimental data that could be used for validation of the numerical results concerning polymer particle retention inside a tablet were found in the open literature. Thus, experiments need to be performed to determine if the semi-empirical equation used to estimate the particle retention rate in the model is valid for the case of pharmaceutical formulation absorption into tablets. The experiments can either confirm the applicability of this equation or suggest a different empirical equation.

The mechanisms of polymer particle coalescence after all the liquid water evaporates from the thin polymer suspension film were not investigated in this thesis (Chapter 6). Previous work investigated latex particle coalescence and the formation of solid coatings (Taylor and Winnik, 2004). Future experimental and theoretical investigation of polymer particle coalescence can provide important information regarding the mechanical properties and the vapor (moisture) permeability of the solid polymer films that cover the surface of the tablet at the end of the film-coating process.

### 7.6.2 Broader recommendations

The models developed during this research work, which are solely based on physics and are specific to the tablet coating process, allow predicting the coating suspension behavior onto and into a porous pharmaceutical tablet. It would be interesting to combine the current models with models that predict tablet movement (as well as tablet orientation), polymer film adhesion, tablet exposure and resident time under the spray, and spray atomization and evaporation. Such models were discussed in Chapter 2 of this thesis.

The final combined model will be able to provide useful information regarding the entire coating process and help optimize this. The validation of this model will be possible by performing actual coating runs and comparing the model output (film thickness, defect formation, water content) with the observations of the final coated tablets.

To conclude, the combined model would be able to assist the end user (the pharmaceutical company) in understanding how changing controllable process conditions (such as inlet air temperature, drum rotation speed) can affect the phenomena at the point of contact between the tablet and the coating formulation and subsequently the water content and coating polymer distribution onto and into the tablets.

## **Publications that have arisen from this work**

Publications that have arisen during this project are listed below:

Christodoulou, C., Sorensen, E., García-Muñoz, S. and Mazzei, L., 2019. Mathematical modeling of spray impingement and film formation on pharmaceutical tablets during coating. Submitted.

Christodoulou, C., Sorensen, E., García-Muñoz, S. and Mazzei, L., 2018. Mathematical modelling of water absorption and evaporation in a pharmaceutical tablet during film coating. *Chemical Engineering Science*, 175, pp.40-55.

Christodoulou, C., Mazzei, L., García-Muñoz, S. and Sorensen, E., 2018. Modeling of spreading and drying of aqueous polymer coatings on pharmaceutical tablets during film coating. In *Computer Aided Chemical Engineering (Vol. 44, pp. 2095-2100)*. Elsevier. (Conference article)

Christodoulou, C., Mazzei, L., García-Muñoz, S. and Sorensen, E., 2017. Modelling of Droplet Absorption and Evaporation during Pharmaceutical Tablet Coating. In *Computer Aided Chemical Engineering (Vol. 40, pp. 85-90)*. Elsevier. (Conference article)

## **Conference participation**

Process Systems Engineering, PSE2018. San Diego, USA, 2018. Oral presentation: Modeling of spreading and drying of aqueous polymer coatings on pharmaceutical tablets during film coating.

Advanced Process Modelling Forum 2018, London, UK. Oral presentation: Mathematical modeling of spray impingement and film formation on pharmaceutical tablets during coating.

American Institute of Chemical Engineers Annual Meeting. 2017. Minneapolis, USA. Oral presentation: Modeling of Flow and Drying of Aqueous Polymer Coatings on Porous Pharmaceutical Tablets.

10<sup>th</sup> World Congress of Chemical Engineering. 2017. Barcelona, Spain. Oral presentation: Modeling of Droplet Absorption and Evaporation during Pharmaceutical Tablet Coating.

American Institute of Chemical Engineers Annual Meeting. 2016. San Francisco, USA. Oral presentation: Modelling of Droplet Absorption and Evaporation in a Pharmaceutical Tablet.

ChemEngDay UK. 2016. Bath, UK. Poster Presentation: Modelling of Water Absorption in a Pharmaceutical Tablet.

## **Research stay**

Visiting scholar at Carnegie Mellon University, Pittsburgh, USA (April 2018 - August 2018). Advisor: Professor Aditya Khair.

# Notation

Some of the symbols used infrequently in this thesis are not listed here, but are defined where they first appear in the text.

## Roman symbols

$a$	Particle radius (m)
$A$	Surface area (m <sup>2</sup> )
$c_p$	Heat capacity (J K <sup>-1</sup> )
$C_v$	Vapor concentration (mol m <sup>-3</sup> )
$\mathcal{D}$	Diffusion coefficient (m <sup>2</sup> s <sup>-1</sup> )
$D_0$	Initial droplet diameter (m)
$D_d$	Droplet wetted area diameter (m)
$d_p$	Pore diameter (m)
$E$	Evaporation velocity (J)
$E_G$	Gravitational potential energy (J)
$E_K$	Kinetic energy (J)
$E_S$	Surface potential energy (J)
$f$	Gravitational potential energy per unit volume (J m <sup>-3</sup> )
$F_d$	Dissipation factor (-)
$\mathcal{F}_p$	Filter coefficient (m <sup>-1</sup> )
$g$	Gravitational field (m s <sup>-2</sup> )
$h$	Droplet height profile (m)
$\hat{h}$	Precursor film thickness (m)
$H_c$	Porous crust thickness (m)
$H_f$	Cylindrical film thickness (m)
$h_H$	Heat transfer coefficient (W m <sup>-2</sup> K <sup>-1</sup> )
$h_m$	Droplet mass centre height (m)
$h_{max}$	Maximum droplet height (m)
$h_p$	Wetting front depth (m)
$H_p$	Evaporation front depth (m)
$\mathcal{H}_{rs}$	Mean curvature of the surface $\mathcal{S}_{rs}$ (m <sup>-1</sup> )
$\mathbf{I}$	Identity tensor (-)
$\mathbf{j}$	Particle migration flux (m s <sup>-1</sup> )
$k$	Thermal conductivity (W m <sup>-1</sup> K <sup>-1</sup> )

$k_B$	Boltzmann coefficient ( $\text{J K}^{-1}$ )
$k_m$	Mass transfer coefficient ( $\text{m s}^{-1}$ )
$\mathcal{K}_p$	Porous media permeability ( $\text{m}^2$ )
$\dot{m}$	Mass flux ( $\text{kg s}^{-1} \text{m}^{-2}$ )
$M$	Disjoining pressure parameter (-)
$M_w$	Molecular weight ( $\text{kg mol}^{-1}$ )
$m_0$	Consistency index ( $\text{Pa s}^n$ )
$n$	Flow index (-)
$N$	Disjoining pressure parameter (-)
$\mathbf{n}_{rs}$	Unit vector normal to $\mathcal{S}_{rs}$ pointing from phase $r$ to phase $s$ (-)
$p$	Pressure (Pa)
$p_c$	Laplace pressure (Pa)
$Q_s$	Surface flux ( $\text{m}^2 \text{s}^{-1}$ )
$\mathbf{q}$	Heat flux ( $\text{W m}^{-2}$ )
$\mathcal{R}$	Spatial region ( $\text{m}^2$ )
$\mathfrak{R}$	Universal gas constant ( $\text{J mol}^{-1} \text{K}^{-1}$ )
$R_0$	Tablet characteristic length (m)
$R_d$	Droplet wetted area radius (m)
$R_f$	Cylindrical film radius (m)
$RH$	Relative humidity (-)
$T$	Temperature (K)
$t_i$	Kinematic characteristic time (K)
$\mathbf{u}$	Velocity vector ( $\text{m s}^{-1}$ )
$U_m$	Velocity of the droplet center of mass ( $\text{m s}^{-1}$ )
$U_0$	Droplet velocity before impact on the tablet ( $\text{m s}^{-1}$ )
$v$	Radial velocity component of the coating mixture ( $\text{m s}^{-1}$ )
$V$	Volume ( $\text{m}^3$ )
$w$	Vertical velocity component of the coating mixture ( $\text{m s}^{-1}$ )
$W_a$	Absorption velocity ( $\text{m s}^{-1}$ )
$W$	Rate of work done on the droplet by the surroundings (W)

## Dimensionless numbers

Bo	Bond number
Nu	Nusselt number
Oh	Ohnesorge number
Pe	Peclet number
Pr	Prandtl number
Re	Reynolds number
Sc	Schmidt number
Sh	Sherwood number
St	Stokes number
We	Weber number

## Greek symbols

$\Gamma$	Particle retention rate ( $s^{-1}$ )
$\dot{\gamma}$	Shear rate ( $s^{-1}$ )
$\gamma_s$	Surface tension ( $N\ m^{-1}$ )
$\delta$	Boundary layer thickness (m)
$\Delta H$	Enthalpy of vaporization ( $J\ kg^{-1}$ )
$\epsilon$	Carrier fluid volume fraction
$\epsilon_p$	Volume fraction of the particles retained in the tablet pores (-)
$\eta$	Effective viscosity (Pa s)
$\theta$	Contact angle (rad)
$\Lambda$	Dissipation parameter (-)
$\mu$	Viscosity (Pa s)
$\pi_c$	Disjoining pressure (Pa)
$\rho$	Density ( $kg\ m^{-3}$ )
$\sigma$	Stress tensor (Pa)
$\tau_a$	Absorption time (s)
$\tau$	Deviatoric stress tensor (Pa)
$\varphi$	Porosity (-)
$\phi$	Particle volume fraction (-)
$\Phi$	Rate of viscous dissipation of kinetic energy (W)
$\xi$	Boundary immobilisation variable (-)

## Subscripts

<i>d</i>	Droplet
<i>e</i>	Liquid phase
<i>f</i>	Film
<i>g</i>	Gas
<i>i</i>	Disconnected film on tablet
<i>max</i>	Maximum
<i>p</i>	Inside the tablet pores
<i>s</i>	Solid phase
<i>sat</i>	Saturated
<i>TD</i>	Dried tablet region
<i>TW</i>	Wetted tablet region
<i>w</i>	Water
0	Initial value
1	Phase 1 (coating formulation)
2	Phase 2 (air over the tablet)
3	Phase 3 (solid tablet)

## Bibliography

- Agrawal, A.M. and Pandey, P., 2015. "Scale up of pan coating process using quality by design principles", *Journal of Pharmaceutical Sciences*, 104(11), pp. 3589-3611.
- Alam, N., Sharma, M., Ahmad, S., Ali, M.S., Alam, M.S. and Alam, M.I., 2015. Formulation development, evaluation and accelerated stability studies of entecavir tablet dosage form. *The Pharma Innovation*, 4(9, Part A), p.1.
- Aliseda, A., Hopfinger, E.J., Lasheras, J.C., Kremer, D.M., Berchielli, A. and Connolly, E.K., 2008. Atomization of viscous and non-Newtonian liquids by a coaxial, high-speed gas jet. Experiments and droplet size modeling. *International Journal of Multiphase Flow*, 34(2), pp. 161-175.
- Alleborn, N. and Raszillier, H., 2004. Spreading and sorption of a droplet on a porous substrate. *Chemical Engineering Science*, 59(10), pp.2071-2088.
- am Ende, M.T. and Berchielli, A., 2005. A thermodynamic model for organic and aqueous tablet film coating. *Pharmaceutical development and technology*, 10(1), pp.47-58.
- Amidon, G.L., Lee, P.I. and Topp, E.M. (eds.), 1999. *Transport processes in pharmaceutical systems*. New York, NY, United States: Marcel Dekker.
- Attané, P., Girard, F. and Morin, V., 2007. An energy balance approach of the dynamics of drop impact on a solid surface. *Physics of Fluids*, 19(1), p.012101.
- Aulton, M. E. and Twitchell, A. M., 1995. Film coat quality, In Graham Cole. *Pharmaceutical Coating Technology*, Bristol: Taylor & Francis.
- Barnes, H.A., Hardalupas, Y., Taylor, A.M.K.P. and Wilkins, J.H., 1999, July. An investigation of the interaction between two adjacent impinging droplets. In *Proceedings of the 15th ILASS, Toulouse*. pp. 1-7.
- Batchelor, G.K., 1976. Brownian diffusion of particles with hydrodynamic interaction. *Journal of Fluid Mechanics*, 74(1), pp.1-29.
- Bechtel, S.E., Bogy, D.B. and Talke, F.E., 1981. Impact of a liquid drop against a flat surface. *IBM Journal of Research and Development*, 25(6), pp.963-971.
- Bird, R.B., Stewart, W.E. and Lightfoot, E.N., 2007. *Transport phenomena*. John Wiley & Sons.
- Bisighini, A., Cossali, G.E., Tropea, C. and Roisman, I.V., 2010. Crater evolution after the impact of a drop onto a semi-infinite liquid target. *Physical Review E*, 82(3), p.036319.
- Bolleddula, D.A., Berchielli, A. and Aliseda, A., 2010. Impact of a heterogeneous liquid droplet on a dry surface: Application to the pharmaceutical industry, *Advances in Colloid and Interface Science*, 159(2), pp. 144-159.
- Bradford, S.A., Simunek, J., Bettahar, M., van Genuchten, M.T. and Yates, S.R., 2003. Modeling colloid attachment, straining, and exclusion in saturated porous media. *Environmental science & technology*, 37(10), pp.2242-2250.

- Bradford, S.A., Yates, S.R., Bettahar, M. and Simunek, J., 2002. Physical factors affecting the transport and fate of colloids in saturated porous media. *Water Resources Research*, 38(12), pp.63-1.
- Brady, J.F., 1993. The rheological behavior of concentrated colloidal dispersions. *The Journal of Chemical Physics*, 99(1), pp.567-581.
- Buyevich, Y.A. and Kapbsov, S.K., 1999. Segregation of a fine suspension in channel flow. *Journal of non-Newtonian fluid mechanics*, 86(1-2), pp.157-184.
- Cacuci, D.G., Cacuci, C.G., 2003. *Sensitivity and Uncertainty Analysis*. Chapman & Hall/CRC Press, Boca Raton.
- Chen, Y. and Porter, W.R., 2008. *Developing solid oral dosage forms: Pharmaceutical theory and practice*. Edited by Yihong Qiu, Lirong Liu, and Zhang. Amsterdam: Academic Press Inc. (London).
- Christodoulou, C., Sorensen, E., Garcia-Munoz, S. and Mazzei, L., 2018. Mathematical modelling of water absorption and evaporation in a pharmaceutical tablet during film coating. *Chemical Engineering Science*, 175, pp.40-55.
- Civan, F., 2011. *Porous media transport phenomena* (pp. 152-159). Hoboken: Wiley.
- Cole, G.C., 1995. Introduction and overview of pharmaceutical coating. In *Pharmaceutical coating technology* (pp. 11-15). CRC Press.
- Collins, J.H.P., Gladden, L.F., Hardy, I.J. and Mantle, M.D., 2007. Characterizing the evolution of porosity during controlled drug release. *Applied Magnetic Resonance*, 32(1-2), pp.185-204.
- Colorcon, 2019. *Film coatings – Product literature – General information* [online]. Available at: <https://www.colorcon.com/products-formulation/all-products/film-coatings/immediate-release/> [Accessed 12 June 2019].
- Cossali, G.E., Marengo, M. and Santini, M., 2005. Single-drop empirical models for spray impact on solid walls: a review. *Atomization and Sprays*, 15(6).
- Coussot, P. and Ancey, C., 1999. Rheophysical classification of concentrated suspensions and granular pastes. *Physical Review E*, 59(4), p.4445.
- Croll, S.G., 1987. Heat and mass transfer in latex paints during drying. *JCT, Journal of coatings technology*, 59(751), pp.81-92.
- Davis, S.H. and Hocking, L.M., 2000. Spreading and imbibition of viscous liquid on a porous base. II. *Physics of fluids*, 12(7), pp.1646-1655.
- De Gennes, P.G., 1985. Wetting: statics and dynamics. *Reviews of modern physics*, 57(3), p.827.
- Delhaye, J.M., 1974. Jump conditions and entropy sources in two-phase systems. Local instant formulation. *Int. J. Multiph. Flow* 1 (3), 395–409.
- Denesuk, M., Zelinski, B.J.J., Kreidl, N.J. and Uhlmann, D.R., 1994. Dynamics of incomplete wetting on porous materials. *Journal of Colloid and interface science*, 168(1), pp.142-151.

- Elimelech, M., Gregory, J. and Jia, X., 2013. Particle deposition and aggregation: measurement, modelling and simulation. Butterworth-Heinemann.
- Felton, L.A., 2013. Mechanisms of polymeric film formation. *International journal of pharmaceuticals*, 457(2), pp.423-427.
- Fluent, A.N.S.Y.S., 2019. Ansys Fluent, Academic Research, Release, 19.
- Freireich, B., Ketterhagen, W.R. and Wassgren, C., 2011. Intra-tablet coating variability for several pharmaceutical tablet shapes, *Chemical Engineering Science*, 66(12), pp. 2535-2544.
- Freireich, B., Kumar, R., Ketterhagen, W., Su, K., Wassgren, C. and Zeitler, J.A., 2015. Comparisons of intra-tablet coating variability using DEM simulations, asymptotic limit models, and experiments, *Chemical Engineering Science*, 131, pp. 197-212.
- García Muñoz, S., Moreno, M., Cano, A., Leyland, S., 2012. Modeling the Dynamics of the Film Coating Operation for Pharmaceutical Tablets. Paper presented at the AIChE Annual Meeting, Pittsburgh, PA.
- Golman, B., Julklang, W., 2013. Analysis of drying kinetics of a slurry droplet in the falling rate period of spray drying. *Int. J. Chem. Mol. Nucl. Mater. Metall. Eng.* 7 (9), 685–689.
- Hein, T., 2017. The benefits of multiple oral solid dosage forms. [online] *EPM Journal*. Available at: <https://www.epmmagazine.com/news/top-form-the-benefits-of-multiple-oral-solid-dosage-forms/> [Accessed 15 Jul. 2019].
- Hiby, J.W., 1962. Longitudinal and transverse mixing during single-phase ow through granular beds. *Interaction between Fluids & Particles*, pp.312-325.
- Holloway, W., Aristoff, J.M. and Stone, H.A., 2011. Imbibition of concentrated suspensions in capillaries. *Physics of Fluids*, 23(8), p.081701.
- Hu, H. and Larson, R.G., 2005. Analysis of the microfluid flow in an evaporating sessile droplet. *Langmuir*, 21(9), pp.3963-3971.
- Iwasaki, T., 1937. Some notes on sand filtration. *Journal American Water Works Association*, 29(10), pp.1591-1597.
- Jackson, R., 2000. *The dynamics of fluidized particles*. Cambridge University Press.
- Jamshidi, R., Angeli, P. and Mazzei, L., 2019. On the closure problem of the effective stress in the Eulerian-Eulerian and mixture modeling approaches for the simulation of liquid-particle suspensions. *Physics of Fluids*, 31(1), p.013302.
- Kadja, M. and Bergeles, G., 2003. Modelling of slurry droplet drying. *Applied Thermal Engineering*, 23(7), pp.829-844.
- Kalantari, D. and Tropea, C., 2007. Spray impact onto flat and rigid walls: Empirical characterization and modelling. *International Journal of Multiphase Flow*, 33(5), pp.525-544.
- Kalbag, A., Wassgren, C., Penumetcha, S., Perez-Ramos, J., 2008. Inter-tablet coating variability: residence times in a horizontal pan coater. *Chem. Eng. Sci.* 63, 2881-2894.

- Ketterhagen, W., Aliseda, A., am Ende, M., Berchielli, A., Doshi, P., Freireich, B. and Prpich, A., 2017. Modeling tablet film-coating processes. In *Predictive Modeling of Pharmaceutical Unit Operations* (pp. 273-316). Woodhead Publishing.
- Ketterhagen, W.R., 2011. Modeling the motion and orientation of various pharmaceutical tablet shapes in a film coating pan using DEM. *International journal of pharmaceutics*, 409(1-2), pp.137-149.
- Kiil, S., 2006. Drying of latex films and coatings: Reconsidering the fundamental mechanisms. *Progress in Organic Coatings*, 57(3), pp.236-250.
- Kim, H., Chun, J., 2001. The recoiling of liquid droplets upon collision with solid surfaces. *Phys. Fluids* 13 (3), 643–659.
- Krieger, I.M. and Dougherty, T.J., 1959. A mechanism for non-Newtonian ow in suspensions of rigid spheres. *Transactions of the Society of Rheology*, 3(1), pp.137-152.
- Krok, A., Vitorino, N., Zhang, J., Frade, J.R. and Wu, C.Y., 2017. Thermal properties of compacted pharmaceutical excipients. *International journal of pharmaceutics*, 534(1-2), pp.119-127.
- Kumar, R., Freireich, B. and Wassgren, C., 2015. DEM-compartment-population balance model for particle coating in a horizontal rotating drum”, *Chemical Engineering Science*, 125, pp. 144-157.
- Kutluay, S., Bahadir, A.R., Ozdes, A., 1997. The numerical solution of one-phase classical Stefan problem. *J. Comput. Appl. Math.* 81 (1), 135–144.
- Landau, H.G., 1950. Heat conduction in a melting solid. *Quarterly of Applied Mathematics* 8 (1), 81–94.
- Leal, L.G., 2007. *Advanced transport phenomena: fluid mechanics and convective transport processes* (Vol. 7). Cambridge University Press.
- Leáang, M., Pauchard, L., Lee, L.T. and Giorgiutti-Dauphine, F., 2019. Imbibition on a porous layer: dynamical and mechanical characterization. *Soft matter*, 15(10), pp.2277-2283.
- Lee, J.B., Radu, A.I., Vontobel, P., Derome, D. and Carmeliet, J., 2016. Absorption of impinging water droplet in porous stones. *Journal of colloid and interface science*, 471, pp.59-70.
- Lee, S.H. and Ryou, H.S., 2001. Development of a new model and heat transfer analysis of impinging diesel sprays on a wall. *Atomization and Sprays*, 11(1).
- Lefebvre, A.H., Wang, X.F. and Martin, C.A., 1988. Spray characteristics of aerated-liquid pressure atomizers. *Journal of Propulsion and Power*, 4(4), pp.293-298.
- Levi-Hevroni, D., Levy, A., Borde, I., 1995. Mathematical modelling of drying of liquid/solid slurries in steady state one-dimensional flow. *Drying Technol.* 13 (5–7), 1187–1201.
- Manninen, M., Taivassalo, V. and Kallio, S., 1996. On the mixture model for multiphase flow.

- Mezhericher, M., Levy, A., Borde, I., 2008. Modelling of particle breakage during drying. *Chem. Eng. Process.* 47 (8), 1404–1411.
- Mikulic, M., 2017. Pharmaceutical market worldwide revenue 2001-201 — Statista. [online] Statista. Available at: <https://www.statista.com/statistics/263102/pharmaceutical-market-worldwide-revenue-since-2001/> [Accessed 5 Jun. 2019].
- Möltgen, C.V., Puchert, T., Menezes, J.C., Lochmann, D. and Reich, G., 2012. A novel in-line NIR spectroscopy application for the monitoring of tablet film coating in an industrial scale process. *Talanta*, 92, pp.26-37.
- Moreira, A.L.N., Moita, A.S. and Panao, M.R., 2010. Advances and challenges in explaining fuel spray impingement: How much of single droplet impact research is useful?. *Progress in energy and combustion science*, 36(5), pp.554-580.
- Mowery, M.D., Sing, R., Kirsch, J., Razaghi, A., Bechard, S. and Reed, R.A., 2002. Rapid at-line analysis of coating thickness and uniformity on tablets using laser induced breakdown spectroscopy, *Journal of Pharmaceutical and Biomedical Analysis*, 28(5), pp. 935-943.
- Mueller, S., Llewellyn, E.W. and Mader, H.M., 2009. The rheology of suspensions of solid particles. *Proceedings of the Royal Society A: Mathematical, Physical and Engineering Sciences*, 466(2116), pp.1201-1228.
- Muliadi, A.R. and Sojka, P.E., 2010. A review of pharmaceutical tablet spray coating. *Atomization and Sprays*, 20(7).
- Müller, R. and Kleinebudde, P., 2006. Comparison study of laboratory and production spray guns in film coating: effect of pattern air and nozzle diameter. *Pharmaceutical development and technology*, 11(4), pp.425-433.
- Niblett, D., Porter, S., Reynolds, G., Morgan, T., Greenamoyer, J., Hach, R., Sido, S., Karan, K. and Gabbott, I., 2017. Development and evaluation of a dimensionless mechanistic pan coating model for the prediction of coated tablet appearance. *International journal of pharmaceutics*, 528(1-2), pp.180-201.
- O'brien, S.B.G. and Schwartz, L.W., 2002. Theory and modeling of thin film flows. *Encyclopaedia of surface and colloid science*, 1, pp.5283-5297.
- Pandey, P., Turton, R., Joshi, N., Hammerman, E. and Ergun, J., 2006. Scale-up of a pan-coating process. *AAPS PharmSciTech*, 7(4), pp.E125-E132.
- Page, S., Baumann, K.H. and Kleinebudde, P., 2006. Mathematical modeling of an aqueous film coating process in a Bohle Lab-Coater, Part 1: Development of the model. *AAPS PharmSciTech*, 7(2), pp.E79-E86.
- Park, H., Carr, W.W., Zhu, J. and Morris, J.F., 2003. Single drop impaction on a solid surface. *AIChE journal*, 49(10), pp.2461-2471.
- Pasandideh-Fard, M., Qiao, Y.M., Chandra, S. and Mostaghimi, J., 1996. Capillary effects during droplet impact on a solid surface. *Physics of fluids*, 8(3), pp. 650-659.
- Pham, T. and Kumar, S., 2019. Imbibition and evaporation of droplets of colloidal suspensions on permeable substrates. *Physical Review Fluids*, 4(3), p.034004.

- Popov, Y.O., 2005. Evaporative deposition patterns: spatial dimensions of the deposit. *Phys. Rev. E* 71 (3), 036313.
- Process Systems Enterprise Ltd., 2019. Release 5.1.1. London, UK.
- Rafai, S. and Bonn, D., 2005. Spreading of non-Newtonian fluids and surfactant solutions on solid surfaces. *Physica A: Statistical Mechanics and its Applications*, 358(1), pp.58-67.
- Rein, M. and Delplanque, J.P., 2008. The role of air entrainment on the outcome of drop impact on a solid surface. *Acta mechanica*, 201(1-4), p.105.
- Reis Jr, N.C., Griffiths, R.F., Mantle, M.D. and Gladden, L.F., 2003. Investigation of the evaporation of embedded liquid droplets from porous surfaces using magnetic resonance imaging. *International Journal of Heat and Mass Transfer*, 46(7), pp.1279-1292.
- Roberts, I.D. and Griffiths, R.F., 1995. A model for the evaporation of droplets from sand. *Atmospheric Environment*, 29(11), pp.1307-1317.
- Roisman, I.V., 2004. Dynamics of inertia dominated binary drop collisions. *Physics of Fluids*, 16(9), pp.3438-3449.
- Roisman, I.V., Horvat, K. and Tropea, C., 2006. Spray impact: rim transverse instability initiating fingering and splash, and description of a secondary spray. *Physics of Fluids*, 18(10), p.102104.
- Roisman, I.V., Prunet-Foch, B., Tropea, C. and Vignes-Adler, M., 2002. Multiple drop impact onto a dry solid substrate. *Journal of colloid and interface science*, 256(2), pp.396-410.
- Roisman, I.V., Rioboo, R. and Tropea, C., 2002. Normal impact of a liquid drop on a dry surface: model for spreading and receding. *Proceedings of the Royal Society of London. Series A: Mathematical, Physical and Engineering Sciences*, 458(2022), pp.1411-1430.
- Russel, W.B., Russel, W.B., Saville, D.A. and Schowalter, W.R., 1991. *Colloidal dispersions*. Cambridge university press.
- Rutgers, I.R., 1962. Relative viscosity of suspensions of rigid spheres in Newtonian liquids. *Rheologica Acta*, 2(3), pp.202-210.
- Sahota, M.S. and Pagni, P.J., 1979. Heat and mass transfer in porous media subject to fires. *International Journal of Heat and Mass Transfer*, 22(7), pp.1069-1081.
- Schwartz, L.W. and Eley, R.R., 1998. Simulation of droplet motion on low-energy and heterogeneous surfaces. *Journal of Colloid and Interface Science*, 202(1), pp.173-188.
- Schwartz, L.W. and Weidner, D.E., 1995. Modeling of coating flows on curved surfaces. *Journal of engineering mathematics*, 29(1), pp.91-103.
- Schwartz, L.W., 1999. Theoretical and numerical modeling of coating flow on simple and complex substrates including rheology, drying and Marangoni effects. *Advances in coating and drying of thin films*, pp.105-128.
- Schwartz, L.W., Roy, R.V., Eley, R.R. and Petrash, S., 2001. Dewetting patterns in a drying liquid film. *Journal of colloid and interface science*, 234(2), pp.363-374.

- Shaari, K.Z.K., 2007. Coating uniformity on a pharmaceutical tablet: An experimental study and finite volume modeling of droplet impact behavior. West Virginia University.
- Siregar, D. P., 2012. Numerical simulation of evaporation and absorption of inkjet printed droplets Eindhoven:Technische Universiteit Eindhoven
- Siregar, D.P., Kuerten, J.G. and Van der Geld, C.W.M., 2013. Numerical simulation of the drying of inkjet-printed droplets. *Journal of colloid and interface science*, 392, pp.388-395.
- Siregar, D.P., Kuerten, J.G.M., Wijshoff, H.M.A. and Van der Linden, L.T.M., 2010. Numerical simulation of the absorption of a droplet in a porous medium. In *AIP Conference Proceedings* (Vol. 1254, No. 1, pp. 135-140). AIP.
- Sirignano, W.A., 1999. Fluid dynamics and transport of droplets and sprays. Cambridge University Press (CUP).
- Slattery, J.C., Sagis, L. and Oh, E.S., 2007. Interfacial transport phenomena. Springer Science & Business Media.
- Suzzi, D., Toschkoff, G., Radl, S., Machold, D., Fraser, S.D., Glasser, B.J. and Khinast, J.G., 2012. DEM simulation of continuous tablet coating: Effects of tablet shape and fill level on inter-tablet coating variability. *Chemical Engineering Science*, 69(1), pp.107-121.
- Szeri, A.Z., 2010. Fluid film lubrication. Cambridge university press.
- Tag, C.M., Toiviainen, M., Ridgway, C., Juuti, M. and Gane, P.A., 2013. Dynamic ink oil absorption in a pigmented porous coating medium studied by near-infrared diffuse reflectance spectroscopy. *Transport in porous media*, 99(1), pp.145-160.
- Taylor, J.W. and Winnik, M.A., 2004. Functional latex and thermoset latex films. *Jct Research*, 1(3), pp.163-190.
- Tropea, C. and Marengo, M., 1999. The impact of drops on walls and films. *Multiphase Science and Technology*, 11(1).
- Tufenkji, N. and Elimelech, M., 2004. Correlation equation for predicting single-collector efficiency in physicochemical filtration in saturated porous media. *Environmental science & technology*, 38(2), pp.529-536.
- Twitchell, A. M., Hogan, J. E., and Aulton, M. E., 1995. The behaviour of film coating droplets on their impingement onto uncoated and coated tablets". *STP Pharma Sci.*, (5) pp. 190-195.
- Varga, C.M., Lasheras, J.C. and Hopfinger, E.J., 2003. Initial breakup of a small-diameter liquid jet by a high-speed gas stream, *Journal of Fluid Mechanics*, 497, pp. 405-434.
- Wang, J., Hemenway, J., Chen, W., Desai, D., Early, W., Paruchuri, S., Chang, S.Y., Stamato, H. and Varia, S., 2012. An evaluation of process parameters to improve coating efficiency of an active tablet film-coating process. *International journal of pharmaceutics*, 427(2), pp.163-169.
- Weidner, D.E., Schwartz, L.W. and Eley, R.R., 1996. Role of surface tension gradients in correcting coating defects in corners. *Journal of colloid and interface science*, 179(1), pp.66-75.

- Woodside, W., Messmer, J.H., 1961. Thermal conductivity of porous media. I. Unconsolidated sands. *J. Appl. Phys.* 32 (9), 1688–1699.
- Yamane, K., Sato, T., Tanaka, T., Tsuji, Y., 1995. Computer simulation of tablet motion in coating drum. *Pharm. Res.* 12, 1264-1268.
- Yarin, A.L. and Weiss, D.A., 1995. Impact of drops on solid surfaces: self-similar capillary waves, and splashing as a new type of kinematic discontinuity. *Journal of fluid mechanics*, 283, pp.141-173.
- Yiantsios, S.G. and Higgins, B.G., 2006. Marangoni flows during drying of colloidal films. *Physics of Fluids*, 18(8), p.082103.
- Yoon, J.S., Germaine, J.T. and Culligan, P.J., 2006. Visualization of particle behavior within a porous medium: Mechanisms for particle filtration and retardation during downward transport. *Water resources research*, 42(6).
- Yortsos, Y.C. and Stubos, A.K., 2001. Phase change in porous media, *Current Opinion in Colloid & Interface Science*, 6(3), pp. 208-216.